RELEVANCE OF MIDLATITUDE DYNAMICS DURING BREAK-ACTIVE CYCLES OF SUMMER MONSOON, WITH EMPHASIS ON INDIA AND BEYOND

A thesis submitted during 2015 - 2021 to the University of Hyderabad in partial fulfilment of the award of a Ph. D. degree in Earth and Space Sciences

by

Govardhan Dandu
Reg. No: 15ESPE05

Under the supervision of
Prof. Karumuri Ashok

Centre for Earth, Ocean and Atmospheric Sciences
School of Physics

University of Hyderabad
(P.O.) Central University, Gachibowli,
Hyderabad
Telangana
India

CERTIFICATE

This is to certify that the thesis entitled **"RELEVANCE OF MIDLATITUDE DYNAMICS DURING BREAK-ACTIVE CYCLES OF SUMMER MONSOON, WITH EMPHASIS ON INDIA AND BEYOND"** submitted by **Govardhan Dandu** bearing Reg. No. **15ESPE05,** in partial fulfilment of the requirements for the award of Doctor of Philosophy in Earth & Space Sciences, is a bonafide work carried out by him under my supervision and guidance.

This thesis is not been submitted previously in part or in full to this or any other University or Institution for the award of any degree or diploma.

Prof. Karumuri Ashok
(Supervisor)

Prof. KARUMURI ASHOK
Centre for Earth, Ocean & Atmospheric Sciences
University of Hyderabad
Hyderabad-500 046, INDIA.

08.11.2021

Head
Centre for Earth, Ocean and Atmospheric Sciences

Head
Centre for Earth, Ocean & Atmospheric Sciences
University of Hyderabad
Hyderabad-500 046, INDIA.

Dean
School of Physics

DEAN
School of Physics
University of Hyderabad
Hyderabad-500 046, INDIA

CERTIFICATE

(For Ph. D. Dissertations)

This to certify that thesis entitled **"RELEVANCE OF MIDLATITUDE DYNAMICS DURING BREAK-ACTIVE CYCLES OF SUMMER MONSOON, WITH EMPHASIS ON INDIA AND BEYOND"** submitted by Govardhan Dandu bearing registration number 15ESPE05 in partial fulfilment of the requirements for award of Doctor of Philosophy in the School of Physics is a bonafide work carried out by him under my supervision and guidance.

This thesis is free from plagiarism and has not been submitted previously in the part of in full to this or any other University or Institution for award of any degree or diploma.

Further, the student has the following publications before submission of the thesis/monograph for adjudication and has produced evidence for the same in the form of acceptance letter or the reprint in the relevant are of this research: (Note: at least one publication in referred journal is required)

1. Govardhan, D., V. B. Rao and K. Ashok, 2017: Understanding the dynamics of breaks in the Indian Summer Monsoon and its revival. *J. Atmos. Sci.*, 74, http://dx.doi.org/10.1175/JAS-D-16-0325.1 I.F. 3.578 3 citations. Chapter 5 of dissertation where there this publication appears.

2. Rao, V. B., Govardhan, D, Ashok, K., Mary Toshie Kayano, Julio Pablo Reyes Fernandez and Marcelo Barbio Rosa, (2020): A unified view of breaks in Indian, South America and North American monsoons. (*JGR, under review*). Chapter 3 & chapter 4 of dissertation where there this publication appears.

3. Feba, F., D. Govardhan, C. T. Tejavath, Karumuri Ashok, 2021, ENSO Modoki teleconnections to Indian summer monsoon rainfall—A review, *Elsevier*, Book title: Indian Summer Monsoon Variability ElNiño-Teleconnections and Beyond, 1st Edition, ISBN: 9780128224021. Chapter 7 of dissertation where there this publication appears.

and has made presentations in the following conferences:

1. Presented a poster at IMSP, Annual Monsoon Workshop - 2015 and National Symposium on "Understanding and Forecasting the Monsoon Extremes", at IITM, Pune during February 23-24, 2016.

2. Presented a poster at International Conference at CLIVAR Early Career Scientists Symposium at First Institute of Oceanography/State Oceanic Administration of China, Qingdao, China during September 18-25, 2016.

3. Presented a poster at TROPMET – 2016; National Symposium on Tropical Meteorology: Climate Change & Coastal Vulnerability at Indian Institute of Technology, Bhubaneswar during December 18-21, 2016.

Further, the student has passed the following course towards fulfilment of coursework requirement for Ph.D. / was exempted from doing coursework (recommended by Doctoral Committee) on the basis of the following courses during his Ph. D. program

Course code	Name	Credits	Pass/Fail
ES 801	Earth System Sciences	4	Pass
ES805	Research Methodology	3	Pass
ES 806	Mathematics for Earth Sciences	4	Pass
ES 807	Interdisciplinary Course	3	Pass
ES 811-830	Special paper on a specified Research Topic	2	Pass

Prof. Karumuri Ashok
(Supervisor)

Prof. KARUMURI ASHOK
Centre for Earth, Ocean & Atmospheric Sciences
University of Hyderabad
Hyderabad-500 046, INDIA.

(Head, CEOAS)

05.11.2021

Head
Centre for Earth, Ocean & Atmospheric Sciences
University of Hyderabad
Hyderabad-500 046, INDIA.

(Dean, School of Physics)

DEAN
School of Physics
University of Hyderabad
Hyderabad-500 046, INDIA

DECLARATION

I, Govardhan Dandu, hereby declare that this thesis entitled **"RELEVANCE OF MIDLATITUDE DYNAMICS DURING BREAK-ACTIVE CYCLES OF SUMMER MONSOON, WITH EMPHASIS ON INDIA AND BEYOND",** submitted by me under the guidance and supervision of Prof. Karumuri Ashok, Centre for Earth, Ocean and Atmospheric Sciences, School of Physics, University of Hyderabad, is a bonafide research work. I also declare that it has not been submitted previously in part or in full to this University or any other University or Institution for the award of any degree or diploma.

Date: 08/11/2021

Place: Hyderabad

Govardhan Dandu

Reg. No. 15ESPE05

Ph. D. Earth and Spcace Sciences

Centre for Earth, Ocean and Atmospheric Sciences

School of Physics

University of Hyderabad

Coursework Report

Exams| 1301
31|5|17

UNIVERSITY OF HYDERABAD
NOTIFICATION OF RESULTS

Course Work: Ph.D., Centre for Earth and Space Sciences,

Month & Year: April'2017
Semester -II

Sl. No	Regn.No.	Name of the Student	CORE/COMPULSORY COURSES & NO OF CREDITS AND GRADES				
			ES 801 Credits 4	ES 805 Credits 3	ES 806 Credits 4	ES 807 Credits 3	ES 811-830 Credits 2
1	13ESPE01	KONETI SUNITHA	Pass	Pass	Pass	Pass	Pass
2	13ESPE03	DEBASHRI GARAI	Pass	Pass	Pass	Exempted	Pass
3	15ESPE01	FABA FRANCIS	Pass	Pass	Pass	Pass	Pass
4	15ESPE02	HEMADRI BHUSHAN AMAT	Pass	Pass	Pass	Fail	Pass
5	15ESPE03	K. MALLESH	Pass	Pass	Pass	Exempted	Pass
6	15ESPE04	CHENNU RAMU	Pass	Pass	Pass	Pass	Pass
7	15ESPE05	GOVARDHAN DANDU	Pass	Pass	Pass	Pass	Pass
8	15ESPE07	BOYAJ ALUGULA	Pass	Pass	Pass	Pass	Pass
9	15ESPE09	TEJAVATH CHARAN TEJA	Pass	Pass	Pass	Pass	Pass
10	15ESPE10	BILLINGI TARUN KUMAR	Pass	NA	Pass	NA	Pass
11	16ESPE01	RESHMA M.R.	Pass	NA	Pass	Exempted	Pass
12	16ESPE02	SEEDABATTULA V BALAJI MANASA RAO	Pass	NA	Pass	NA	Pass
13	16ESPE04	SUNIT MOHANTY	Pass	NA	Pass	NA	Pass
14	16ESPE05	TARUN THOMAS T.	Pass	NA	Pass	NA	Pass

Course No.	Title of the Course
ES 801	Earth system sciences -4
ES 805	Research Mehtodology -3
ES 806	Mathematics for Earth Sciences -4
ES 807	Interdisciplinary course -3
ES 811-830	Special Paper on Spectified Research Topic -2

NA - NOT APPEARED

Dated: 29.05.2017

Controller of Examination 30-5-17

To

Head, Centre for Earth and Space Sciences
Dean School of Physics

07-06-2017

Dedicated to XO ” ‘*-_|_-*` “ OX…

“One day, in retrospect, the years of struggle will strike you as the most beautiful.”

— Sigmund Freud

CONTENTS

ACKNOWLEDGEMENTS

It gives me immense pleasure to express my heartfelt gratitude to everyone who has made this research journey possible.

First and foremost, I thank my thesis advisor, *Prof. Karumuri Ashok*, for his able guidance, support and discussions spanning from dynamics, to statistics to carrying out model experiments, etc. His vast knowledge, continues motivation as a teacher & mentor, and holistic perspective on research have left a deep-seated mark on me. He has always been motivating and taught me to work hard, think critically, and evaluate my work, as well as to develop a scientific understanding and the importance of seizing every opportunity. I am grateful to him for his patient guidance and support, which enabled me to overcome challenges during my PhD work and finish this thesis.

I am fortunate to be associated with the stalwart of theoretical Meteorology, *Dr. Vadlamudi Brahmananda Rao, Emeritus Scientist*, INPE, Brazil, with whom we have a strong collaboration. His continuous guidance during the research process, his wisdom and profound knowledge of climate sciences, and his encouragement to perform my research from a theoretical viewpoint resulted in the establishment of this theoretically based thesis. Our close collaboration with him, and guidance stemming from his vast experience of research in theoretical meteorology, have been critical for realization of the thesis. He has been a great motivation for us.

I thank my Ph. D. doctoral committee members, *Dr. S. Maqbool Ahmed*, Principal Scientific Officer and Head of Central Instruments Laboratory, UoH, *Dr. S. Sri Lakshmi*, Assist. Professor and *Dr. Vijay P. Kanawade*, Assist. Professor, CEOAS, UoH, for their valuable suggestions & comments in improving quality of research, through continues assessments.

I thank *Prof. K. S. Krishna*, Head of the Department, CEOAS, UoH, and former HoD *Prof. M. Jayananda* for providing facilities to carry out research work in the department. I also sincerely thank other faculty members of CEOAS, *Honorary Prof. A. C. Narayana, Prof. V. Chakravarthi*, *Dr. T. Devleena Mani*, *Dr. M. Ismaiel*, *Dr. Aliba Ao*, and visiting faculty *Prof. D. V. Bhaskar Rao*,

K. L. University, Vijayawada, Andhra Pradesh, *Dr. Y. V. Rama Rao*, TSPDS, and *Dr. B. Chakrapani, Associate professor, CUSAT, Cochin,* for their encouragement

I express my warm thanks to *Dr. Nagaraju Chilukoti*, Assistant Professor, NIT, Rourkela for his help in model installation and technical support. I am also happy to acknowledge *Dr. Krishna Kishore* Osuri, NIT, Rourkela, for discussions and advice during my visit to their laboratory. I thank *Dr. Somenath Dutta*, Scientist F, IMD, climate research & services, for his valuable discussions with me during course of research.

I thank my colleagues, *A. Boyaj*, *H. B. Amat, T. Charan Teja*, *F. Francis, S. Bidyabati*, and *K. Vikas Kumar*, for all their valuable discussions and moral support. I particularly acknowledge *A. Boyaj*, for his continuous discussions and collaboration during course of PhD. I would also like to extend my warm thanks to all my other *fellow doctoral students* of the CEOAS, for their immense support.

I thank my *father Late Chandra Sekhar D*, *mother Lakshmi Devi D* and *elder brother Durga Prasad D & family* for inspiring me to pursue higher education and loving me through the times of difficulty. I convey my warm thanks to my dearest friends *K. Ashok Immaniel*, *T. Ravi Teja, B. Naresh, V. N. K. Chaitanya*, *Usman Syed* and *R. Jagdeep Kumar* and others for their support and encouragement.

I'd like to express my gratitude to the *Council of Science and Industrial Research* (CSIR) for providing research support in the form of JRF and SRF scholarships. This grant was facilitated through qualifying the national CSIR-NET exam. I thank the CLIVAR committee for providing funds to attend an international conference at Qingdao, China during 2016.

I would like to thank all *CEOAS non-teaching staff* for their support at various stages of my course. Finally, I would like to thank all those people who have been helping me directly and indirectly during my research. I am thankful to all of them.

My deepest gratitude to all…

Govardhan Dandu

LIST OF JOURNAL PUBLICATIONS

1. **Govardhan, D**., V. B. Rao and K. Ashok**,** 2017: Understanding the dynamics of breaks in the Indian Summer Monsoon and its revival. *J. Atmos. Sci*.**, 74,** http://dx.doi.org/10.1175/JAS-D-16-0325.1 **I.F. 3.578** ***3 citations***

2. Rao, V. B.,**Govardhan, D**, Ashok, K. , Mary Toshie Kayano, Julio Pablo Reyes Fernandez and Marcelo Barbio Rosa, (2020): A unified view of breaks in Indian, South America and North American monsoons. **(JGR, under review)**

BOOK CHAPTER

1. Feba, F., **D. Govardhan**, C. T. Tejavath, Karumuri Ashok, 2021, ENSO Modoki teleconnections to Indian summer monsoon rainfall—A review, *Elsevier*, *Book title: Indian Summer Monsoon Variability ElNiño-Teleconnections and Beyond, 1st Edition, ISBN: 9780128224021*.

OTHER PUBLICATIONS

1. Boyaj A., K. Ashok, S. Ghosh, P. Devanand, and **D. Govardhan**, 2017: The Chennai extreme rainfall event in 2015: The Bay of Bengal connection, *Climate Dynamics*. DOI: 10.1007/s00382-017-3778-7 **I.F. 4.048.** ***7 citations***

2. Rao, V. B., Koteswara Rao, K, Mahendranath, B., Lakshmi Kumar, T. V., **Govardhan, D**., (2020): Large-scale connection to deadly Indian heat waves, *Quart. J. Royal. Met. Society* (https://doi.org/10.1002/qj.3985)

CONFERENCE & WORKSHOP PROCEEDINGS

1. Attended an international workshop at INCOIS under the ITCO-ocean program entitled **"Indian Ocean Dynamics: From the Large-scale Circulation to Small-scale Eddies and Fronts"** during November 16-27, 2015 under Julian P. McCreary, Professor and Director, IPRC, University of Hawaii, Manoa. He also familiarized himself with the WRF model installation and preliminary analysis in this semester.

2. Presented a poster at IMSP, Annual Monsoon Workshop - 2015 and National Symposium on **"Understanding and Forecasting the Monsoon Extremes"**, at IITM, Pune during February 23-24, 2016.

3. Presented a poster in international conference at **CLIVAR** Early Career Scientists Symposium at First Institute of Oceanography/State Oceanic Administration of China, Qingdao, China during September 18-25, 2016.

4. Presented a poster at **TROPMET – 2016**; National Symposium on Tropical Meteorology: Climate Change & Coastal Vulnerability at Indian Institute of Technology, Bhubaneswar during December 18-21, 2016.

5. Participated in a national workshop on **"Extreme Weather and Climate Variability: Observation, Understanding and Prediction Training Workshop"** conducted by **GIAN** during December 22-31, 2016 at Indian Institute of Technology, Bhubaneswar.

6. Participated in the **"TERI-NORCE Research School: Global Climate Anomalies, Teleconnections and Regional Implications",** during the period August 05th -08th 2019 held at TERI Institute, New Delhi.

7. Participated in a workshop on **"Thermodynamics in Earth System"**, by Prof. Axel Kleidon, Max Plank Institute, during the period 10th-15th October 2019 held at IISER, Pune.

LIST OF ACRONYMS

ASM	:	Asian Summer Monsoon
BoB	:	Bay of Bengal
CBI	:	Barotropic instability
CMKE	:	Rate of conversion of mean kinetic energy to eddy kinetic energy
CMR	:	Core Monsoon Region
CTL	:	Control experiment
DCW	:	Daily Climatological Winds
DCWNC	:	Daily Climatological Winds with convection scheme switched off
ENSO	:	El Niño-Southern Oscillation
EP	:	Eliassen - Palm
FAA	:	Federal Aviation Administration
FGGE	:	First Global Experiment
GARP	:	Global Atmospheric Research Programme
HIF	:	High-index flow
IMD	:	Indian Meteorological Department
ISM	:	Indian Summer Monsoon
ISO	:	Intraseasonal oscillations
ITCZ	:	Inter-tropical convergence zone

IV	:	Intaseasonal variability
JJAS	:	June, July, August, and September
LBA	:	Large-Scale Biosphere Atmosphere
LBC	:	Lateral boundary conditions
LIF	:	Low-index flow
LLJ	:	Low-level jet
MCZ	:	Maximum cloud zone
MJO	:	Madden Julian Oscillation
MT	:	Monsoon trough
NAM	:	North American Monsoon
NCAR	:	National Centre for Atmospheric Research
NCEP	:	National Centres for Environmental Prediction
NCEP-FNL	:	National Centers for Environmental Prediction-Final Analysis
NE-SW	:	Northeast to Southwest
NH	:	Northern Hemisphere
NW-SE	:	Northwest to South east
QRA	:	Quasi-Resonant Amplification
SACZ	:	South Atlantic Convergence Zone
SAH	:	South Asian High
SAM	:	South American Monsoon

SLP	:	Sea level pressure
SMO	:	Sierra Madre Occidental
SWJ	:	Subtropical Westerly Jet
TEJ	:	Tropical Easterly Jet
TRMM	:	Tropical Rainfall Measuring Mission
USA	:	United States of America
WETAMC	:	Wet Season Atmospheric Mesoscale Campaign
WRF	:	Weather Research & Forecasting model

LIST OF SYMBOLS

Symbol	Definition
Φ	Geopotential Height
U	Zonal wind
V	Meridional wind
D/2	Latitudinal distance between Jets
L_c	Critical wavelength
$\overline{K}$	Mean Kinetic energy
K'	Eddy Kinetic energy
ζ	Absolute vorticity
f	Coriolis force
m	mass
u'	eddy zonal wind
v'	eddy meridional wind

LIST OF FIGURES

LIST OF TABLES

ABSTRACT

The summer monsoon Intraseasonal variability is primarily associated with active and break spells of rainfall. In this thesis, I investigate a few noteworthy aspects of the intraseasonal variability of the Indian summer monsoon in connection to midlatitude upper level circulation. I conducted several dynamical and statistical analyses, and sensitivity simulations with a regional model, to this end. The Indian summer monsoon rainfall (ISMR) is essentially a primary source of basic human life and a long-standing source of reliance for the Indian economy. My primary focus in this research is on the initiation and development of a break phase, as well as the revival of active conditions following a break phase over the Indian subcontinent. Furthermore, I investigated the break monsoon dynamics of North and South American summer monsoon systems and explored commonalities to the Indian summer monsoon.

The monsoon breaks in the core monsoon region or central region of India, lasting a few days-rarely even up to two weeks, are periods of low to no rainfall. Throughout summer monsoon, a seasonal high pressure region, extending from the Tibetan plateau, prevails over north India at 200 hPa. Our analysis of various observed and reanalyses data sets for the 1979-2007 period shows that breaks are characteristically preceded by an upper-tropospheric transient blocking high over north India, which extends to low levels. The formation of this blocking high is found to be due to the penetration of mid-latitude baroclinic waves into lower latitudes. Importantly, this transient blocking high is weaker than the seasonal High pressure at this level. The weakening of the high pressure due to the presence of this transient blocking leads to a sinking motion relative to the prebreak or after-break period which in turn leads to a filled up surface low, and an eventual

reduction in daily rainfall, Importantly, this mechanism is found to be associated with monsoon breaks in the North America, and South America as well.

The blocking high over the core monsoon region during breaks is associated with the convergence of Eliassen-Palm fluxes, which causes the upper-level zonal westerlies to decelerate. This holds the blocking high in place over the core monsoon region without being advected by the zonal wind. Also, I find that the resonance and amplification of planetary Rossby waves play a vital role in the block formation over the northwest of India. This sequence of events associated with the Indian breaks, that is, the initiation due to the formation of upper level blocking high due to resonance of planetary Rossby waves at mid-latitudes, followed by the break event and a relative sinking over the core monsoon region, also explains the North and South American summer monsoon breaks.

Following the initiation of a break phase over the Indian region, I observe an anomalous southward shift of a subtropical westerly jet stream during the peak of a significant break phase, followed by an anomalous northward shift of a stronger-than-expected tropical easterly jet stream. These major changes during a break facilitate an instability mechanism, which evidently contributes to the development of a synoptic disturbance, and subsequent revival of the Indian summer monsoon into the active phase in about 61% of the cases.

Our computations of energetics indicate an increase in the eddy kinetic energy at the expense of the mean kinetic energy during the breaks, in agreement with the formation of the synoptic disturbance. This demonstrates that barotropic instability in the presence of a monsoon basic flow is the primary physical mechanism that controls the subsequent revival of the monsoon. This entire life cycle of monsoon break formation and reversal to normal monsoon can be seen as the barotropic adiabatic cycle, similar to the index cycle of midlatitudes in a barotropic atmosphere. I propose these oscillations as ‘Monsoon Index Cycles’.

Apart from the above dynamical analysis carried out using NCEP reanalysis 2 data and gridded Indian summer monsoon rainfall data sets for the 1979-2007 period on the revival phase of monsoon from the break, I conducted a few sensitivity experiments using WRF regional climate model in order to ascertain the aforementioned dynamical mechanism for the revival of active conditions after a break phase of Indian summer monsoon, for one typical break case 01-09 August 2000. The sensitivity experiments essentially examine the role of the break-related circulation, particularly the role of the horizontal shear at upper level between the subtropical Westerly jet and tropical Easterly jet, eddy momentum flux and associated energetics. The results from the model confirm my interpretation of the mechanisms from analysis of observational and reanalysis data.

Chapter 1

Introduction

Outline of the chapter:

In this chapter, I discuss the available literature on the intraseasonal variability of the Indian summer monsoon with main focus on active to break conditions. I also discuss the intraseasonal variability of South and North American summer monsoonal regions.

Based on the scientific gaps identified during the review of the literature, we developed four objectives and further discussed the scope of the thesis. It will also be interesting to see if some of the mechanisms that cause the Indian summer monsoon, North American monsoon, and South American monsoon breaks have little in common and can be unified into a theory.

1.1 Pioneering studies of Indian Summer Monsoon

Scientific interest in the monsoon is not new. The earliest theory explaining the monsoons, which is based on the importance of the differential heating between ocean and land, was espoused by Edmund Halley (1686). Eliot (1884) has been credited with the identification of “minor cyclones of the Southwest monsoon season” which we now refer to as monsoon depression. Since then, there has been tremendous interest in studying the monsoon, its variability, and its relevance for applications.

Fig 1.1 shows the mean sea level pressure during June, July, August, and September (JJAS) months, which together comprise the Indian summer monsoon (ISM) season, for the 1979-2007 period. The low-pressure zone across the Indian region is conventionally referred to as a monsoon trough (MT) (Fig. 1.1.), which is a part of the Inter-tropical convergence zone (ITCZ), and is associated with the large-scale monsoon flow. To distinguish the presence of the ITCZ at the equatorial region for a few days and times during the same season, Gadgil (2003) proposed the nomenclature of convective tropical convergence zone. Fig. 1.2, based on the Indian Meteorological Department (IMD) observations for the 1901-2019 period, shows the mean seasonal rainfall over India. It is clear that there is a lot of spatial variability of rainfall distribution during the Indian summer monsoon. The Indian summer monsoon also varies on different time scales. Fig. 1.3, for example, shows the interannual variability of rainfall anomalies over the Indian region, indicating normal, above normal, and below-normal rainfall years.

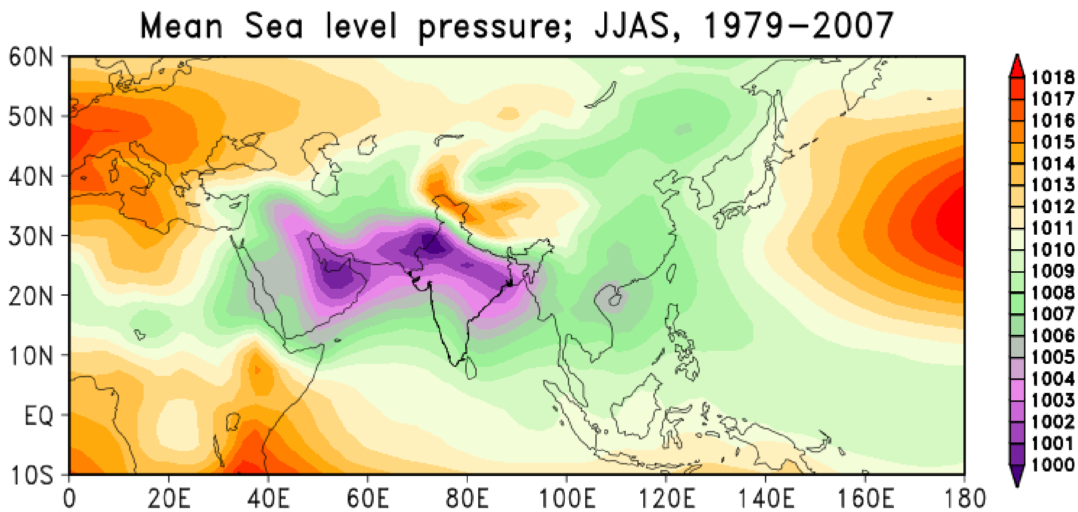

Figure 1.1: Spatial distribution of climatological mean sea level pressure (mb) during the June through September months (JJAS), over the 1979-2007 period.

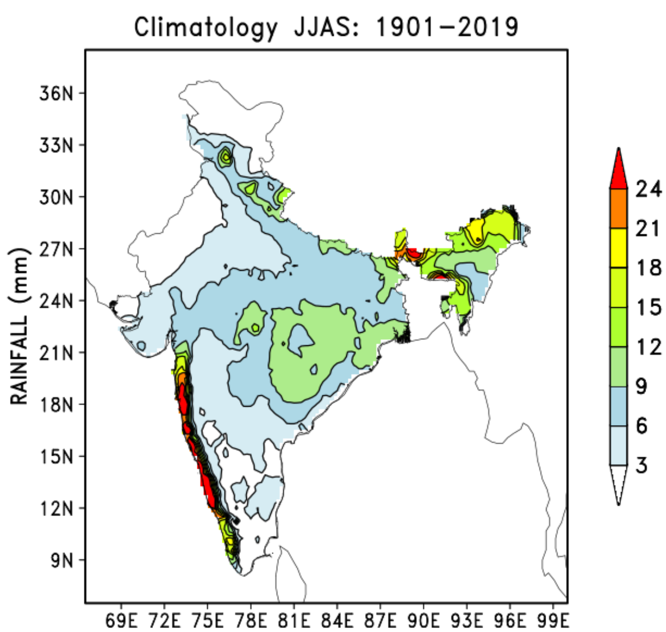

Figure 1.2: Climatology of rainfall (mm/day) over the Indian region for the JJAS season during the period 1901-2019.

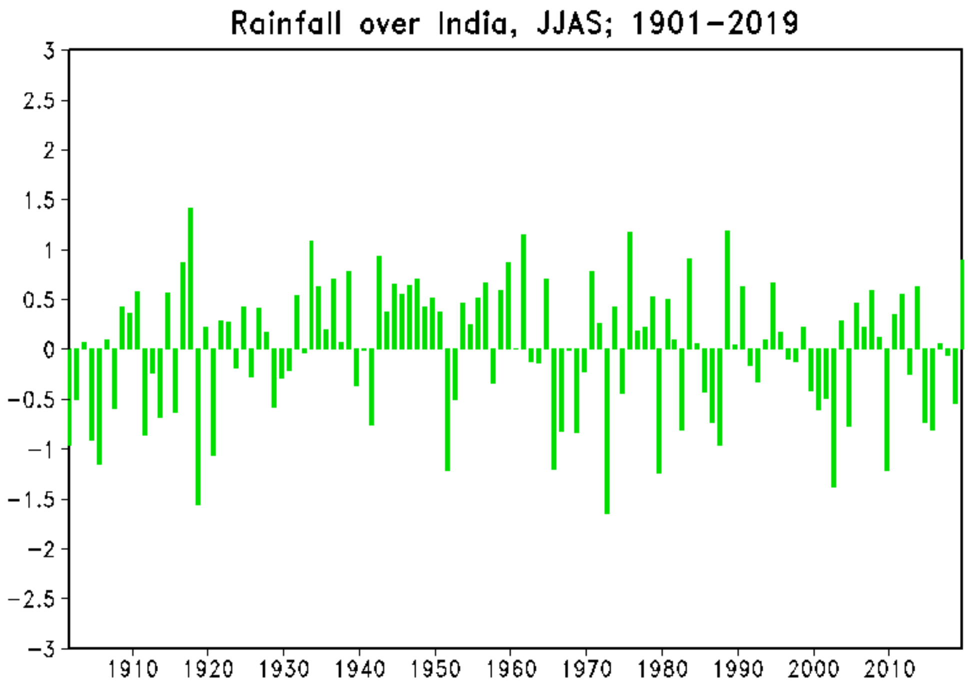

Figure 1.3: Interannual variability of the Indian summer rainfall over the Indian region during 1901-2019, provided as example of its temporal variations.

Recent investigations (Gadgil 2008), to be sure, have pointed out that while the summer onset in India is fundamentally affected by the differential heating of land and ocean, but its evolution is rather more significantly related to the complex high-frequency atmospheric disturbances, extra-monsoonal perturbations, and by the teleconnections between various climate drivers and monsoonal region. Studies suggest that the ISM rainfall varies at interannual, intraseasonal, decadal and multi-centennial time scales. From the statistical sense, a dominant mode of the Indian summer monsoon is interannual variability (Fig. 1.3), driven by the well-known El Niño-Southern Oscillation (ENSO), etc. The variability is forced by both external and internal drivers (e.g., Webster et al., 1998; Pant and Rupa Kumar,1997). In addition to the interannual variability, the

ISM also varies on intraseasonal time scales (e.g., Chatterjee and Goswami, 2004). For example, there are cycles of active and break episodes. “During the active monsoon spell, the Indian region receives adequate rainfall over the majority of the Indian region; however, during the break, the rains are reduced or no none across most of the Indian region, primarily the monsoonal core region (central parts) of India” (Ramamurthy 1969, Goswami et al. 1998 and Lawrence & Webster 2001). This is also a major mode of variability of the ISM.

Therefore, in this thesis, my primary focus lies on the intraseasonal variability in the ISM rainfall, specifically to document the hitherto unexplored potential mechanisms behind the break monsoon and the consequent revival of the Indian summer monsoon. In the next sub-section, we review the available literature on the observational and theoretical aspects of break phase initiation and its development, and those on the subsequent revival of active conditions of ISM rainfall.

1.2 Intraseasonal Variability of rainfall during the Indian summer monsoon

During summer monsoon months, there occur a few low-rainfall periods/spells or void situations over most of the Indian region. Blanford (1886) named these “intervals of drought” during July & August, the peak summer monsoon months, as the break periods. These intervals with low rainfall situations over a major portion of the Indian region are now routinely called “breaks”. Breaks are typically announced as when the MT shifts northward from its mean position for at least 3 days. Consequently, the Himalayan foothill region receives high rainfall during this period, while the rainfall along the climatological MT position decreases drastically. For example, Fig. 1.4 depicts the mean sea level pressure during the break (01-09 August 2000) and prebreak period (23-31 July 2000), as well as the corresponding rainfall distribution over India. This break period was generated using the Rajeeven et al. (2010) criterion. In Fig. 1.4, we see the MT weakening or shifting towards the Himalayan foothills during the break period, with massive rainfall across the Himalayan foothills. This causes a decrease in rainfall in the central parts of India, as well as the majority of the country. The monsoon revives after the break periods, often entering into the 'active' phase, which is, in a sense, exacerbation of the mean conditions.

Several researchers (e.g., Goswami et al. 2018) suggest that the total rainfall during any summer monsoon season critically depends on the number and intensity of the breaks. Therefore, understanding the intraseasonal variability of the ISM and diagnosing the mechanisms is important to enrich the seasonal prediction of the ISM, which has immense economic value. Thus, it is clear that the ISM rainfall is irregular in its occurrence and intensity. However, there is a lot of temporal and spatial variability in the ISM.

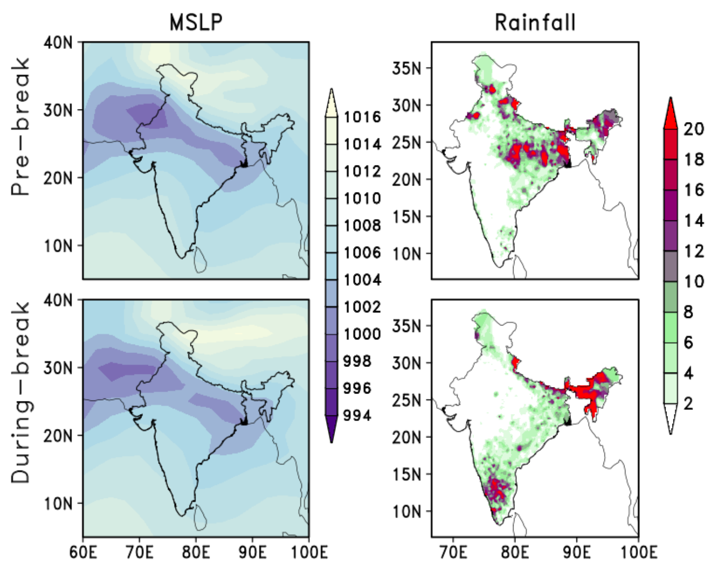

Fig. 1.4: Spatial distribution of mean sea level pressure and rainfall averaged over the duration of a break event (01-09 August 200) and corresponding prebreak conditions (23-31 Jul 2000). The break event has been identified Based on the Rajeevan et al. (2010) criterion.

As per Koteswarm (1950), who studies 19 break events, the 'break phase' begins two days before or later than the formation of a 'low' at 700 hPa in low latitudes. The movement of such lows weakens the North-south pressure gradient over the Peninsula. According to Koteswaram (1950), the monsoon frequently revives after a “break” by the formation of a synoptic low or a depression in the North Bay of Bengal (BoB) or a shift towards the north of the BoB from lower latitudes, resulting in the gradual revival of the MT to its normal position.

Using IMD observations, Ramamurthy (1969) classified active and 'break' periods based on MT fluctuations in the apex monsoon months of July and August from 1888 to 1967. Ramamurthy (1969) adopted the criteria of the movement of the MT moving northward from its mean position, i.e., close to the foot hills of Himalayas for more than two days as a 'break’, and a southward shift from its mean position as an active event. He also claims that August is slightly more prone to longer 'break' periods. Later, Ramaswamy (1971) observed a trough (active) and ridge (break) pattern of westerly waves in the lower troposphere at 500 hPa near the Himalayas in a case study during the 1965 summer monsoon using satellite data. Raghavan (1973) suggests that the beak and active phase of ISM are associated with the fluctuation of MT, and with the tropical synoptic low-pressure systems developing in the Bay of Bengal region. Then the normal/active monsoon conditions of rainfall are re-established when the monsoon trough returns and intensifies over India. When a synoptic low-pressure system moves in the northerly direction towards the Himalayas, then the monsoon trough of low pressure also moves from the plains to Himalayan foothills. This weakens rainfall over the plains of northern India brings about the break-monsoon.

Ramanadham et al. (1973), studying a single case study 1967 summer monsoon, suggested that the break monsoon situation sets in over the Indian region in association with the eastward movement of the high amplitude 500 hPa middle-latitude westerly trough, that extends into western parts of Pakistan and northern India. At the same time, Ramanadham et al. (1973) observed the subtropical anticyclonic ridge over Arabian region extends into central and peninsular India. At this particular time, the monsoon trough moves northward from its normal location over the Gangetic plains to the foothills of Himalayan region triggering break monsoon conditions.

The Monsoon Experiment was conducted during 1979 as a regional sub-program of the First GARP (Global Atmospheric Research Programme) Global Experiment (FGGE). This program has sourced valuable first time data related to the ISM and led to further investigation in different aspects. Studies from the project suggest that during the boreal summer monsoon, the intraseasonal variability of Asian Summer Monsoon (ASM) is dominated by the quasi-periodic intraseasonal oscillations (ISO) on time scales longer than 10 days but shorter than a season (Krishnamurti and Bhalme 1976; Krishnamurti and Ardunay 1980; Yasunari 1980 and Goswami & Ajaya Mohan 2001). Apart from the important 30-60 day oscillations, some of the experiments were carried out to explore the 10-20 day oscillation of the Indian monsoon as the intraseasonal variability is extremely important for rainfall predictions and their socioeconomic applications (Murakami 1979; Das 1979 and Goswami 1997).

Krishnamurti and Ardanuy (1980) suggest that the break spells of ISM are accompanied by westward propagating trough-ridge systems of surface pressure with a periodicity of about 10–20 days, which have a steady quasi-linear propagation of phase. From a power spectral density analysis, they revealed that zonal wavenumbers 3–6 made a significant contribution to this quasi-biweekly mode. Krishnamurti and Ardanuy (1980) also suggest that the extrapolation of the phase information of the steady westward propagating quasi-biweekly mode predicts monsoon breaks moderately well. Sikka & Gadgil (1980) showed that there are two favourable and important locations for maximum cloud zone (MCZ) during JJAS for 1973–1977 period over the Indian region, i.e., over the longitudes 70° - 90°E and in the monsoon zone north of 15° at 700 hPa, and the secondary MCZ in the equatorial region, i.e., between 0–10°N. In monsoon months JJAS, a break phase develops just before the temporary disappearance of the MCZ from the mean summer monsoon location, i.e., over the latitudes 15° - 28°N, and the active monsoon is established again by the northward shift of the secondary MCZ over the monsoon zone.

Results from Pant (1983) suggest that Tibetan Plateau cooling (warming) leads to break (active) periods over the Indian region. He showed that a ‘break’ period is associated with a zonally oriented trough between 10° - 15°N at 700 hPa over south Indian region and the adjoining seas; there is also a sharp decline in the temperature over the Tibetan Plateau region at 500 hPa level. Subsequently, as the plateau warms, the trough shifts northward over the North Indian region and leads to normal/active monsoon around 20°N. As per Pant, the Hadley cell has its upward limb in the trough at 10°–15°N over south India and descent further north during the break monsoon conditions. Whereas during the active phase of the monsoon, the Hadley cell is associated with a rising limb at ~20°N, and southward descent is prominent.

Yasunari (1986) demonstrated the inter-correlations between ISM active/break cycles and westerly circulation changes in the middle and high latitude, which are relevant to the low frequency 30–50 day oscillations. The oscillation of the monsoon system of this 30-50 day period is closely related with the east-west oscillation of the geopotential height with the node over Tibet. The lag correlations between the northern hemisphere monsoon trough and the 500 hPa geopotential height, suggested that this east-west oscillation is part of the response of the middle and high latitude westerly waves to the northward moving monsoon heat source. Yasunari (1986) suggest that the transition from the active to break phase of ISM, may be regarded as the transformation in the thermodynamical process from the "diabatic limit" to the "advective limit" (Webster, 1981) and vice versa.

Using atmospheric models, in a case study of the 1994 monsoon, Rodwell (1997) proposed a mechanism that includes the infusion of dry, high negative potential vorticity air from the Southern Hemisphere midlatitudes into the low-level monsoon inflow. Rodwell (1997) even suggests that altering moisture fluxes in South Asia and the perturbation activity of Southern Hemisphere midlatitudes associated with the cross-equatorial flow of monsoon can trigger monsoon breaks. Furthermore, De et al. (1998) discovered a few more additional features of the monsoon basic flow, which in turn leads to the monsoon break conditions during the 1968–1997 period, such as, a) The movement of cyclonic circulation or a trough over low latitudes, b) existence of a trough in mid-tropospheric westerlies over northern India, c) weak pressure gradient over the west coast of India, and d) strong westerly winds over the northern India.

Krishnan et al. (2000) defined break. The study, using both observations and modelling experiments, suggests that a quick northwest movement of anomalous Rossby waves from the Bay of Bengal into northwest and central India initiates break conditions over Indian region. Importantly, the intensification of “convective stable anomalies” over the Bay of Bengal triggers these anomalous Rossby waves. Goswami and Ajaymohan (2001) using dynamical climate models, that both the intraseasonal and interannual variability is governed by the mode of spatial variability. As a result, if the frequency of occurrence of active (break) phases of Intraseasonal oscillations (ISO) is larger than that of the opposite phases in a season, the seasonal mean monsoon could be strong (weak). In further analysis, they have shown that the strong (weak) monsoon years are indeed characterized by a higher frequency of occurrence of active (break) conditions and vice-versa. Gadgil and Joseph (2003) obtained a significant negative correlation between all India summer monsoon rainfall and the number of rain break days between 1901-1989 (i.e., r = -0.56). They also obtained a significant positive relationship between active days and monsoon rainfall between 1901-1989 (r = 0.47). Gadgil and Joseph's (2003) rainfall break composite is very similar to Ramamurthy's (1969) rainfall break composite, as they have identified positive rainfall anomalies over the Himalayan foothills and southeastern peninsular region.

AS per Joseph and Sijikumar (2004), when the strong cross-equatorial low-level Jetstream (LLJ) oriented southeastwards with its core at 850 hPa changes its direction towards east between Sri Lanka and the equatorial region, it triggers a break monsoon condition. During active monsoon conditions, the LLJ axis passes from the central Arabian Sea eastwards through peninsular India and it provides moisture for increased convection in the Bay of Bengal and the formation of a monsoon depression. Ramesh Kumar & Dessai (2004) analyzed break monsoon cases during the 1901-2002 period. They find that during the breaks, the overall daily Indian rainfall is < 9 mm/day and this condition lasts at least three days during July and August. The majority of the breaks lasted for 3–4 days duration (49%) in the July and August months. Furthermore, the correlation between the JJAS rainfall and break (active) days is −0.80 (0.38).

In a case study by Rao et al (2004), the authors suggest that the upper troposphere relative humidity reduces between 600 hPa and 200 hPa by ~30% at least ~3days before the break period over the ITCZ along with a weakening of the low-level convergence by ~50%. These lead to the drying of the middle troposphere and trigger break monsoon conditions over the Indian region. Wang et al, (2005) suggest that ISO of the Indian monsoon is associated with western equatorial Indian ocean warming. As the beginning of the rain, conditions in the western equatorial Indian Ocean is preceded by local surface wind convergence and central equatorial Indian Ocean warming. a “self-induction mechanism" of eastern Indian ocean warming appears to be operating in the maintenance of the active-break cycle of monsoon.

Mandke et al (2007) suggested a criterion for identifying active and break days based on the rainfall anomalies over the Indian core region (73°–82°E, 18°–28°N). The periods were acknowledged as active (break) events, when the standardized rainfall anomaly over the Indian core/central region exceeds (below) 0.7 (−0.7) for at least three uninterrupted days between 15 June - 15 September. Using observations of daily gridded rainfall datasets from 3700 stations, Krishnamurthy and Shukla (2000) shown the above normal rain over central India and below normal rain across Himalayan foothills (North India) and southern peninsular India, and that this pattern is transposed during the break phase. The authors also suggest that the largescale droughts are associated with huge negative rainfall anomalies across the central Indian region. Krishnamurthy and Shukla also pointed out that the success in long-range forecasting will essentially depend on precise quantitative estimates of the external factors affecting ISM due to high nonlinearity in the intraseasonal prediction of ISM.

Krishnamurthy and Shukla (2007) found two dominant intraseasonal oscillations with periods of 45 and 20 days in the seasonal rainfall of ISM, using multichannel singular spectrum analysis of the daily rainfall anomalies. Interestingly, they suggest that the active and break monsoon events contribute very little to the seasonal mean rainfall of 45-day and 20-day oscillations. They discovered that the lows and depressions formed during these active and break periods are consistent, and that the number of depressions formed during the active phase is approximately seven times that of the break phase. Rajeevan et al. (2010) suggest the active and break events are the normalized anomaly of the rainfall over a critical area, called the monsoon core zone (18°-28°

N & 65°-85° E), which exceeds 1.0 or is less than −1.0 respectively, provided that this criterion is satisfied for at least three consecutive days.

The Madden Julian Oscillation (MJO) is a dominant mode of tropical intraseasonal variability in the tropics. While it is relatively during the boreal summer, studies suggest that it is associated with northward propagation of cloud-bands over the Indian monsoon region. The work by Joseph et al. (2009) indicates that very long break periods can be deemed as a divergent Rossby response due to a dry phase of equatorial convection which can be due to a prevailing MJO signal. Pai et al., (2011) claim that 83% of the break cases are coincident with Phases 7, 8, 1, and 2 of the MJO. They also suggest an association between the active phase obf the ISM with certain phases of the MJO. Madhu and Bhatla (2020) suggest a stronger association of the MJ with breaks than with active monsoon conditions over the Indian region. However, despite the aforementioned apparent association between the active-break cycle and MJO, it is possible that a particular phase of MJO in the equatorial Indian Ocean is actually triggered by the intraseasonal phase of the ISM itself, or that both of these are part of an encompassing phenomenon of the same periodicity.

Umakanth et al. (2014) suggested a new criterion for breaks during the ISM, primarily based on the threshold of area-averaged rainfall over each grid considered. They also suggest a strong association between breaks and total seasonal summer monsoon rainfall in India. Umakanth et al. (2019) suggest that the development of a mid tropospheric cyclonic circulation anomaly stretching over the sub-tropical/mid-latitude Asian continent may trigger break conditions over the Indian region.

Interestingly, they propose a strong association between El Niño and below-average monsoon rainfall. Pai et al. (2014)'s analysis of long term trends in lows, also suggests, in agreement with Raghavan (1969) the importance of the lows and depressions for revival after a break phase.

The spatial and temporal variability of ISM is unique throughout the world, owing to all of the complex features of the monsoon basic flow. Apart from the theories of the break phase discussed above, the Indian northern boundary is also associated with midlatitude interactions during ISM. In this context, the following subsection discussed the interactions between midlatitudes and ISM, prominently the role of upper tropospheric Jet streams and Blocking high.

1.3 Interactions between Indian summer monsoon and Midlatitudes

1.3.1 The impact of Jet streams on the Indian summer monsoon

Essentially, Jet streams are formed by the thermal contrast between the equator & the polar regions as a result of differential solar insolation and role of Coriolis force acting on the moving masses. These are characteristically continuous over long distances, but a discontinuity is also common. The pathway of the jet is normally meandering, and these meanders propagate eastward at slower speeds than the actual wind within the flow. These large meanders of waves within the Jetstream are known as long or ultralong Rossby waves or planetary waves. In the Northern hemisphere, the intraseasonal variability of ISM is associated with the upper-level Subtropical Westerly Jet (SWJ) and the Tropical Easterly Jet (TEJ). The SWJ core sustains at 200 hPa at 42° N, while the TEJ core is found at 150 hPa at 9° N during summer months i.e., June, July, August, and September (JJAS). For example, Fig. 1.5 shows the climatological wind vectors at 200 hPa for the season JJAS during the period 1979-2019. From Fig. 1.5, I observe a large anticyclonic circulation over the Indian region during climatological JJAS season, which is normally called

South Asian High (SAH). The SAH intensity depends on the distribution of heterogeneous diabatic heating over the Tibetan Plateau region and the summer monsoon regional area (Wu and Liu 2003; Wu et al. 2007). The SAH is another typical synoptic system over the Asian continent during boreal summer (Mason and Anderson 1963), which indeed forms near the tropopause over the Indo-Chinese peninsular region before the BoB monsoon onset (He et al. 2006; Liu et al. 2009, 2012). Figure 1.5 depicts the climatology of SWJ ranging from 30° to 40° N, as well as TEJ ranging from 0° to 20° N. Large meanders of Rossby waves, however, extend beyond 50° N, accompanied by a spatial shift of the jet core in day-to-day SWJ and TEJ beyond 20° N, due to diurnal variation, seasonal shift, climate change, and so on. The detailed discussion of SAH and its influence over the Indian region during the summer monsoon is detailed in the next subchapter.

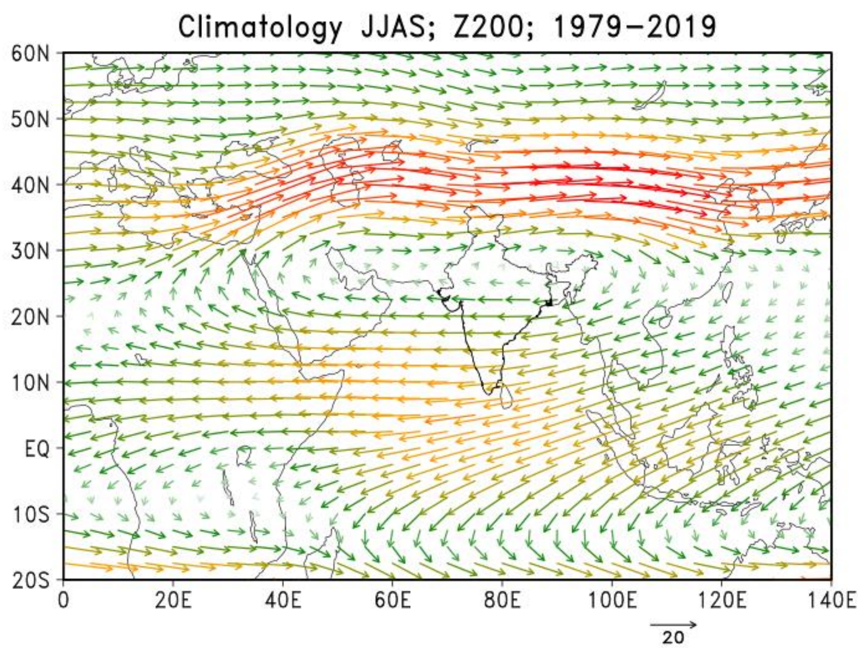

Figure 1.5: Climatological mean JJAS wind vector and magnitude (m/s) at a height of 200 hPa for the 1979 - 2019 period.

According to Rao et al. (1970) the changes in SWJ and TEJ flow result in four kinds of manifestations: a) intensifying or developing lower tropospheric lows or troughs, b) enhancing rainfall in pre-existing systems, c) re-curvature of depressions and lows and d) the onset of break conditions. Furthermore, even when the break is traced to westerly troughs, rainfall is increased by mid-latitude troughs before the break occurs over Indian region. During breaks, the subtropical ridge becomes more prominent and swings southwards. As a result, whether or not a break occurs after the passage of a westerly trough may be determined by the intensity of the ridge in the rear rather than the passage of the trough itself. Even after a break burst of rain along the Himalayas moving eastwards appear to be associated with the passage of subsequent troughs in westerlies, which are perhaps unable to break up the warm high that had formed earlier. A warm high forming and strengthening the seasonal subtropical ridge may explain 'breaks' that last for one to two weeks at times. The passage of a trough cannot account for the subsequent lengthy break. However, it is consistent with the behaviour of warm highs.

The STJ is a narrow band of fast-moving air that flows from west to east. Wind magnitude in a westerly jet stream typically varies between 40~60 m/s. Malurkar (1950) demonstrated that during ISM, the southward extension of an extratropical westerly trough into northern India results in a break condition. Later, Ramaswamy (1962) discovered that during a summer 'break' monsoon over India, large amplitude troughs in the middle latitude westerlies protrude into the Indo–Pakistan area based on break phase case studies during ISM. These eastward moving Rossby waves get retarded and elongated meridionally during movement across Tibetan Plateau and weakening Tibetan high at 500 hPa. Ramaswamy (1962) also showed that the ridge in the rear of the trough causes the extension of the anticyclone from the Tibetan plateau over to the northwest and central India. The associated upperlevel divergence causes heavy rainfall over and near the Himalayas. In a few case studies, Ramaswamy (1962) also observed that the large amplitude trough remains quasi-stationary over the northern India same as the 'break' lasts for a week or more. Thus, during break conditions, I witness the remarkable spectacle of two jets of completely different types - the Easterly and sub-tropical Westerly jets - passing within a short latitudinal distance of each other and dynamically interacting with each other.

Bedi et al. (1981) noticed that a strong monsoon is associated with strong westerlies and weak monsoon is associated with weak westerlies and westerly systems of middle-latitude are more active during a weak monsoon. Sikka and Grossman (1981) found that a large amplitude trough in the regime of subtropical westerlies was present during the break period of monsoon during the year 1979. Further, very weak spells of the ISM are associated with the signature of what is called as a low-index Rossby regime in the atmospheric general circulation over northern as well as southern hemispheres (Ramaswamy and Pareek,1978).

The TEJ is a critical feature of the ISM circulation (Koteswaram 1958; Alaka 1958; Krishnamurti and Bhalme, 1976) with the strongest winds of ~ 0– 50 m/s positioned just to the west of the southern tip of India and adjoining Arabian Sea (Reiter, 1961). The first detailed study on the TEJ was carried out by Koteswaram et al. (1958), who showed that the TEJ is sourced due to the large-scale arrangement of landmasses, the ocean, and the elevated heat source of the Tibetan Plateau. Chen and Yen (1991) noticed that the interannual variability of TEJ follows the interannual variability of stationary eddies over the summer monsoon region. Earlier studies also explained that the interannual variation of TEJ can be related to the interannual variation of summer rainfall (Chen and Yen 1991; Chen and Van Loon 1987; Kobayashi 1974). According to these studies, TEJ is found to be weaker (stronger) during the deficient (excess) summer monsoon rainfall over India.

The TEJ has a distinct intraseasonal oscillation south of its core, according to Chen and Van Loon (1987). The systematic shifting of locations caused by convection, low-level monsoon flow, and TEJ during different phases of the monsoon suggests that they all possibly related (Sathiyamoorthy et al., 2007). During the weak (strong) monsoon season of 1987 (1988), the middle and upper tropospheric meridional temperature gradient between the Tibetan High and the Indian Ocean region decreased (increased) (Pattanaik and Satyan 2000). There have been few studies on the relationship between the long-term trend of TEJ and the Indian summer monsoon due to a lack of persistent long-term data over the upper troposphere.

Sathiyamoorthy, et. al. (2007) has shown that the 30-60 day ISO of the TEJ reported in individual case studies occurs during the 1979–1990 period of study. The Axis of the TEJ, at the east of ∼70° E, and at 200 hPa is found along the near-equatorial latitudes during monsoon onset/revivals and the axis of TEJ propagates northward as the monsoon basic inflow advances across India. Also, they have found the axis is along ∼5° N and ∼15°N during active and break monsoon situations, respectively.

The next sub-chapter discusses extratropical systems, such as Blocking high and its interaction with ISM, particularly from the context of intraseasonal variability.

1.3.2 Relevance of Midlatitude Blocking High with Indian summer monsoon

The extratropical systems are associated with (a) troughs and (b) ridges of the SWJ. It may be presumed that the ridges can sometimes develop into a Blocking and the northern Indian region is just at the periphery of this system. Atmospheric blocking (hereafter as blocking) is a large-scale quasi-stationary low-frequency circulation pattern occurring in midlatitudes with a lifetime of ~10 to 20 days (Berggren et al. 1949; Rex 1950; Shukla and Mo 1983).

Blocking is defined as a continuous occurrence of high geopotential height for a relatively persistent time in a confined region or a quasi-stationary form (Hartmann & Ghan 1980). Early investigators (Berggren et al., 1949; Elliott and Smith, 1949 and Rex, 1950a, b) ascertained the synoptic behaviour and blocking climatology. Berggren et al. (1949) demonstrated that the formation of a blocking ridge is associated with the deepening of some extratropical wave cyclones over central Europe. This quasi-stationary blocking 'wave' disrupts the zonal flow of fast-moving frontal waves approaching from North America, resulting in extreme weather events. According to Rex (1950a), blocking occurs when the basic westerly current at upper level splits into two branches, each of which transports a significant amount of mass. The double-jet system must cover at least 45° of longitude. Across the current split, a sharp transition from zonal type flow upstream to meridional flow downstream must be observed, and this pattern must persist for at least ten days.

Rex (1950b) noted that blocking most frequently occurs over the North eastern portions of the Atlantic Ocean at 10° W and Pacific Ocean at 150° W (their Fig. 1), and normally this blocking persists for 12 – 16 days and relatively stable in position. According to Rex (1950b), the climatological mean position of the block is just downstream from the normal position of the major mid-latitude jet streams, with noticeable warming occurring in the northern part of the blocked zone and cooling occurring in the southern parts. During recent years it has also been shown that planetary-scale waves influence atmospheric blocking (Lejenas and Madden, 1989). Using the barotropic channel model, Egger (1978) showed that blocking could result from the nonlinear interactions between the forced stationary waves and the slowly moving free waves. Using the equation of motion, Hasanean and Hafez (2003) explained how the main westerly air current splits into two branches leading to the formation of a blocking high. Later, Shutts (1983) conducted a few numerical experiments to confirm a hypothesis that barotropic eddies reinforced blocking flow patterns mostly through Reynolds stresses. This propagation of barotropic eddies into the split Jetstream amplifies vorticity fields, resulting in blocking enhancement.

Tanaka (1998) defines atmospheric blocking as an abnormally persistent, quasi-stationary anticyclone that blocks the mid-latitude jet stream and the onset of blocking is generated by Rossby wave breaking. A blocking anticyclone forms at latitudes higher than where the normal sub-tropical high forms and is frequently accompanied by a cutoff low in low latitudes. However, in the Southern Hemisphere (SH), blocking highs tend to have a shorter lifetime than in the Northern Hemisphere (NH) and form at somewhat lower latitudes in general (Van Loon, 1956; Taljaard, 1972).

Another characteristic feature widely recognized is that even when a blocking high does break down or move away, there is a strong tendency for another high to form and intensify in the same location (Taljaard, 1972; Wright, 1974). Blocking phenomenon in a barotropic atmosphere can result due to resonant enhancement of Rossby lee waves forced by two stationary sources of potential vorticity (Kalney and Merkine 1981). Resonant interactions among planetary-scale waves may be an important physical mechanism in generating certain atmospheric blocking (Colliucci et al., 1981). A block may be initiated by a deep cyclonic storm development, which locks the flow pattern into a blocking equilibrium, or vice-versa when it drives the flow out of a blocking equilibrium (Charney et al., 1981). All the above discussion gives a detailed idea of blocking high genesis and its implications with the surrounding areas.

The blocking during the summer months is critical to the monsoonal regions, affecting the monsoon basic flow directly or indirectly. This blocking is also known as SAH over the Asian region. Wei et al. (2015) demonstrated a diagnostic analysis on the interannual time scale of SAH and its movement southeast-northwest, which is closely related to the Indian and East Asian summer monsoon rainfall. The SAH's reallocating towards southeast (northwest) is closely related to weak (more) Indian summer monsoon rainfall and high (less) rainfall in the Yangtze River valley of the East Asian summer monsoon region. There have only been a few studies that look at the relationship between ISM blocking and intraseasonal variability. They are as follows:

Unninayar and Murakami (1978) found that during weak monsoon situation anticyclonic circulation (at 200 hPa) over Himalaya bifurcates into two cells due to penetration of the midlatitude trough into sub-tropics, and at lowerlevel 700 hPa, they found that the easterlies around 20° N and 30° N over India are replaced by westerlies and north-westerlies intensified in the Arabian Sea. Keshvamurty et al. (1980) noticed a shift in the quasi-stationary large-scale features, i.e., Tibetan anticyclone and other monsoon disturbances of extratropical regions at 300 hPa and 200 hPa of tropospheric circulation in active-break monsoon situations. They also suggest that such shifts of quasi-stationary flow features and the associated changes in meridional and vertical shears may have a significant effect on summer monsoon circulation with the interactions of midlatitude westerly regime.

Raman and Rao (1981) suggested that the prolonged breaks causing severe summer monsoon droughts over the Indian sub-continent are due to upper tropospheric blocking high over East India (90° to 120°E) associated with baroclinic waves. Thus, this blocking high is considered as the initiator of the monsoon break. Recent studies have shown, the extreme cold spells during winter (Buehler et al. 2011), European temperature extremes during spring (Brunner et al. 2017), and heatwaves during summer (Della-Marta et al. 2007; Schaller et al. 2018) are often related to the formation and maintenance of mid-high latitude blocking, this has been an important research topic in past decades (for example, Yeh 1949; Shutts 1983; Colucci 1985; Haines and Marshall 1987; Holopainen and Fortelius 1987; Luo 2000, 2005; Luo et al. 2014, 2019; Zhang and Luo 2020; Nakamura and Huang 2017, 2018; Aikawa et al. 2019; Paradise et al. 2019).

All these studies indicate that the Indian monsoon is more than a local phenomenon and interacts significantly with midlatitude circulation. We see a potential impact of upper-level jet streams and blocking high on the monsoonal circulation over the Indian region based on the literature reviewed above. In a similar vein, in the following sub-chapter 1.3, we will discuss whether the intraseasonal variability of North and South American monsoons has few similarities with ISM.

1.3.3 Quasi-Resonant Amplification

Another important aspect of the atmospheric upper level midlatitude phenomenon is Quasi-Resonant Amplification (QRA). In general, large-scale midlatitude atmospheric circulation is associated with free and forced Rossby waves (Charney and Drazin, 1961; Hoskins and Karoly 1981; Dickinson 1970; Held et al., 2002 and Branstator 2002). Petoukhov et al. (2013) hypothesized the effect of QRA of planetary waves and recent occurring weather extremes. A brief explanation of QRA hypothesis as follows

Assume, k and m are the zonal wave numbers of free synoptic waves and forced/quasi-stationary planetary-scale Rossby waves. The upperlevel atmospheric circulation is characterized as per Petoukhov et al. (2013)

- free synoptic-scale Rossby waves with zonal wave numbers $k \geq 6$ propagate mainly in the longitudinal direction with a phase speed $c \approx 0$, and

- forced/quasi-stationary planetary-scale Rossby waves with zonal wave numbers m, with a phase speed $c \approx 0$, and frequency $\omega \approx 0$, are response of quasi-stationary spatially inhomogeneous diabatic sources/sinks and orography.

The midlatitude free synoptic-scale waves with zonal wavenumbers $k \approx 6$ - 8 are normally weak, with the meridional velocity less than 1.5 – 2 m/s (Eliasen and Machenhauer (1965); Fraedrich and Böttger (1978); Whitham (1960)).

Charney and DeVore (1979) shown that there is a “low-index” flow with a relatively weaker zonal component and a strong wave component which is intertwined close to linear resonance; the other is a “high-index” flow with a weak wave component and a relatively stronger zonal component which is much distant from linear response of resonance using a barotropic channel model with topographical forcing to study the planetary-scale circulations. It is suggested that the phenomenon of blocking is a metastable equilibrium state of the low-index near-resonant character.

Later, Petoukhov et al. (2013) proposed that the extreme summer events occur due to the certain persistent high-amplitude wave structures evolved in the field of the large-scale midlatitude atmospheric meridional velocity to which the quasi-stationary component of free synoptic waves with k ≈ 6 - 8 made an exceptionally large contribution. These structures may arise from changes in the midlatitude zonal mean state. When the aforementioned changes result in latitudinal trapping within the midlatitude waveguides of quasi-stationary free synoptic waves with zonal wavenumbers $k \approx 6$ - 8, the typically weak midlatitude response of wave numbers m 6 - 8 to quasi-stationary thermal and orographic sources/sinks may be strongly amplified via quasi-resonance.

Hence the QRA plays an important role in extreme weather events. In recent years, the Northern Hemisphere has experienced several regional weather extremes during summer, such as the heatwave in the United States in 2011, the Russian heatwave and the Indus River flood in Pakistan in 2010, and the European heatwave in 2003. In this regard, I began to investigate the genesis of quasi-stationary anticyclones (blocking highs) as a result of the QRA, followed by the break phase development during the summer monsoon.

Kornhuber et al. (2016) showed that QRA explains roughly a third of all high-amplitude events with wave numbers 6 to 8 and that amplitudes of quasi-stationary waves of that wave number range are significantly higher when resonance conditions are met. They also showed that planetary waves amplified by QRA exhibit specific preferred phases due to the characteristic stationary orographic forcing of the Northern Hemisphere midlatitudinal orographic profile. Their analysis shows that the central United States and western Europe are specifically susceptible to persistent heat waves during QRA episodes (Kornhuber et al., 2017). Later Mann et al. (2018) have shown that the zonally averaged surface temperature field can be used to define a signature for the occurrence of QRA by examining the Coupled Model Intercomparison Project Phase 5 climate model projections. Mann et al. (2018) also suggest that QRA events are likely to increase by 50% this century under business-as-usual carbon emissions, but there is significant variation among climate models. The following subchapter discusses the importance of NAM & SAM.

1.4 Intraseasonal variability of North and South American monsoon regions

The classical monsoon definition was solely based on the annual reversal of prevailing surface winds (Ramage 1971). Monsoons are not the same throughout the tropics because they are influenced by the specific locations of continents, oceans, and regional wind and rain patterns. Figure 1.6, for example, depicts the climatology mean sea level pressure across global tropical regions. The black dashed line box in Fig. 1.6 (a) represents the North American, North African, Indian, and East Asian monsoonal regions during the JJAS season, and in Fig. 1.6 (b) represents the South American, South African, and Australian monsoonal region during the DJF season. In this section, we discuss the monsoons of both Americas in comparison to ISM. Even though the geographical characteristics of specific monsoon regions significantly differ due to the vast continental region and much larger ocean basins that are adjacent to the monsoonal regions. In Fig. 1.6, we see a high on both sides of the American continent in the mean sea level pressure field, which is not seen in the Indian, East Asian, or African summer monsoons. In this regard, the environments of the monsoon systems are not comparable, but nonetheless have. Of course, they also have a few general similarities.

North American Monsoon (NAM) and South American Monsoon (SAM) circulation systems have a few similarities to other monsoons around the globe, which develop in response to thermal contrast between the continent and adjacent oceanic regions and provide a major component of continental warm season precipitation regime. Similar to other tropical monsoons, the evolution of the NAM and SAM system can be characterized in terms of onset, mature/peak, and subsidence phases. Importantly, A similar characteristic of intraseasonal variability in different American regions reveals a considerable commonality in the events occurring in ISM, despite the monsoons' distinct climatic conditions. Several examinations support the idea that intraseasonal rainfall within the NAM and SAM regions shows oscillatory behavior, though the specification of the preferred periodicities remains uncertain, the monsoon season consists of irregular burst and break periods and that the length (and number) of these periods is an important factor concluding the overall quality of the monsoon season. The goal of this research is to better understand the similarities between ISM, NAM, and SAM, in the genesis of a break phase during the summer monsoon.

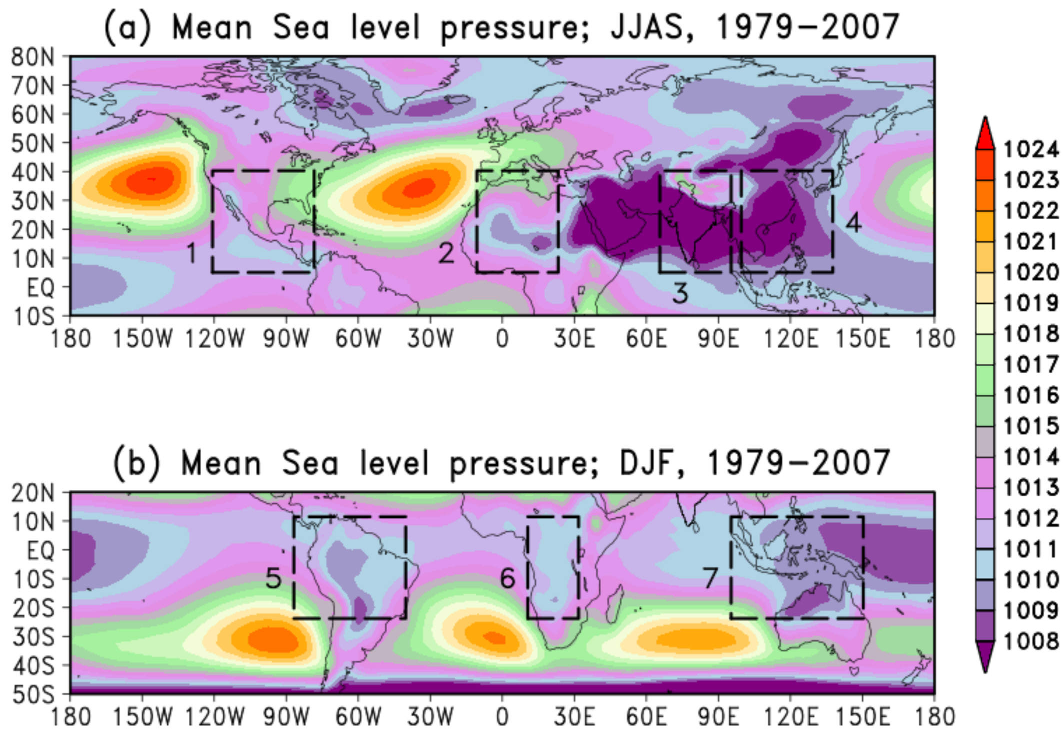

Fig. 1.6: (a) The black dashed line box denotes 1. North American, 2. African (northern western parts of the continent) 3. Indian and 4. East Asian monsoonal regions in the northern hemisphere and the shading represents the climatology mean sea level pressure of the JJAS season for the 1979-2007 period. **(b)** The black dashed line box denotes the 5. South American, 6. African (middle and southern African countries), and 7. Australian monsoonal regions in the southern hemisphere, and the shading represents the DJF season climatology mean sea level pressure for the 1979-2007 period.

1.4.1 Intraseasonal variability of North American summer monsoon

Importantly, the NAM exhibits substantial interannual variability, which is also connected with intraseasonal variability. For example, a good (poor) monsoon is often associated with an early (late) start (Douglas and Englehart 1996; Higgins et al. 1999). The intaseasonal variability (IV) of the NAM is also of great importance, as New Mexico and the Southwestern states of the United States of America (USA) still depend on the summer rainfall and as well as human basic needs.

Douglas et al. (1993) showed that the onset of the Mexican monsoon, which is part of the NAM is characterized by heavy rainfall over southern Mexico, which quickly spreads northward along the western slopes of the Sierra Madre Occidental (hereafter SMO) and into Arizona and New Mexico by early July. Higgins et al. (1996) and Wallace (1975) have shown that there are increases in the amplitude of the diurnal precipitation cycles during the summer monsoon. Mo & Berbery (2004) shown the inverse relationship between the low-level jet (LLJ) over Great Plains and NAM, i.e., a strong jet with diurnal variations during summer between the mountains and the Great Plains at 925 hPa (e.g., Bonner 1968; Higgins et al. 1997). The NAM is accompanied by a decrease in midlatitude synoptic-scale transient activity over the adjacent United States of America (USA) and northern Mexico as the extratropical storm track weakens and migrates poleward close to the Canadian border by late June (Whittaker and Horn 1981; Parker et al. 1989).

In the case of NAM, the IV is associated with various factors such as a weak monsoon circulation, blocking high, intrusion of LLJ’s, and moisture subsidence in the monsoon basic flow. The NAMS fully develops during the mature phase of boreal summer, and can be related to the seasonal evolution of the precipitation regime. Surges of maritime tropical air northward over the Gulf of California are linked to active and break periods of the monsoon rains over the deserts of Arizona and California (Hales 1972). Among others, Bryson and Lowry (1955), Carleton (1986), and Cavazos et al. (2002) shows the northward shifts in the subtropical ridge axis incline to promote active monsoon convection (bursts) with southward shifts inducing drying (break) periods.

Mullen et al. (1998) suggest a dominant 12–18 day oscillation in the precipitation over South eastern Arizona, which was later ascertained by Cavazos (2002), who, through a detailed analysis, also identified a secondary peak at 40–60 days in the region. Mo (2000) identified a 22-day mode in the summer rainfall over New Mexico and Arizona. Higgins and Shi (2001) define the NAM rainfall as the rainfall over the 5°–35°N, 125°–80°W region. They claim that a major portion of the intraseasonal variability in this area is due to a 30–60 day signal connected to the Madden–Julian oscillation. Similarly, used wavelet analysis to study monsoon rainfall in Arizona and New Mexico. While a wavelet analysis on the monsoonal rainfall in 1990 over southeast Arizona, which was above average, isolated strong periodicities in the 10–20 and 20–40 day ranges, but no such dominant periodic variations were observed for the monsoonal rains in 1993 over the region (Hall-McKim et al., 2002)

1.4.2 Intraseasonal variability of South American summer monsoon

The South American monsoon system (SAM) is distinguished by the seasonal change in precipitation and moisture caused by alterations in the trade winds, and associated processes such as surface pressure, convection, thermodynamic instability, etc. The SAM summer seasonal cycle is essentially due to a variance in heating between South American land mass and the Atlantic Ocean, analogous to the Indian monsoon scenario. In the pre-monsoon season, the insolation amplifies the diabatic heating over the central-western tropical South America, and the ensuing thermal gradient between the land and ocean facilitate the setup of the monsoonal circulations, enhances the moisture advection across the equator by trade winds towards the continent centre. Just as the ISM, the diabatic processes trigger convective instabilities. A combination of large scale and small scale processes make sure that the monsoon persists throughout the wet season (Fu et al. 1999; Fu and Li 2004, Fisch et al. 2004).

The South Atlantic Convergence Zone (SACZ) is a critical feature of the SAM during the wet season. It is distinguished by a quasi-permanent cloud band, oriented north-west to south-east, and associated with low level wind and moisture convergence (Kodama 1992; Carvalho et al. 2002; 2004). It has an impact on densely populated areas throughout tropical and subtropical South America. Heavy rain begins in late August in north western South America and moves south eastward until it reaches the Brazilian highlands. The wet season in the Amazon core peaks during austral summer (*December–February).*

Other than interannual, decadal time scales, SAM exhibits persistent “active” and “break” periods/events in the intensity of rainfall, commonly known as Intraseasonal oscillations. Deep convection over the Amazon begins to weaken in early March, and the dry season lasts for the majority of the austral winter (Horel et al. 1989; Jones 1990). The SAM is a feature that has become increasingly popular to describe the strong summertime convective activity, intense precipitation, and large-scale atmospheric circulation features. The study of Zhou and Lau (1998) reviewed the early definitions of monsoon systems, originally formulated to account for reversals in the large-scale circulation that are driven by differential heating between landmasses and oceans. In addition, the analysis by Zhou and Lau (1998), which was based on monthly averaged data, indeed demonstrated that the summer season in South America contains the main ingredients to be characterized as a monsoon system. Zhou and Lau (1998) also suggest that the easterly winds prevail in the tropical Atlantic and eastern South America throughout the entire year, and seasonal reversal of surface winds is not immediately apparent. However, when the annual mean is removed from summer (January) and winter (July) composites of surface winds, the characteristic reversal in anomalous low-level circulation becomes evident (see Zhou and Lau 1998, their Fig. 9 and Grimm et al., 2021). In the context of monsoon systems, an important characteristic observed in the Asian–Australian region relates to the persistent “active” and inactive (or “break”) periods in the intensity of rainfall amounts. In this respect, tropical intraseasonal oscillations have been found to strongly modulate these “active” and “break” periods of the Asian–Australian monsoon system (Vernekar et al. 1993). Thus, the Madden–Julian oscillation (MJO; Madden and Julian 1994) is key in the occurrence of active and break phases of the Asian–Australian monsoon. Paegle et al., (2020) suggest that IV of rainfall over South America is examined using singular spectrum analysis. The dipole convection pattern with centres of action over the SACZ and the subtropical plains is modulated by modes of different timescales. Both oscillatory modes with periods of 36–40 days (mode 40) and 22–28 days (mode 22) influence convection over the SACZ with the faster mode (mode 22) leading the variability over the subtropical plains.

In the recent Large-Scale Biosphere Atmosphere (LBA) experiment of the intensive field campaign in January–March 1999, some limited observational evidence of variations in the structure of convection and different large-scale circulation regimes was gathered. This experiment took place in the Brazilian state of Rondônia over the southwest part of the Amazon as part of the Wet Season Atmospheric Mesoscale Campaign (WETAMC) and LBA Tropical Rainfall Measuring Mission (TRMM) validation experiment (Silva Dias et al. 2000). Periods of easterly and westerly 850-hPa winds in several Rondônia locations appear to be associated with different physical and structural characteristics of mesoscale convective systems (Cifelli et al. 2002; Petersen et al. 2001; Carvalho et al. 2002).

The MJO is a key tropical intraseasonal process, which controls and varies convection and winds over the tropical and sub-tropical regions of South America (Carvalho et al. 2004; Jones and Carvalho 2002; Liebmann et al. 2004a & b). Circulation Changes due to intraseasonal variations, notwithstanding whether they are due to the MJO or otherwise, influence the moisture transport in the monsoon region (Herdies et al. 2002; Carvalho et al. 2010b). Over central Brazil, active phases of the SAM are seen to co-occur with westerly wind anomalies, and break phases with easterly wind anomalies (Jones and Carvalho 2002). Such changes in circulation are noted in association with changes in the vertical distribution of moist static stability, which changes the 24-hour cycle of convection, and thereby, the characteristics of mesoscale convective systems (Petersen et al. 2002; Cifelli et al. 2002; Rickenbach et al. 2002; Carvalho et al. 2002b). The synoptic scale activity is associated with the active and break phases of the SAM regime, as well as variations in circulation and thermodynamic properties. Propagating frontal systems facilitate convection in the SACZ during active phase over central and eastern South America, (Garreaud 2000; Rickenbach 2002; Vera et al. 2006; Marengo et al. 2010; Cunningham and Cavalcanti 2006).

With all of these similarities in the three summer monsoons, I discuss the research objectives and scope in the following sub-chapter.

1.5 Objectives and Scope of the study

1.5.1 Objectives

From the review of literature carried out in the previous sections, it is clear that there are certain gaps in understanding the midlatitude interactions with the tropics during monsoons in India as well as Americas from the context of monsoonal intraseasonal variations. and in. Based on these gaps, I have framed four objectives. These are as follows:

1. To Delineate dynamic interactions between mid-latitudes and ISM from the context of the initiation and development of a break phase over the Indian region, through analysis of multiple cases.

2. Examine if the mid-latitude-tropical interactions are also seen for the North and South American summer monsoons as well.
3. Diagnosing the dynamical mechanisms behind the revival of ISM after a typical break phase through analysis of multiple cases
4. To ascertain dynamical mechanism for revival of active conditions of ISM after a break phase using WRF model.

1.5.2 Scope of the present study

The next section describes the datasets used in this study and the methodology adopted in this study is discussed. In chapters 3 & 4, a detailed analysis establishes a similar evolution of the breaks in the ISM, NAM, and SAM, and proposes a uniform mechanism based on the QRA and blocking that causes these breaks. In chapter 5, I propose a mechanism for the revival of summer monsoon rainfall after a break phase over the Indian region. In chapter 6, using the WRF regional model, we diagnose the mechanism proposed for the revival of active conditions after a break phase during ISM. In the final chapter 7, I discuss the conclusion of this research and the future scope of the study.

Chapter 2

Data & Methodology

Outline of the chapter

In this chapter, I discuss the source of the datasets used for the analysis. I also discuss the methodology followed to analyse the genesis of the Blocking high, the sustenance of the break phase in all three monsoonal regions and the mechanism for the revival of active conditions after a break phase during Indian summer monsoon. In addition, I briefly discuss about the Weather Research & Forecasting model and its importance.

2.1 Data used

2.1.1 Observational data

I use gridded daily rainfall data (Pai et al., 2014) of 0.25° X 0.25° resolution, derived from the observations of the India Meteorological Department (IMD) to observe the rainfall over the Indian during break situations for the 1979-2007 period. IMD (Cyclone eAtlas- IMD) data is also used to identify the dates of formation of Lows at the Head of the Bay of Bengal during the above period.

In addition, I have also used Daily gridded precipitation data derived from the Global Precipitation Climatology Centre (GPCC) Full Data Reanalysis V.7 version (Schamm et al., 2016) to see the spatial distribution of rainfall over North American and South American regions during summer monsoon. This product is developed using weather stations data on a regular grid with a spatial resolution of 1.0° latitude X 1.0° longitude. This dataset is based on data provided by NCEP-PSL.

2.1.2 Reanalysis data

I use reanalysed daily data sets of globally gridded Zonal wind (U), Meridional wind (V) and Geopotential (Φ) from the NCEP-DOE Reanalysis II (Kanamitsu et al., 2002) of 2.5° latitude x 2.5° longitude resolution for the period 1979-2007. NCEP-II reanalysis datasets are developed using available large data from Physical Sciences Laboratory, satellite data from 1979 to the present and uses an updated forecast model, updated data assimilation system, improved diagnostic outputs.

Table 2.1: A list of source/weblinks of datasets used in the present study.

Sr. No.	Dataset	Source	Weblink
1	Rainfall	IMD	http://www.imd.gov.in/
2	Rainfall	GPCC	https://www.esrl.noaa.gov/psd/data/gridded/
3	Zonal wind, Meridional wind, Sea level pressure, Geopotential height	NCEP-II	https://www.esrl.noaa.gov/
4	Lows	RMC, IMD	http://14.139.191.203/Login.aspx ; http://www.imdchennai.gov.in/

2.2 Dates of break periods, and study region

Rajeevan and co-authors (2010) identified active and break events of ISM, and are defined as periods during the peak monsoon months of July and August in which the normalized anomaly of the rainfall over the core monsoon region (CMR) (18° N-28° N & 65° E- 88° E), exceeds 1 or is less than −1.0, respectively, provided the criterion is satisfied for at least three consecutive days. They have shown the CMR is almost the same as that of the average all-India rainfall, and also shown that the interannual variation of the all-India summer monsoon rainfall is highly correlated with a correlation coefficient of 0.91 with that of the summer monsoon rainfall over the CMR and suggesting that it is a critical region for the interannual variation.

Following this identification method by Rajeevan et al. (2010), 41 break events have been identified through the 1979-2007 period. Various datasets over these breaks are used to generate the weather and climate statistics for the break phases during the summer monsoon months over India as tabulated below (Table 2.2).

Table 2.2: A list of break days based on Rajeevan et al., 2010 for the period 1979-2007 (J-July & A-August)

Sr. No.	**Break Monsoon days (< 3mm/day)**	**Year**
1	2–6J, 14–29A	1979
2	17–20J, 13–15A	1980
3	24–27A	1981
4	1–8J	1982
5	23–25A	1983
6	27–29J	1984
7	23–25A	1985

8	22–31A	1986
9	23–25J, 30J–4A, 8–13A, 16–18A	1987
10	14–17A	1988
11	18–20J, 30J–3A	1989
12	-	1990
13	-	1991
14	4–11J	1992
15	20–23J, 7–13A, 22–28A	1993
16	-	1994
17	3–7J, 11–16A	1995
18	10–12A	1996
19	11–15J, 9–14A	1997
20	20–26J, 16–21A	1998
21	1–5J, 12–16A, 22–25A	1999
22	1–9A	2000
23	31J–2A, 26–30A	2001

25	-	2003
26	10–13J, 19–21J, 26–31A	2004
27	7–14A, 24–31A	2005
28	-	2006
29	18–22J, 15–17A	2007

Mo (2000) has shown the 7-day running mean precipitation (mm/day) averaged over Arizona and New Mexico, i.e., 107.5°–112.5°W, 32°–36°N based on daily precipitation analysis by Higgins et al. (1996). Based on this study, we have chosen (from their Fig.6) three cases of North American break monsoon (Table 2).

Table 2.3: List of North American break monsoon days

Sr. No.	Break Monsoon days (< 3mm/day)	Year
1	17-25 July	1981
2	25 July -02 August	1995
3	16-24 July	2000

Gan et al. (2004) have shown the daily precipitation (mm/day) of west-central Brazil (primary region of South American monsoon), i.e., 10°–20° S, 60°–50° W, during month of January for the

1979-1996 period. Following Gan et al. (2004), six break spells are chosen (from their Fig. 19) using the daily rainfall (Table 3) with less than 3mm rainfall of the west-central Brazil region.

Table 2.4: List of South American break monsoon days

Sr. No.	Break Monsoon days (< 3mm/day)	Year
1	22-24 Jan	1980
2	05-10 Jan	1981
3	16-19 Jan	1988
4	21-26 Jan	1990
5	02-05 Jan	1993
6	25-27 Jan	1996

2.3 Methodology applied

Atmospheric waves transport moisture, energy and momentum from their source. Atmospheric waves extending large spatial extent are called planetary waves, and are a type of inertial waves naturally occurring in rotating fluids. These waves are associated with pressure systems and the Jet streams. Planetary waves play a major role in bringing the atmosphere to balance by transferring heat, moisture and momentum from equator towards the poles and vice-versa. For example, it is well known (e.g., Palmen 1951) that planetary waves in the subtropical westerly Jet streams play a primary role in the maintenance of weather in mid-latitudes, and therefore seasonal climate as well.

Hide (1953), based on his laboratory experiments noted periodic changes in the shape of propagating of planetary atmospheric waves. He named this kind of flow with regular periodic change in the shape as a vacillating flow. Lorenz (1963) classified these waves into four categories based on their progression and shape as a) a steady symmetric regime, b) a steady-wave regime, c) a vacillating wave regime and d) an irregular wave regime. For example, Hadley circulation can be seen as a steady symmetric regime; and a steady-wave regime & a vacillating wave regime together form a Rossby regime. A Rossby regime is a group of waves such as steady waves as well as steady waves with periodical change in the shape during progression. For example, SWJ is a typical example of the vacillating flow in a barotropic atmosphere. The westerly waves propagate from west to east and are associated with trough and ridges due to various factors such as, for example, earth's rotation, thermal gradient between equator and poles, etc.

Later, Charney and Devore (1979) found three equilibrium states for orographically-forced Rossby waves in a simple barotropic channel model, of which two were stable: a high index (resonant) type state of blocking with strong waves, and a low index (non-resonant) zonal state. Most of the subsequent observational studies identified quasi-stationary resonant waves in winter. In this context, the subtropical westerly Jetstream undergo meridional changes along with the zonal changes, such as low-index flow (LIF) and high-index flow (HIF) (Charney and DeVore 1979). During LIF, the jet is weakened and tends to develop elongated troughs and ridges. In the case of HIF, however, the jet is stronger than normal and narrower. As the jet weakens, the associated troughs and ridges have considerable effect on the nearby regions. During southwest monsoon of India, middle latitude westerlies exercise considerable influence on the monsoon weather over northern India, essentially during breaks (for relevant studies, see subsection 1.3.2) In this context, it will be interesting to examine the relevance of vacillating flows in facilitating break monsoon conditions.

<u>2.3.1 Dynamical analysis carried out</u>

<u>2.3.1.1 Eliassen–Palm fluxes</u>

From the view point of understanding the midlatitude interactions with the tropics at the upper level, it’s important to observe the changes in the planetary baroclinic waves. To study the maintenance of blocking high episodes, computation of the Eliassen–Palm (1961) (EP) fluxes will be very useful as they represent the effect of transient and stationary eddy fluxes on the zonal-mean circulation. The properties and application of EP fluxes have been discussed by several other authors as well (Andrews and McIntyre, 1976a; 1978a; Edmon et al., 1980; Tung, 1986) in detail in previous studies.

We summarize them here in the Quasi-Geostrophic ambit for simplicity. Briefly, the EP flux is a useful diagnostic of the propagation of waves (both magnitude and direction) in the meridional plane. In the case of small amplitude waves, it represents the flux of wave activity, and its divergence is zero for steady conservative waves. EP fluxes are also an important diagnostic for wave propagation, so we try to figure out the Rossby wave propagation and its importance in the formation of blocking high and its maintenance. Meridionally propagating eddies transport momentum towards their generation region (Held, 1975; 2000).

The EP flux in pressure coordinates on the sphere is given, following Andrews et al., (1983), by

$$F_{(\phi,P)} = r_o \cos(\phi)[-\overline{(u'v')},\ f\,\overline{(v'\phi')}/\theta_P] \qquad \text{--------------------} \ (2.1)$$

Where φ is the latitude, P is the pressure, θ is the potential temperature, r_o is the radius of the earth. Bars ($\overline{\ }$) and primes (`) denote zonal means and deviations respectively, and u, v are zonal and meridional velocities.

2.3.1.2 Energetics computations

Lorenz (1955) and Oort et al., (1962) defined the importance and consequences of the growth of perturbations through the expense of the mean available potential energy and the mean kinetic energy in a baroclinic and barotropic atmosphere respectively. They also have given mathematical expressions for the spatial and temporal variations of the energetics. In our case, during break phase of ISM, quantifying the energy exchange between the SWJ and TEJ (e.g., Rao 1971) is important.

The rate of conversion of mean kinetic energy to eddy kinetic energy is expressed as

$$C(\overline{K},K') = \int U \frac{\partial}{\partial y}\overline{v'u'}dm \text{--------------------------}(2.2)$$

Where m is the mass, $\overline{K}$ is the Mean kinetic energy (Joule/sec), K' is the Eddy kinetic energy, U is the zonal wind (m/s) and V is the meridional wind (m/s). The u' and v’ have been obtained as the daily anomalies from the zonal mean of the U averaged over 20° E and 120° E, and v', similarly from the zonal mean of V. Equation 2 means that if there is divergence (convergence) of eddy momentum transport in region of westerlies, $\overline{K}$gets converted into K'(K' gets converted into $\overline{K}$), that is, the disturbance is barotropically unstable (stable).

The eddy momentum flux $\overline{u'v'}$ controls the structure of the mean zonal surface wind and of meridional cells. This flux is significant for global circulation because it fulfils the global momentum balance equation. The equatorial region's zonal momentum is transported to the midlatitudes, where a flux convergence zone can be found. This is due to the global wind pattern, which consists of easterlies in the equatorial region and westerlies in the midlatitudes. Whereas the atmospheric waves are responsible for the transfer of zonal momentum.

Hence, the structure of the eddy momentum flux is fundamental to the mean state of Earth’s atmosphere.

Assuming the stream function ψ as a function of latitude and longitude,

Given,

$$\psi = R_{\psi}(y)\sin[Kx + \delta(y)]$$

leads to

$$\frac{\partial \psi}{\partial x} = v = KR\cos(Kx + \delta)$$

Therefore, $u = -\dfrac{\partial \psi}{\partial y} = -[\dfrac{\partial R}{\partial y}\sin(Kx + \delta) + \dfrac{\partial \delta}{\partial y}R\cos(Kx + \delta)]$

and $\overline{vu} = -KR\dfrac{\partial R}{\partial y}\sin(Kx + \delta)\cos(Kx + \delta) - \dfrac{\partial \delta}{\partial y}KR^2\cos^2(Kx + \delta)$

In the above, $\overline{()}$ represents the zonal mean. From the above equation, the mean zonal momentum can be expressed as

$$\overline{(vu)} = \frac{\overline{-v^2}}{K}\frac{\partial \delta}{\partial y} \qquad \text{--(2.3)}$$

1. If $\frac{\partial \delta}{\partial y}$ is negative, the wave tilts Northeast to Southwest (NE-SW).

2. if $\frac{\partial \delta}{\partial y}$ is positive, the wave tilts Northwest to South east (NW-SE), in the first case (1) the eddy momentum transport is northward and while in the second case (2) the transport of eddy momentum is towards southward.

<u>2.3.1.3 Condition for unstable waves</u>

My research problem is closely connected to barotropic stability theory, and previously a few authors have discussed different mathematical methods of which three important methods are detailed below.

- The eigen-value problem of linearized equation: Kuo (1951), by using linearized vorticity equation, defined the distinct profile conditions of zonal mean flow that would decide whether a disturbance would grow or dampen. Kuo also discussed the implications of such growing or weakening perturbations to the zonal mean flow.
- Initial value problem of non-linear equation: Platzman (1952), Kuo (1953) and Syono & Aihara (1957) treat this problem as an initial value problem. This is done by prescribing certain initial conditions for the distributions of zonal mean flow and perturbations. Then, the higher order time derivatives of their kinetic energies are computed.

- A method with statistical assumption: While Lorenz (1953) also acknowledges that this is an initial value problem, he confines to prescribing only a few initial statistics of the flow, rather than the whole profile of the flow pattern.

In steps of Kuo (1953), Syono & Aihara (1957) and Rao (1968; unpublished thesis) found an analytical solution of the growing waves in a barotropic atmosphere. Rao 1971 introduced the concept of neutral wavelength' 'L', which isolates the stable shorter waves and unstable longer waves in to two distinguished groups. It is to be noted that the final output of the solution is not associated with the contribution of earth's rotation. The detailed derivation is found in appendix I. From this theory, it is proposed that the expression for the time change of perturbation kinetic energy at the initial time is given by Rao (1968) as

$$\left(\frac{\partial^2 K_r}{\partial t^2}\right)_o \quad = \quad 0 \qquad \text{when } L=2D/\sqrt{3} \qquad (2.4)$$

$$> \quad 0 \qquad \text{when } L>2D/\sqrt{3}$$

$$< \quad 0 \qquad \text{when } L<2D/\sqrt{3}$$

K_r is perturbation kinetic energy and the left hand side of the above equation is a measure of barotropic instability. Indeed, the associated waves longer than L (wavelength) become unstable and below L are stable (Starr & White, 1954; Aihara, 1959). Whereas D/2 is the zonal width between subtropical westerly jet and tropical easterly jet.

2.3.1.4 Condition for barotropic instability

In our analysis, we use the criterion by Kuo (1949), which states that, for barotropic instability to happen at a location, the meridional gradient of the absolute vorticity has to be either maximum or minimum.

$$\frac{d}{dy}\left(\frac{-d\overline{U}}{dy}+f\right)=0 \qquad \frac{d\zeta}{dy}=0 \tag{2.5}$$

Where $\overline{U}$ is the mean zonal wind, f is the Coriolis force and ζ is the absolute vorticity. We use the criterion shown in equation (3) to explain the mechanism behind the formation of the after-break synoptic disturbances over the Indian region and the Bay of Bengal, which reactivate the Indian summer monsoon.

2.3.2 Statistical methods

2.3.2.1 One sample Student's t test for composite analysis

In our composite analysis, the statistical significance of the composited signal is assessed by computation of the 't' statistic from a 2-tailed Student's t-test. This is a standard test for composite analysis. The 't' is calculated as

$$t=\frac{X-\mu}{\sigma/\sqrt{n}} \tag{2.6}$$

Where X is the sample mean, μ is the population mean, σ is the standard deviation of the population mean and n is the number of cases.

2.3.2.2 Student’s t test for two unequal variances

Two-sample T-Test with unequal variance can be applied as the samples are normally distributed, and the standard deviation of both populations are unknown and assumed to be unequal with sufficiently large sample size (>30)

$$t_{df} = \frac{(\overline{x_1} - \overline{x_2}) - (\mu_1 - \mu_2)}{\sqrt{(\frac{{s_1}^2}{n_1} + \frac{{s_2}^2}{n_2})}} \tag{2.7}$$

$$df = \frac{(\frac{{s_1}^2}{n_1} + \frac{{s_2}^2}{n_2})^2}{\frac{(\frac{{s_1}^2}{n_1})^2}{n_1 - 1} + \frac{(\frac{{s_2}^2}{n_2})^2}{n_2 - 1}}$$

x_1= values of the first sample; $\overline{x}$ = mean of the values of the first sample; x_2=values of the second sample; $\overline{y}$=mean of the values of the second sample, and df=degrees of freedom

2.3.2.3 Pearson’s correlation coefficient

Pearson’s correlation is also referred as Pearson's r. It is a measure of linear correlation between two sets of data, such that the result always has a value between −1 and 1.

$$r = \frac{\sum(x_i - \overline{x})(y_i - \overline{y})}{\sqrt{\sum(x_i - \overline{x})^2 \sum(y_i - \overline{y})^2}} \tag{2.8}$$

r = correlation coefficient; x_i= values of the x-variable in a sample; $\overline{x}$ = mean of the values of the x-variable; y_i=values of the y-variable in a sample, and $\overline{y}$=mean of the values of the y-variable

2.4 A brief introduction to the Weather Research and Forecasting model

I prefer carry out few sensitivity experiments using a regional climate model in order to validate the theory proposed in the present study. Here in our case, we use the Weather Research and Forecasting (WRF) Model for its wide range of applicability in prediction & validation. WRF model is mesoscale numerical weather prediction system designed for both atmospheric research and operational forecasting applications. The model is useful for a variety of meteorological applications at scales ranging from tens of metres to thousands of kilometres. It features two dynamical cores, a data assimilation system, and the other one is a software architecture supporting parallel computation and system extensibility.

WRF model is a collaborative output from the National Centre for Atmospheric Research (NCAR), National Centres for Environmental Prediction (NCEP) and the Earth System Research Laboratory, the U.S. Air Force, the Naval Research Laboratory, the University of Oklahoma, and the Federal Aviation Administration (FAA). WRF offers operational forecasting a flexible and computationally-efficient platform, while reflecting recent advances in physics, numeric, and data assimilation contributed by developers from the expansive research community.

Importantly, all the sensitivity experiments conducted using WRF model and their discussion is carried out in the chapter 6.

Chapter 3

Breaks in Indian Summer Monsoon

Outline of the chapter

In this chapter, I carried out a few dynamical and statistical analyses, to understand the interactions between the upper level midlatitude circulation features and the tropical summer monsoon circulation of Indian region. Based on the results from the analyses, I propose a mechanism for the genesis of the Blocking high and how it facilitates a monsoon break phase over the core monsoonal region of the Indian region.

3.1 Introduction

The ISM experiences intraseasonal variability associated with higher and lower rainfall patterns. The lower spells of rainfall are called breaks in monsoons. These are characterized by relatively sparse rainfall over the core monsoon region (CMR) of India, which is bounded by 18° N to 28° N, and 65° E to 88° E. The region is referred to as the core monsoon region because the summer monsoon rainfall in this region is highly correlated with the area-averaged summer monsoon rainfall over the whole of India (correlation coefficient=0.91) (Rajeevan et al., 2010). The rainfall variations in CMR are very important for several aspects such as agricultural production and energy generation. Intraseasonal variations of rainfall are manifested as (a) monsoon breaks of low rainfall, (b) normal (c) or heavy rainfall in the CMR region, which are referred to as active periods. Hence the years with low rainfall in the CMR region associated with prolonged breaks are of vital importance. In this context, we propose to study the dynamics leading to break situations.

From a dynamical perspective, Raman and Rao (1981) suggested that the prolonged breaks causing severe summer monsoon droughts over the Indian sub-continent are due to upper tropospheric blocking high over East India (90° E to 120° E) associated with baroclinic waves. Thus, this blocking high is perceived to be the initiator of the monsoon break. However, Raman and Rao (1981)'s conclusions are based on studying a small number of cases. In this context, I evaluate the potential importance of large-scale circulation that leads to the blocking high and subsequent generation of break monsoon conditions. In this analysis, we find the fundamental characteristics that are suggested to lead to the blocking high, namely, the planetary wave resonance as envisaged by Charney and DeVore (1979).

In this context, the following subchapters 3.2 & 3.3 discusses the results of the conditions that lead to break phase and conditions for the genesis of blocking high using reanalysis data in the Indian monsoonal region. The key findings are summarized in the subchapter 3.4 by proposing a robust method to identify a break phase in the monsoon regions with the interactions of midlatitudes.

3.2 Breaks in the Indian Monsoon Season: Rainfall characteristics and associated synoptic situation

Fig. 3.1 illustrates 200 hPa composite geopotential height (Z_{200}) zonal anomalies for a) prebreak, b) break, and c) after-break periods for the 41 cases of Indian break monsoon (Table 2.1). The hatched areas in Fig. 3.1 indicate composite Z_{200} anomaly significant the 95% confidence using a two tailed student's t-test. The composites of the zonal anomaly of Z_{200}, shown in various panels of Fig. 3.1, indicate that the high pressure region is split into two vortices, as already noted earlier (Siu & Bowman, 2020). Siu & Bowman (2020), who refer to this *quasi-stationary high-pressure zone during the summer season* as the 'Asian monsoon anticyclone', claim that the split structure is due to a combination of various factors such as diabatic heating, its interactions with Rossby waves propagating along with the subtropical jet, and internal dynamics within the anticyclone. Notably, during the break phase, we see this high over India extending to lower levels at the 1000 hPa (figure not shown).

Differences in zonal anomaly of Z_{200} are not immediately perceivable among figures 3.1a, 3.1b and 3.1c. Therefore, to focus on the changes in the upper tropospheric high during the break monsoon situation, we present in Fig. 3.2a the difference obtained by subtracting the composite daily zonal anomalies of Z_{200} for the prebreaks from that over the breaks. We have also subtracted the composite zonal anomalies of Z_{200} during the after-breaks from that over the breaks (Fig. 3.2b). Similar differences have also been generated for the SLP (figures 3.2c & 3.2d). In figures 3.2a and

3.2b, we see negative values of the Z_{200} over northern and central India, statistically significant at 95% confidence levels from a 2-tailed Student's t-test.

Fig. 3.2a suggests, in a relative sense, a substantially weak high and so an increased convergence over the north Indian region during breaks compared to the prebreaks and also relative to the after-breaks (Fig. 3.2b). The positive values of the SLP in figures 3.2c & 3.2d suggest a relative filling up of the surface low, i.e., increase in the SLP. In other words, the various panels in Fig. 3.2 suggest a relative sinking of air from the upper level to lower level over north India during breaks compared to the prebreak and post break conditions. This is because of the differences that are indicative of a relative upper level 200 hPa convergence and a relative low level divergence during the breaks. This is also clear from a similar composite difference of the daily 1000 hPa geopotential height zonal anomaly between monsoon breaks and prebreaks (Fig. 3.3a) and that between monsoon breaks and after-breaks (Fig. 3.3b).

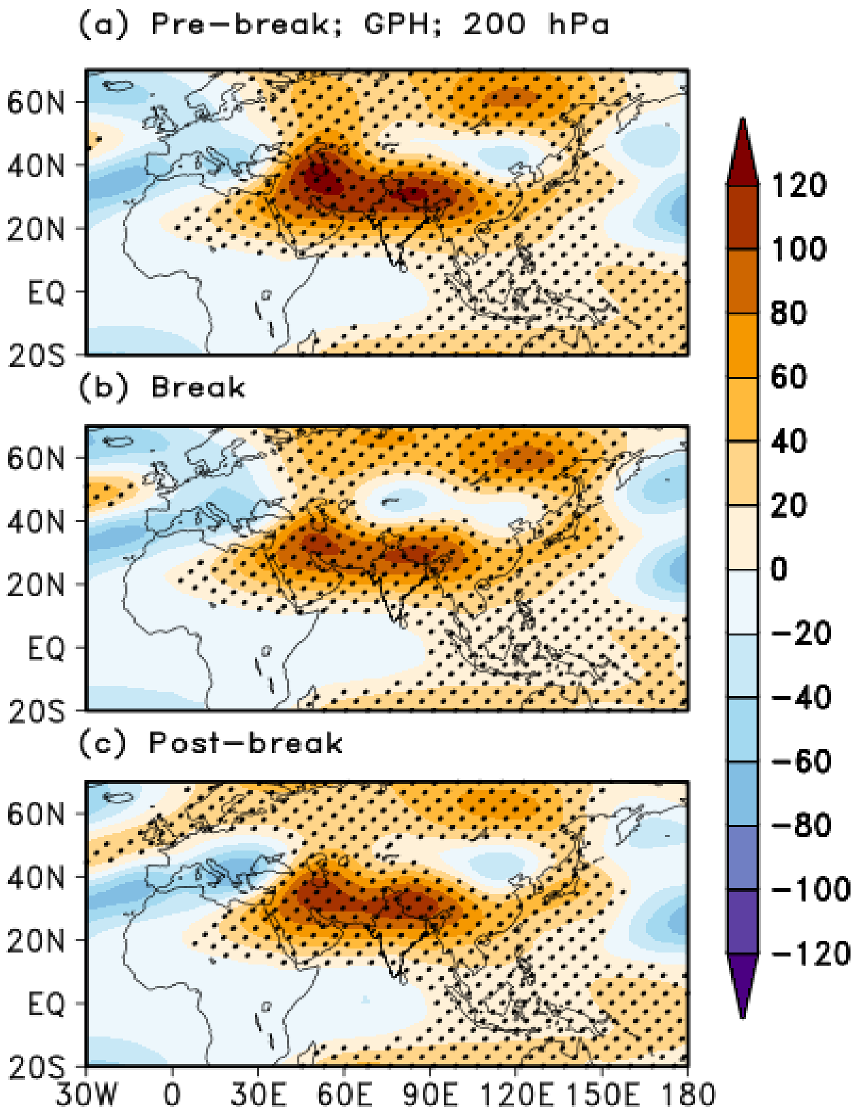

Figure 3.1: Composite daily zonal anomalies of Geopotential height (m) over the monsoon season of 1979-2007 in the Indian region during **(a)** prebreak periods, **(b)** break periods, and **(c)** after-break periods. The hatching in the Figures 1 a-c indicates the regions where the composite Geopotential height is significantly different from zero at 95% confidence level. Statistical significance has been obtained using a two-tailed one sample Student's t test. Note that

significance test has not been applied to negative values. The shaded region vary between -120 m to 120 m, with an interval of 20 m.

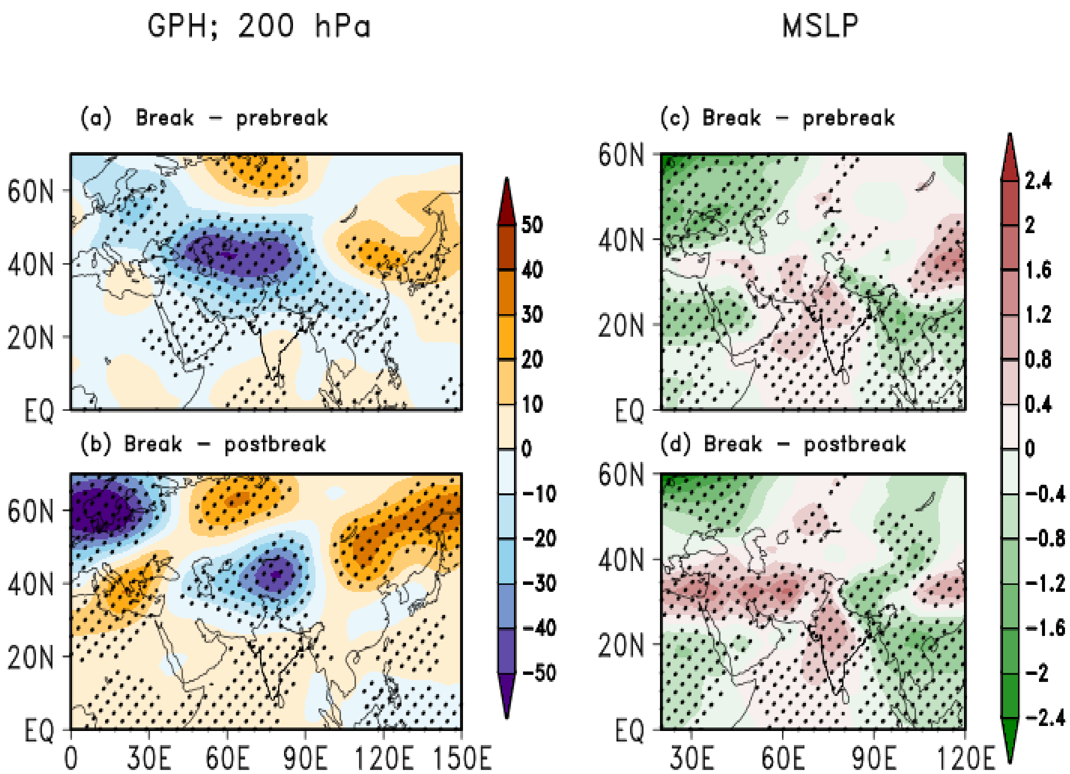

Figure 3.2: Difference between the composite daily zonal anomalies of Geopotential height (m) during the 1979-2007 period over the Indian region between **(a)** break and prebreak periods **(b)** break periods and after-break periods. Difference in composites of zonal anomalies of daily mean sea level pressure (hPa) over the Indian region during the 1979-2007 period between **(c)** during-break and prebreak periods, and **(d)** during-break and after-break periods. The shaded region in the panels (a) & (b) vary between -50 m to 50 m, with an interval of 10 m and those in panels (c) & (d) vary between -2.4 hPa to 2.4 hPa, with an interval of 0.4 hPa. The hatched regions indicate locations of significant differences, at 95% confidence level, in daily zonal anomalies of Geopotential height in panels (a) & (b), and that of daily mean sea level pressure in panels (c) &

(d). Statistical significance has been obtained using a two-tailed two sample Student's t-test with unequal variances.

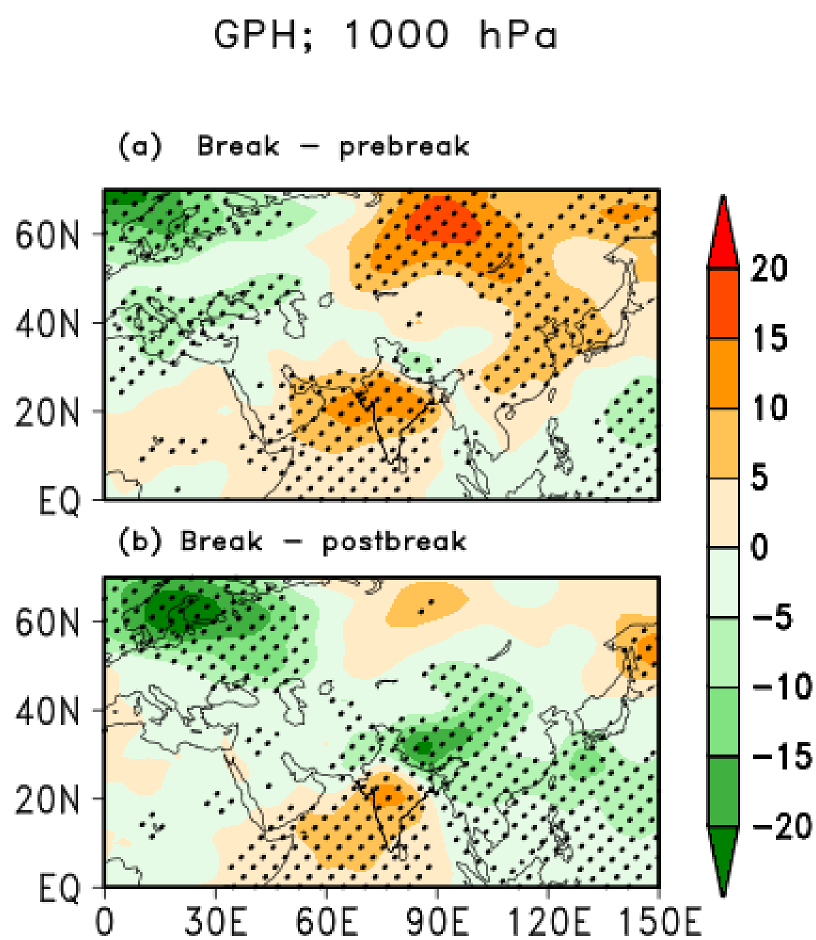

Figure 3.3: Difference between the composite daily zonal anomalies of Geopotential height at 1000 hPa (m) during the 1979-2007 period over the Indian region between **(a)** break and prebreak periods **(b)** break periods and after-break periods. The shaded region in panels (a) & (b) vary between -20 hPa to 20 hPa, with an interval of 5 hPa. The hatched regions indicate locations of significant differences, at 95% confidence level.

In addition to Ramaswamy (1962), Krishnan et al. (2009) also note the intensification of the anomalous westerly troughs was accompanied by retardation in their eastward movement from west central Asia toward the Tibetan plateau for 20 years mean boreal summer season. Krishnan et al. (2009) also suggest that, using upper-level circulation charts during weak monsoon periods indicate zonally asymmetric variations of the Tibetan high under the influence of southward penetrating midlatitude troughs (lows) over west central Asia and the formation of stagnant blocking highs between 90° and 115° E over East Asia (Raman and Rao 1981). According to Raman and Rao (1981) at 200 hPa, a dominant ridge on the North, with a cut off high or blocking high on the southern side of the westerly jet, tends to associate with a break phase over the Indian region. Raman and Rao (1981) show the various stages of blocking high over Southwest Asian region (their Fig. 1), of which the first stage is with an amplified ridge at 200 hPa. This amplification is clearly akin to the increase of amplitude of wave number 7, (in their Fig. 1 we note an approximate distance between two ridges or wave length of about 50 degrees) and this amplification is a sign of resonating affect between the planetary Rossby waves of the westerly jet. Further, we also see this amplification associated with the ridge in the individual case study of ISM of *daily geopotential heights at 200 hPa* & 1000 hPa and rainfall distribution, and are shown in supplementary information (figures 3.4 a-c, 3.5 a-c & 3.6 a-c). The daily area-averaged normalised rainfall anomaly over the core monsoon region during this event was lower than ~3 for at least three of the 10 days over which the long break event occurred. Qualitatively, the other features, such as the anomalous shift of the monsoon trough northward have also been observed during this case (figure not shown).

This dominant ridge remains for about a few days up to two weeks. Also, these authors found a closed “warm” high extending the entire column with an increase of surface pressure by about 20 hPa. The warmth of the high indicates sinking motion. Raman and Rao (1981) also noted a trough at upper levels. From this context, it is a typical case with a few days of exacerbated break conditions. This typical case study provides a glimpse into the blocking high dynamics, which are critical in understanding the characteristics of sub-seasonal variability.

Fig. 3.7 depicts the vertical velocity (ω; in Pa/s) of the Indian summer monsoon during the prebreak, break, and after-break periods, as well as the difference in it between the break and prebreak periods and that between the break and after-break periods. A raising motion can be seen in the composites of prebreak, break, and after-break in figures 3.7a, 3.7b, and 3.7c, but the magnitudes differ as shown in figures 3.7d & 3.7e. In figures 3.7d & 3.7e, we see a sinking motion (positive ω values extending vertically) at 20° N. The observed positive ω values confirm the sinking motion during breaks, as previously discussed in Fig. 3.2. The changes in the ω (figures 3.7 a-e) are significant at 95% confidence level from a two tailed students t-test.

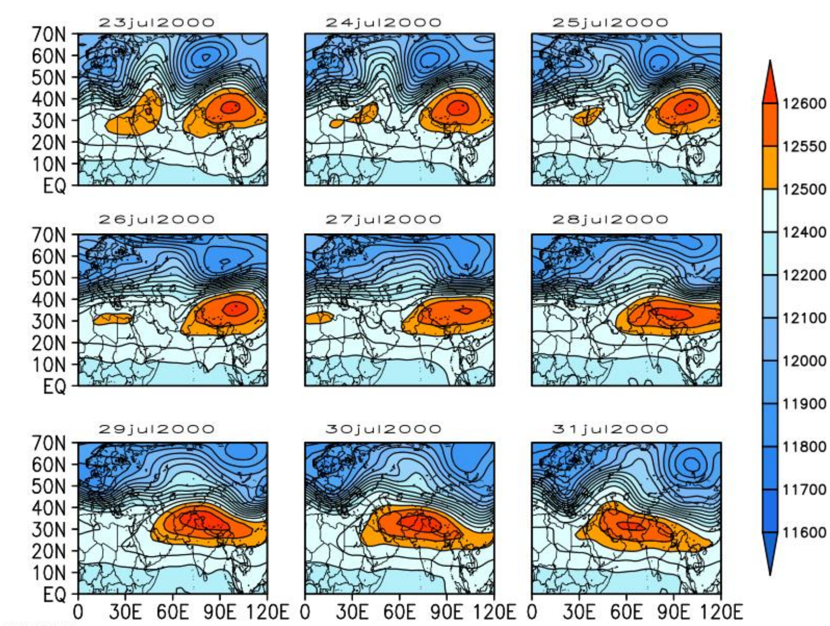

Figure 3.4a: Daily geopotential height distribution at 200 hPa level for a prebreak period (23-31 July 2000) over the Indian region.

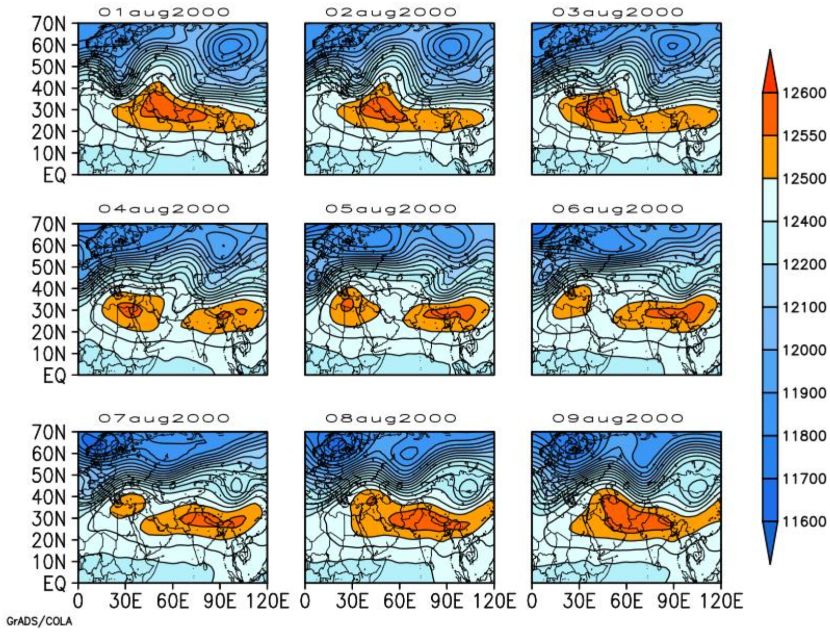

Figure 3.4b: Daily geopotential height distribution at 200 hPa level for a break period (01-09 August 2000) over the Indian region.

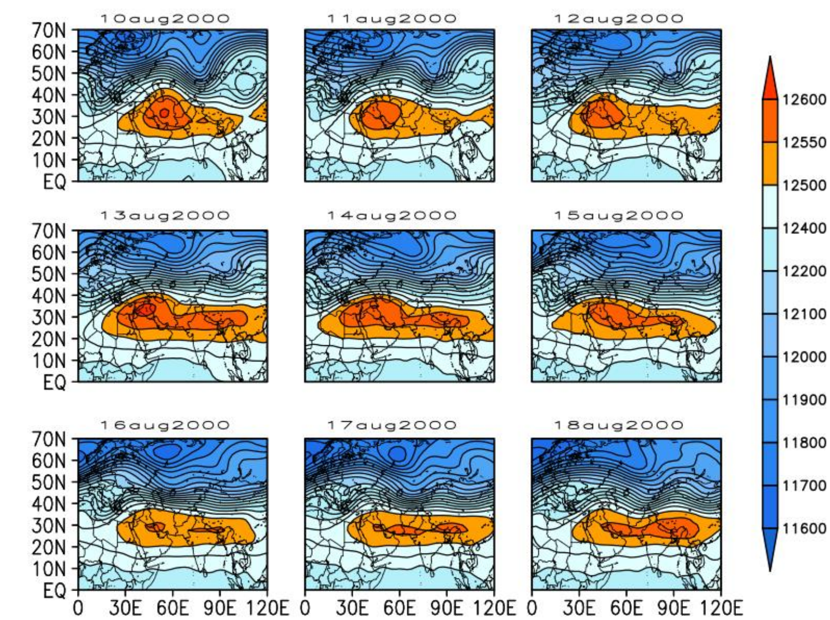

Figure 3.4c: Daily geopotential height distribution at 200 hPa level for a after-break period after (10-18 August 2000) over the Indian region.

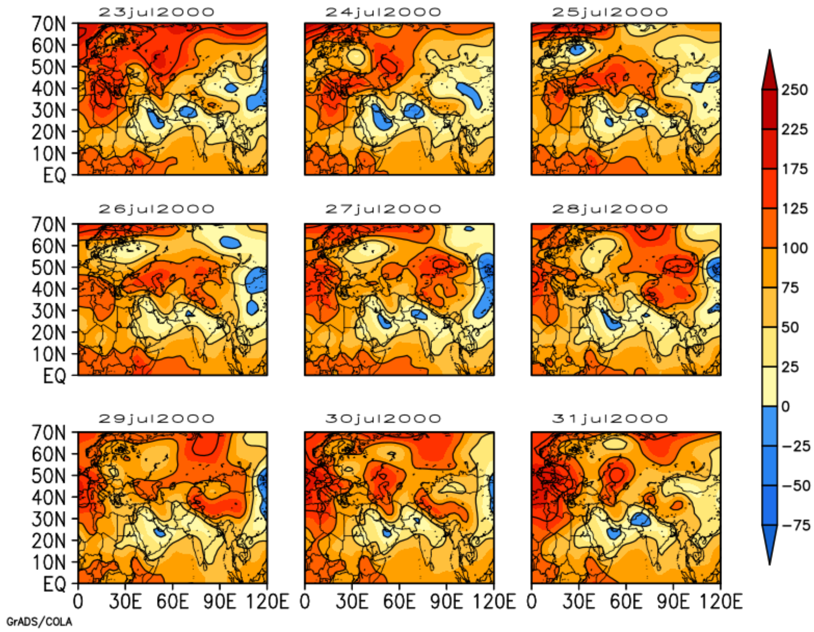

Figure 3.5a: Daily geopotential height distribution at 1000 hPa level for a prebreak period (23-31 July 2000) over the Indian region.

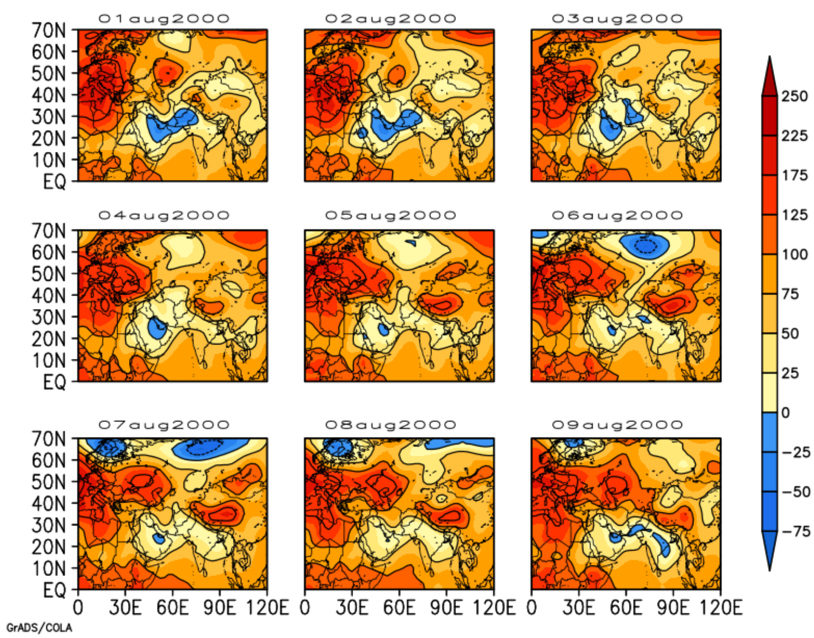

Figure 3.5b: Daily geopotential height distribution at 1000 hPa level for a during-break period (01-09 August 2000) over the Indian region.

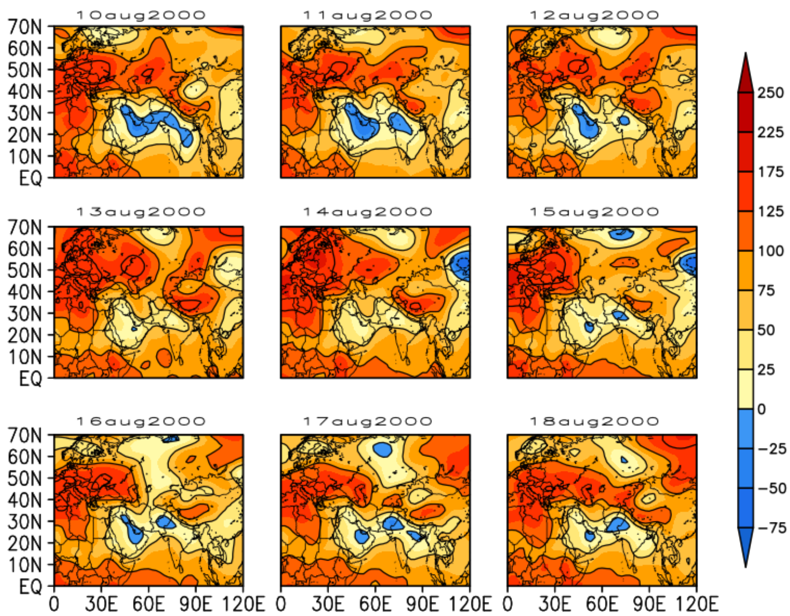

Figure 3.5c: Daily geopotential height distribution at 1000 hPa level for a after-break period (10-18 August 2000) over the Indian region.

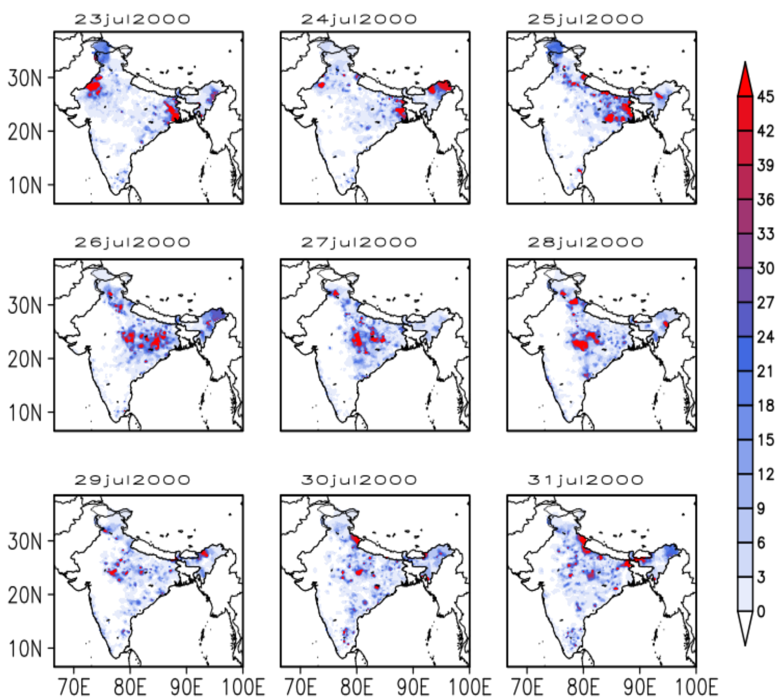

Figure 3.6a: Daily spatial rainfall distribution for a prebreak period (23-31 July 2000) over the Indian region.

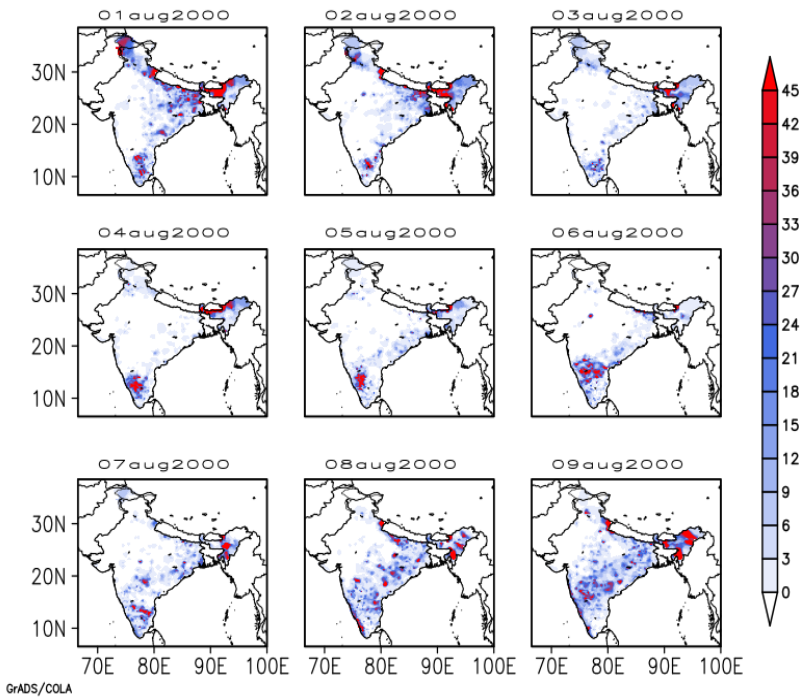

Figure 3.6b: Daily spatial rainfall distribution during (01-09 August 2000) a break period over the Indian region.

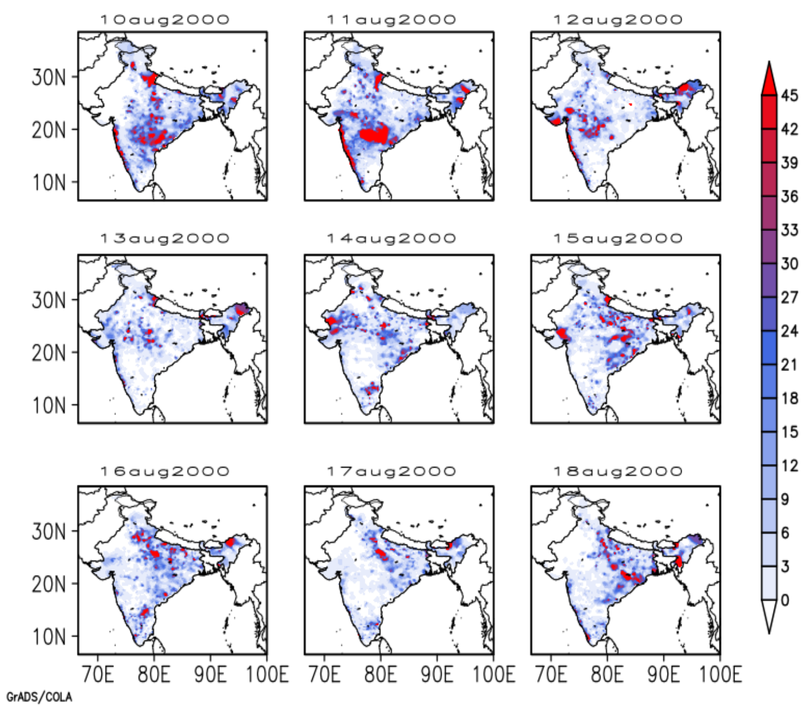

Figure 3.6c: Daily spatial rainfall distribution for the after-break period (10-18 August 2000) over the Indian region.

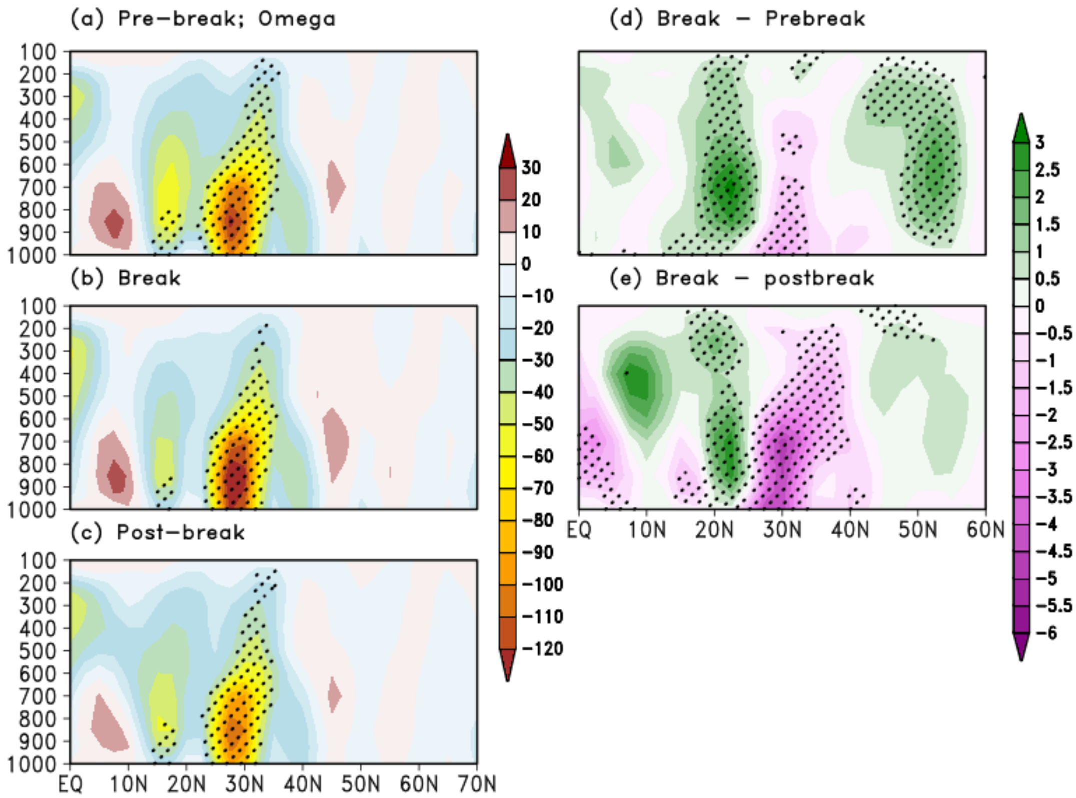

Figure 3.7: Composite vertical wind zonal anomalies (x10^{-3}) (omega) (Pa/s) over Indian region and longitudinally averaged along 60°E to100° E during the summer monsoon for the 1979-2007 period, **(a)** prebreak periods **(b)** during-break periods, and **(c)** after-break periods, **(d)** difference between the composite break and composite prebreak periods, and **(e)** difference between the composite break and composite after-break periods. The shaded region in panels (a) (b) & (c) vary between -120 hPa to 30 hPa, with an interval of 10 hPa and those in panels (d) & (e) vary between -6 hPa to 3 hPa, with an interval of 0.5 hPa. The hatched regions indicate composite omega zonal anomalies are significant at 95% confidence from a two-tailed Student’s t-test.

Nonetheless, enhanced subsidence should be associated with reduced rainfall., figures 3.8a, 3.8b & 3.8c show the corresponding composite daily rainfall over the Indian region for the prebreak, break, and after-break periods, respectively. The rainfall changes, shown in figures 3.8a, 3.8b & 3.8c are significant at 95% confidence level from a two tailed students t-test. Figures 3.8d & 3.8e show the difference in rainfall between the composites of break & prebreak, and that between the break & after-break periods, respectively. Figures 3.8d & 3.8e demonstrates that the Indian region undergoes a decline in rainfall during the breaks as compared to the prebreak, and after-break composite periods. The low or no rainfall in the CMR of India during the breaks is evident due to the relative sinking motion (Figures 3.2 & 3.7) and the changes in the panels of figures 3.8d & 3.8e are significant at 95% confidence level using two tailed students t-test.

From the above observations, we notice two significant findings after conducting composite analyses (Figures 3.1, 3.2, 3.7 & 3.8) and individual study of each case (figures not shown)

- The sinking due to upper level (200 hPa) convergence and SLP divergence at lower level.
- A blocking high forming due to the increase of amplitude of the wave, provoking “sinking” and this condition is discussed further below.

Also noted is that, in all the “break” monsoon cases, there is an increase of rainfall near “foot hills of the Himalayan region”. We note that at the lower levels (figures 3.2c & 3.2d), the monsoon trough shifts to the foot hills of the Himalayan region during the breaks (e.g., Raghavan, 1973). Apart from the raising motion in the monsoon trough in this location, we also note that there are “northerlies (or north westerlies)” near the foothills. These strong north westerlies at Himalayan foothills are along the monsoon trough, cannot cause high rainfall as explained below (fig. 2). However, we see a good rainfall across the foot hills of the Himalayan region, and a low or no rainfall situation at the core monsoon region or most of the Indian region with the sinking conditions during the break phase. The rising motion at the foothills as explained below

$$w = u\frac{\partial h}{\partial x} + v\frac{\partial h}{\partial y},$$

Here, h is the height of the mountain in the northwest (x) direction, and u is the daily zonal wind. Here in the first term, u is positive because of the westerlies *during the break*. *T*he $\frac{\partial h}{\partial x}$ is positive because the trough is on the west side of the foot hills, and the height increases towards east. The other term is almost zero because along the foot hills for the Northerlies $\frac{\partial h}{\partial y}$ is very small or zero. Note that figures 3.2c & 3.2d show a strong gradient of SLP zonal anomalies at North of 20° N and East of 90° E, indicating approximately, a geostrophic westerly zonal wind $u_g = -\frac{1}{f}\frac{\partial P}{\partial y}$, i.e., we note a high pressure zone on the left of the Himalayan and central Indian region, low pressure zone on Tibetan region i.e., right of the Himalayan region (figures 3.2c & 3.2d), and the Himalayan region height gradient is $\frac{\partial h}{\partial x}$ is strong along the monsoon trough region, indicating a pressure decrease from south to north. Thus, a strong raising motion and high rainfall occurs. Also, as we suggested, in "all" cases of break monsoon a Blocking high forms. By considering anomalies of all the cases, we see in composite Fig. 3.2, a relative "upper level low". This low, together with the implied convergence at 200 hPa and a high with divergence at the surface as indicated by the SLP (figures 3.2c & 3.2d) provokes the sinking ahead of the trough, as inferred above.

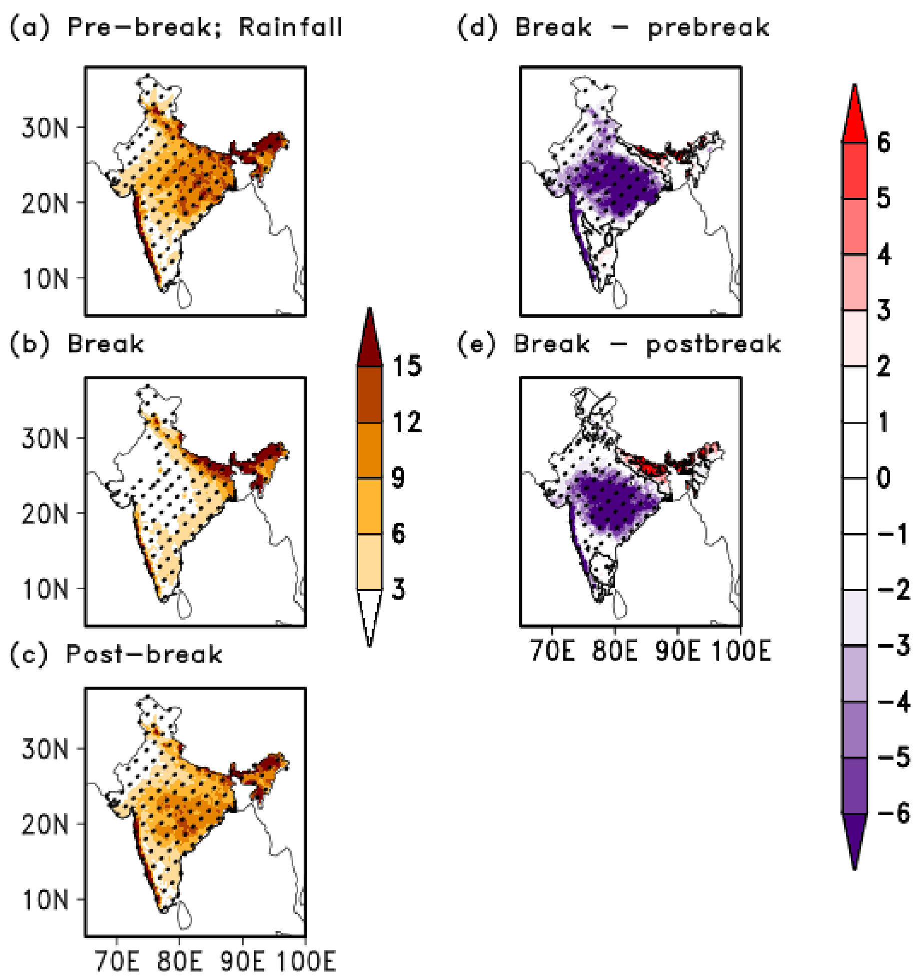

Figure 3.8: Composite Rainfall (mm) over Indian region during the Indian summer monsoon for the 1979-2007 period, **(a)** prebreak periods **(b)** during-break periods, and **(c)** after-break periods, **(d)** difference between the composite break and composite prebreak periods, and **(e)** difference between the composite break and composite after-break periods. The shaded region in the panels (a) (b) & (c) vary between 3 mm/day to 15 mm/day, with an interval of 3 mm/day. The shaded region in panels (d) &(e) vary between 2 to 6 mm/day & -2 to -6 mm/day, with an interval of 1 mm/day. The hatched regions indicate composite rainfall are significant at 95% confidence from a two-tailed Student’s t-test.

3.3 Genesis and Maintenance of the Blocking High Episode

From the context of Figures 3.1 3.2, 3.6 & 3.7, the occurrence of monsoon breaks boils down to the question of how the blocking forms, develops, and subsides with time. Some theoretical aspects on blocking high formation, maintenance, and dissipation were proposed in the previous studies. The pioneering theory on the formation of blocking high by Charney and DeVore (1979), for example, envisages interactions of free Rossby waves of different wavelengths with those of stationary waves. They suggested that the resonance of stationary free (Rossby, 1939) planetary waves interacting with stationary Rossby waves forced by topography and/or differential heating generates large-amplitude planetary waves which are essential in the formation of a block.

In continuance, Fig. 3.9a depicts the global average of zonal wind composite at 200 hPa (hereafter as U_{200}), for prebreak, during-break and after-break periods. We see a peak of ~20 m/s, at 40^0N in all three composites. This indicates a strong and narrow jet peak in the northern hemisphere, which is prevalent around mid-latitudes during the northern summer. Such strong and narrow jets form stable, zonally oriented waveguides, as per Kornhuber et al., 2017. Kornhuber et al., (2017) show that the preferred phase position of the zonal wind peak at a single location is conducive for QRA of waves with wavenumbers 7 and 8 (Kornhuber et al., 2017). This suggests that we can expect an amplification of such waves due to QRA. Sometimes, we also find bimodal peaks in zonal winds in the Northern hemisphere, from June to August (also includes Indian summer monsoon). As an example, we present, in Fig. 3.9b, the zonal wind at 200 hPa as a function of latitude during various stages of a strong break event, i.e., prebreak (23-31July 2000), during-break (01-09 Aug 2000), and after-break (10-17 Aug 2000) period. During the prebreak phase, we note a maximum U_{200} of 23 m/s at 45° N and a secondary peak of about 7 m/s at 75^0 N. During the break phase, the peak U_{200} with a magnitude of 18 m/s is located at 50° N, and with a secondary peak at 80° N of value 11 m/s. These profiles are very similar to those given by Mann et al., (2018) (their Fig. 1b). The secondary peak at 80^0 N is highly favourable for the resonant amplification of the waves with wavenumbers 5-8 range. The profile during the break with a double peak structure of the zonal wind is also an efficient waveguide as noted by Manola et al., (2013). If the waveguide is circumpolar, then the wave energy is efficiently trapped and waves constructively interfere with the forced waves leading to resonance.

To verify the possible application of Charney and DeVore (1979) theory, we show in Fig. 3.10, a composite of the amplitude spectra of the first ten harmonics of 200 hPa meridional wind during the prebreak conditions, at 45° N. We note that wave number 7 is prominent for the individual case, with an amplitude of ~14 m/s (Fig. 3.10). Indeed, the corresponding composite for the prebreak shows that the wavenumbers 5, 6 & 7 are dominant, with an amplitude of ~7 m/s (Fig. 3.10). The increase in the amplitude of the wavenumber 7 as compared to its amplitude during prebreak is twice its prebreak value. Kornhuber et al (2017) suggest that most QRA events are found for wave number 7, which also is associated with the longest duration. This shows the important role of QRA for the formation of the Blocking high over India during the 41 break monsoon cases in agreement with several authors (Manola et al 2013; Kornhuber et al., 2017l Mann et al., 2018).

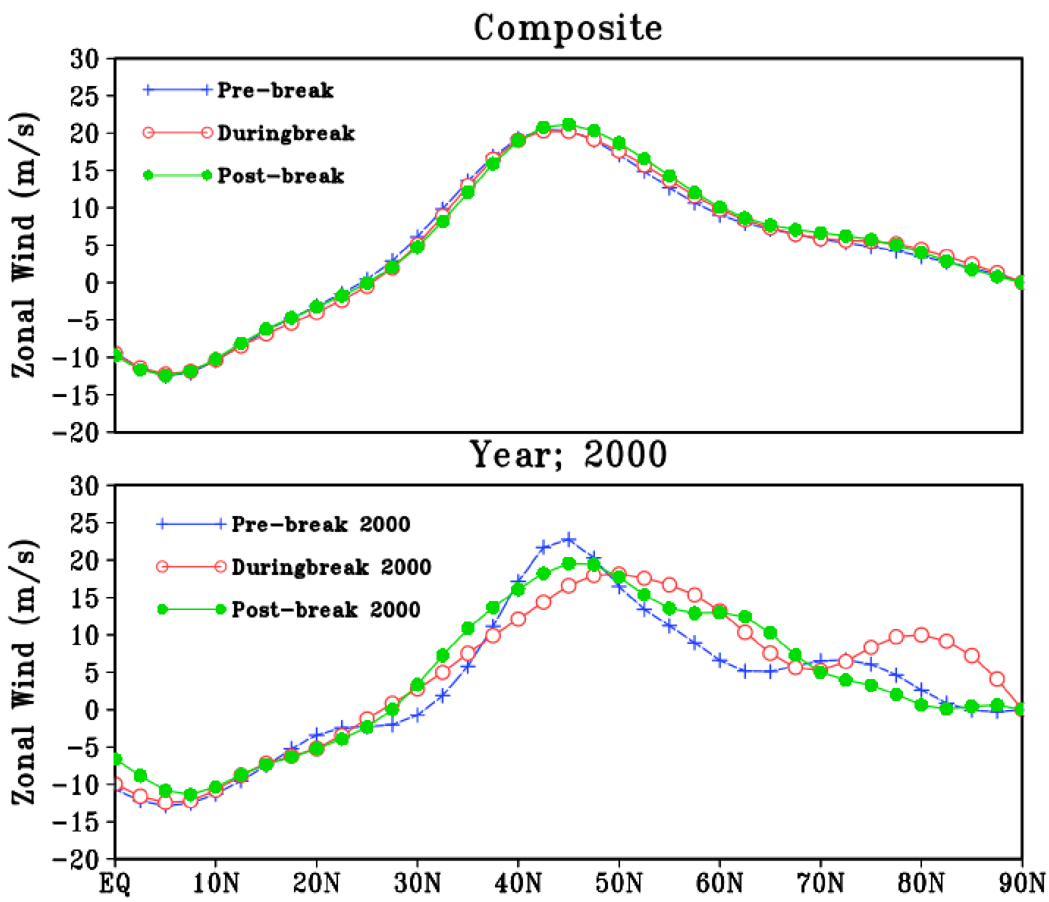

Fig. 3.9: Globally zonal averaged U wind (m/s); **(a) (upper panel):** for the composite prebreak, composite during-break & composite after-break periods of ISM (Table 1), cases available during the 1979-2007 period; **(b) (lower panel):** Similarly, for the case study, prebreak 23-31July 2000, during-break: 01-09 Aug 2000 and after-break 10-17 Aug 2000 of ISM.

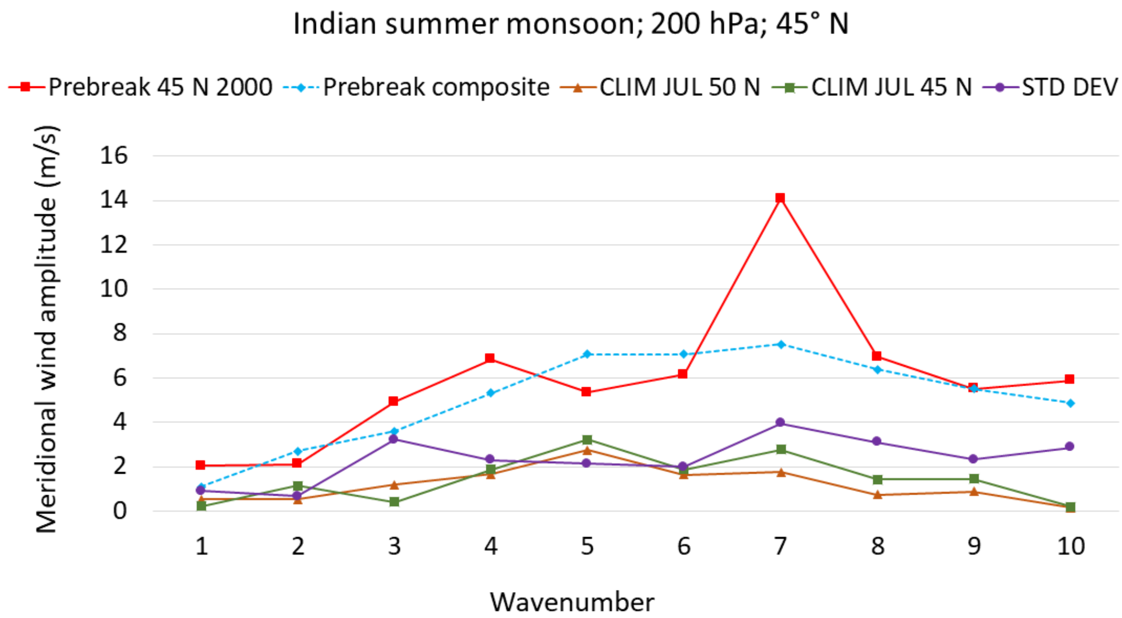

Fig. 3.10: Wavenumber spectrum using meridional wind (m/s) at 200 hPa level for; the case study prebreak: 23-31July 2000, composite prebreak periods during 1979-2007 of the Indian summer monsoon, climatological mean of month July during the 1979-2018 period at latitude 45^0 N & 50^0 N, and standard deviation for all the ten harmonics of July at 45^0 N for the period 1979-2018.

As mentioned earlier, Edmon et al., (1980) derived the EP flux (vector$F_{(\varphi,P)}$, from equation 1) from the quasi-geostrophic equation for the large-scale studies (Andrews et al., 1983). The EP flux is a direct measure of the total eddy forcing of the zonal mean state by eddies. Edmon et al., (1980) suggest that the $F_{(\varphi,P)}$ (see equation 1) is also a measure of net wave propagation in the vertical and the latitudinal direction. Edmon et al., (1980) also mentioned that for quasi-geostrophic planetary waves, the sense of arrow representing $F_{(\varphi,P)}$ gives the sense of the group velocity. Also, the contours of $F_{(\varphi,P)}$ represent the role of zonal force on the mean state by the total effect of the quasi-geostrophic eddies.

Fig. 3.11a shows the EP flux for the composite of 41 break cases during the period 1979 - 2007. In this figure, we see a convergence maximum at 150 hPa level near 30°N, and even at 200 hPa, close to 30°N. This convergence of EP fluxes implies a deceleration of zonal wind, thus keeping the blocking high in place during the period of the breaks. Also, this high over the main monsoon region provokes sinking and scanty or no rainfall or a break monsoon. Subsequently, Fig. 3.11b depicts EP fluxes for the JJAS climatology during the 1979 – 2019 period, which shows much more weakened convergence at 150 hPa & 200 hPa. Similarly, in the single case study (Fig. 3.11c), the EP cross-section shows a very strong convergence at 200 hPa around 30°N during the 01-09 August 2000 period, particularly when the blocking high is observed over the Indian region.

Further, during the amplification of the Rossby waves of the sub-tropical westerly jet due to QRA, we observe the development of two remarkable features during the break phase i.e., (1) strong zonal wind shear in the lower latitudes and (2) a split in the jet (core) structure is seen in the higher latitudes, these are the typical characteristics of the blocking high, as noted by Trenberth (1986) for the Southern Hemisphere (SH) scenario. In this context, Fig. 3.12 shows the cross-section of mean zonal wind anomalies averaged over 60°E to 100°E for all prebreak, during-break and after-break periods. Here, this feature is noted for the first time during the southwest monsoon break case and is statistically significant at 95% confidence using a two tailed student's t-test. The strong zonal wind shear is known to cause barotropic instability generating a monsoon depression (Rao, 1971; Govardhan et al., 2017). In the case of a single case study, Fig. 3.13 shows the cross-section of daily mean zonal wind averaged over 60^0 E to 100^0 E from 23July – 18 August 2000. Initially on 23July 2000, a westerly jet shifts south to 50^0 N and an easterly jet to 5°N. At the beginning of the break phase, over CMR on 31 July 2000, the easterly jet intensifies and shifts north to 20° N, and the westerly jet shifts south to 35° N, generating a strong zonal wind shear in the upper troposphere in lower latitudes. Then, further to the north of 60° N, the increasing speed of the sub-tropical westerly jet is associated with a split jet structure on 06 August 2000.

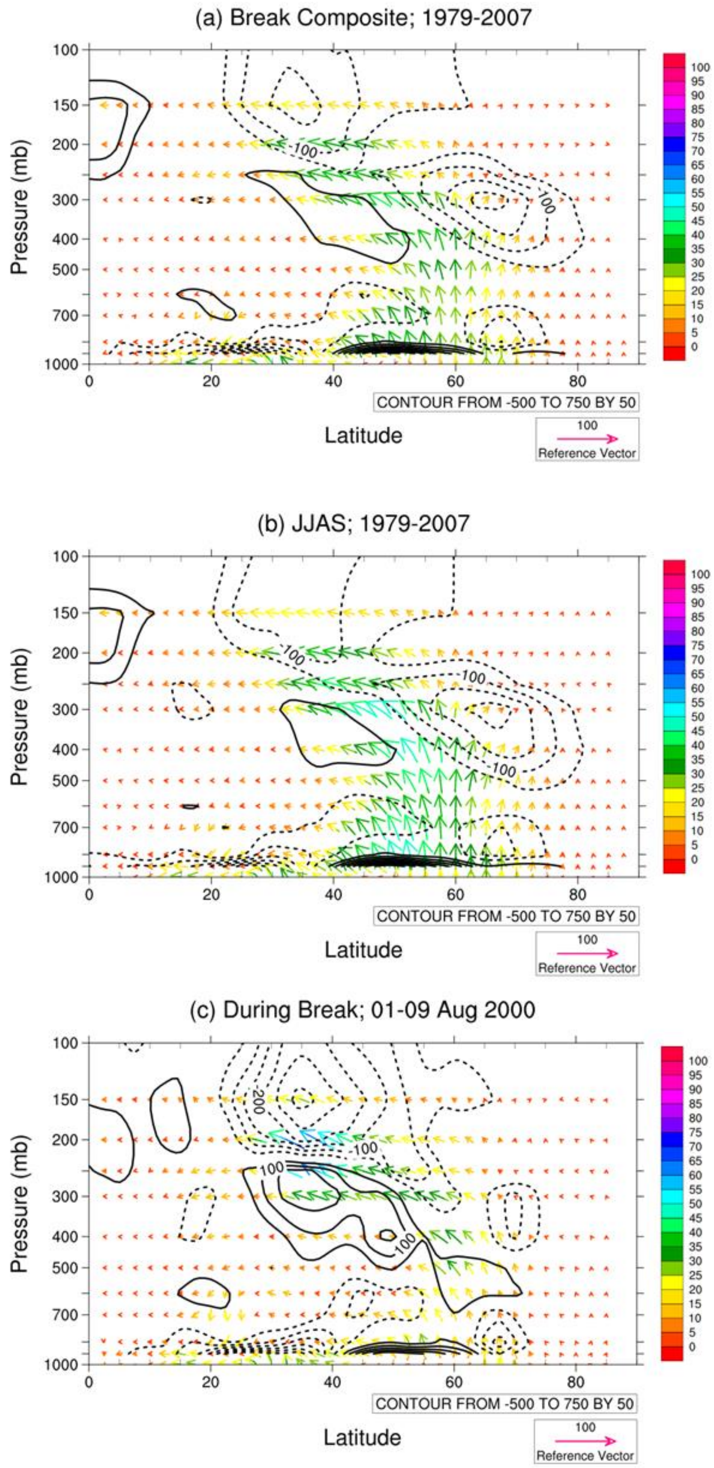

Fig. 3.11 (a): Eliassen-Palm fluxes cross-section of composite during-break periods of Indian summer monsoon; **(b):** Climatological Eliassen-Palm fluxes for the summer season, JJAS during the 1979 – 2007 period. **(c):** Eliassen-Palm fluxes for the case study during the break period 01-09 August 2000 of ISM. In all the figures, the contour interval is 50 m^3. The dashed lines represent convergence and continuous lines represent divergence.

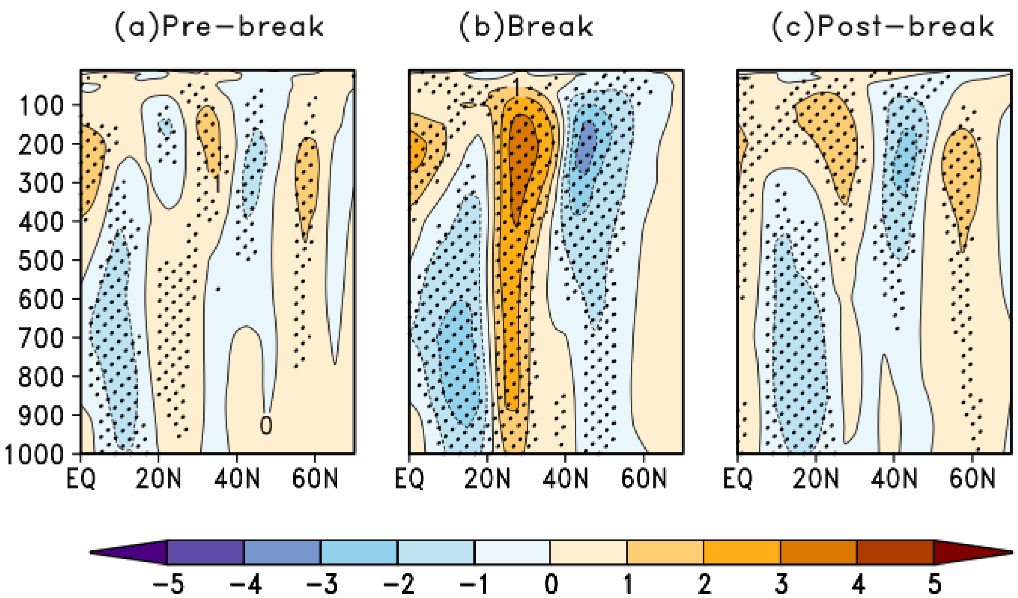

Figure 3.12: Vertical-latitude structure of zonal anomalies of daily U wind (m/s) which are longitudinally averaged between 65°E to100° E, for **(a)** ccomposite prebreak, **(b)** composite during-break and **(c)** composite after-break spells of Indian summer monsoon. The hatched region is significant at 95% confidence using a two-tailed Student's t test. In all the figures, contouring vary between -5 to 5 (m/s) with an interval of 1 m/s

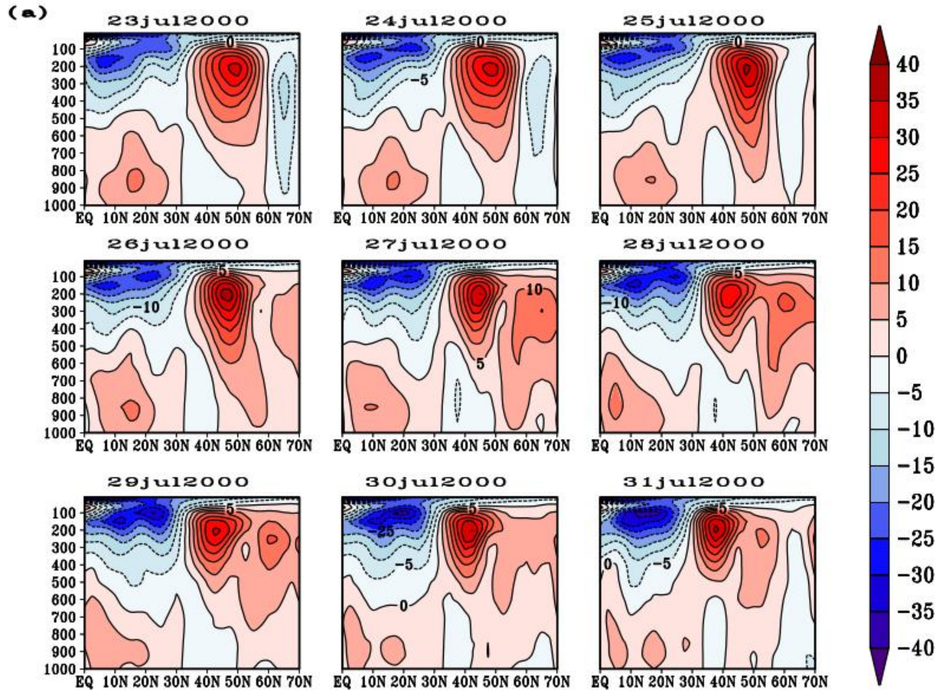
(a)
23jul2000
24jul2000
25jul2000
26jul2000
27jul2000
28jul2000
29jul2000
30jul2000
31jul2000
EQ 10N 20N 30N 40N 50N 60N 70N
100 200 300 400 500 600 700 800 900 1000
40 35 30 25 20 15 10 5 0 −5 −10 −15 −20 −25 −30 −35 −40

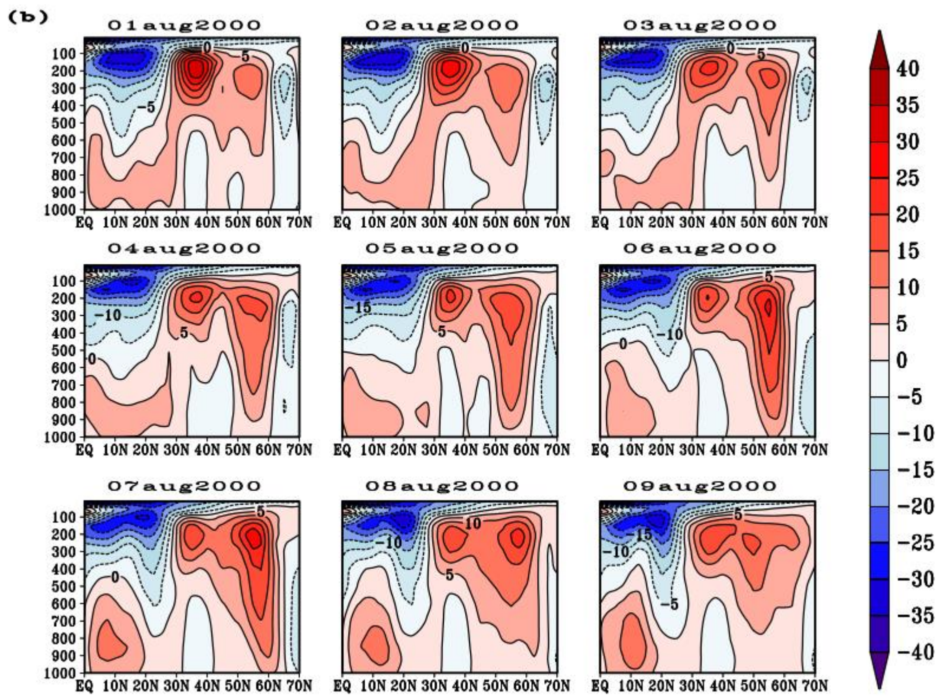
(b)
01aug2000
02aug2000
03aug2000
04aug2000
05aug2000
06aug2000
07aug2000
08aug2000
09aug2000
EQ 10N 20N 30N 40N 50N 60N 70N
100 200 300 400 500 600 700 800 900 1000
40 35 30 25 20 15 10 5 0 −5 −10 −15 −20 −25 −30 −35 −40

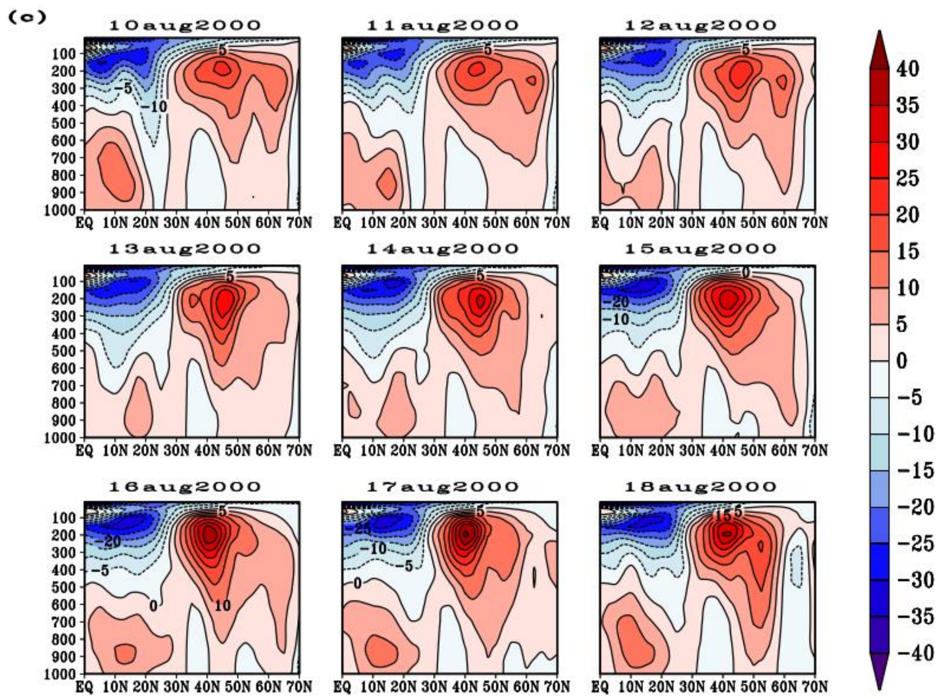

Figure 3.13: Structure of daily zonal wind anomalies which are zonally averaged between 60^0E to100^0 E, before a break **(a)** prebreak (23-31 July 2000); **(b)** during-break (01-09 August 2000) and **(c)** after-break (10-18 August 2000).

Fig. 3.14a shows the latitudinal variation of composite zonal wind, eddy momentum transport, and condition for the barotropic instability (henceforth as CBI) variation for prebreak, during-break and after-break periods. Similarly, the case study (Fig. 3.14b) illustrates the break period 01-09 August 2000 at 200 hPa. A subtropical westerly jet at 35° N and a high latitude jet at 55° N are noted. The eddy momentum transport increases from the equator to around 42° N, decreases to a minimum at 60° N, and then increases again. The necessary condition for barotropic instability (Kuo, 1949; 1951),$\beta - \frac{d^2u}{dy^2} = 0$ occurs at 20° N, 40° N, 60° N and near 80° N. A split jet can be seen at 45° N with mean zonal wind less than 10 m/s.

A similar study by Trenberth (1986) (Fig. 2 in Trenberth's paper) shows the existence of CBI, indicating that eddies may grow locally at the expense of the kinetic energy of the zonal flow, on the poleward flanks of the two jets. A minor difference was observed between our results and Trenberth’s (1986) analyses, that the zonal wind values in our study for the Northern Hemisphere (NH) summer are much lower than in his work for the SH. In our case (Fig. 3.14), there is a divergence of eddy momentum $\overline{u'v'}$ between 30° N and 45° N and the zonal wind (U) is positive from 30° N and 45° N. Thus, from equation 2 of methodology, we can infer an increase of eddy kinetic energy or barotropic instability. Similarly, on the poleward side of the mid-latitude jet, there is a divergence of momentum from 65° N to near about 80° N and U is positive. Again, this indicates the occurrence of barotropic instability. This instability is similar to that noted by Rao (1971) and Govardhan et al., (2017).

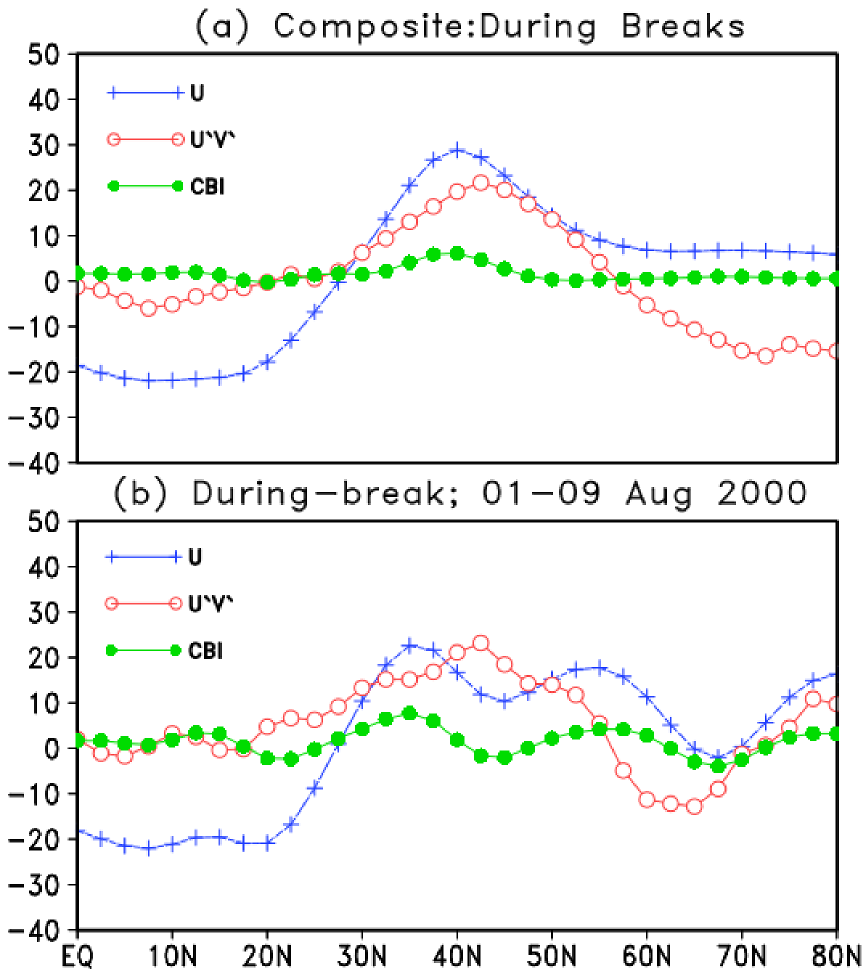

Fig. 3.14: (a) Latitudinal variation of zonal wind (m/s), eddy momentum (m^2/s^2) transport and condition for the barotropic instability (CBI), which are zonally averaged between 60^0 E to100^0 E; for composite during-break periods at 200 hPa during the 1979-2007 period of ISM. **(b)** Latitudinal variation of zonal wind (m/s), eddy momentum (m^2/s^2) transport and condition for the barotropic instability (CBI) for the case study during the break period 01-09 August 2000 at 200 hPa height of ISM.

3.4. Summary of the chapter

Using observed rainfall datasets and NCEP/NCAR II reanalysed datasets over the broad period 1979-2007, I study 41 known break cases in the Indian break summer monsoon. I find that the formation of a blocking high over sub-tropical west Asia a few days earlier is crucial for the manifestation of break monsoon conditions over the India region. Importantly, our study essentially shows that the formation of these blocking highs preceding the breaks is due to the quasi-resonant amplification of planetary waves.

For the occurrence of breaks, the aforementioned transient blocking high is weaker than the seasonal high pressure at upper levels over the Indian region. Because of the presence of this transient blocking, the high pressure weakens, causing a sinking motion relative to the prebreak or after-break period, resulting in a filled-up surface low and, eventually, a reduction in daily rainfall. The following chapter examines whether the sequence of events associated with Indian breaks, namely the formation of an upper level blocking high due to resonance of planetary Rossby waves at mid-latitudes, followed by the break and relative sinking over the core monsoon region, could also explain North and South American summer monsoon breaks.

Chapter 4

Breaks in North & South American summer monsoons

Outline of the chapter

In this chapter, I investigate the interactions between the upper level midlatitudes and tropical summer monsoon circulation in North and South American regions, which is similar to the break formation mechanism discussed in chapter 3.

In this context, I look into similarity between the Indian summer monsoon and the North and South American summer monsoon systems, specifically the mechanism for a break phase, with the goal of developing a unified theory.

4.1 Introduction

In continuation of chapter 4, this chapter is primarily concerned with identifying similar break dynamics between ISM and NAM, SAM systems. The mean evolution of the monsoon from Mexico to the USA, together known as NAM region, is characterized by the regular northward progression of heavy precipitation from southern Mexico by early June, which quickly spreads north into the southwest United States of America (USA) by early July (Higgins et al. 1999). Cavzos et al. (2002) made a systematic and important study about the NAM for the period 1980 - 93. They found “bursts” and “breaks” in a monsoon season. In a spectral analysis of daily summer rainfall, they also found a significant peak at 12-18 days period and also a secondary significant peak near 40 days period. A zonal wet mode (enhanced monsoon ridge) is the most typical mode that characterizes the mature phase of the monsoon in the southwest states of the USA. Wet (dry) summers in the southwest states of the USA are linked to strengthening and northward displacement (weakening and southward displacement) of the monsoon anticyclone (Carleton et al., 1990; Douglas et al., 1993; Higgins et al., 1998; Castro et al., 2001). But, Cavazos et al. (2002) found that eastward location of anticyclone is associated with wet conditions.

The onset of monsoon in Arizona is frequently abrupt, due to the sudden replacement of desert air mass with humid air mass (Moore et al., 1989). Very similar conditions happen over the South American Monsoon region and perhaps even over India, the monsoon onset is abrupt (Rao & Ergodan 1989). Higgins and Shi (2001) noted wet and dry periods of NAM, in western Mexico and South West USA and are linked to 30-60 day variations associated with MJO. This could be again seen similar to India's summer monsoon variations. In the case of the South American Monsoon System (SAM), during the austral summer season as well, there exist periods of enhanced (reduced) convection and higher (lower) rainfall in central and South Brazil (Bolivian

Altiplano and northern South America). The direction of wind anomalies in the Rondonia state, Brazil, is used by Jones and Carvalho (2002) to classify a 3-4 day period known as the Westerly and Easterly low-level wind regimes. During the prevalence of westerly (easterly) anomalies, enhanced (reduced) convection and rainfall is observed over the Bolivian Altiplano and in the North of South America (their figure No. 9) (Jones and Carvalho, 2002), which also shows a clear blocking high, similar to the Indian summer monsoon case.

Similar to the mechanism of break phase of ISM, i.e., the potential relevance of mid-latitude blocking high for the break monsoon, it is important to ascertain the robustness of this hypothesis and its implications for changing of meridional zonal wind stress based on examination of the sufficient number of break monsoon cases. Furthermore, it will also be pertinent to examine whether these mechanisms could also apply to the break monsoon condition in the North and South Americas in addition to the Indian Monsoon region. These are the primary goals of the present investigation. In this context, this chapter is structured as follows. The following subchapter 4.2 & 4.3 discusses the results of the conditions that lead to break phase and conditions for the genesis of blocking high using reanalysis data in the North and South American monsoonal regions. The key findings are summarized in section 4.4.

4.2 Breaks in North American Monsoon

Vera et al., (2006) carried out a brief discussion of intra-seasonal variability for the SAM and NAM systems. Vera et al., (2006) noted, a high located east of the United States of America during the dry (or break) period; in contrast, during the wet period, the high is located to the west (their figures 10a &10b). The eastern high during the break period is reminiscent of the blocking high over Indian and South American regions.

Fig. 4.1 shows the composite daily zonal anomalies of Z_{200} during prebreak, break and after-break periods. In all the panels of Fig. 4.1, we note a high at 40° N and 90° W over the United States of America (USA). During the break period, the corresponding composite Z_{200} zonal anomalies (Fig. 4.1a) over the North American region shows a clear blocking high, which is very much similar to the dry period high (Fig. 4.1) of Vera et al., (2006). Also, one can note a high pressure at 40° N in southern parts of the United States of America (USA). In our case, Fig. 4.2 illustrates the dry/break rainfall period for 16-24 July 2000 over the NAM region. Notably, we see the deficit of rainfall over the Mexican country and southern states of the USA.

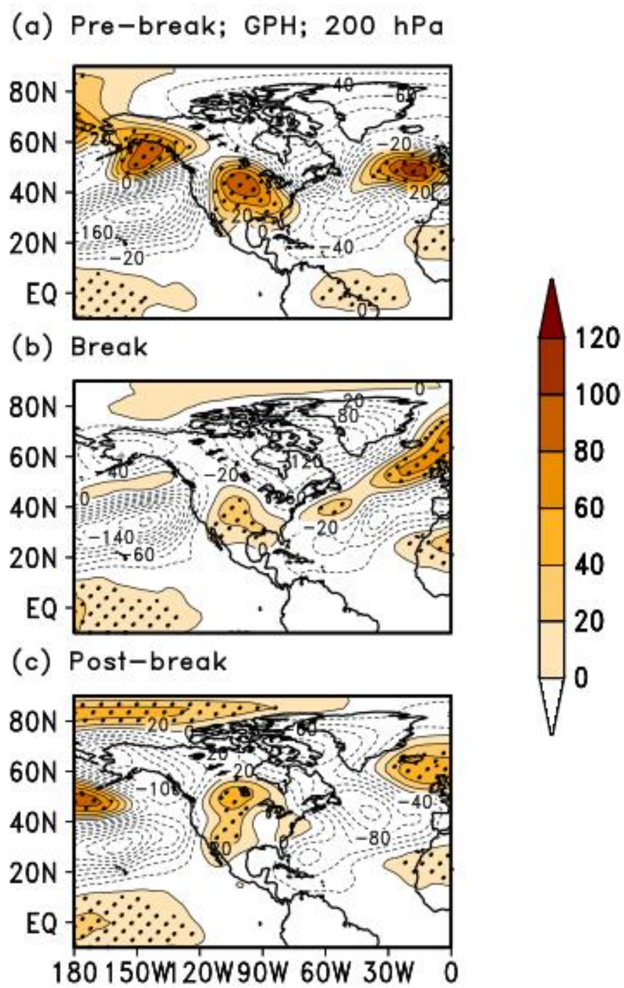

Figure 4.1: Composite daily zonal anomalies of Geopotential height (m) over the monsoon season of 1979-2007 in the North American region during **(a)** prebreak periods **(b)** break periods, and **(c)** after-break periods. The hatching in the Figures 10 a-c indicates the regions where the composite Geopotential height is significantly different from zero at 95% confidence level. Statistical significance has been obtained using a two-tailed one sample Student's t test. In all the figures, positive values are shaded, and negative values are shown in contours. Note that significance test has not been applied to negative values. Contours vary between -120 m to 0 m, with an interval of 20 m. Same interval in shading, as evidenced by the greyscale shown, is used for positive values.

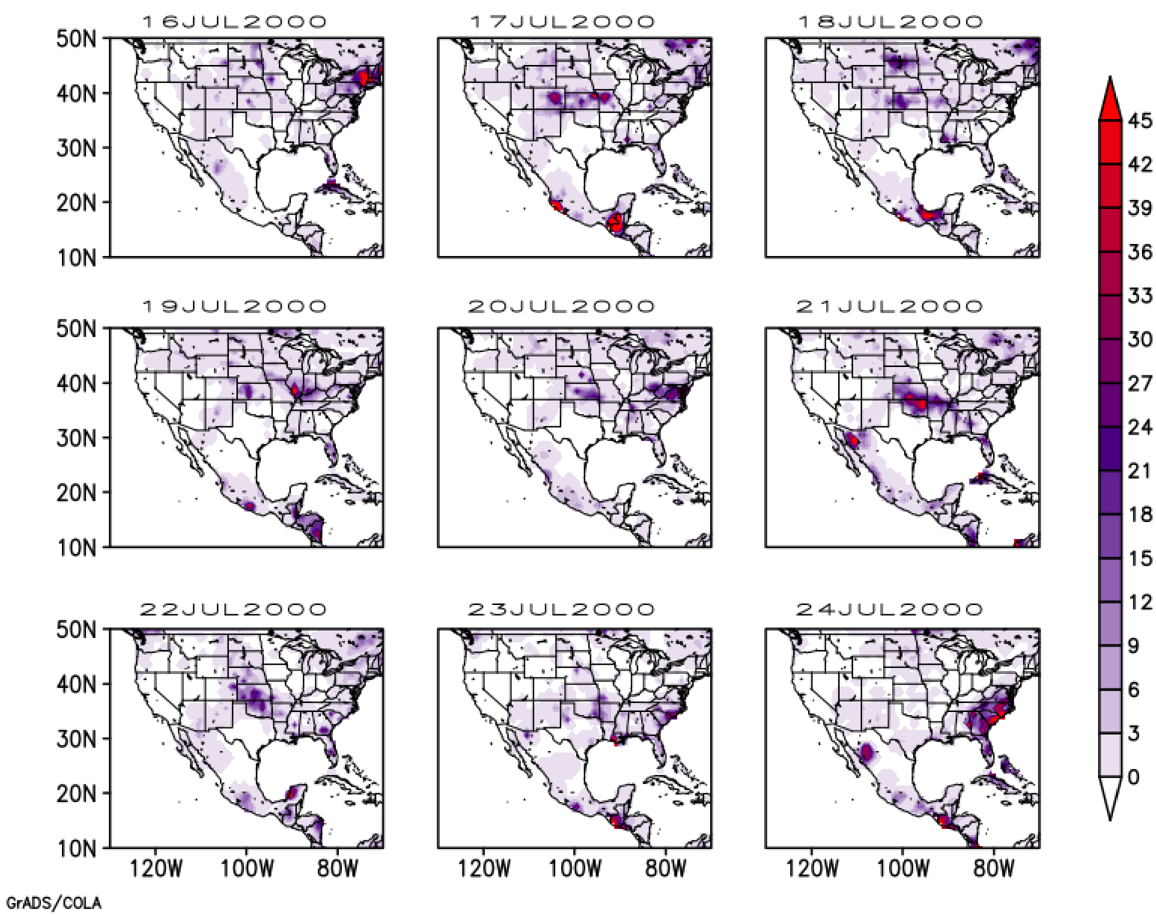

Figure 4.2: Daily rainfall during dry/break period, 16-24 July 2000 over the North American region.

Figures 4.3a & 4.3c show the differences in the composite Z_{200} between break& prebreak periods and that between SLP zonal anomalies. Figures 4.3b & 4.3d show corresponding differences between breaks & after-break periods. Figures 4.3a & 4.3c depict a clear low pressure region at 200 hPa over the Southwest region of the USA during the breaks as compared to prebreaks. The SLP zonal anomalies show a corresponding relatively high pressure region to the eastern United States and a very weak low to the west. This situation, just as in the case of the Indian monsoon breaks, suggests a convergence at a high level and a divergence at a low level indicating sinking motion in accordance with the break conditions. In the after-break situation, figures 4.3b & 4.3d are somewhat similar situation prevails, but to the western side of USA. The similarity to the Indian summer monsoon in terms of the extent of significant signal isn't as obvious statistically because only a few cases were only available for this NAM composite analysis. Fig. 4.4 shows the ω (Pa/s) during the prebreak, break, and after-break periods, as well as the difference between the break and prebreak periods and the difference between the break and after-break periods for NAM system. A similar raising motion can be seen in the composite prebreak, break, and after-break periods in figures 4.4a, 4.4b, & 4.4c, but the magnitudes differ as shown in figures 4.4d & 4.4e. In Fig. 4.4d, we see a strong sinking motion (positive ω values) at 10° N and in Fig. 4.4e we note a very weak raising motion compared to the figures 4.4a, 4.4b & 4.4c. The changes in the ω in figures 4.4a, 4.4b & 4.4c are significant at 95% confidence level, from a two tailed students t-test. Even though the composite ω in figures 4.4d & 4.4e is not as significant as expected, this weak raising motion can be considered as a good observation because we already note sinking motion in Fig. 4.4d, which could be elucidated as a significant result leading to the NAM system’s break phase, although only three break cases were found.

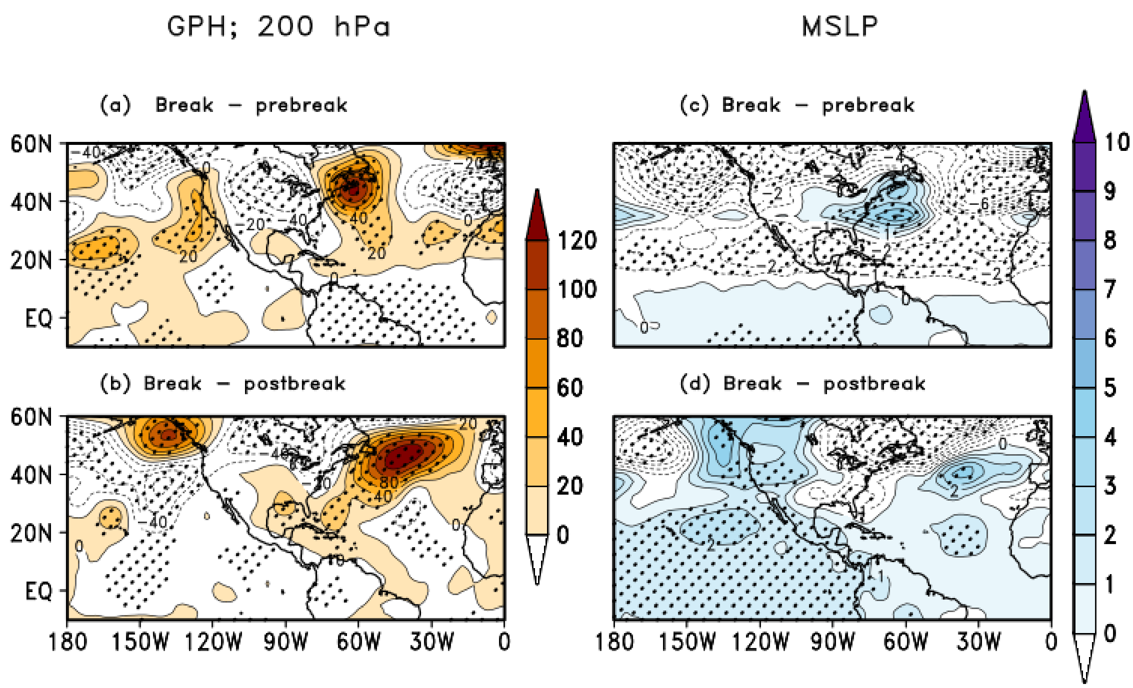

Figure 4.3: Difference between the composite daily zonal anomalies of Geopotential height (m) during the 1979-2007 period over the North American region between **(a)** break and prebreak periods **(b)** break periods and after-break periods. Difference in composites of zonal anomalies of daily mean sea level pressure (hPa) over the North American region during the 1979-2007 period between **(c)** during-break and prebreak periods, and **(d)** during-break and after-break periods. The hatched regions indicate locations of significant differences, at 95% confidence level, in daily zonal anomalies of Geopotential height in panels (a) & (b), and that of daily mean sea level pressure in panels (c) & (d). Statistical significance has been obtained using a two-tailed two sample Student's t-test with unequal variances. In all the figures, positive values are shaded, and negative values are shown in contours. The contours in panels (a) & (b) vary between -120 m to 0 m, with an interval of 20 m and those in panels (c) & (d) vary between -10 hPa to 0 hPa, with an interval of 1 hPa. Same intervals as used for contours are used for the shadings, and indicated in the grayscales shown.

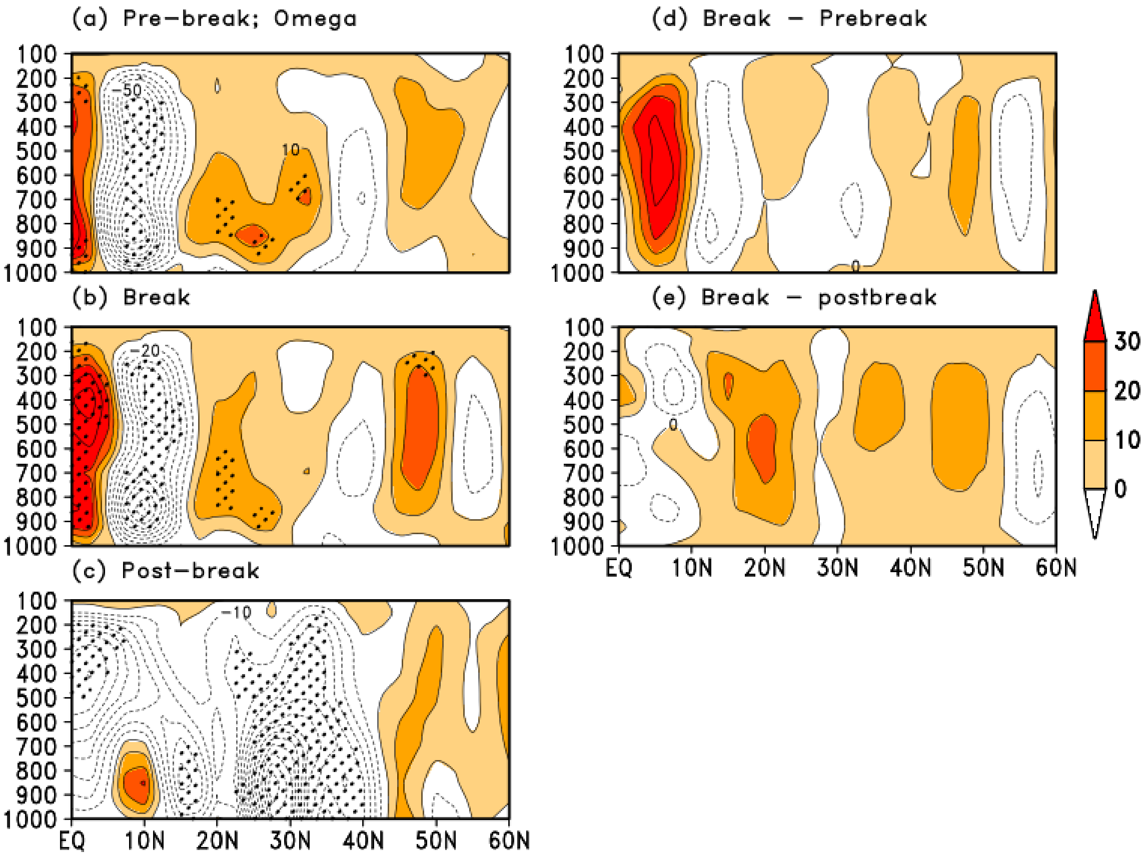

Figure 4.4: Composite vertical wind zonal anomalies (x10^{-3}) (omega) (Pa/s) over North American region and longitudinally averaged along 60^{0} W - 125^{0} W during the summer monsoon for the (a) prebreak periods (b) during-break periods, and (c) after-break periods, (d) difference between the composite break and composite prebreak periods, and (e) difference between the composite break and composite after-break periods. The contours in panels (a) (b) (c) (d) & (e) vary between -30 Pa/s to 0 Pa/s, with an interval of 10 Pa/s. The hatched regions indicate composite omega zonal anomalies are significant at 95% confidence from a two-tailed Student's t test.

To explore the possible occurrence of resonance as suggested by Charney and Devore (1979) for the initiation of the blocking high in the North American monsoon breaks, we constructed the first ten simple harmonics for the meridional wind over the region (Fig. 4.5) for the prebreak at 45° N composite, July climatology at 45° N and 50° N, and an individual case for 1995 prebreak period. For the North American monsoon case, we note a dominant wave number 5 and 6 respectively for the 1995 case and the composite prebreak. Unlike, the wavenumber 7 for Indian summer monsoon case, we do not see a clear dominance of a single wave. This may probably be because of the small number of break cases we used for the NAM system. In any case, compared to the climatology and the standard deviation curves in Fig. 4.5, we do see that wave numbers 5, 6 and 7 are most dominant. This agrees with what is expected from the Charney and Devore perspective and supports the QRA theory for the break monsoon case of North America.

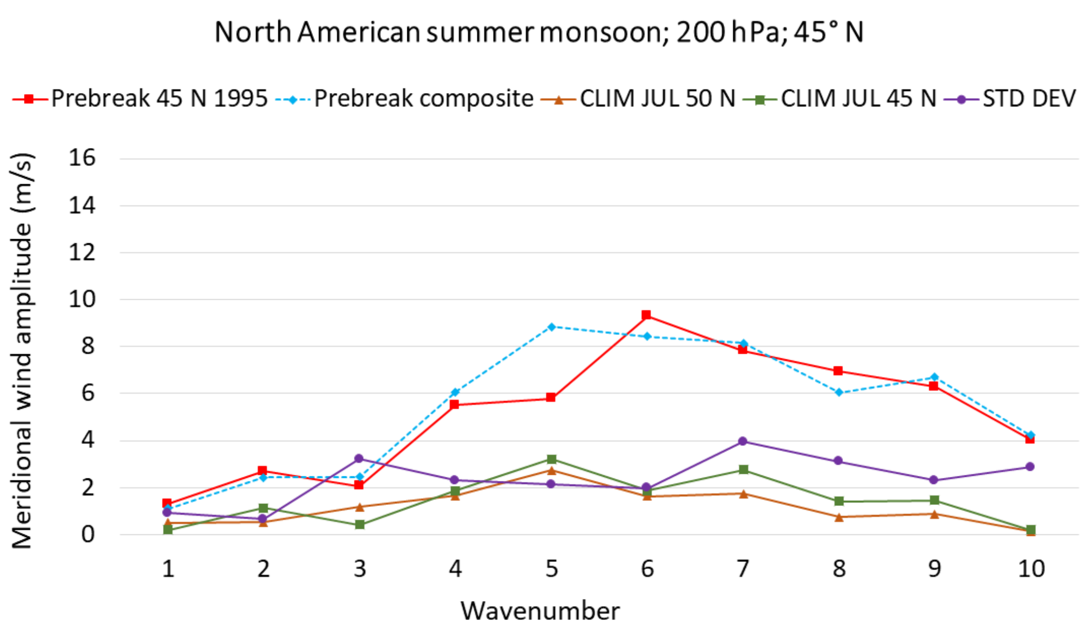

Figure 4.5: Wavenumber spectrum using meridional wind (m/s) at 200 hPa level; for composite prebreak periods of North American monsoon (Table 2.3); case study prebreak period, 10-15 Jul

1995; the climatological mean of month July during 1979-2018 periods at 45^0 N and 50^0 N, and standard deviation for all the ten harmonics of July at 45^0 N for the period 1979-2007.

Fig. 4.6a shows the EP flux for the composite during-break periods of NAM (Table 2.3). In this figure, we see a convergence maximum at 150 hPa level near 30°N, and even at 200 hPa, close to 30°N. This convergence of EP fluxes implies a deceleration of zonal wind, thus keeping the blocking high in place during the period of the breaks. Also, this high over the main monsoon region provokes sinking and scanty or no rainfall or a break monsoon. Subsequently, Fig. 4.6b depicts EP fluxes for a single case study, the EP cross-section shows a very strong convergence at 200 hPa around 30°N during the 16-24 July 2000 period, particularly when the blocking high is observed over the North American region.

Fig. 4.7a illustrates the composite of mean zonal wind and Fig. 4.7b shows the profiles of prebreak periods of each case. Fig. 4.8 shows the zonal wind profiles during the break phase for each case. Here, the composite zonal wind profiles (Fig. 4.7a) prebreak, during-break, and after-break periods show a minimal difference of about 23 m/s. In each case, during prebreak spells, we note zonal wind of 25 m/s and during the break phase (Fig. 4.8) we note 27 m/s. Manola et al., (2013) have shown that stronger and narrower jets tend to stronger zonal waves and smaller wavenumbers (4 and 5). Also, we see a double-jet structure (Fig. 4.9) in the composite zonal wind anomalies and the steep sub-tropical jet is strongly linked to QRA (Kornhuber et al., 2017). The resonance amplification depends on the characteristics of mean zonal wind. In the case of SAM (ISM) the strength of the jet is higher and the stationary free waves are of higher wavelengths or lower wavenumbers (lower wavelengths and higher wavenumbers)

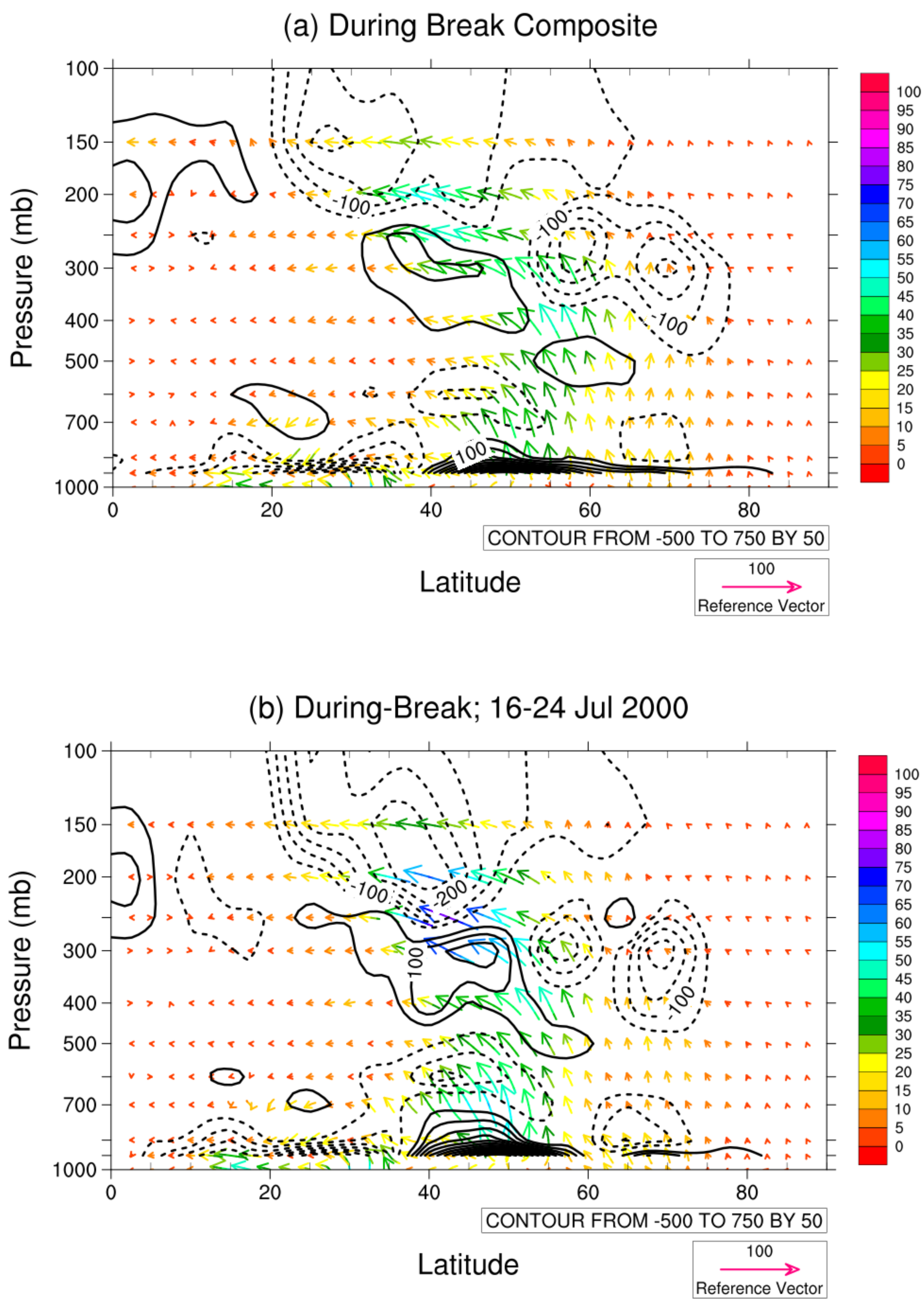
(a) During Break Composite
Pressure (mb)
100
150
200
300
400
500
700
1000
0
20
40
60
80
-100
100
CONTOUR FROM -500 TO 750 BY 50
Latitude
100
Reference Vector
100 95 90 85 80 75 70 65 60 55 50 45 40 35 30 25 20 15 10 5 0
(b) During-Break; 16-24 Jul 2000
Pressure (mb)
100
150
200
300
400
500
700
1000
0
20
40
60
80
-100
-200
100
CONTOUR FROM -500 TO 750 BY 50
Latitude
100
Reference Vector
100 95 90 85 80 75 70 65 60 55 50 45 40 35 30 25 20 15 10 5 0

Figure 4.6: (a) Eliassen-Palm fluxes cross-section of composite during-break periods of NAM; **(b):**Eliassen-Palm fluxes for the case study during the break period 16-24 July 2000 of NAM. In all the figures, the contour interval is 50 m^3. The dashed lines represent convergence and continuous lines represent divergence.

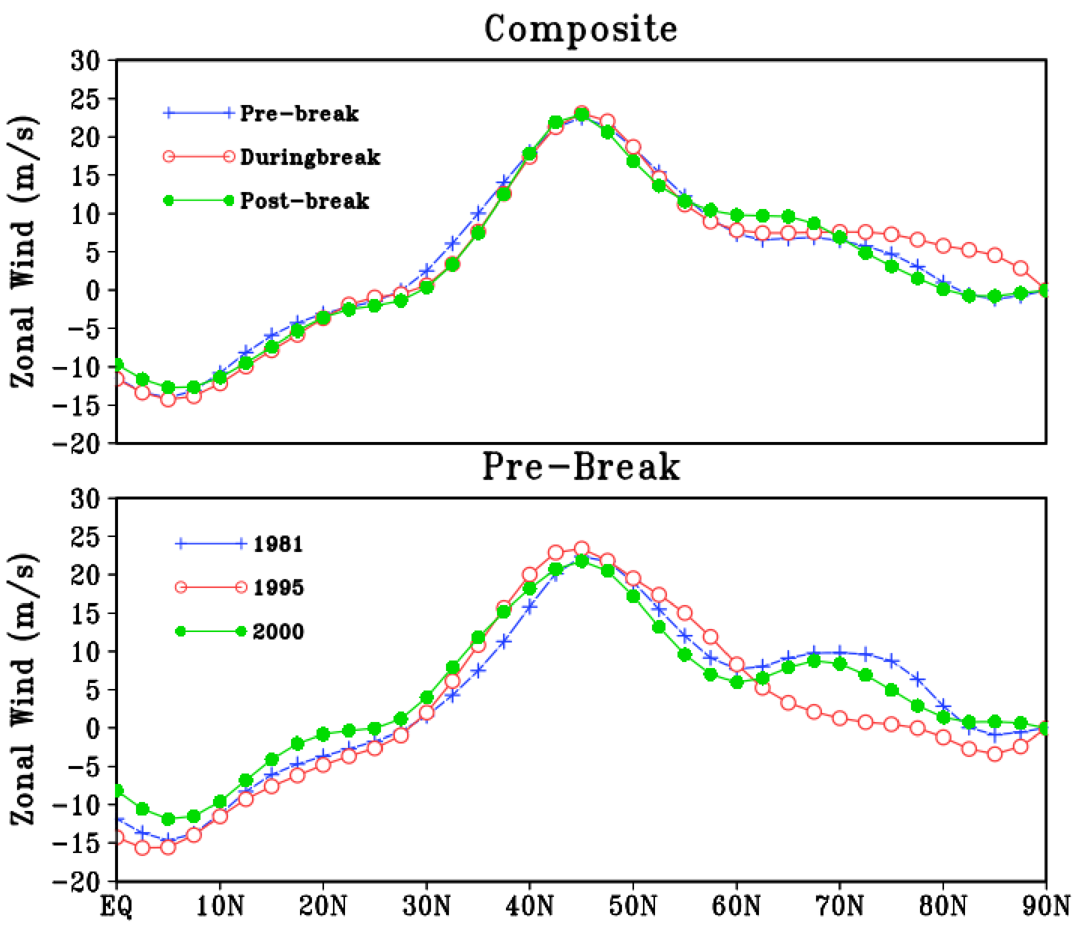

Figure 4.7(a):(Top) Composite globally zonal averaged U wind (m/s) of composite prebreak, composite during-break and composite after-break periods of North American monsoon **(b):** (Bottom) Globally zonalaveraged U wind of prebreak periods in three different cases: 10-16 July 1981, 20 - 24 July 1995 and 10-15 July 2000 of NAM.

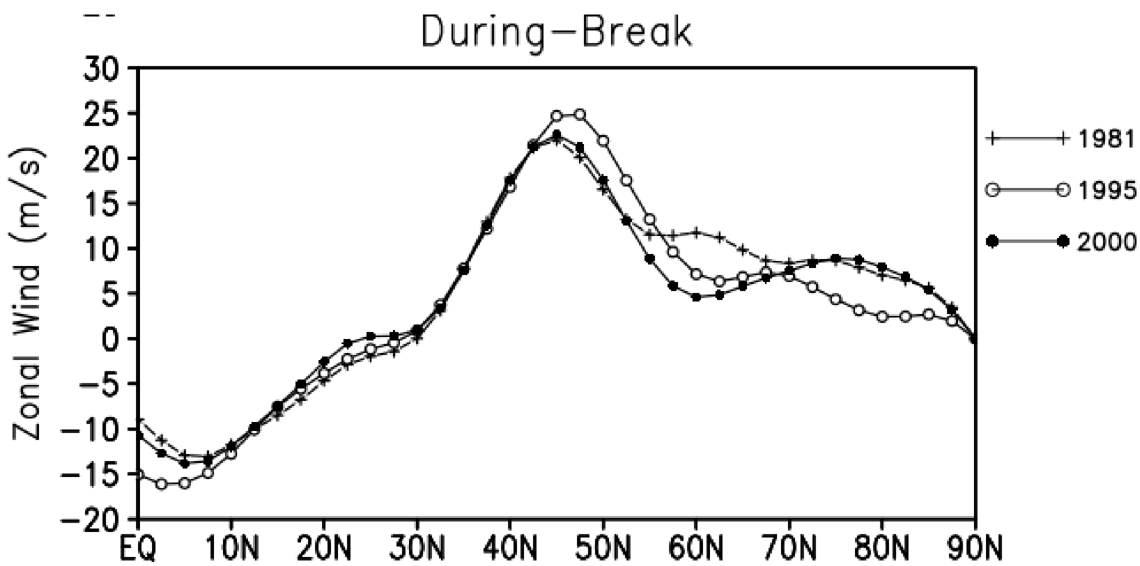

Figure 4.8: (c) Zonal wind profiles during the break phase for 1981, 1995 and 2000 events.

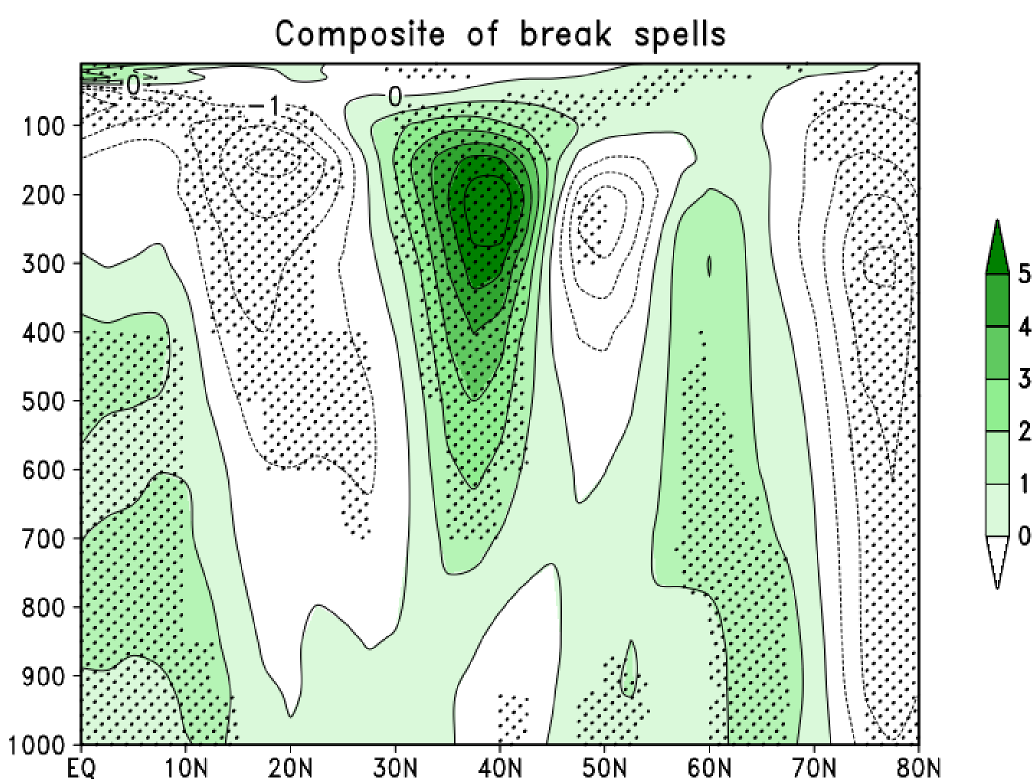

Figure 4.9: Composite structure of daily U wind zonal anomalies (m/s) for the break cases of NAM, 10-16 July 1981, 20 - 24 July 1995 and 10-15 July 2000; which are zonally averaged in between 60^0 W - 125^0 W. The hatched region indicates 95% confidence using a two-tailed Student's t test. In this figure positive values are shaded and negative values are shown in contours. Contouring between -5 to 0 (m/s) with an interval of 1 m/s

4.3 Breaks in South American Monsoon

The strong summer convective activity in South America is associated with large-scale atmospheric circulation. Intra-seasonal variability of SAM is related to convection on a wide range of spatial-temporal scales. Previously, the intra-seasonal variability of the 10-90 days scale is observed over eastern South America and particularly over northeast Brazil (Jones and Carvalho, 2002; Carvalho et al., 2002; Ciffelli et al., 2002; Grimm et al., 2005; Souza et al., 2005). Intra-seasonal variations of SAM mayoccurby the propagation of mid-latitude perturbations into the convection region, and as well as, with a subsequent increase in north-westerly cross-equatorial moisture transport over southern tropical South America (Carvalho et al., 2010) with the amplification of wave activity in the Northern hemisphere.

A study on SAM by Gan et al., (2004) found some similarities and differences with the Indian Monsoon using a 21-year (July 1979-June 2000) period of data. They noted a strong easterly jet maximum at 100 hPa during January, similar to the easterly jet over south India (Halley, 1686; Koteswaram, 1958). They found that only zonal wind anomalies show a perceptible reversal in direction, i.e., when the annual cycle is removed as noted by Zhou and Lau (1998). Further, they had observed wet and dry periods of SAM which are similar to the Asian Monsoon (Jones and

Carvalho, 2002). Thus, the blocking high configuration in the upper troposphere, Fig 9 of Jones and Carvalho (2002) is similar as noted earlier for Indian monsoon breaks.

Fig. 4.10 shows the composite zonal anomalies Z_{200} and all panels are statistically significant at 95% confidence using a two tailed students t-test. We observe a high at 60^0 S & 120^0 W and another high extending between 40° S to 0° and at 60° E, i.e., central and north of South America. Figures 4.11 a-b illustrates theZ_{200} anomaly pattern for the break period in January 1980 & 1981. A clear blocking high over central South America can be noted with two troughs on either side of the blocking high at 20°S. The formation of a blocking high preceding a break/drought situation in this case of SAM is analogous to that for the Indian summer monsoon situation (Fig. 4.11a). Thus, these features are a unifying characteristic for the break in the ISM (Fig. 3.1) and SAM. The troughs which are associated with blocking high are strongly oriented towards NW to SE tilt which implies southward (poleward) transport of eddy momentum. Fig. 4.11b depicts Geopotential Height for the break case during 06-11 January 1981. The characteristics in this figure are very similar to those in January 1980 case.

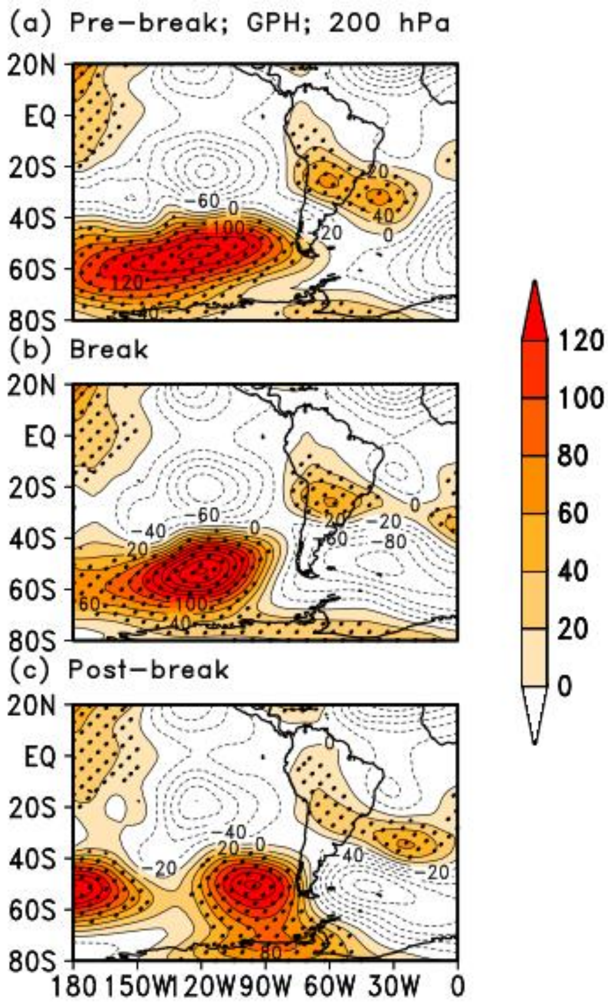

Figure 4.10: Composite daily zonal anomalies of Geopotential height (m) over the monsoon season of 1979-2007 in the South American region during **(a)** prebreak periods **(b)** break periods, and **(c)** after-break periods. The hatching in the Figures 17 a-c indicates the regions where the composite Geopotential height is significantly different from zero at 95% confidence level. Statistical significance has been obtained using a two-tailed one sample Student's t test. In all the figures, positive values are shaded, and negative values are shown in contours. Note that significance test has not been applied to negative values. Contours vary between -120 m to 0 m,

with an interval of 20 m. Same interval in shading, as evidenced by the greyscale shown, is used for positive values.

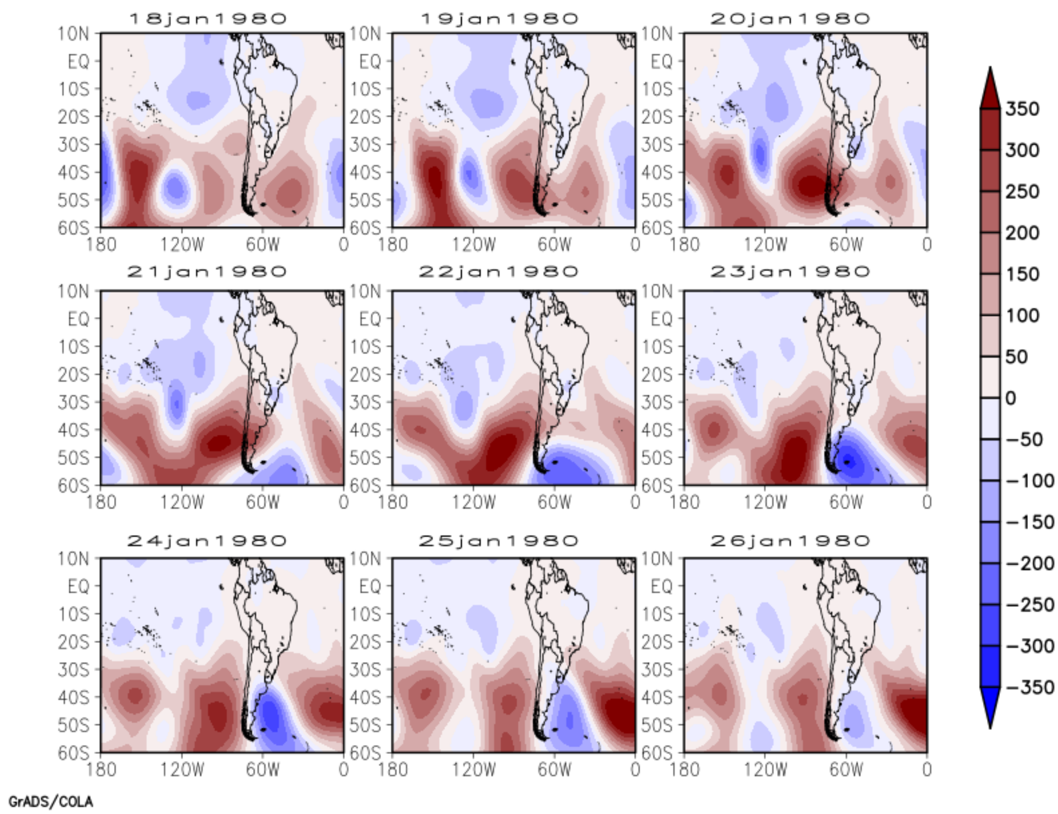

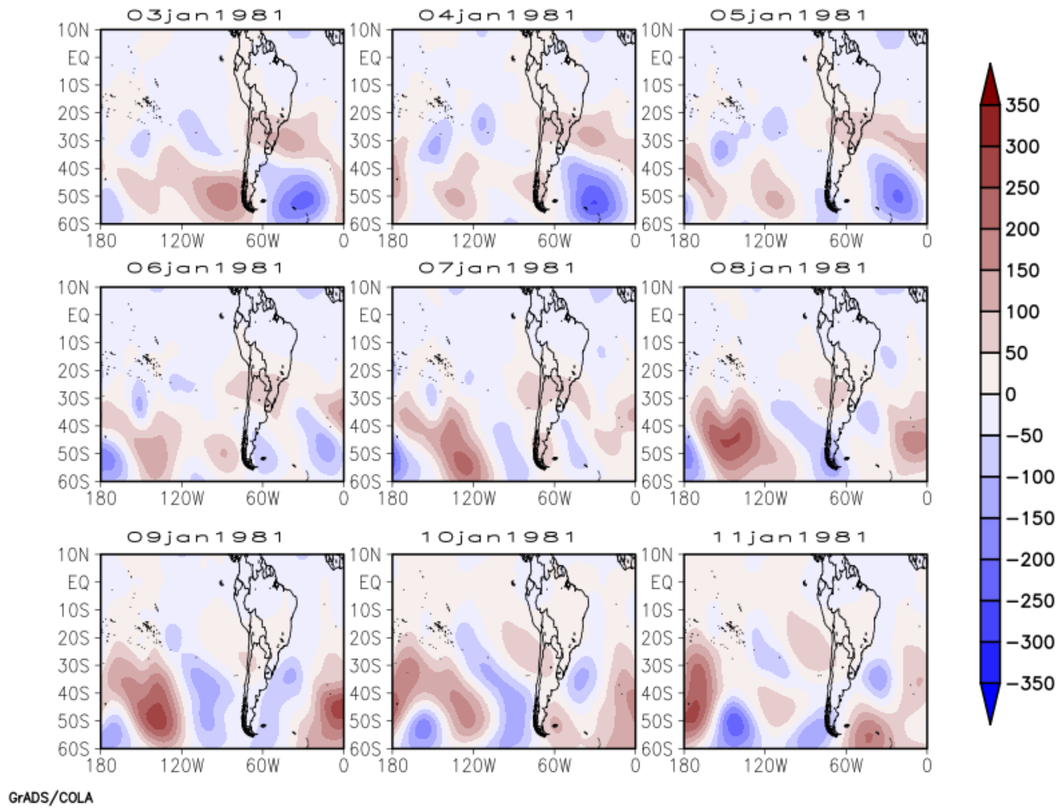

Figure 4.11: **(a)** Geopotential Height anomalies (m) at 200 hPa during the break spell, 21-26 January 1980 over the South American region. **(b)** Geopotential Height anomalies (m) at 200 hPa during the break spell, 06-11 January 1981 over the South American region.

Figures 4.12 a-d show the difference between the composites of break & prebreak periods, and breaks & after-break periods of $Z_{200}$and SLP zonal anomalies. In Fig. 4.12, we note a strong low pressure region at 200 hPa over southern South America and eastern South Atlantic. While in Fig. 4.12(c) we note a relatively high pressure region, this indicates again similar to Indian and North American break monsoons convergence at higher levels and divergence at lower levels (figures 4.12c & 4.12d; SLP figures) indicating a sinking motion. Thus, in all the break monsoon regions very similar conditions exit and the analysis using Z_{200} and SLP zonal anomalies, and strongly supports sinking and reduction of rainfall causing break monsoons. All the changes in the panels of the Fig. 4.12 are statistically significant at 95% confidence level using a two tailed students t-test. Figures 4.13a, 4.13b & 4.13c shows the vertical velocity (omega) (Pa/s) of the South American summer monsoon during the prebreak, break, and after-break periods, as well as the figures 4.13d & 4.13e difference between the break and prebreak periods and the difference between the break and after-break periods. A strong sinking motion is seen in the composite prebreak& break between 10° S - 0° in figures 4.13a & 4.13b, and raising motion in after-break periods between 10° S - 0° in fig. 19c, but the omega magnitudes differ as shown in Figures 4.13d & 4.13e. In Figures 4.13d & 4.13e, we note a narrow region of raising motion at 10° S and strong sinking between 0° – 10° N. The changes in the omega wind in figures 4.13 a-e are significant at 95% confidence level using two tailed students t-test.

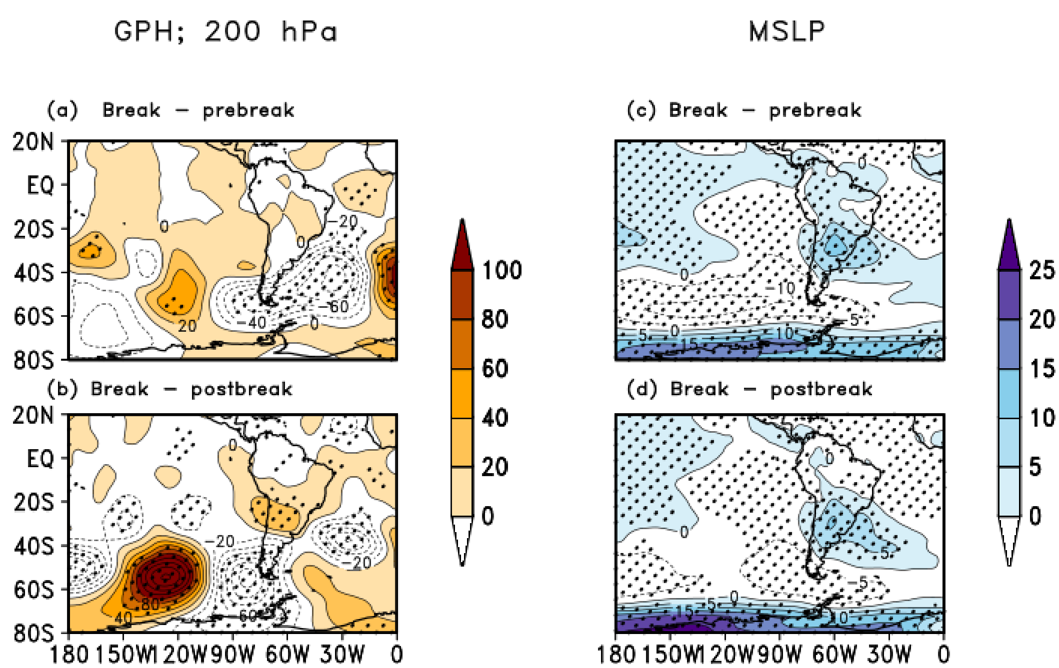

Figure 4.12: Difference between the composite daily zonal anomalies of Geopotential height (m) during the 1979-2007 period over the South American region between **(a)** break and prebreak periods **(b)** break periods and after-break periods. Difference in composites of zonal anomalies of daily mean sea level pressure (hPa) over the South American region during the 1979-2007 period between **(c)** during-break and prebreak periods, and **(d)** during-break and after-break periods. The hatched regions indicate locations of significant differences, at 95% confidence level, in daily zonal anomalies of Geopotential height in panels (a) & (b), and that of daily mean sea level pressure in panels (c) & (d). Statistical significance has been obtained using a two-tailed two sample Student's t-test with unequal variances. In all the figures, positive values are shaded, and negative values are shown in contours. The contours in panels (a) & (b) vary between -100 m to 0 m, with an interval of 20 m and those in panels (c) & (d) vary between -25 hPa to 0 hPa, with an interval of 5 hPa. Same intervals as used for contours are used for the shadings, and indicated in the grayscales shown.

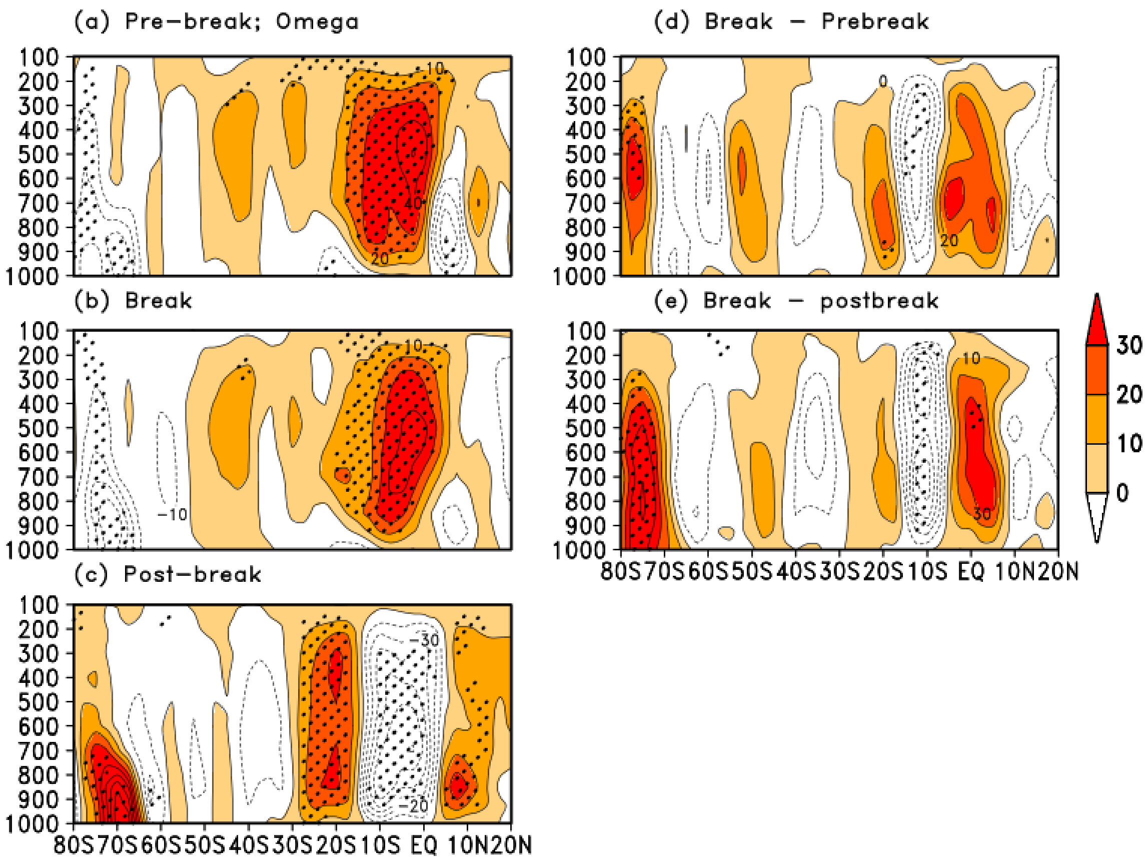

Figure 4.13: Composite vertical wind zonal anomalies (x10^{-3}) (omega) (Pa/s) longitudinally averaged along 60^0 W to 125^0 W over South American region during the summer monsoon for the 1979-2007 period, **(a)** prebreak periods **(b)** during-break periods, and **(c)** after-break periods, **(d)** difference between the composite break and composite prebreak periods, and **(e)** difference between the composite break and composite after-break periods. The contours in panels (d) & (e) vary between -30 Pa/s to 0 Pa/s, with an interval of 10 Pa/s. The hatched regions indicate composite omega zonal anomalies are significant at 95% confidence from a two-tailed Student's t-test.

Fig. 4.14 illustrates the wavenumber spectrum of meridional wind at 200 hPa height for composite prebreak periods, a case study during 1981 January at 45° S, and the climatology of January month for the 1979-2018 period at 45° S & 50° S, and standard deviation. For the South American monsoon case, we see the dominance of wave numbers 4 & 5 for the 1981 prebreak case and 4, 5 & 6 for the prebreak composite. The values of the amplitude for wave number 4 and 5 are much higher than for the climatology and also above standard deviation. In the case of austral summer Kornhuber et al., (2017) found waveguides approximately 70% for the analysed period for wavenumber 4 & 5. In our case, the dominance of wavenumber 4 & 5, thus is very similar to that noted by Kornhuber et al., (2017). This indicates a strong case for wave resonance as suggested by Charney and DeVore (1979) and quasi-resonant amplification for the SH case noted by Kornhuber et al., (2017).

The difference in the dominant wave numbers is due to the difference in the strength of the mean zonal wind. In the Indian break monsoon case, the maximum velocity of the zonal wind is around 22 m⁄s, as explained Kornhuber (2017, their Fig. 1) the QRA is expected for wave numbers ≥6. While in the case of the SH the maximum velocity of composite zonal wind is around 28 m⁄s (Fig. 4.15a), as explained by Kornhuber et al., (2017) leads to the QRA mechanism for wave numbers ≥4. Fig. 4.15b shows the zonal wind profiles for the prebreak period of each case, and Fig. 4.16 shows the during-break and after-break periods for all cases. Jones and Carvalho (2002) studied independent events of westerly and easterly wind samples, 113 and 104 respectively for SAM (their Fig.7). Westerly and easterly phases are associated with lower and higher rainfall over the SAM core monsoon region. Their fig. 9 shows a clear blocking high at 200 hPa level during the westerly regime and break monsoon case. Note that these characteristics are for a composite of 104 break events. Also, they mentioned in their figure, the resemblance to wave trains implying

Rossby wave propagation akin to those envisaged by Charney and DeVore (1979), Kornhuber et al., (2017), and others mentioned earlier. Thus, the break monsoon events in South America are analogous to break events in Indian CMR.

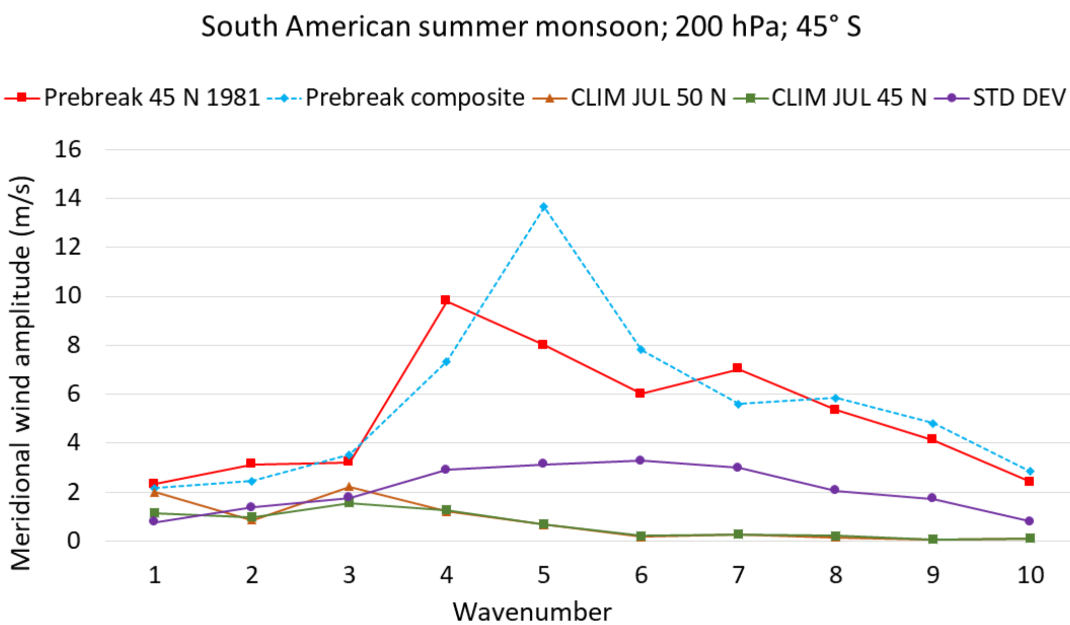

Figure 4.14: Wavenumber vs. Amplitude spectrum using meridional wind (m/s) at 200 hPa, for an individual case 1981 at 45^0 N, composite of prebreak periods of South American monsoon (Table 3), the climatological mean of month July during 1979-2018 periods at 45^0 N and 50^0 N, and standard deviation for all the ten harmonics of July at 45^0 N for the period 1979-2007.

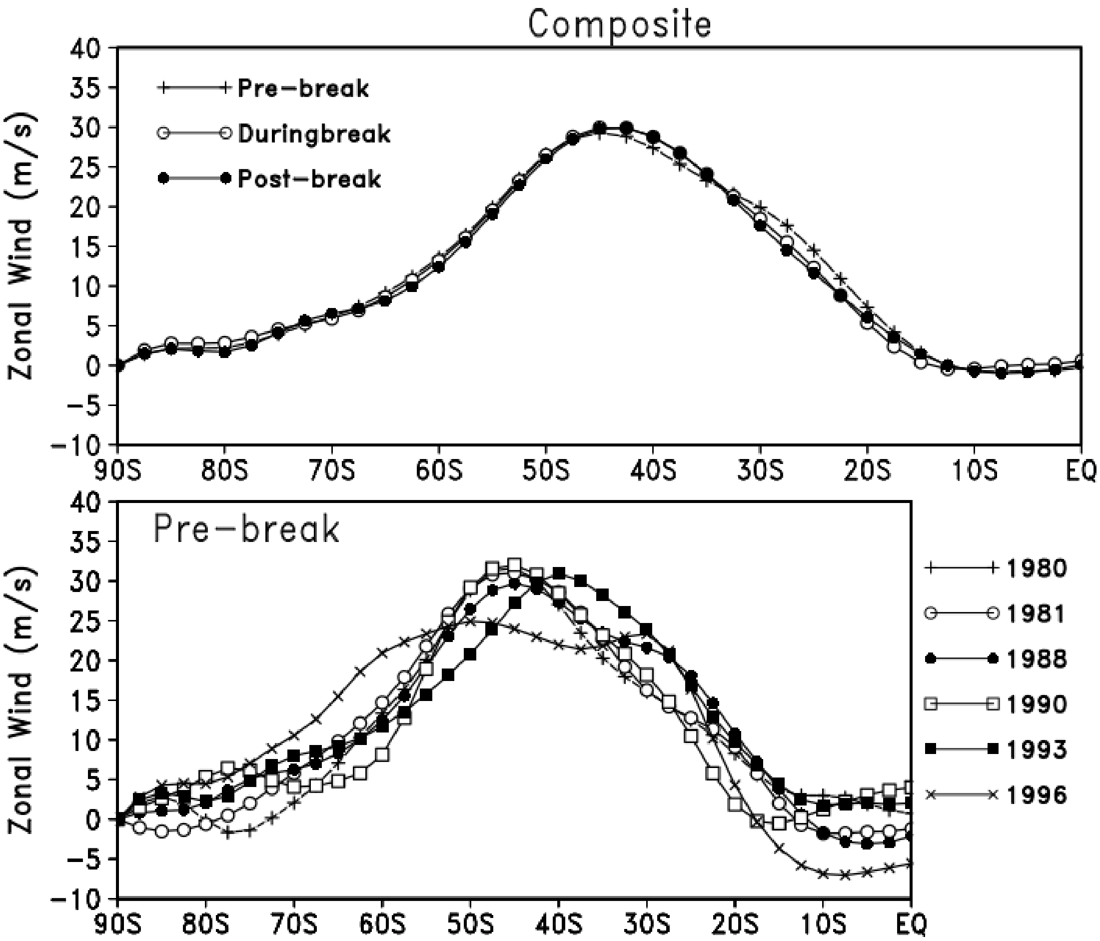

Figure 4.15(a):(Top) Globally zonal averaged U wind (m/s) of composite prebreak, composite during-break and composite after-break periods of SAM (**b): (Bottom)** Globally zonal averaged U wind (m/s) for prebreak periods of six different cases of SAM: 18-21 January 1980, 01-04 January 1981, 10-15 January 1988, 16-20 January 1990, 25 December-01 January 1993, 19-24 January 1996.

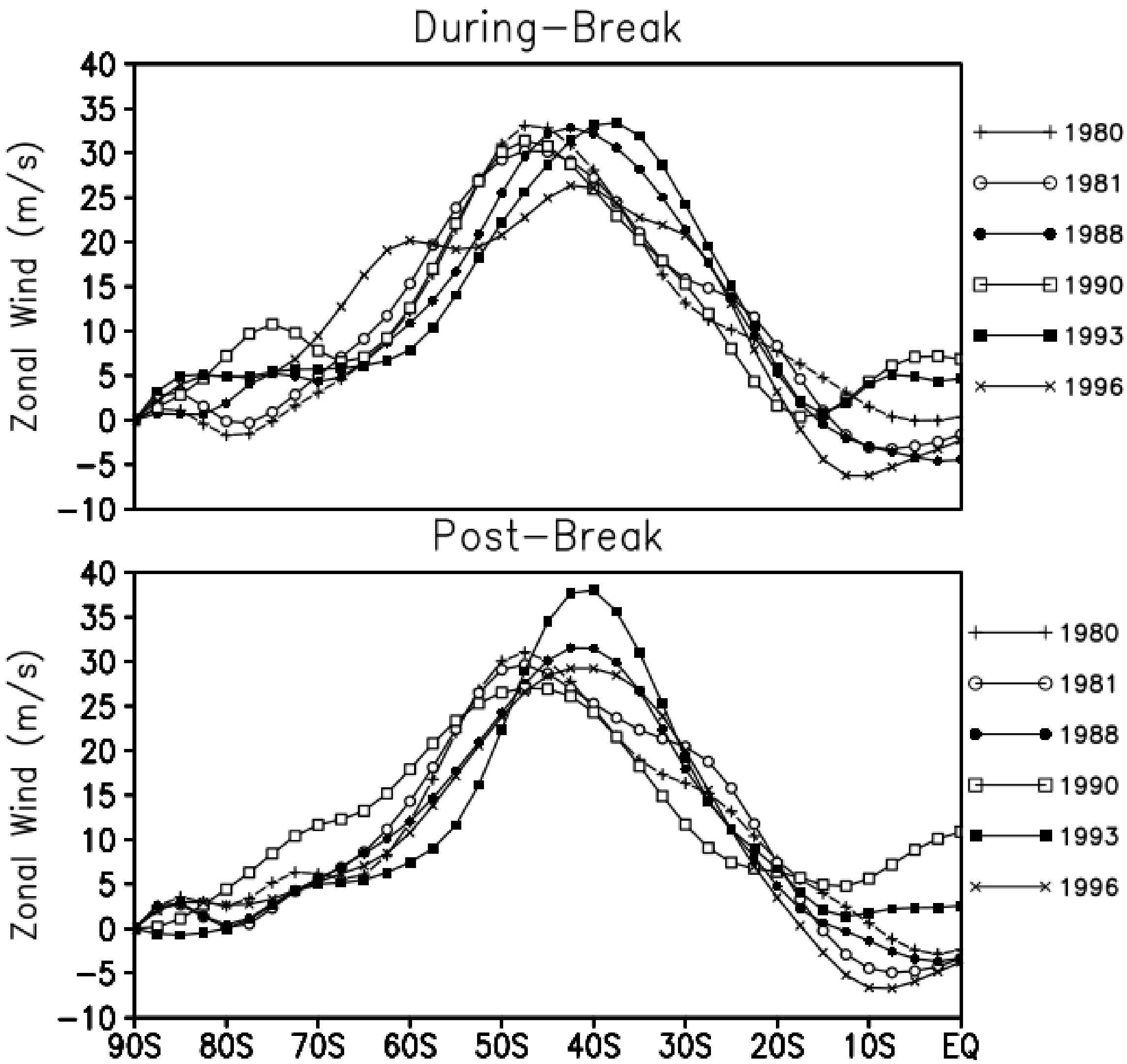

Figure 4.16: (a) (Top) Composite of globally zonal averaged U wind (m/s) for during-break in six different cases. (**b)** (Bottom) Globally zonal averaged U wind (m/s) for after-break periods in six different cases: 18-21 January 1980, 01-04 January 1981, 10-15 January 1988, 16-20 January 1990, 25 December-01 January 1993, 19-24 January 1996.

Fig. 4.17 shows the composite structure of zonal wind anomalies. Two jets, one at 55°S and the other at 35°S can be noted around the height of 250 hPa. Also, a tropical easterly jet can be seen around 15°S at levels above 100 hPa. Similarly, Fig. 4.18 portrays the structure of zonal wind anomalies before the block formation on 4 January 1981. Whereas, the shear between the jets is maximized on 6 January 1981, the day on which the break period starts, indeed the maximized shear can be seen in the composite of during-break (Fig. 4.17b). This occurrence of maximum zonal wind shear during the break is similar to that noted for the Indian case. Further, the strong shear also can be noted in the upper troposphere between the westerly and easterly jets. We noted two regions of convergence, one at 60°S and 400 hPa and the other at 30°S and 250 hPa. Similarly, for the two case studies in January 1980 and 1981 (Fig. 4.19), two large convergence regions are found with a slightly higher magnitude relative to composite EP fluxes during-break period (Fig. 4.20a) and climatology DJF for the 1979-2007 period (Fig. 4.20b). This situation can be seen as similar to that co-occurred over India, the low latitude convergence seems to reduce the zonal wind and maintain the block without being advected, by the zonal current.

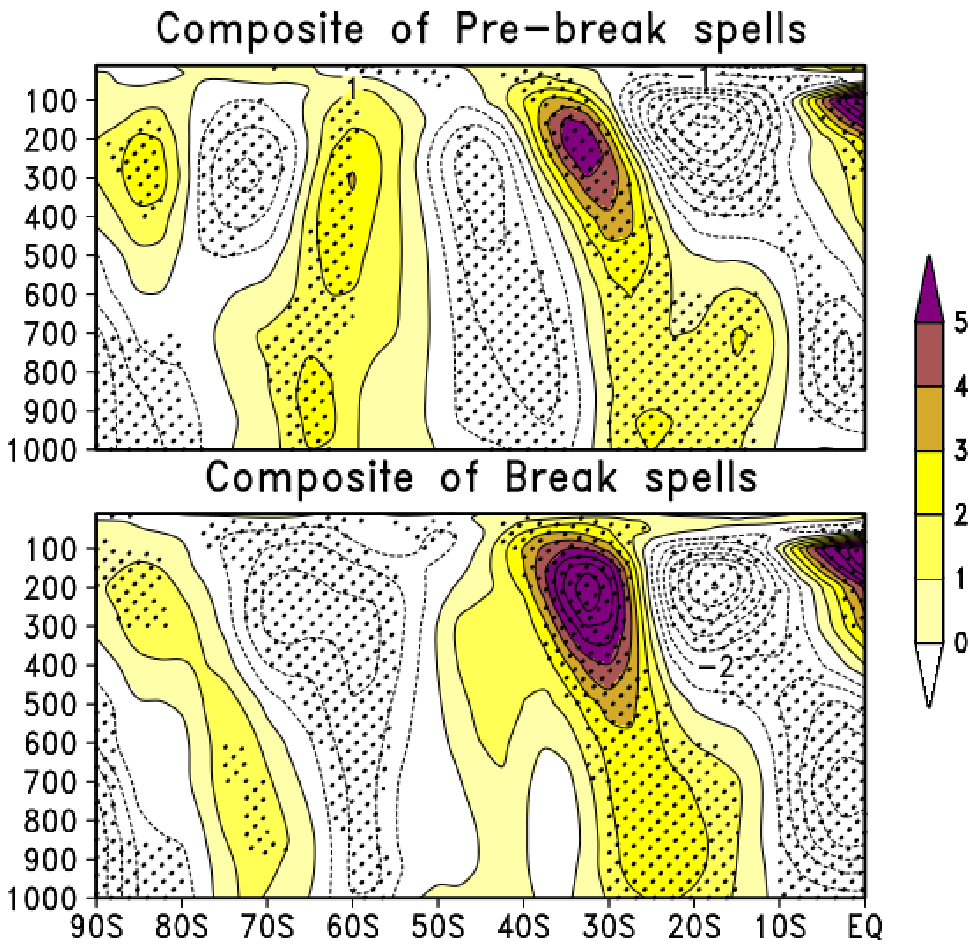

Figure 4.17: (a)(Top) Prebreak composite structure of U wind zonal anomalies of South American monsoon (Table 3) (m/s), **(b)(Bottom)** During-break composite structure of zonal wind anomalies of South American monsoon (m/s) (Table 3), which are zonally averaged between 60^0 W to 125^0 W. The hatched region indicates 95% confidence using a two-tailed Student's t test. In both the figures positive values are shaded and negative values are shown in contours. Contouring between -5 to 0 (m/s) with an interval of 1 m/s.

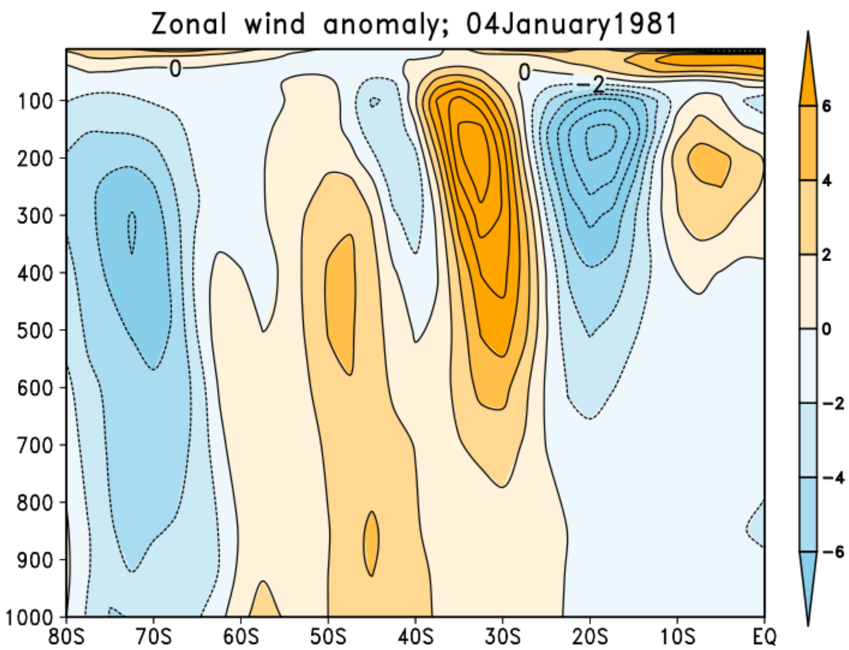

Figure 4.18: Structure of zonal wind anomaly on 4 January 1981, which is zonally averaged over 270^0 E-330^0 E.

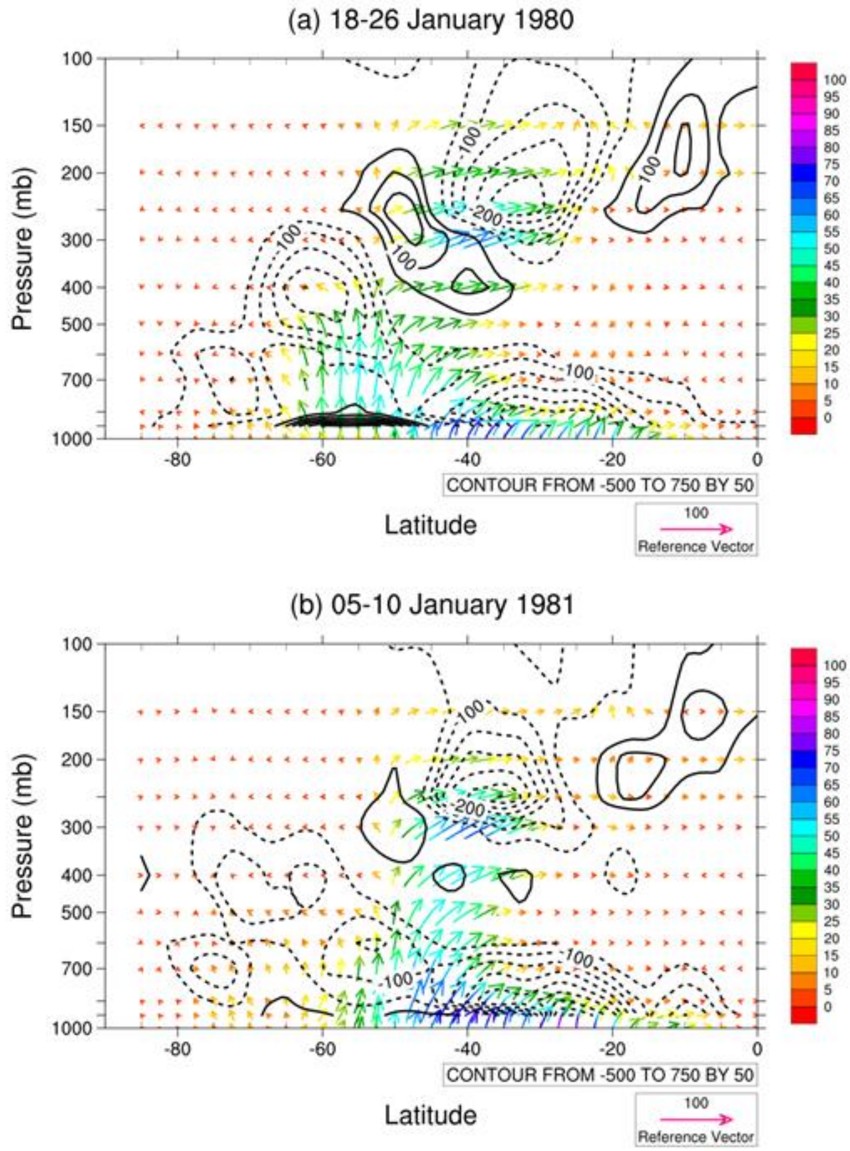

Figure 4.19: Eliassen Palm fluxes for **(a)** 18-26 July 1980 & **(b)** 05-10 July 1981. The dotted lines denote convergence and continues lines denote divergence and contouring at 50 m^3.

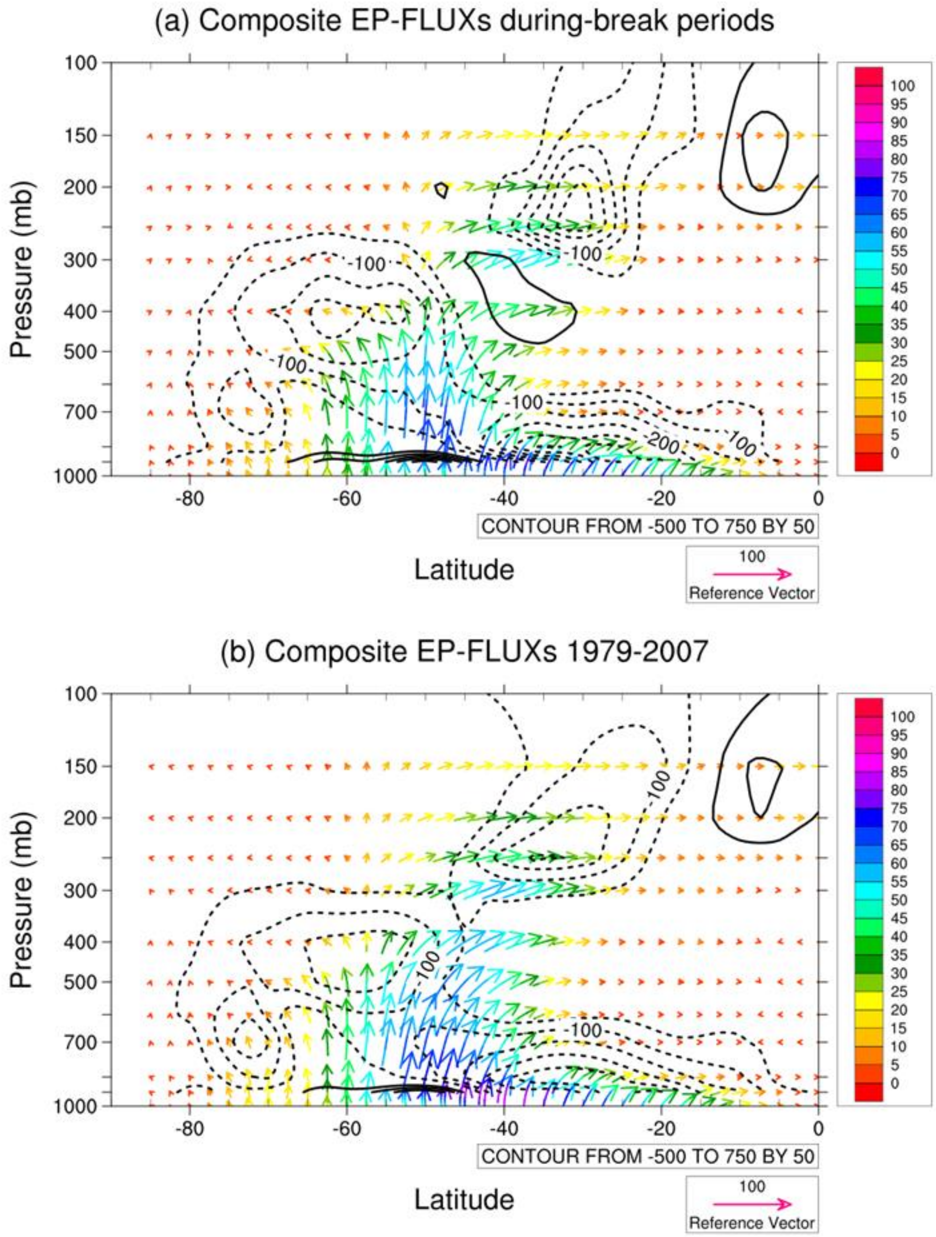

Figure 4.20: Eliassen -Palm flux cross-sections of southern hemisphere**(a)** Composite during-break periods (Table 2.4) of SAM; **(b)** during the season (austral summer) DJF for the 1979-2007 period. The contour interval is 50 m^3. In both the figures dashed lines represent convergence and continuous lines represent divergence.

4.4. Summary of the chapter

I observe a similar sequence of break monsoon characteristics as of the Indian summer monsoon, to those seen in the North and South American summer monsoon systems. These similar characteristics can be viewed as a global monsoon feature, in which extratropical eddies play a significant role in the common ground of the basic characteristics of the breaks in these three monsoons, namely, the ISM, SAM, and NAM. This is referred to as the unified theory.

The following chapter examines the revival of active conditions of rainfall after a break period over the core monsoon region of India during boreal summer.

Chapter 5

Understanding the revival of the Indian Summer Monsoon after Breaks

Outline of the chapter

In this chapter, I discuss a mechanism for reviving ISM after a typical break phase. This mechanism is associated with upperlevel barotropic instability caused by an increase of eddies in the mean zonal flow at 200 hPa, which spurs a subsequent synoptic low formation in the head of Bay of Bengal for the revival of ISM.

5.1 Introduction

In this chapter, I discuss the revival of active conditions of ISM after a break phase is facilitated by the formation of synoptic disturbances in the BoB, namely, monsoon depressions, and low pressure systems that travel toward the northwest from Bay of Bengal into the Indian region. For example, some of the previous studies discussing about the synoptic disturbance in the BoB for the active conditions over Indian region during boreal summer, Chen et al. 2005; Sikka and Dixit 1972; Boos et al. 2015; Sikka and Gadgil 1980.

From a dynamical standpoint, for example, Ramaswamy (1962) emphasise that the relevance of anomalous southward shift of large-amplitude westerly trough from the midlatitudes into the Indo-Pakistan region during ISM breaks. Importantly in a case study by Rao (1971), also documents a manifestation of barotropic instability associated with increased horizontal shear due to the southward shift of the westerly troughs in the subtropical westerly jet at the midtropospheric level in the aforementioned break event and a subsequent revival associated with the formation of a synoptic disturbance. Rao (1971) hypothesized that manifestation of the barotropic instability during break leads to the formation of disturbances that in turn invigorate the ISM an active phase. In a recent study, Krishnamurthy and Ajayamohan (2010) have shown that the absence of low pressure systems, such as lows, depressions, and cyclonic storms, represents the break phase and their presence represents an active phase of ISM. Therefore, the question remains whether instabilities generated by large-scale processes lead to subsequent revival of the monsoon through a barotropic instability mechanism and formation of a synoptic disturbance.

In this chapter, I attempt to answer this question. The availability of reanalysis datasets in the recent decades is a great opportunity in this sense. Analysis of multiple cases will also help us to refine any theoretically based thresholds and indices that represent a phenomenon. For example, theory (Kuo 1953; Starr and White 1954; Aihara 1959) suggests that barotropic instability occurs only in disturbances of very long wavelengths. The case study of a break monsoon Rao (1971) suggests that synoptic waves in the subtropical westerly jet in the Indian region with a wavelength greater than (less than) 3000 km are unstable (stable). We revisit this aspect in this study. We present our results and a discussion in section 5.2 & 5.3, followed by conclusions in section 5.4.

5.2 Barotropic instability in the aftermath of breaks

From the works of Starr and White (1954) and Rao (1971), I can suppose that such a break condition will result in barotropic instability, which may in turn manifest as a synoptic disturbance for the revival of ISM. In this context, from Table 2.2, following Rajeevan et al. (2008), we list the dates of various postbreak revival events of ISM. Of the 41 total break events (Table 5.1), 18 revivals occurred with the formation of low pressure in the Bay of Bengal (e.g., Fig. 5.1) and 7 others with the formation of low pressure on land (figures not shown). This result suggests that about 61% of the postbreak revivals are associated with formation of low pressure in the Bay of Bengal or land regions, providing a general support to the hypothesis of Rao (1971) and Raghavan (1973).

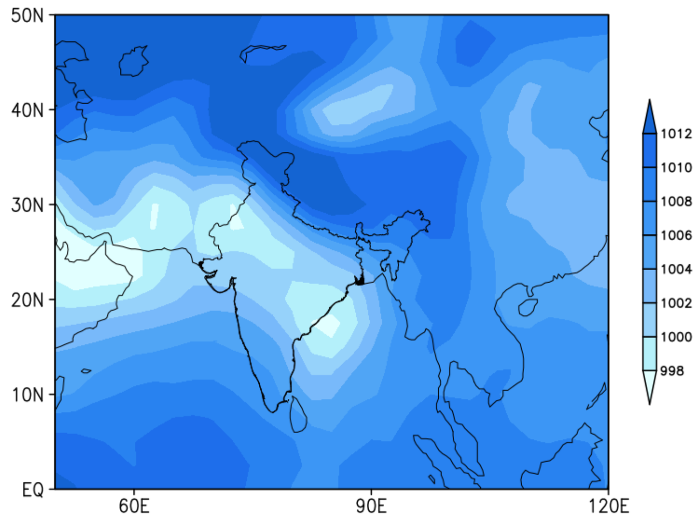

Figure 5.1: Observed Sea Level Pressure (SLP) distribution on 10 Aug., 2000, after a break period.

Table 5.1: Gives the formation of a synoptic disturbance on the particular day after every break event during the 1979-2007 period. ' *** ‘represents the revival of ISM without low formation.

Year	Low formation day after every break event	Condition
1979		***
1979		***
1980	23 July	Bay of Bengal
1980	26 August	Bay of Bengal
1981		***
1982	19 July	Bay of Bengal
1983	4 August	Bay of Bengal

1984	30 July	Bay of Bengal
1985	28 August	Bay of Bengal
1986	9 September	Bay of Bengal
1987	11 August	Land Region
1987	19 August	Bay of Bengal
1988		***
1989	2 August	Bay of Bengal
1989	16 August	Bay of Bengal
1992	18 July	Land Region
1993		***
1993		***
1993	6 September	Bay of Bengal
1995		***
1995		***
1996		***
1997	22 July	Bay of Bengal
1997	16 August	Bay of Bengal
1998	1 September	Land Region
1998	29 July	Land Region
1999		***
1999		***
1999		***
2000	10 August	Bay of Bengal

2001	6 August	Bay of Bengal
2001	11 September	Land Region
2002		***
2002	1 August	Bay of Bengal
2004		***
2004	26 July	Land Region
2004		***
2005	11 September	Bay of Bengal
2005	19 August	Land Region
2007		***
2007	18 August	Bay of Bengal

Now, eddy formation due to barotropic instability would necessitate a conversion of the into, as shown by equation (2.3). Indeed, this is true in 30 out of the 41 cases (i.e., 73% of postbreak revival events), as evidenced by the positive values of rate of conversion of mean kinetic energy to eddy kinetic energy (CMKE) (Table 3) (Fig. 5.2). This indicates that the barotropic instability is the primary possible large-scale dynamical instability mechanism during the ISM breaks, many times leading to the formation of synoptic eddies. Another way to ascertain this further is by checking that there exists a significant negative correlation between the CMKE and wavelength, an indication of barotropic instability (e.g., Rao 1971). We find a strong correlation of −0.285 (Table 5.2), which is significant at 95% confidence level from a student's two-tailed t test. This significant correlation confirms that barotropic instability is indeed manifested after the monsoon break events and is a necessary condition for the revival of Indian summer monsoon after break conditions.

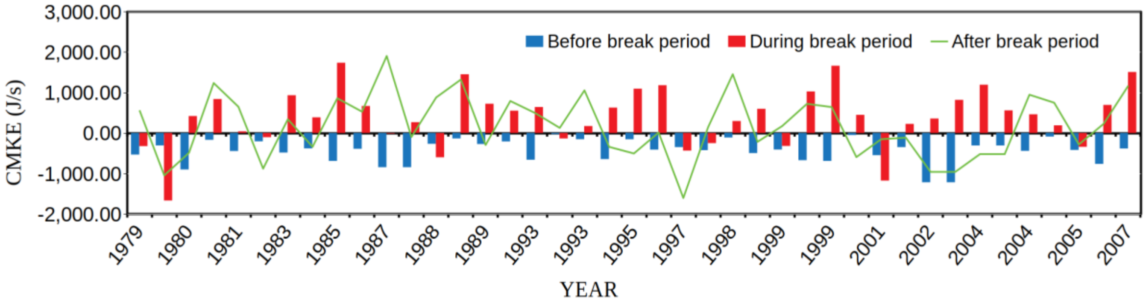

Figure 5.2: Conversion of Kinetic Energy (J/s) anomaly values of 41 break periods during the 1979-2007 period.

Table 5.2: Conversion of Mean Kinetic Energy Values (Joule/second) at 200 hPa.

Year	Pre- break period	Break period	After-break period
1979	-533.85	-324.67	568.11
1979	-307.49	-1668.31	-1040.26
1980	-902.14	419.32	-483.19
1980	-168.76	838.84	1241.05
1981	-445.01	41.06	654.83
1982	-206.31	-104.81	-873.12
1983	-483.50	932.99	345.91
1984	-381.30	386.58	-334.05
1985	-691.33	1736.20	864.34
1986	-391.23	667.50	533.51
1987	-845.24	-15.09	1909.51

1987	-845.24	266.40	-92.27
1988	-267.84	-600.93	884.11
1989	-134.70	1450.52	1326.88
1989	-272.84	722.94	-289.01
1992	-209.65	551.18	796.84
1993	-662.03	641.99	500.70
1993	-27.15	-134.37	132.38
1993	-154.66	171.96	1059.52
1995	-645.48	627.13	-336.83
1995	-155.81	1094.81	-499.51
1996	-410.98	1179.61	18.84
1997	-348.92	-435.35	-1599.46
1997	-424.11	-249.73	147.87
1998	-111.57	296.10	1457.89
1998	-496.43	597.56	-211.52
1999	-409.16	-320.18	178.70
1999	-671.99	1026.46	727.02
1999	-691.03	1662.09	646.58
2000	-51.00	447.82	-588.90
2001	-547.99	-1176.18	-147.23
2001	-348.58	224.42	-108.66
2002	-1218.62	357.86	-950.32
2002	-1218.62	818.58	-950.32

2004	-309.27	1192.99	-520.30
2004	-309.27	558.93	-520.30
2004	-442.18	462.54	952.01
2005	-88.06	188.81	754.90
2005	-418.94	-341.93	-275.85
2007	-763.64	693.70	231.90
2007	-384.59	1507.19	1175.04

What is the potential mechanism for such manifestation of barotropic instability in these subseasonal events? As is known, barotropic disturbances derive energy from the mean kinetic energy. Energy considerations (e.g., Kuo 1951) show that for a disturbance to grow, it must tilt in a direction opposite to that of the meridional gradient of zonal wind. To be specific, a tilt from southwest to northeast (SW–NE) in a westerly zonal flow will meet this criterion. That is, waves with an SW–NE tilt will result in a maximum vorticity to the south [see (3), which is from Kuo (1949)]. Fig. 5.3 (a-e) shows the zonal wind at 200 hPa of 41 break periods during the 1979-2007 period and Fig. 5.4 (a-e) shows the zonal wind on a peak day of the 41 break periods for the 1979-2007 period. Whereas, figures 5.3 and 5.4, it is seen most of the break days are also indeed associated with such an SW–NE tilt in the 200-hPa zonal flow. Such a tilt in the mean 200-hPa subtropical westerly jet over the Indian region on a typical break day (see Fig. 5.5a as an example, along with the corresponding geopotential field in Fig. 5.5b) is associated with a northward transfer of westerly momentum (Kuo 1949). In such a case, the zonally averaged eddy momentum transport will be positive and is, importantly, conducive to the formation of an eddy disturbance (Fig. 5.6a) associated with maximum vorticity to its south (Kuo 1949). Truly, the corresponding zonal wind structure at 200 hPa shows a southward shift of the westerly jet during the break period and a northward shift of the tropical easterly jet (Fig. 5.6b).

(a)

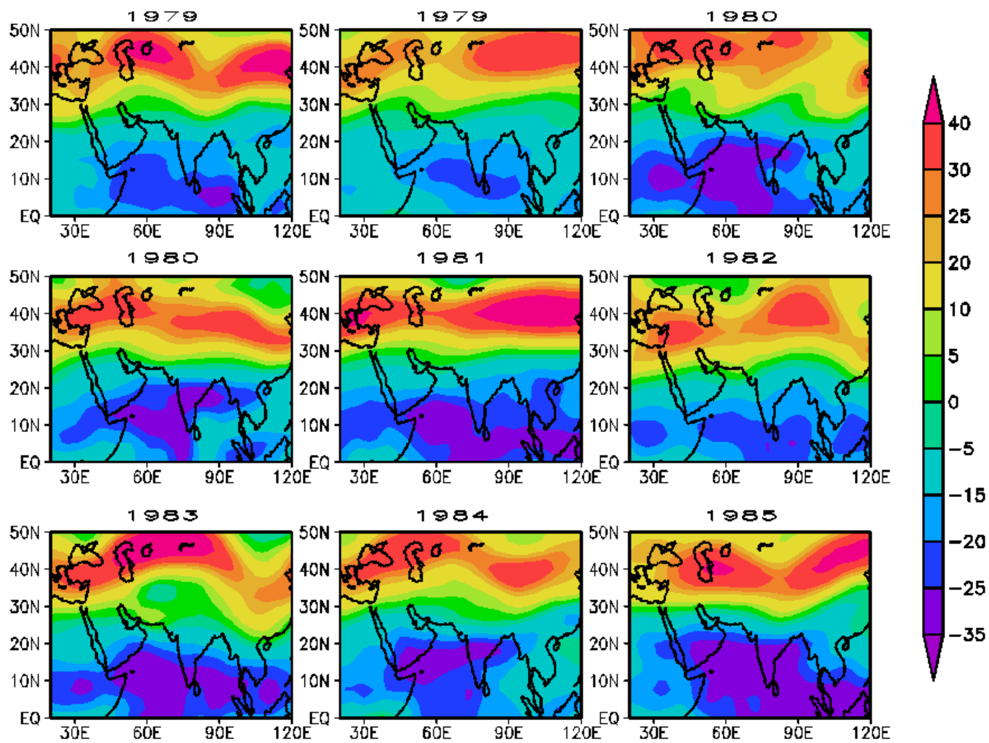

(b)

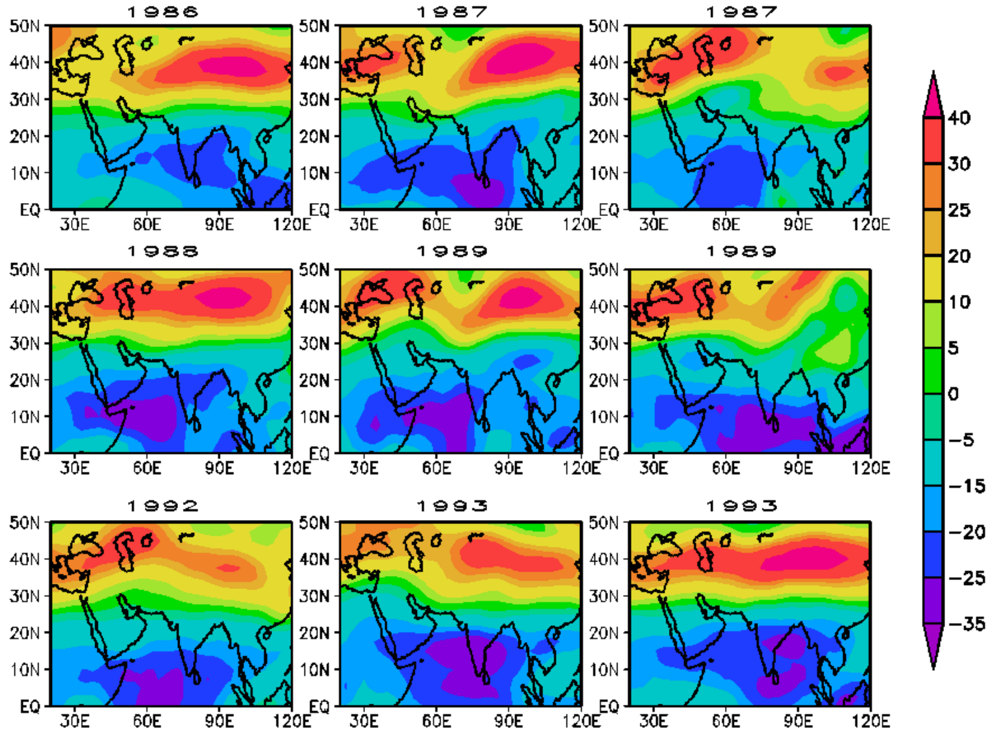
1986
1987
1987
1988
1989
1989
1992
1993
1993
50N
40N
30N
20N
10N
EQ
30E
60E
90E
120E
40
30
25
20
10
5
0
−5
−15
−20
−25
−35

(c)

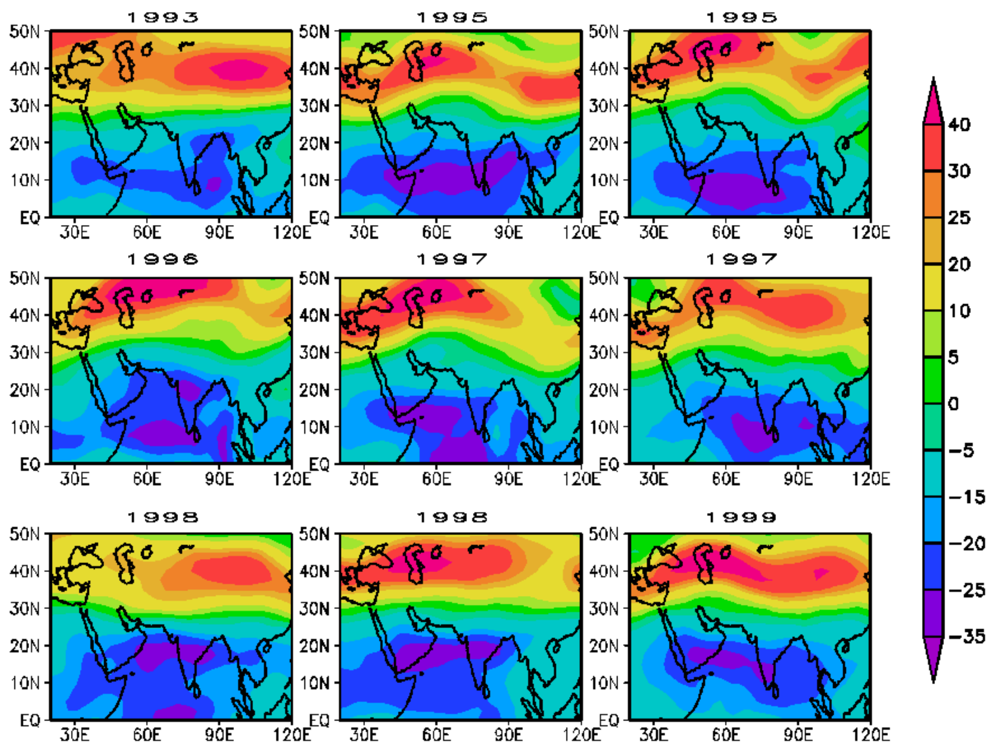
1993
1995
1995
1996
1997
1997
1998
1998
1999
50N
40N
30N
20N
10N
EQ
30E
60E
90E
120E
40
30
25
20
10
5
0
−5
−15
−20
−25
−35

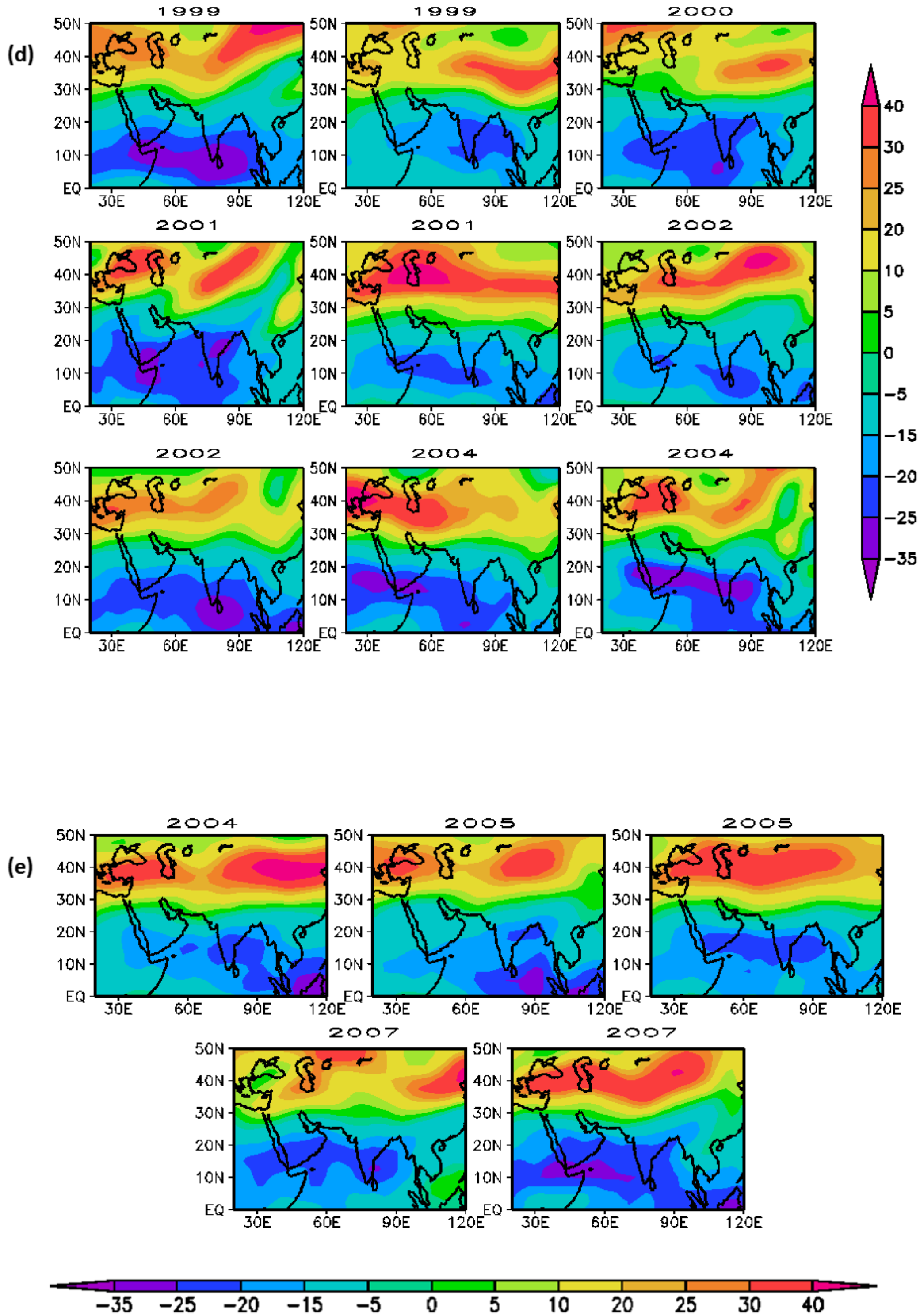

Fig. 5.3 (a-e): Spatial distriubution of zonal wind at 200 hPa for 41 break events (Rajeevan et al. 2008) during the 1979–2007 period for the region 0°–50°N, 20°–120°E.

(1)

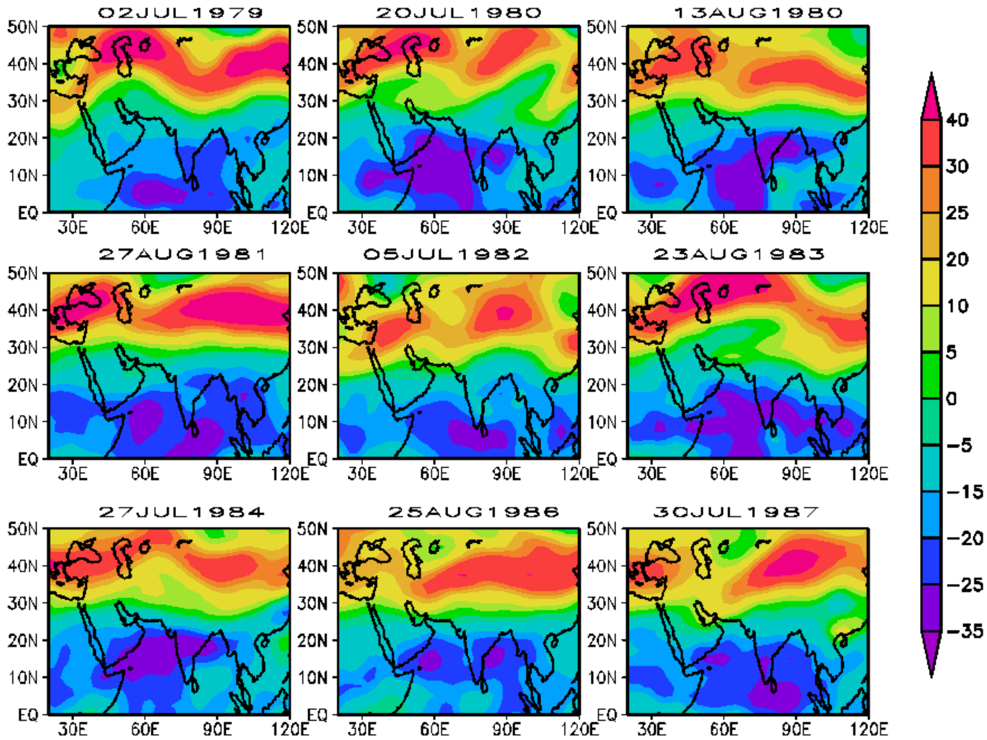
02JUL1979
20JUL1980
13AUG1980
27AUG1981
05JUL1982
23AUG1983
27JUL1984
25AUG1986
30JUL1987
50N
40N
30N
20N
10N
EQ
30E
60E
90E
120E
40
30
25
20
10
5
0
−5
−15
−20
−25
−35

(2)

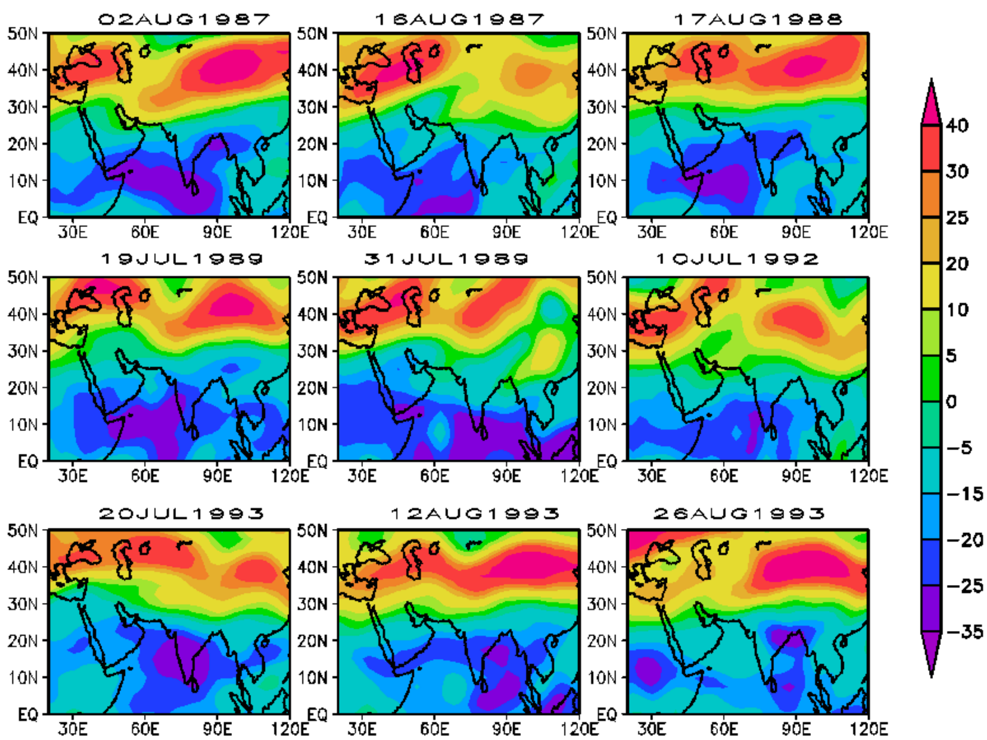
02AUG1987
16AUG1987
17AUG1988
19JUL1989
31JUL1989
10JUL1992
20JUL1993
12AUG1993
26AUG1993
50N
40N
30N
20N
10N
EQ
30E
60E
90E
120E
40
30
25
20
10
5
0
−5
−15
−20
−25
−35

(3)

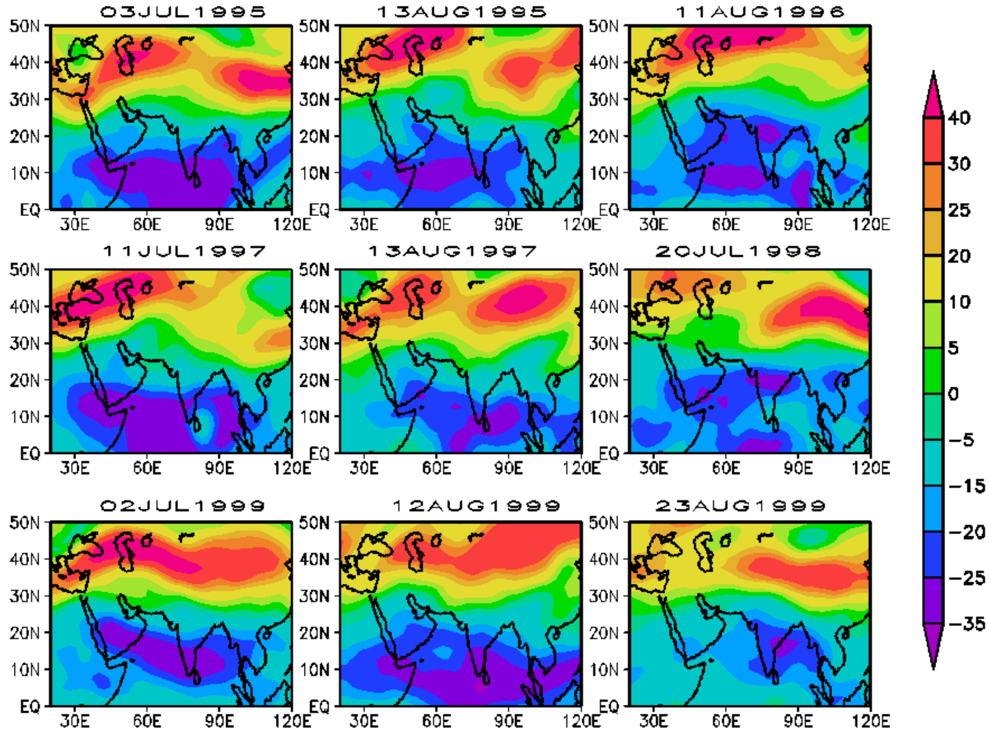
03JUL1995
13AUG1995
11AUG1996
11JUL1997
13AUG1997
20JUL1998
02JUL1999
12AUG1999
23AUG1999
50N
40N
30N
20N
10N
EQ
30E
60E
90E
120E
40
30
25
20
10
5
0
−5
−15
−20
−25
−35

(4)

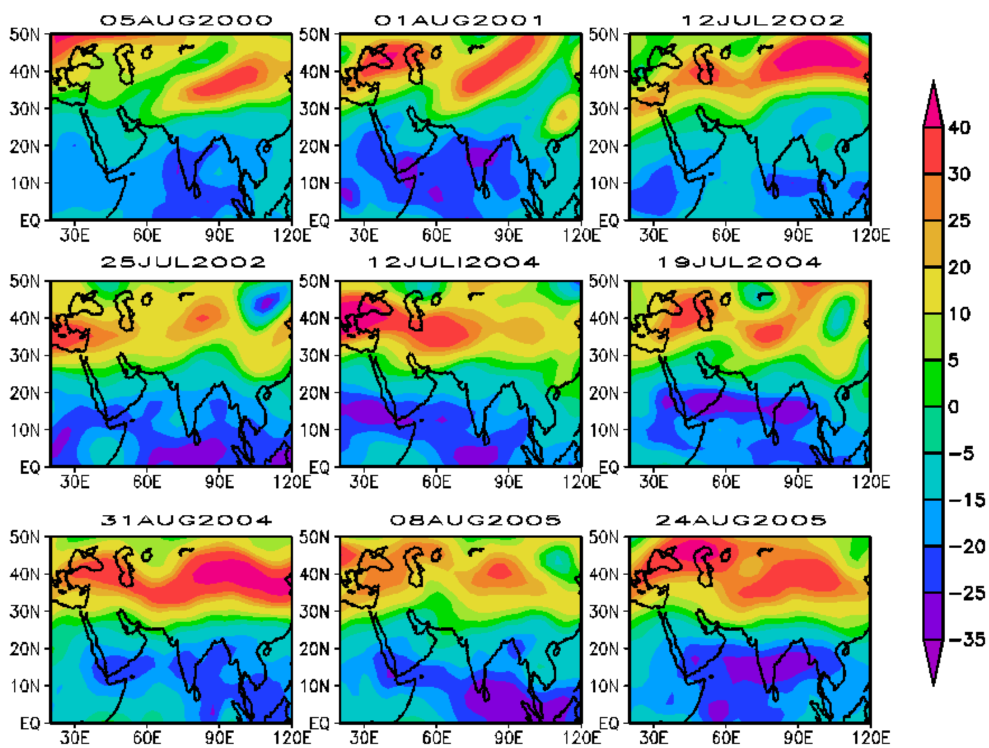
05AUG2000
01AUG2001
12JUL2002
25JUL2002
12JULI2004
19JUL2004
31AUG2004
08AUG2005
24AUG2005
50N
40N
30N
20N
10N
EQ
30E
60E
90E
120E
40
30
25
20
10
5
0
−5
−15
−20
−25
−35

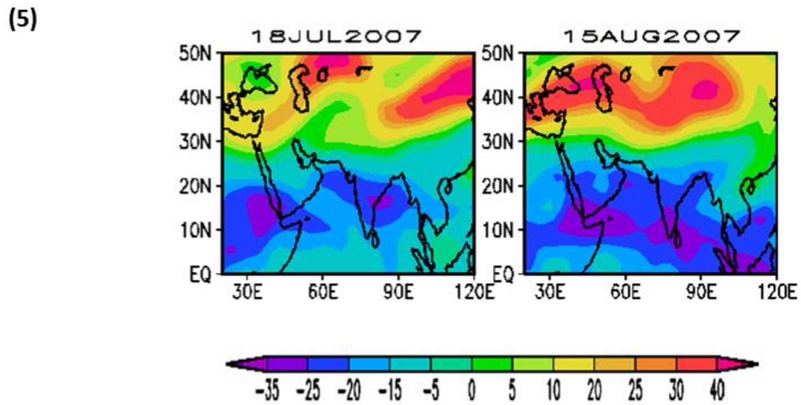

Fig. 5.4 (a-e): Spatial distribution of zonal wind on a peak days of of 41 break events (Rajeevan et al. 2008) during the 1979–2007 period for the region 0°–50°N, 20°–120°E.

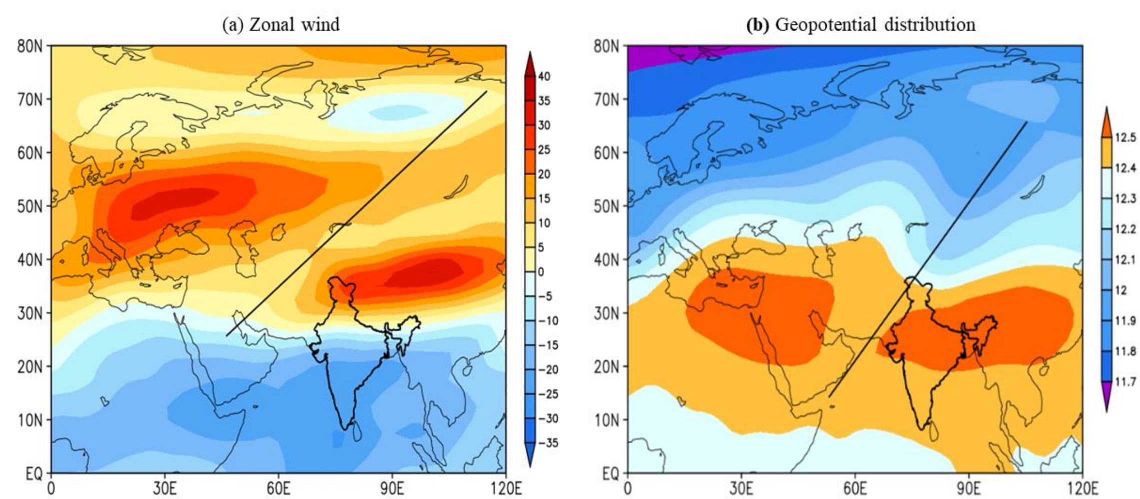

Figure 5.5: (a) Zonal wind at 200hpa on 4august, 2000, a typical break day; **(b)** the corresponding Geopotential distribution (in Km). The black line shows the NE-SW tilt orientation in both the figures.

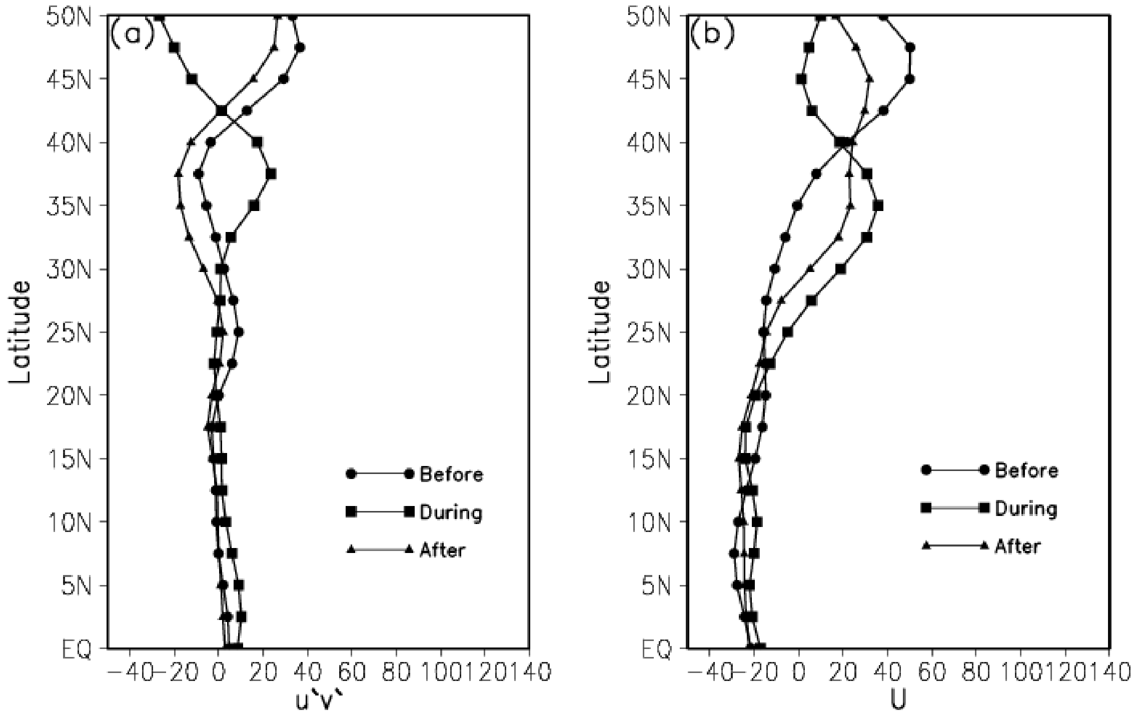

Figure 5.6: (a) Eddy momentum flux transfer during a break (1-9 August); before the break (14-23 July); and after the break (10-15 August), in relation to the 1-9 August break in the year 2000. **(b)** zonal wind profiles (82.5° E) at 200hpa during a break day (4th August); on a day in the prebreak period; (23rd July); on a after-break day (11th August), all for the same event presented in Fig. 5.6(a).

From the point of Rao (1971), it will be instructive to verify that the barotropic instability is a mechanism that would help the aforementioned eddies grow in such situations. To that end, the meridional vorticity distribution of the absolute vorticity ζ in the Indian region composite of during break events is presented in Fig. 5.7a, along with the corresponding all the break events in Fig. 5.7b. Importantly, we see maximum or minimum in absolute vorticity ζ around 29°N in the composite, with the individual values varying between 25° and 30°N. Manifestation of such maximum or minimum values is a necessary condition for the barotropic instability (Kuo 1951) from the individual case also indicates such manifestation (Fig. 5.7b). All this highlights the importance of the mean seasonal zonal wind structure, with westerlies to the north and easterlies to the south of the Indian subcontinent, in facilitating such a dynamical instability manifested by the breaks.

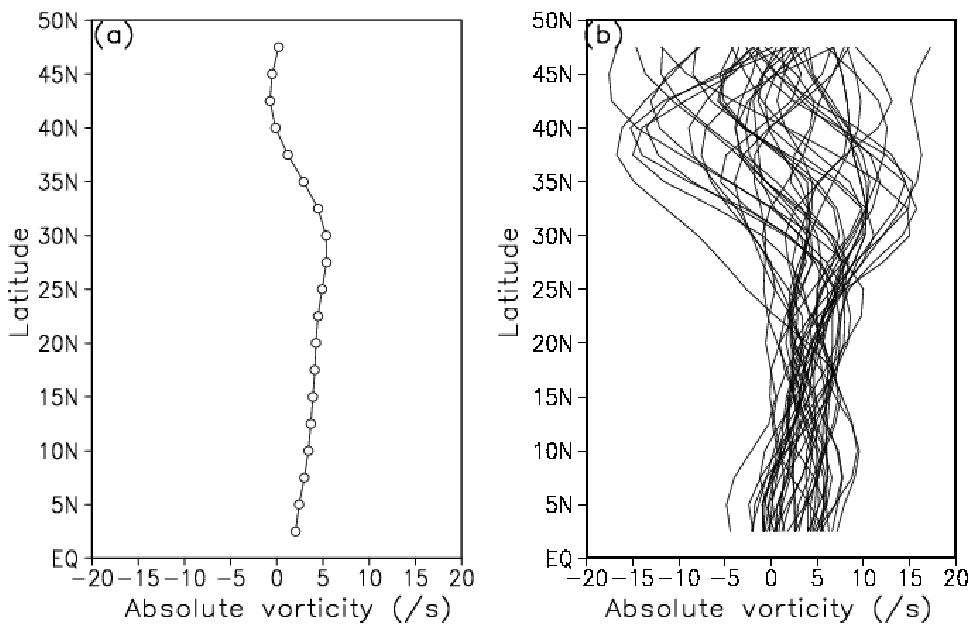

Figure 5.7: (a) Meridional distribution of the composite absolute vorticity (200 hPa), obtained by compositing it over all the break periods for the period of 1979-2007. **(b)** Same as Fig. 5.7(a) but composited over each break periods during 1979-2007.

<u>5.3 Wavelength threshold for manifestation of a postbreak synoptic disturbance</u>

Ramaswamy (1962) and Rao (1971) claim from their individual case studies a decrease in channel width (D/2) between subtropical westerly and tropical easterly jets that manifest as a dynamical instability. We revisit this aspect by computing the D/2 during the break events in the study period.

Our results (Table 5.3 and Fig. 5.8) show that 32 out of 41 break events (78%) indeed show a decrease in channel width. From this, we can deduce that a dynamical instability during the breaks is facilitated either as a result of a transient southward shift of the westerlies over the northern portions of the subcontinent and/or a transient northward shift of the tropical easterly jet stream over the peninsular region. Such a decrease in the channel width in the zonal width can also manifest with a weakening (strengthening) of the upper-level westerlies (easterlies) in the Indian region.

Table 5.3: The channel width (D/2) between the subtropical westerly jet and tropical easterly jet (°) at 200 hPa for 41 break periods during the 1979-2007 period.

Year	Prebreak period	Break period	After-break period
1979	35.43	28.25	26.11
1979	31.00	30.00	34.50
1980	42.25	37.25	34.83
1980	28.88	23.67	31.83
1981	35.00	31.75	34.29
1982	29.88	25.63	34.43
1983	33.29	35.33	36.38
1984	30.63	22.67	43.00
1985	31.00	20.00	36.14
1986	33.57	26.00	26.25
1987	26.10	29.83	22.67

1987	32.14	29.33	39.14
1988	38.00	32.75	30.83
1989	26.43	28.00	43.29
1989	48.86	40.20	44.00
1992	31.22	28.88	39.63
1993	30.43	25.75	42.43
1993	33.86	22.29	31.43
1993	30.14	28.57	38.43
1995	34.57	26.80	37.71
1995	35.29	28.67	37.83
1996	37.38	39.00	37.83
1997	41.71	39.20	34.29
1997	34.43	30.83	41.00
1998	29.00	23.00	30.67
1998	24.29	23.14	35.43
1999	24.43	25.80	26.14
1999	39.57	35.80	25.86
1999	31.43	20.50	39.43
2000	34.63	28.89	37.33
2001	25.43	26.33	37.43
2001	34.00	29.40	29.57
2002	29.86	31.43	38.86
2002	29.86	30.82	38.86

2004	28.13	32.25	40.20
2004	28.13	23.67	40.2
2004	29.70	23.33	31.00
2005	31.86	24.25	38.63
2005	32.71	33.63	34.86
2007	25.38	25.20	29.43
2007	37.57	37.00	40.57

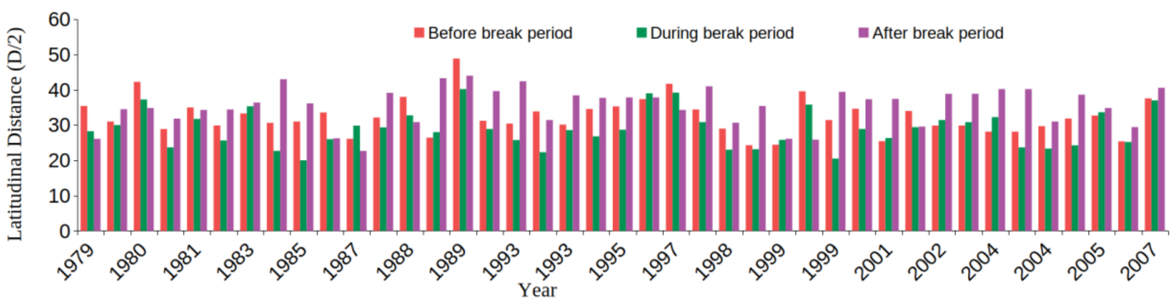

Figure 5.8: Latitudinal distance (degrees) between westerlies and easterlies at 200 hPa for various phases associated with observed break events.

Theory (Kuo 1953; Syōno and Aihara 1957) shows that barotropic instability occurs only in zonal waves of wavelength shorter than a critical wavelength L_c [see chapter 2]. Rao (1971), from his sole case study, estimates L_c of the upper-level westerly jet stream in the Indian region to be ~3000 km. However, given that it was only a single case and the relatively poor quality of the upper-air data during that period, we use the reanalyzed gridded datasets for multiple monsoon break cases to revisit this important finding by Rao (1971). Our analysis using (1) (Table 5.4) shows that (i) wavelengths in the upper-level westerlies north of Indian region during the summer monsoon reach a minimum value during breaks as compared to a few days prior to and after the event and (ii) the critical mean value of the aforementioned wavelength, obtained by averaging it over all break events, is 7411 km. The minimum Lc we find is just 5127 km (Fig. 5.9).

Table 5.4: Critical wavelength (L_c Km) for prebreak, break and after-break periods.

Year	**Prebreak period**	**Break period**	**After-break period**
1979	9082	7310	6693
1979	7947	7690	8844
1980	10831	9549	8929
1980	7402	6067	8160
1981	8972	8139	8789
1982	7658	6569	8826
1983	8533	9057	9324
1984	7851	5810	11023
1985	7947	5127	9265
1986	8606	6665	6729
1987	6691	7648	5810
1987	8240	7519	10034
1988	9741	8395	7904
1989	6775	7178	11096
1989	12524	10305	11279
1992	8004	7402	10158

1993	7800	6601	10876
1993	8679	5713	8057
1993	7727	7324	9851
1995	8862	6870	9668
1995	9045	7349	9698
1996	9581	9997	9698
1997	10693	10049	8789
1997	8826	7904	10510
1998	7434	5896	7861
1998	6225	5933	9082
1999	6262	6614	6702
1999	10144	9177	6628
1999	8057	5255	10107
2000	8876	7405	9570
2001	6518	6750	9595
2001	8716	7536	7580
2002	7654	8057	9961
2002	7654	7900	9961
2004	7210	8267	10305
2004	7210	6067	10305
2004	7613	5981	7947
2005	8166	6216	9901
2005	8386	8620	8935

2007	6505	6460	7544
2007	9631	9485	10400

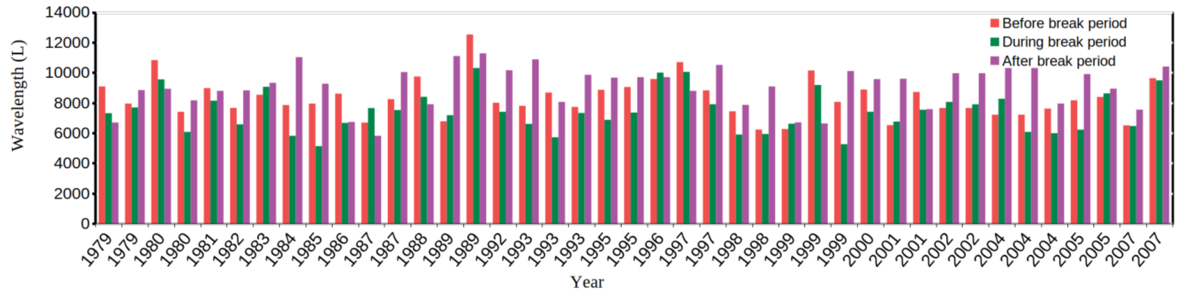

Figure 5.9: Wavelength anomalies (Km) of the zonal wind at 200 hPa, averaged over the span of each break event

5.4 Summary of the chapter

In this chapter, using the atmospheric circulation datasets from the NCEP–NCAR Reanalysis 2 (Kanamitsu et al. 2002) for the period 1979–2007, I explore the potential role of monsoon break conditions in subsequent revival of the monsoon through formation of a synoptic disturbance in the Indian region. I find that barotropic instability manifests in the Indian region during monsoon breaks in 61% of the cases. Such a revival is found to be associated with a reduction of the zonal width between the upper-level subtropical westerlies and tropical easterlies. Further, the anomaly correlation between the wavelength of zonal winds in the Indian region and the local rate of conversion of mean kinetic energy values for the study period is −0.285, statistically significant at 95% confidence level, which confirms the role of barotropic instability for formation of the post break synoptic disturbance. During the monsoon break period there is no rainfall over most of the country, and therefore the succeeding disturbances are not generated by the condensational heating. Thus, the argument that generation of monsoon depressions and synoptic disturbances due to the break-induced barotropic instability is reasonable. I also find that the mean wavelength of westerlies during boreal monsoon events north of the Indian region, which leads to the revival of the monsoons, is about 7400 km. While Rao (1971) suggests a threshold wavelength of 3000 km from his single case study, my analysis of the 41 cases (adopted from Rajeevan et al. 2008) suggests an apparent threshold to be above 5000 km.

The following chapter accesses the revival of active conditions of rainfall after a break period over the core monsoon region of India during boreal summer using the WRF model.

Chapter 6

Assessment of a dynamical mechanism for the revival of active summer rainfall conditions over India following a break phase

Outline of the chapter

This chapter mainly focuses on various WRF model sensitivity experiments, which I have carried out to confirm the active role of the dynamical mechanism for the revival of active monsoon after a break phase, as proposed in Chapter 5. In this regard, we have carried out a variety of simulations to see the sensitivity of the simulated break to active transition to changes in the various meteorological parameters.

6.1 Introduction

Chapter 5 proposes, using nearly 30-years of reanalysis data, that, the monsoon revival after a break is caused by the barotropic instability of the zonal current. They found that during the peak of monsoon break, the tropical Easterly Jet, which is normally located around 9° N, invariably shifts northward. Also, the Subtropical Westerly Jet normally located around 40° N, shifts southward. These meridional shifts in the position of the jet streams increase the zonal wind shear, which results in the generation of barotropic instability. This instability results in the formation of a synoptic disturbance at least in about 61% of the cases, thereby reviving to the active monsoon phase.

To ascertain that the formation of barotropic instability associated with the closing of jet streams is indeed important for the subsequent revival of the monsoon, we have carried out few sensitivity experiments using the Weather Research and Forecasting (WRF) model version 3.8 (Skamarock et al., 2008) for a typical break case. The results are discussed in this chapter. We also verify the role of convection is also important in this process.

In the next section 6.2, I provide a description of the model configuration detailed experimental setup, and other datasets used in this study. I discuss the experimental results in section 6.3 and finally provide conclusions in the last section 6.4.

6.2 WRF model description and sensitivity experiments performed

The WRF model version 3.8 is a mesoscale numerical weather prediction system. It has both hydrostatic and non-hydrostatic options with the latter needing a fully compressible condition. The model has a sigma coordinate system designed for atmospheric research and operational forecasting needs. Several studies have been used this regional model to study the monsoon problems from weather scale (e.g., Srinivas et al., 2017; Mohanty, Rao, 2014), intra-seasonal variability of ISM (e.g., Taraphdar et al. 2010; Kolusu et al., 2014; Chen et al., 2018), and even the relevance of interannual variations and background changes for extreme rainfall events (e.g., Boyaj et al., 2017, 2020). Various authors used the WRF model to successfully simulate and diagnose the break monsoon over the Indian region. For example, Taraphdar et al., (2010) used the WRF model to estimate the predictability of active and break phases of ISM from 2001 to 2009. Taraphdar et al., (2010) reported that the predictability is more for the break phases than the active phases of the monsoon over the Indian region.

We configured the model with two nested domains at 60 and 20 km horizontal resolutions, and 30 vertical levels. The mother domain covers the large-scale region encompasses 20°S-60°N, 10°E-160°E, the and nested domain 0°-50°N, 40°E–120°E region (Fig. 6.1). The selected physics options follow those of Rao et al. (2014), Boyaj et al., (2020), given that the simulation is mainly for the Indian region. Some of the physics schemes chosen are shown in Table 6.1.

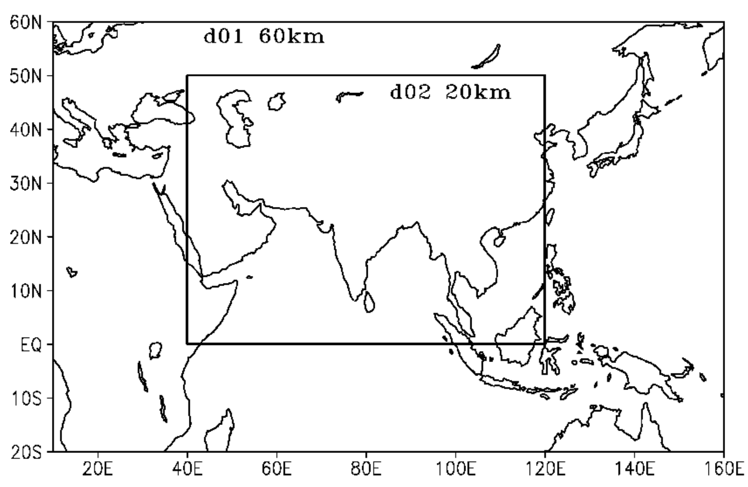

Figure 6.1: Schematic figure of the WRF model domain chosen, two nested domains of 60 and 20 km horizontal resolutions, and 30 vertical levels. The mother domain covers the large-scale

region encompasses 20°S-60°N, 10°E-160°E, the and nested domain 0°-50°N, 40°E–120°E region.

Table 6.1: List of physics schemes/parametrizations used in the sensitivity experiments of WRF model

Sr. No.	Physics schemes	Citation
1	Goddard Ensemble scheme for microphysics	Tao et al., 2016
2	Short-wave radiation scheme	Dudhia et al., 1989
3	Rapid Radiation Transfer Model (RRTM) for long-wave radiation	Mlawer et al., 1997
4	Yonsei University (YSU) non-local scheme	Hong et al., 2006
5	Planetary boundary layer and NOAH scheme	Tewari et al., 2004
6	The Kain-Fritsch (KF) scheme	Kain, 2004

The initial and lateral boundary meteorological conditions for the model are obtained from the National Centers for Environmental Prediction-Final Analysis (NCEP-FNL) data, available for every six hours at 1°x1° horizontal resolution (NCEP, 2000). From the break case we selected, from those suggested by Rajeevan et al. (2010), is from 1August to 9August, 2000 (hereafter referred to as B2000).

The experiments carried out in this study using the WRF model are tabulated below (Table 6.2). We have carried out three experiments. In all the experiments, the model simulation spans from 01 to 15 August 2000, and the model initial boundary conditions start at 0000 UTC on 01 August 2000. In all the experiments, the lower boundary conditions are obtained from NCEP-FNL data.

The first experiment is what we refer is the control experiment (hereafter CTL). In this experiment, the lateral boundary conditions (LBC) for the outermost domain are adapted from the NCEP-FNL datasets. The second experiment is referred as the Daily Climatological Winds (hereafter DCW) experiments, respectively (Table 6.2). The DCW experiment is similar to that as the CTL, except that the LBCs are from the daily NCEP reanalysis-II climatological winds (generated 1980 to 2000). The third experiments are similar to DCW experiments, except that the convection scheme is switching off (DCWNC).

Table 6.2: A list of Experiments carried out using WRF model.

Sr. No.	Brief experiment details	Acronym
1	Real simulation using NCEP-FNL data as LBC’s, from 31 July to 15 August 2000	CTL
2	Same as CTL but the experiment is forced with daily climatology of NCEP-II reanalysis zonal and meridional winds (1980-2000) as initial conditions.	DCW
3	Same as DCW experiment with the cumulus convection scheme switched off	DCWNC

6.3 Results and Discussion

6.3.1 Wavelength characteristics and energetics exchange for the revival of active conditions over India

We recall from chapter 5 that the critical wavelength (L_c) above which barotropic instability can occur during monsoon breaks is equal to or greater than ~5000 km. The L_c for the B2000 break event from the NCEP/NCAR reanalysis II is 7405 km (Table 6.3). During the break, the average latitudinal distance between the two upper level jets was 30°. The corresponding values simulated in the CTL experiment with latitudinal distance of 30º, and L_c of 7690 km, which are well in agreement with the values from the NCEP-II reanalysis. The DRW experiment simulates a significant latitudinal distance between the SWJ and TEJ during the B2000 break event, particularly in comparison to NCEP II reanalysis data. Interestingly, the latitudinal distance simulated in the DRW is 24º. We believe that the relatively better results from the CTL simulation, compared to the NCEP II reanalysis data, whereas the FNL data sets are relatively coarser. Furthermore, all of the experiments show L_c values greater than the average (~5000 Km), indicating that there is a basis for barotropic instability at 200 hPa.

Table 6.3: Latitudinal distance (D/2) (°) and Critical wavelength (L_c) (Km) during the break period B2000 in the NCEP II reanalysis data and conducted sensitivity experiments.

Year	**Lat. Dist. (°), B2000**	**Wavelength (Km), B2000**
NCEP II reanalysis	**29**	**7405**
CTL	30	7690
DCW	32	8203
DCWNC	31	8175

As discussed so far, horizontal atmosphere, the barotropic instability develops due to an increase in horizontal shear of the zonal flow. From the context of Lorenz cycle (1955), this involves the conversion of mean kinetic energy to eddy kinetic energy of the zonal flow, a term we represent by C_k. In this context, in Fig. 6.2, I illustrate the evolution of the C_k at 200 hPa over the CMR through the break phase B2000 from the NCEP II reanalysis as well as that from all the simulation experiments. Its evolution from the NCEP reanalysis suggests a significant fall in the C_k during 1-5 August, 2000 in association with the peaking of the break, after which its magnitude increases; it peaks on 8 August. The CTL experiment also broadly captures the general weakening phase and its intensification later. The DCW and DCWNC experiments, which are forced with daily climatological winds do not simulate the fall in the C_k well. On the other hand, Fig. 6.2 also shows that the evolution of the C_k from the simulation is qualitatively reasonable.

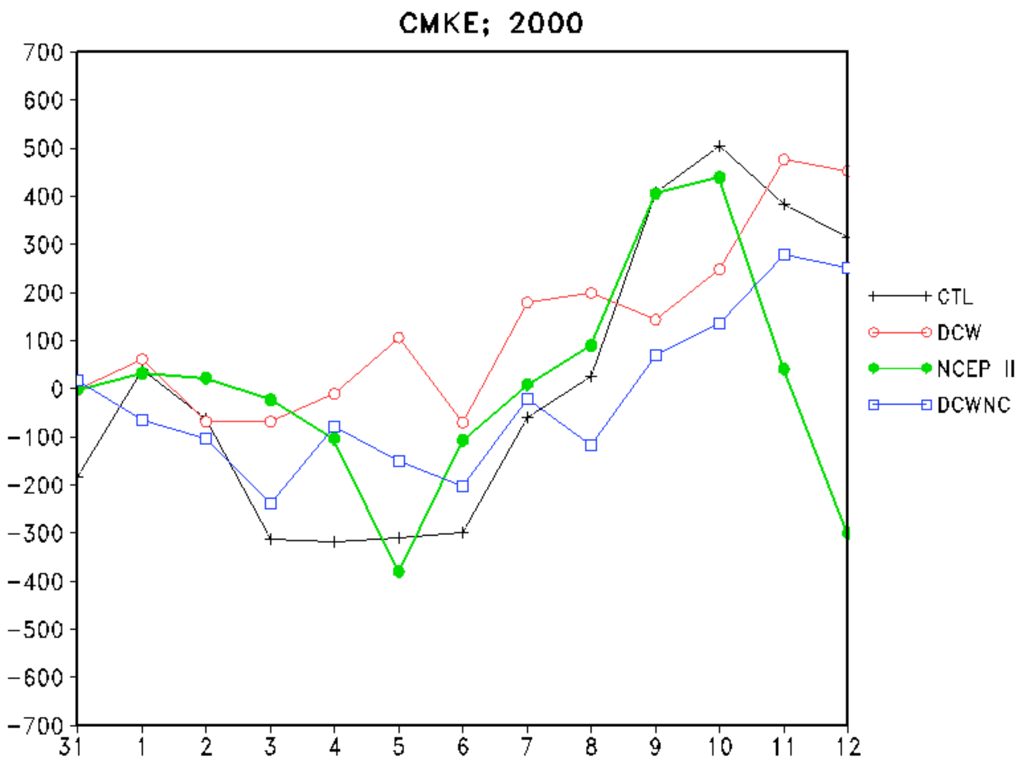

Figure 6.2: Daily mean C_k, the rate of conversion of mean kinetic energy to eddy kinetic energy (J/s) during break event from 31 July-09 August 2000 over core monsoon region of India, from the NCEP II reanalysis data, and from the CTL, DCW, and DCWNC experiments. The abscissa shows the dateline from 31st July-12th August 2000 and the ordinate shows the rate of conversion of energy.

The Fig. 6.3a shows the SLP from the NCEP II reanalysis data on 10th August 2000, which is the day after the demise of the B2000 break event. In this figure, we see the formation of a low in the north BoB. It is widespread and close to the eastern Indian coast, and located in the southern portion of the MT, which is aligned along the CMR. The CTL experiment simulates the low (Fig. 6.3d) with an intensity similar to that in Fig. 6.3a at the head of the BoB, with though the MT has been simulated slightly North of its observed position. However, the DCW experiment shows a weak low and MT (Fig. 6.3b). Despite DCWNC experiment (Figures 6.3c) do neither simulate the low nor the MT.

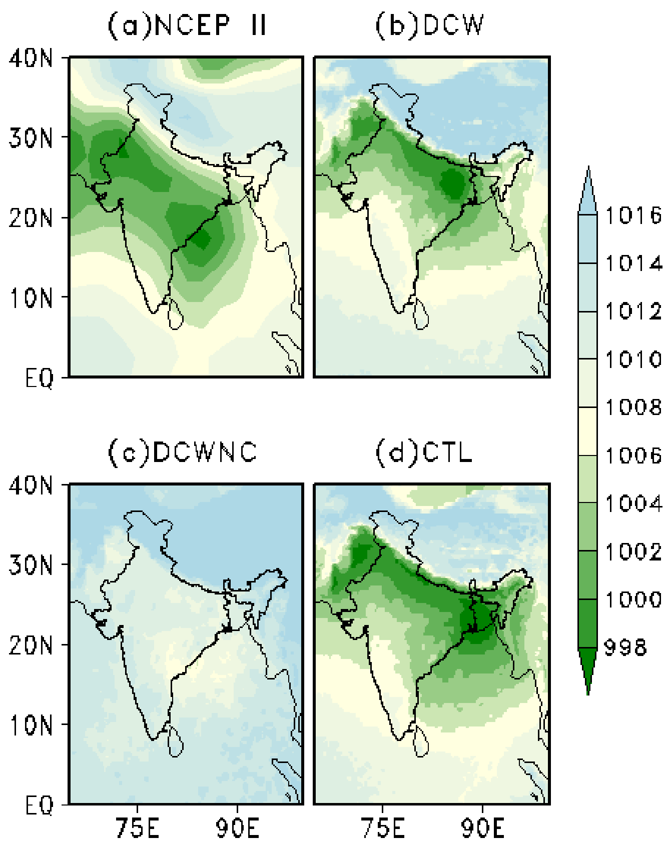

Figure 6.3: Sea level pressure on 10 August 2000 over the Indian region from (a)NCEP II reanalysis data, (b) DCW, (c) DCWNC, and (d) CTL experiments

6.3.2 Eddy momentum flux and rainfall characteristics during a break phase.

The energy to grow the barotropic disturbances is derived from the mean kinetic energy. Energy considerations show that for a disturbance to grow, it must tilt in a direction opposite to that of the meridional gradient of zonal wind (Kuo 1949). That is, waves with an SW–NE tilt will result in maximum vorticity to the south (Kuo 1949), and are associated with a northward transfer of westerly momentum. In such a case, the zonally averaged eddy momentum transport will be positive and is, importantly, conducive to the formation of an eddy disturbance associated with maximum vorticity to its south (Kuo 1949). The transport of eddy momentum flux ($\overline{u'v'}$) is associated with large-scale eddies. Fig. 6.4 depicts the eddy momentum flux for the B2000 break event over the CMR from the NCEP II and all simulations. The evolutions of the simulated eddy momentum flux from the CTL experiment is comparable to that from the NCEP II (Fig. 6.4), though the magnitudes of the eddy momentum flux simulated by the DCWNC, DCW are much weaker.

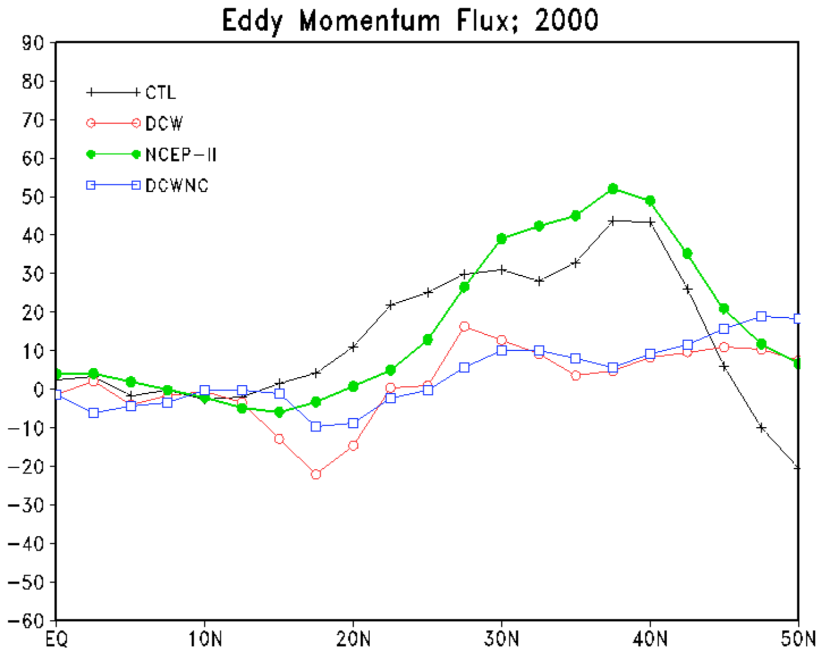

Figure 6.4: Evolution of the eddy momentum flux (m^2/s^2) through the break event 01-09 August 2000 over the core monsoon region of India using NCEP II, DCW, DCWNC, and CTL. The abscissa shows the dateline from 31st July-12th August 2000 and the ordinate shows the rate of conversion of energy.

As per Kuo (1949), the occurrence of neutral waves requires that the absolute vorticity (Z) of zonal flow possess an extreme value ($\frac{dZ}{dy} \equiv \beta - U'' = 0$) at some point. This is the condition for barotropic instability (CBI) of the zonal Rossby waves. If no such critical point exists in the velocity profiles of waves, there can be no neutral waves with phase velocity in the range of the minimum and maximum zonal magnitude of the Rossby waves. Unstable waves manifest the growth of the eddies, which are associated with the transport of momentum flux depending upon the orientation of the troughs of vacillating flow. Kuo (1951) further extended the "*the study of wave motions from the very long and slowly moving or retrograding waves into the realm of* *ordinary waves and cyclone waves and it is found that, for nondivergent barotropic motion, the condition for the presence of neutral and amplified waves with a phase velocity whose value is between the maximum and minimum wind velocity in the belt is the existence of critical points where the absolute vorticity has an extreme value. If no such point exits, then all perturbations must be damped. When this condition is satisfied, both amplified (unstable) and neutral waves can be expected. The waves moving with a velocity equal to the current velocity at the critical point is neutral while those with a velocity less than this values but greater than the minimum wind velocity will be amplified. The amplification will be greatest when the phase velocity is the intermediate between the latter two values; therefore, both fast and slowly moving waves will have little amplification. The degree of instability will also depend upon the sharpness of the velocity profile. When the wave is unstable, the trough line will be directed from southeast toward northwest to the south of the point of the minimum absolute vorticity and from southwest toward northeast to the north of the point of maximum vorticity.*"

In this sense, Fig. 6.5 shows the zonal wind (u) and condition for barotropic instability (CBI) during a break event B2000. In chapter 5, I show the composite CBI or absolute vorticity (chapter 5, Fig. 5.6 & Fig. 5.7) using NCEP II zonal wind data and declining meridional width between SWJ and TEJ. In comparison to NCEP II reanalysis data, CTL, DCW, and DCWNC experiments show a weak zonal wind magnitude on peak days of break phase, along with weaker vorticity. Importantly, the unstable waves are located to the north of the point of maximum vorticity and the westerly waves orient along NE-SW direction (Kuo 1951), indeed, the geopotential height distribution at 200 hPa on B2000 break event show the trough oriented along NE-SW direction (Fig.6.5). Fig. 6.6 shows the 200 hPa geopotential height distribution for the average of break period B2000 and Fig. 6.7 shows the 200 hPa geopotential height difference between the NCEP II and conducted sensitivity experiments, for the break B2000. The observed westerly jet trough orientation along the NE-SW direction is seen in all the experiments with a minor spatial shift.

Similarly, I note the trough NE-SW orientation in the zonal wind distribution at 200 hPa during the break B2000 in all the sensitivity experiments conducted with a slight spatial shift and changes in the magnitude to the SWJ (Fig. 6.8). Fig. 6.9 shows the zonal wind difference between the reanalysis data and model experiment results. In comparison to the reanalysis data, the experiments CTL, and DCW seem to show a good shifting of SWJ and TEJ towards each other during the B2000 break event (Fig. 6.9). Notably, the experiments DCWNC show weaker magnitudes of zonal winds and meridional distribution of SWJ and TEJ. In addition to the geopotential height distribution, all the experiments of the zonal wind distribution at 200 hPa also demonstrate the westerly jet trough orientation along the NE-SW direction (figures 6.8 & 6.9).

Thus, all the model results show a weak rainfall situation over CMR. Fig. 6.10 shows the daily rainfall over the CMR of India for the B2000 break event. Apart from rainfall IMD gridded data, all the experiments show an overestimated daily rainfall during the break period B2000.

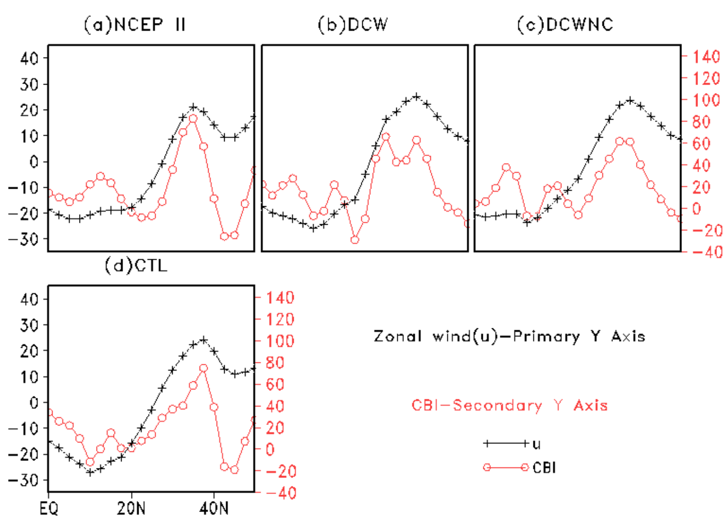

Figure 6.5: Zonal wind (u; Black) and Condition for barotropic instability (CBI) (/s) for break event 01-09 August 2000 over core monsoon region of India using (a)NCEP II, (b) DCW, (c) DCWNC, (d) CTL, (e) DNW, and (f) DNWNC

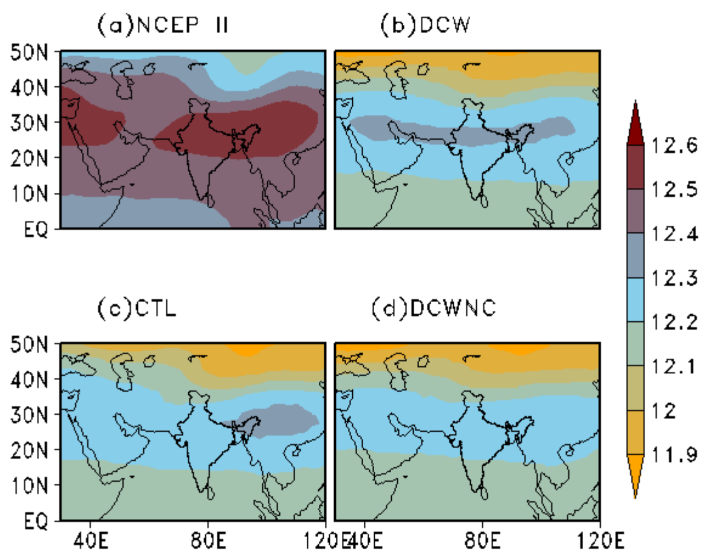

Figure 6.6: Geopotential height (m) at 200 hPa on break event 01-09 August 2000 of (a) NCEP II, (b) DCW, (c) DNW (d) CTL, (e) DCWNC, and (f) DNWNC

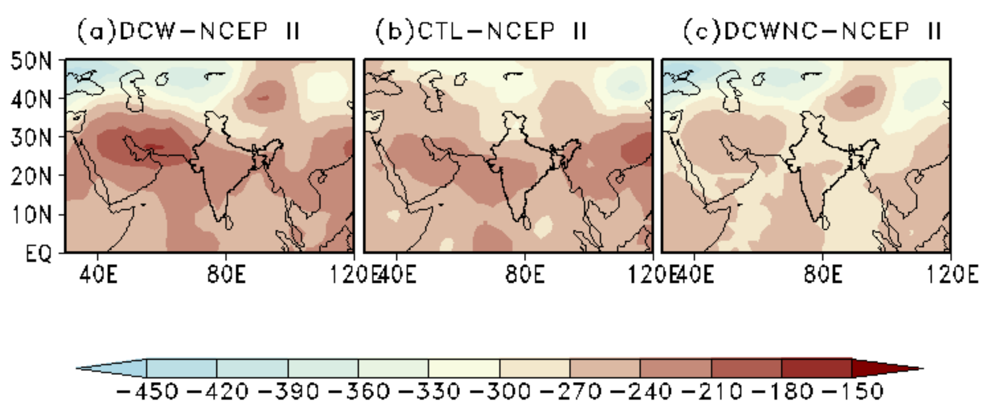

Figure 6.7: Geopotential height (m) at 200 hPa on break event 01-09 August 2000 of (a) difference between DCW-NCEP II, (b) difference between DNW-NCEP II, (c) difference between CTL-

NCEP II, (d) difference between DCWNC-NCEP II, and (e) difference between the DNWNC-NCEP II

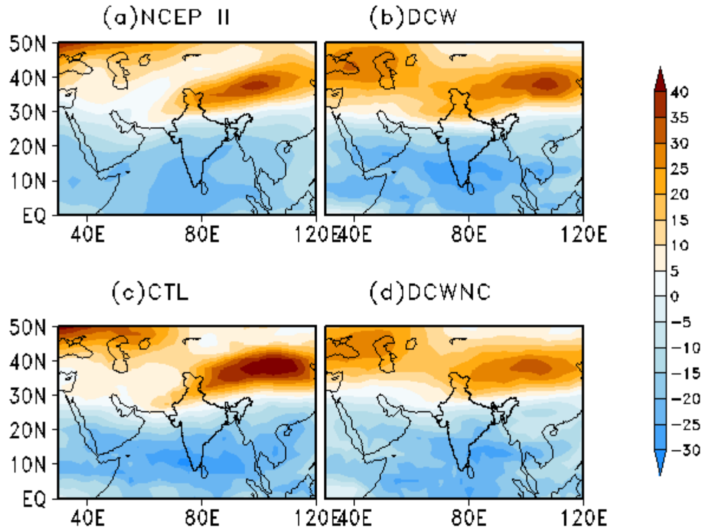

Figure 6.8: Zonal wind (m/s) at 200 hPa on break event 01-09 August 2000 of (a) NCEP II, (b) DCW, (c) DNW (d) CTL, (e) DCWNC, and (f) DNWNC

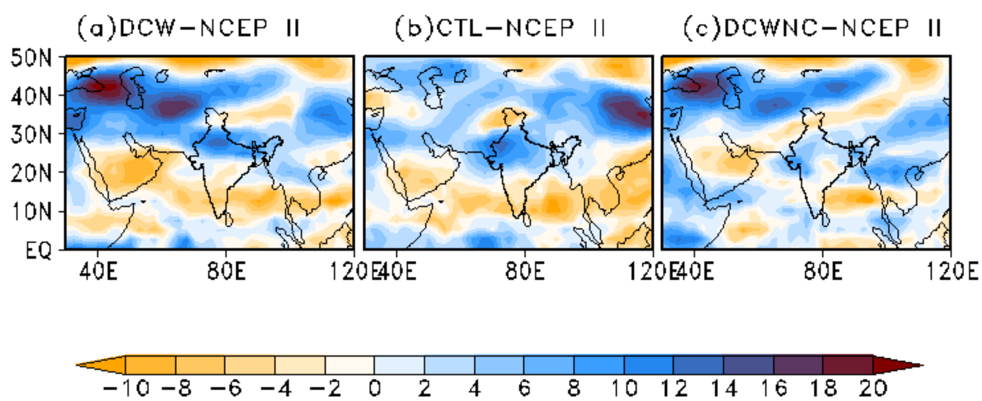

Figure 6.9: Zonal wind (m/s) at 200 hPa on break event 01-09 August 2000 of (a) difference between DCW-NCEP II, (b) difference between DNW-NCEP II, (c) difference between CTL-NCEP II, (d) difference between DCWNC-NCEP II, and (e) difference between the DNWNC-NCEP II

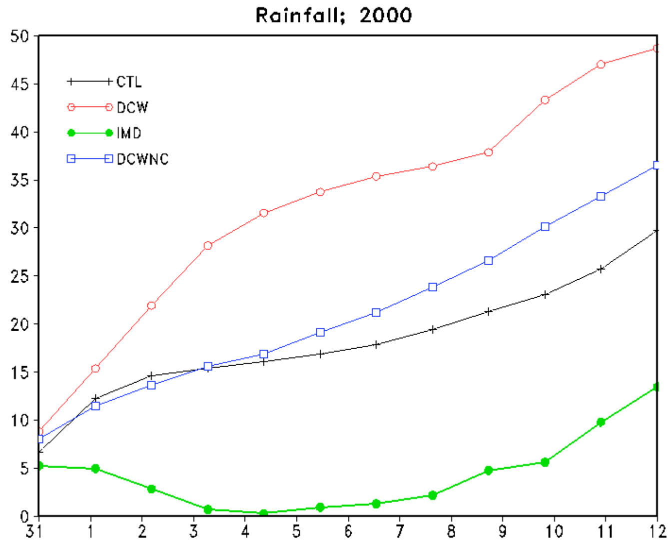

Figure 6.10: Daily Rainfall over core monsoon region of India, using NCEP II, DCW, DNW, CTL, DCWNC, and DNWNC. The abscissa shows the dateline from 31st July-12th August 2000 and the ordinate shows the rate of conversion of energy.

6.4 <u>Summary of the chapter</u>

As the study on monsoon break case i.e., 01-09 August 2000, is assessed using the WRF model to ascertain the changes in the upper atmosphere during a break phase for the revival of summer monsoon over India. The primary goal of the study is to see the characteristic changes in the zonal flow of the upper atmosphere with the conditions variable initial conditions provided in the WRF model, which is the key component to the development of dynamical shear at 200 hPa and subsequently followed by the formation of a low in the head of the Bay of Bengal for the revival of ISM.

Our study suggests the experimental results have shown a qualitative similarity to the NCEP II reanalysis data. The experiment CTL (real run of the model using NCEP-FNL as LBCs), have proven with the significant energy exchange between the SWJ and TEJ, as the jets move close to each other tend to develop a horizontal shear. The associated geopotential height and zonal wind spatial distribution at 200 hPa during the break period B2000 of the experiments DCW, DCWNC, and CTL experiments show a good agreement with the reanalysis data.

The horizontal shear developed is associated with a synoptic low formation in the head of BoB for the revival of ISM. The experiment DCWNC with KF convection scheme turned off, using SLP daily distribution, do not show a low formation in the BoB after a break phase, which is understandable. The experiments DCW and CTL show a low formation with a minor spatial shift towards the Himalayan region or the coastal regions of India.

Nonetheless, apart from upper atmosphere characteristics, the model results of the rainfall over the CMR of India are pretty vague. This could be due to the model's initial conditions, which are developed through the assimilation of limited observational data and ocean features. From this context, it is evident that the inclusion of the observational ocean characteristics/data into the model is very much necessary, this needs further analysis to be carried out using a coupled model.

Chapter7

Summary, conclusion and future scope of the thesis

Outline of the chapter

In this chapter, I discuss the entire summary and conclusion of the research conducted, as well as a brief outline of the thesis's future scope.

7.1 Conclusion

This primary focus of the thesis is to the break monsoon characteristics of ISM and a comparison of these characteristics with those over the Americas, and the role of breaks in the ISM in its subsequent revival. For this, using observed rainfall datasets and NCEP/NCAR II reanalysed datasets, over the broad period from 1979 to 2007, I study 41 known break cases of ISM, which were identified by Rajeevan et al. (2010).

I find that the formation of a blocking high over sub-tropical west Asia a few days earlier is crucial for the manifestation of break monsoon conditions over the India region. While there has been a single case study earlier (Raman and Rao, 1971) that mentioned about the relevance of a blocking high for the formation of a break monsoon event, the study is essentially of historic relevance given the limited data that was used in that study. Interestingly, my results from the analysis of these 41 cases are in conformation with a conclusion from this single case study. My study shows that the formation of these blocking highs preceding the breaks is due to a quasi-resonant amplification of planetary waves. Importantly, I also discover similar conditions associated with break monsoon conditions in the NAM and SAM, respectively. The above discussion on how the extratropical eddies potentially play a major role in the common ground of the basic characteristics of the breaks in these three monsoons i.e., ISM, SAM, and NAM is indicative of a potential global monsoon feature. This motivates us to propose as a unified theory for the development of breaks during summer monsoon.

In addition, I find a dynamical mechanism involved in the revival of the summer monsoon after a break. During the peak of significant breaks, the southward shift of the subtropical westerly jet stream and northward shift of a stronger-than-normal easterly jet facilitate local generation of barotropic instability mechanism, which apparently leads to formation of a synoptic disturbance. Indeed, my other computations of energetics and correlation analysis, suggest an increase in the eddy kinetic energy at the expense of the mean kinetic energy during the breaks, which is also apparently with the formation of the synoptic disturbances in many cases. Indeed, formation of such a disturbance is critical to the subsequent revival of the summer monsoon in 61% of the observed break-to-active revivals.

To verify this hypothesis, I have carried out a few sensitivity experiments using the WRF model. My sensitivity experiments yield energetics and zonal wind changes quantitatively and qualitatively comparable to those from the analysis of the NCEP reanalysis 2 data, and thereby support the afore-proposed mechanism for the revival of active conditions after a break phase.

Thus, the transformation from break to active conditions is also a barotropic process (Rao, 1971, and Govardhan et al., 2017 which has been reported in this thesis). In this context, the entire life cycle of formation of the monsoon breaks and reversal to normal monsoon can therefore be seen as a barotropic adiabatic cycle. This is somewhat similar to the index cycle in a barotropic atmosphere of the middle and polar latitudes, confirming the hypothesis put forth by Arakawa, (1961). This conceptual similarity will be elucidated later. Rao (1971) have first pointed out that the study by Arakawa (1961) is relevant for break-normal cycles. What is more, this concept seems to apply to the SAM and NAM as well. For example, Webster and Curtin (1975), using constant density balloon data, suggested that the 18-23 day variations in the SH seem to be a barotropic interaction between the midlatitudes mean westerlies and ultralong perturbations. They also mention the potential relevance of the findings from the study by Arakawa (1961) on index cycles in a barotropic atmosphere. The real test would be to see whether these variations in the zonal index occur in the observational data over the monsoonal regions. The divergence of eddy momentum in the region of the jet, decelerating the mid-latitude jet implies, a decrease of zonal kinetic energy and a corresponding increase of eddy kinetic energy or barotropic instability, very similar to the Indian break monsoon case (Rao, 1971 and Govardhan et al., 2017; also see equation (2.2)). Note that the regional variations can also be viewed as a regional manifestation of global waves as suggested by Mishra (2018) for the ISM. Fig. 7.1 illustrates the time latitude cross section of 200 hPa zonal wind averaged for the period June to September 2000. As discussed earlier, I see an increase in zonal wind shear during the break period. Fig. 7.1, which shows the longitudinally averaged 200 hPa zonal winds, shows a 50m/s per 20° latitude meridional shear of zonal winds between 20°N and 40°N on 1st July. While on 1 August, the meridional shear of horizontal wind was 50m/s per 10° latitude, between these latitudes, which is twice the value recorded for 1 July. As shown in chapter 5, this increase in shear generates barotropic instability.

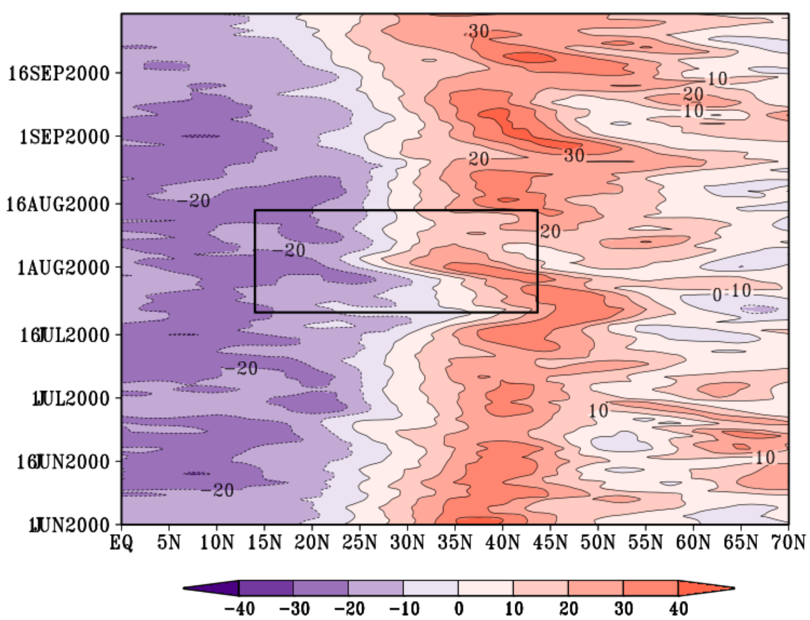

Figure 7.1: Structure of daily U (zonal) wind averaged along 60° E - 95° E over the Indian region, during the period 1 June – 30 September 2000. Black box highlights the Sub-tropical Westerly jet

and Tropical Easterly jet moving close to each other during a break period 01-09 Aug 2000 (case study). Contouring between -40 to 40 (m/s) with an interval of 10 m/s.

One potential reason for the higher latitude westerly jet and lower latitude easterly jet coming closer to one another, in all the three monsoonal regions, is the formation of the blocking high, as conjectured by Ramaswamy (1956, 1962) and confirmed by Fig. 7.1. Similar to the index cycles, during a break, I find that the upper level sub-tropical westerlies and tropical easterlies shift closer. This is analogous to the changes in the westerlies for mid-latitude index cycles. In my case, apart from the blocking, it is still not known exactly what makes these westerly and easterly jets come closer and later move farther. At this moment, I only conjecture that such shifts in the upper level zonal winds in the context of monsoons are closely related to the barotropic processes, as suggested by Chapter 5. As noted earlier, the index cycle variations in the westerly jet can be periodic Arakawa (1961). However, the variations in the Tropical Easterly jet are irregular. This can be understood in a general sense; the variations in the westerlies, extending almost across the globe are more related to the mid-latitude process. The variations in the easterlies may be associated with the changes in the Tibetan plateau, and even due to changes in the monsoon regions, and North Indian Ocean. Therefore, the shifts in both jet streams can be purely due to internal variability, and in some cases, also due to forcing from a co-occurring phenomenon such as an ENSO, IOD, Atlantic zonal mode, etc., which can modulate the jet streams (e.g. Guan and Yamagata, 2003 GRL; . These aspects need to be explored further in detail. Before the break, all waves with wavelengths above 10,000 km are only unstable. This value is manifested through the $2D/\sqrt{3}$ limit Rao (1971). That is, as there are hardly any waves with some lower wavelength, prior to a break, practically there is no instability during the normal conditions. However, during the break the corresponding limit is 5000 km; this value is the lowest found by Govardhan et al., (2017; also see chapter 5) cases. Thus, this jet-induced barotropic instability can generate monsoon disturbances.

A careful examination of Fig. 7.1 shows clear periods of high westerlies in the latitudinal band 30°N-50°N. In the period 1 June- 1 October 2000, there are six varying intervals of high westerlies of about 30 m/s. Also, one can note from 1st September the westerlies in lower latitudes, with the change of the seasons. Further, westerlies increase in speed from 1st September. During the break period, starting at the end of July, the easterly jet (-20m/s) moves northward and the westerly jet (20m/s) southward. In the first week of August, I see a strong shear. Thus, in general, I see regular westerly jet cycles, reminiscent of index cycles between 30°N-50°N. The easterly cycles are very irregular. Fig. 7.1, thus shows the existence of "*Monsoon Index Cycle*", with growth and decay of westerlies over the monsoon region. It would be interesting to speculate the origin of these "*Monsoon Index Cycle*". One possibility, as mentioned earlier, is the barotropic and adiabatic interactions as suggested by Arakawa (1961). Breaks in monsoon occur in one or more cycles. As noted earlier, a typical break is preceded by the formation of blocking high, which occurs due to the penetration of midlatitudes baroclinic wave as shown by Raman and Rao (1981). In Fig. 7.1, I note the southward shift of westerlies in the last week of July 2000. This southward extension of westerlies favours the penetration of midlatitudes baroclinic wave, since easterlies will not permit propagation of a midlatitude baroclinic wave (Charney, 1969). Overall, I note the occurrence of "*Monsoon Index Cycles*" at least in this monsoon season of 2000. A simple schematic, which elucidates the same, r is shown in Fig. 7.2. It would be interesting to see whether these cycles occur in other seasons over India and in other monsoon regions. Considering the regularities in westerlies, interestingly it contributes to the predictability of block formation and consequently breaks.

We should also note that that the breaks in the monsoon could occur due to various other factors also. For example, a recent study by Umakanth et al., (2019) suggests the importance of high-frequency latent heat changes over the central Indian region, foothills of the Himalayas, and Indo-China region for the manifestation of breaks through triggering of meridional wave train trough Artic. As mentioned in the introduction, the monsoon breaks can be manifested due to the MJO.

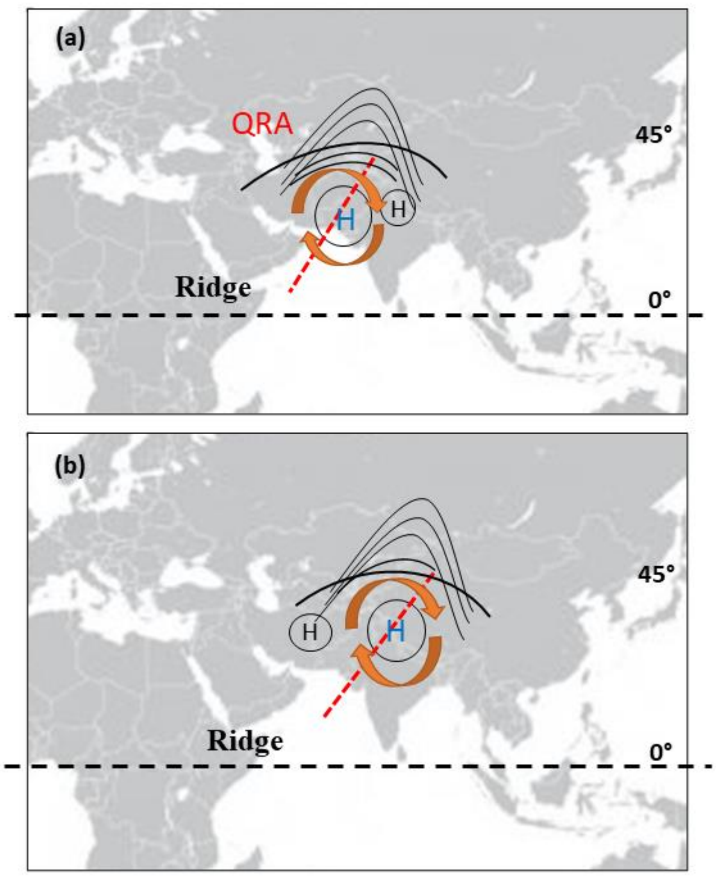

Figure 7.2: A simple schematic picture of a barotropic adiabatic cycle at the upper level. The bold curved arrows represent the Blocking high. The thin angular continuous lines above the Blocking high represent the planetary Rossby waves amplification. The dotted line is the ridgeline and is

inclined along the NE-SW direction. **(a)** Prebreak situation: the genesis of Blocking high due to the QRA **(b)** Break situation: the sustenance of the Blocking high over Indian region due to the deceleration of the zonal wind as shown in the prior Eliassen-Palm flux analysis.

Of course, the Indian summer monsoon variability is controlled by several other factors and drivers. For example, both monsoons and MJO are modulated by the ENSO (e.g., Pai et al., 2016). Pai et al. (2016) show anomalously high number of the ISM break events, which are longer than normal, during the summers when El Niños occur. On the other hand, La Niñas, which are traditionally associated with anomalously surplus ISM rainfall, do not seem to have any association with the frequency of the active cases of the ISM. Importantly, we know that a new type of ENSO, named as ENSO Modoki has been occurring since late 1970s (Ashok et al., 2007; Marathe et al., 2015). In this context, I have carried out a preliminary analysis to document the relative impacts of ENSO types on the active and break monsoon events. I find that both canonical and modoki El Niños anomalously increase the break events, there is a difference in the associated circulation patten and the distribution of negative rainfall anomalies between them. Interestingly, in a general conformation with Pai et al. (2016), the both La Niña types do not indicate a significant association with active event statistics. Further details are provided in Appendix II, and have been published as part of a book chapter (Feba et al., 2020). As it is, as the ENSO impacts and associated circulation patterns last throughout the season, and importantly act from a relatively remote region, any effect of ENSO must be through the ENSO-associated circulation changes in the Indian theatre. Indeed, formation of a synoptic disturbance, which revives the monsoon from breaks, depends on various other factors such as local SST and moisture availability. The monsoon can also revive as a result of large-scale circulation changes that are forced by external drivers, without the explicit formation of a synoptic disturbance. In such cases, the manifested instability may be different. From this context, the other large-scale processes likely explain the remaining cases of the break–active transitions that are not explained by the formation of the synoptic disturbances. We should also be mindful that the mechanism for the revival proposed by us is not necessarily out of the purview of the MJO. For example, a particular phase of an MJO co-occurring during a break induced by a blocking high, may potentially cause an anomalous northward shift of the TEJ and expedite the revival of ISM after a break phase. These possibilities need to be explored.

7.2 Future Scope

Finally, there is also a need to explore the synergies and distinctions in the various mechanism proposed for the active and break cycles.

1. The relative roles of the impact of the midlatitudes versus the role of MJO during breaks and active conditions of ISM.
2. To observe the future changes of instabilities associated with intraseasonal variability of ISM due to the increasing GHGs, aerosols, and land use land cover changes.

Appendix-I

Barotropic instability problem

These are two ways of studying the development of disturbances, namely,

1. Eigen value problem (Dynamic Meteorology by Holton (2004))
2. The initial value problem (Kuo 1953; also see Chapter 6 of Tropical meteorology: An Introduction by Krishnamurti (2013))

Here we have adopted the initial value problem. The symbols/notations representing various variables/parameters in the appendix are listed below (Table A1).

In order to estimate the energy exchange between the basic zonal current and a superimposed disturbance in a barotropic, non-divergent and frictionless atmosphere, we use the barotropic vorticity equation in the form.

$$\frac{d}{dt}(f + v_E) = 0 \qquad (1)$$

where

$$\frac{d}{dt} = \frac{\partial}{\partial t} + u\frac{\partial}{\partial x} + v\frac{\partial}{\partial y}$$

$f = 2\Omega sin(\phi)$; Coriolis force term

ϕ – Latitude

$v_E = \nabla^2\psi$- Relative vorticity

ψ- Stream function

u and v are the zonal and meridional components of the horizontal velocity vector, and can be expressed as

$$u = \frac{-\partial\psi}{\partial y}\,;\, v = \frac{\partial\psi}{\partial x}$$

As can be understood, x & y are the co-ordinate axes taken positive towards east and north respectively.

Linearization of equation (1) yields

$$\frac{\partial}{\partial t}\nabla^2\psi + U\frac{\partial}{\partial x}\nabla^2\psi + \frac{\partial\psi}{\partial x}\left(\beta - \frac{\partial^2 U}{\partial y^2}\right) = 0 \qquad (2)$$

U is the mean zonal current and ψ is the stream function for the perturbation flow.

$\beta = \frac{df}{dy}$ --- Rossby factor

A typical solution for equation (2) will be

$$\psi = A(y,t)sin(kx) + B(y,t)cos(kx) \qquad (3)$$

Where $k = \frac{2\pi}{L}$ is the wave number, and L the Wavelength

Substituting solution (3) in the equation (2) and equating the coefficients of Sin (kx) and Cos (kx) terms, we get the following equations:

$$\frac{\partial^2}{\partial y^2}\left(\frac{\partial A}{\partial t}\right) - k^2\frac{\partial A}{\partial t} = -U\left(k^3 B - K\frac{\partial^2 B}{\partial y^2}\right) + kB\left(\beta - \frac{\partial^2 U}{\partial y^2}\right) \qquad (4)$$

$$\frac{\partial^2}{\partial y^2}\left(\frac{\partial B}{\partial t}\right) - k^2\frac{\partial B}{\partial t} = U\left(k^3 A - K\frac{\partial^2 A}{\partial y^2}\right) - kA\left(\beta - \frac{\partial^2 U}{\partial y^2}\right) \qquad (5)$$

(4) and (5) are two unknown equations in two unknowns, $\frac{\partial A}{\partial t}$ and $\frac{\partial B}{\partial t}$ and so form a closed system of equations.

From the prescribed initial values of u, A, B, and $\frac{\partial^2 U}{\partial y^2}$, and with proper boundary conditions, we can find solutions for $\frac{\partial A}{\partial t}$ and $\frac{\partial B}{\partial t}$.

Initial conditions

A_o =0 and B_o=a sinly , $l = \frac{\pi}{D}$ (6)

where D is the channel width, and suffix ‘o’ represents the initial value . As pointed by Platzman (1952), it is desirable to take initial conditions in such a way as to make the first derivative of perturbations kinetic energy zero. As would be shown later specifically in equation (10), the above condition (6) will fulfil the requirement.

Boundary conditions-- Meridional direction

A=0 at y=0 and y=D; $\frac{\partial A}{\partial t}$=0 and $\frac{\partial B}{\partial t}$=0 at y=0 and y=D (7)

In the X-direction we assume that the disturbance quantities have cyclic periodicity at intervals of one wavelength L. If Q is any disturbance quantity, then Q(x.y)=Q(x±L,y). Thus it is sufficient to consider the domain of integration as the area bounded by one wavelength 'L' in the X- direction and distance D in the y- direction to evaluate various kinds of energies.

Time tendency of Amplitudes

Amplitudes A and B after a time Δt are given by the Taylor's series

$$A(\Delta t) = A_o + \left(\frac{\partial A}{\partial t}\right)_o \Delta t + \frac{1}{2}\left(\frac{\partial^2 A}{\partial t^2}\right)_0 \Delta t^2 \pm - - \quad (8)$$

$$B(\Delta t) = B_o + \left(\frac{\partial B}{\partial t}\right)_o \Delta t + \frac{1}{2}\left(\frac{\partial^2 B}{\partial t^2}\right)_0 \Delta t^2 \pm - - \quad (9)$$

If Δt is sufficiently small, the above series can be truncated after the second derivative. This will no doubt introduce some error in the forecasted amplitudes. Nevertheless, it is not an essential shortcoming as shown by the results.

With initial conditions (6), (5) becomes

$$\frac{\partial^2}{\partial y^2}\left(\frac{\partial B}{\partial t}\right) - k^2\left(\frac{\partial B}{\partial t}\right) = 0 \quad (10)$$

It can easily be shown from (10) and (7) that $\left(\frac{\partial B}{\partial t}\right)_o = 0$, everywhere,

Equations for $\left(\frac{\partial^2 A}{\partial t^2}\right)_0$ and $\left(\frac{\partial^2 B}{\partial t^2}\right)_0$ can be obtained by differentiating (4) and (5) with respect to time. They take the form

$$\frac{\partial^2}{\partial y^2}\left(\frac{\partial^2 A}{\partial t^2}\right) - k^2\frac{\partial^2 A}{\partial t^2} = -U\left(k^3\frac{\partial B}{\partial t} - K\frac{\partial^2}{\partial y^2}\left(\frac{\partial B}{\partial t}\right)\right) + k\frac{\partial B}{\partial t}\left(\beta - \frac{\partial^2 U}{\partial y^2}\right) \tag{11}$$

$$\frac{\partial^2}{\partial y^2}\left(\frac{\partial^2 B}{\partial t^2}\right) - k^2\frac{\partial^2 B}{\partial t^2} = U\left(k^3\frac{\partial A}{\partial t} - K\frac{\partial^2}{\partial y^2}\left(\frac{\partial A}{\partial t}\right)\right) - k\frac{\partial A}{\partial t}\left(\beta - \frac{\partial^2 U}{\partial y^2}\right) \tag{12}$$

Initial conditions (6) are used to obtain (11) and (12) since $\left(\frac{\partial B}{\partial t}\right)_o = 0$from equations (11) and (7) it can easily be shown that $\left(\frac{\partial^2 A}{\partial t^2}\right)_0 = 0$ everywhere, so (8) and (9) reduce to

$$A(\Delta t) = \left(\frac{\partial A}{\partial t}\right)_o \Delta t \tag{13}$$

$$B(\Delta t) = B_o + \frac{1}{2}\left(\frac{\partial^2 B}{\partial t^2}\right)_o \Delta t^2 \tag{14}$$

so after time Δt,ψ is given by

$$\psi(\Delta t) = A(\Delta t)sin(kx) + B(\Delta t)cos(kx)$$

$\psi(\Delta t) = R_\psi cos(kx - \delta\psi)$ where $R_\psi = [A^2(\Delta t) + B^2(\Delta t)]^{1/2}$

and $tan(\delta\psi) = \frac{A(\Delta t)}{B(\Delta t)}$ (15)

Thus the amplitude and phase of ψ wave can be found after time Δt from (15)

Initial change of kinetic energy

The rate of change of kinetic energy may be regarded as the rate of amplification of the disturbances. If it is positive, kinetic energy tends to increase with time, and disturbance is said to be unstable. If it is negative, kinetic energy tends to decrease, and the disturbance is said to be stable or damping. If the rate of change of kinetic energy is zero, the kinetic energy remains constant, and the disturbance is said to be neutral.

The kinetic energy of the disturbance is given by

$$K_r = \int_0^D \int_0^L \frac{u^2+v^2}{2} dxdy \tag{16}$$

But

$$u = \frac{-\partial\psi}{\partial y} = -\left[\frac{\partial A}{\partial y} sin(kx) + \frac{\partial B}{\partial y} cos(kx)\right] \tag{17}$$

$$v = \frac{\partial\psi}{\partial x} = -k[Acos(kx) - Bsin(kx)] \tag{18}$$

Inserting (17) and (18) into (16) we get

$$K_r = \frac{\pi}{2k} \int_0^D \left[\left(\frac{\partial A}{\partial y}\right)^2 + \left(\frac{\partial B}{\partial y}\right)^2 + k^2(A^2 + B^2)\right] dy \tag{19}$$

Differentiating (19) with respect to time and using (4), (5) and (7) we get

$$\frac{\partial K_r}{\partial t} = -\pi \int_0^D U \left[A \frac{\partial^2 B}{\partial y^2} - B \frac{\partial^2 A}{\partial y^2}\right] dy \tag{20}$$

The equation for the time change of the zonal wind is

$$\frac{\partial U}{\partial t} = \frac{-\partial}{\partial y} \overline{uv} \tag{21}$$

where the overbar denotes a zonal average.

Multiplying (21) by U and integrating over the region we get the equation for the time change of zonal kinetic energy as

$$\frac{\partial}{\partial t} K_{r_z} = -\int_0^D \int_0^L U \frac{\partial}{\partial y} \overline{uv} dxdy \tag{22}$$

Where $K_{r_z}$is the zonal kinetic energy given by

$$K_{r_z} = -\int_0^D \int_0^L \left(\frac{U^2}{2}\right) dxdy$$

Using (17) and (18)

$$\overline{uv} = \frac{k}{2}\left[B \frac{\partial A}{\partial y} - A \frac{\partial B}{\partial y}\right] \tag{23}$$

Using (23) and (22) becomes

$$\frac{\partial}{\partial t} K_{r_z} = \pi \int_0^D U \left[A \frac{\partial^2 B}{\partial y^2} - B \frac{\partial^2 A}{\partial y^2} \right] dy \tag{24}$$

It is seen from (20) and (24) that the right hand side of (24) is the same as the right hand side of (20) but with opposite sign. Thus this term represents the interaction between the zonal and perturbation kinetic energies.

In view of our initial conditions,

$$\left(\frac{\partial K_r}{\partial t} \right)_0 = \left(\frac{\partial K_{r_z}}{\partial t} \right)_0 = 0 \tag{25}$$

Thus, as pointed out, earlier our initial conditions are such that the first derivative of perturbation kinetic energy is made equal to zero. So we have to consider the second derivative of perturbation kinetic energy K_r, in order to find out the initial change of kinetic energy, then

$$\frac{\partial^2}{\partial t^2} K_{r_z} = -\pi \int_0^D U \left[\left(\frac{\partial A}{\partial t} \right)_o \frac{\partial^2 B_o}{\partial y^2} - B_o \frac{\partial^2}{\partial y^2} \left(\frac{\partial A}{\partial t} \right)_o \right] dy \tag{26}$$

Initial conditions are used to get (26)

Now, we will study the stability properties of different zonal currents with initial disturbance

$\psi = asin(ly)cos(kx)$, i.e.., $B_o = asin(ly)$and $A_o = 0$ (27)

The actual forms of the zonal current will be selected in such a way as to study different aspects of the problem.

(i) the zonal current U is given by

$U = c\cos(2ly)$ Where $l = \frac{\pi}{D}$

We shall discuss this symmetric mean zonal current. This profile has two inflections points (where $\frac{\partial^2 u}{\partial y^2} = 0$) midway between the axis of the flow and the walls. Kuo (1949) found that the presence of flex points plays an important role in the barotropic stability problem.

We now need to solve equation (4) for the above prescribed zonal wind profile and B_o (given by equation 27). β is given as

$$\beta = \frac{2\Omega\cos(\phi)}{R} = \frac{\Omega}{R}\left(1 + \cos(2\phi)\right)^{1/2} = \frac{\Omega}{R}\left(1 + \alpha\cos(ly)\right) \qquad (28)$$

where R is the radius of the earth and $\alpha < 1$,

With the prescribed expressions for U, B and β, equation (4) is solved with the boundary conditions (7) to give

$$\left(\frac{\partial A}{\partial t}\right)_o = \frac{-E}{k^2+l^2}\sin(ly) - \frac{F}{k^2+4l^2}\sin(2ly) - \frac{G}{k^2+9l^2}\sin(3ly) - - - - \qquad (29)$$

Where

$$E = \frac{ka\Omega}{R} + \frac{k^3ac}{2} - \frac{3kacl^2}{2}$$

$$F = \frac{ka\Omega\alpha}{2R}$$

$$G = \frac{3}{2}l^2kac - \frac{k^3ac}{2}$$

with the expressions for $\left(\frac{\partial A}{\partial t}\right)_o$, B_o and U, the integral in (26) is evaluated to give

$$\left(\frac{\partial^2 K_r}{\partial t^2}\right)_o = \frac{ka^2c^2l^2\pi D}{k^2+9l^2}(3l^2 - k^2) \tag{30}$$

$$\left(\frac{\partial^2 K_r}{\partial t^2}\right)_o \quad = \quad 0 \quad \text{when } L = \frac{2D}{\sqrt{3}} \tag{31}$$

$$> \quad 0 \quad \text{when } L > \frac{2D}{\sqrt{3}}$$

$$< \quad 0 \quad \text{when } L < \frac{2D}{\sqrt{3}}$$

Thus, the neutral wavelength $L < \frac{2D}{\sqrt{3}}$ separates the stable shorter waves and unstable longer waves. It is to be noted that the terms due to earth's rotation will not appear in (30). So earth's rotation will not contribute to $\left(\frac{\partial^2 K_r}{\partial t^2}\right)_o$ with the symmetric profile for U considered. $\left(\frac{\partial^2 K_r}{\partial t^2}\right)_o$ is maximum at a wavelength 2.1 D and so is the most unstable disturbance.

Table A1: A complete list of the symbols/notations representing various variables/parameters in the appendix.

Symbol	Definition
f	Coriolis parameter
ϕ	Latitude
$v_E = \nabla^2\psi$	Relative vorticity
ψ	Stream function for perturbation flow
u	Zonal wind
v	Meridional wind
U	Mean zonal wind
$\beta = \frac{df}{dy}$	Rossby factor
$k = \frac{2\pi}{L}$	Wave number
t	time
L	Wavelength
D	Channel width
Q	Any disturbance quantity
A,B	Amplitude
K_r	Perturabation Kinetic energy
K_{r_z}	Zonal kinetic energy
R	Radius of Earth
dx & dy	Incremental zonal & meridional distances used in integration/differentiation
a,α,c	

	Wavelength
Ω	Vertical ‘p’ velocity
ω	Angular speed of the earth
$\mathit{\Delta}$	Del operator applied to a quantity which varies on an isobaric surface
$\mathit{\Delta}^2$	Laplacian operator

Appendix - II

Intraseasonal Variability of ENSO Modoki - ISM Teleconnections

The intraseasonal variability of the Indian Summer Monsoon (ISM) rainfall has is characterized by periods of wet (active) and dry (break) rainfall activity mainly prominent over the monsoon core region of central India. It is manifests as a 30-60-day oscillation (Gadgil and Joseph 2003; Goswami and Mohan 2001; Goswami and Xavier 2003; Keshvamurthy and Sankar Rao 1992; Krishnamurti and Bhalme 1976; Krishnamurti and Subrahmanyam 1982; Sikka and Gadgil 1980; Yasunari 1979). Goswami and Chakravorty elaborate on these aspects of active and break spells of monsoon in their recent review (Goswami and Chakravorty 2017).

Pai et al. (2016) showed that the composite rainfall patterns of active days during El Niños in the 1901-2014 period show only a slight difference from those during La Niñas, except for slightly stronger negative rainfall anomalies along the foothills of Himalayas during El Niños. However, in the case of break monsoon, the positive composite rainfall anomalies along the foothills of Himalayas during La Niña years are both stronger and extending more westwards (North-eastern states) compared to that of El Niño years.

Motivated by this, in my study, I carried out composite analysis of intraseasonal summer monsoon rainfall anomalies for each type and phase of ENSOs during the 1951-2019 period was obtained by averaging daily rainfall anomalies during the break monsoon and active monsoon periods identified by Rajeevan et al. (2006; 2010), and are shown in Figures A2.1 and A2.2, respectively. TableA2.1 lists the aggregate number of break and active monsoon days in all the canonical El

Niño years, those in El Niño Modoki years, and those in two types of La Niña years respectively (Marathe et al., 2015), during the 1951-2007 period. The El Niño and El Niño Modokis are seen to be predominantly associated with higher number of break conditions over India (Figures A2.1). Interestingly, unlike its seasonal signature (e.g., Figure 5, Ashok et al., 2019), the El Niño Modoki events are associated with negative rainfall anomalies along the monsoon trough during the break periods (Figure A2.1). However, the association between the type and phase of ENSO events with the active monsoon condition is not clear, unlike for the break events. Heuristically, I would expect that the number of active days is more during La Niñas. But we also see many active days during El Niños as well. Of course, the relatively high rainfall during El Niño Modokis over the core monsoon region may be due to the fact that the anomalously negative seasonal rainfall anomalies during these events are more concentrated in peninsular India, with a positive association in the core monsoon region (Fig. 3.4; also see Ashok et al., 2007 and 2019). There is an argument that propensity of the break and active cycles in any monsoon season decide whether the relevant seasonal monsoonal rainfall is below or above normal (Goswami and Chakravorty, 2017; Lau et al., 2012 and references therein).

Table A2.1 List of total number of active and break monsoon days (and spells) during El Niño, El Niño Modoki, La Niña Modoki and La Niña years during the period of 1951-2007.

Event	**Years**	**Total No. of active rainfall days over CMR**	**Total average rainfall over CMR (mm)**	**Total No. of break rainfall days over CMR**	**Total average rainfall over CMR (mm)**

All	1951-2007	414	7.67	404	-4.06
El Niño Modoki	1967, 1977, 1991, 1994, 2002, 2004	36	8.84	52	-2.25
El Niño	1957, 1965, 1972, 1982, 1987, 1997	40	5.24	74	-4.29
La Niña Modoki	1975, 1983, 1998, 1999	19	7.37	32	-2.12
La Niña	1970, 1973, 1988, 2007	43	8.39	25	-3.05

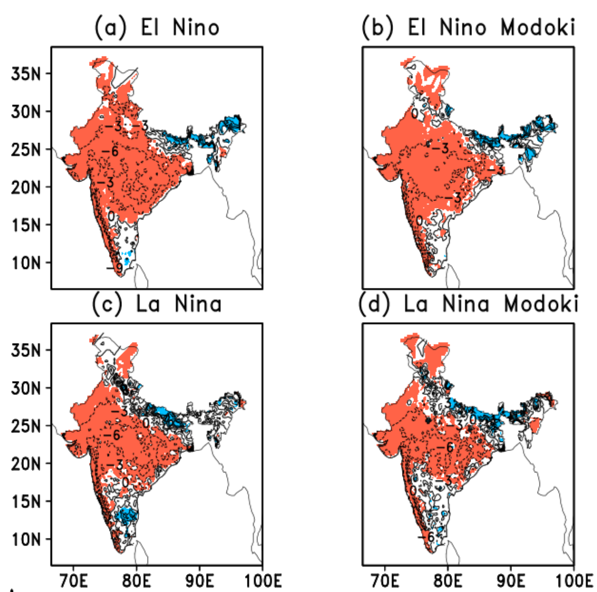

Figure A2.1: (clockwise) Composite of rainfall anomalies during break monsoon days in the El Niño, El Niño Modoki, La Niña Modoki & La Niña years (in contours, at 5 mm/day intervals).

The shaded region indicates 95% confidence using two tailed Student’s t test (orange - negative; sky-blue - positive).

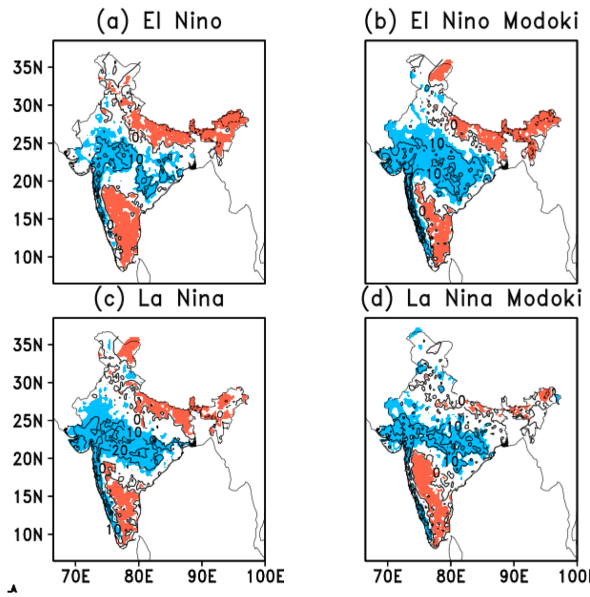

Figure A2.2: (clockwise) Composite of rainfall anomalies during active monsoon days of Indian region in the El Niño, El Niño Modoki, La Niña Modoki & La Niña years (in contours, at 10 mm/day intervals). The shaded region indicates 95% confidence using two tailed Student’s t test (orange - negative; sky-blue - positive).

We see from Figure A2.3(b) that the highest number of break days in a year are seen in 2002, associated with a strong El Niño Modoki. The 1965 El Niño seems to be also associated with the third-highest number of break monsoon days. When the total number of break days are concerned (Table A2.1), the canonical El Niño events are more proficient. During years with a warm-phased event in the tropical Pacific, break spells of longer length are more common, such as the El Niño years during 1951-2007 showing longer break spells compared to the active spells & El Niño Modoki in 2002 & 2004, rather than during the La Niña years. All this suggests that the ENSOs affect the intraseasonal variability of the ISM through the modulation of background seasonal circulation. Moreover, there should be a significant role of internal variability, as evidenced by that the second-highest number of breaks has occurred in 1966 (Table A2.1) when neither a strong warm ENSO nor a positive IOD have co-occurred (Figures not shown).

Interestingly, we also see from Table A2.1 that the number of active days during either of these two El Niños is not negligible. The number of active days associated with La Niñas during 1951-2007 is higher than those associated with the La Niña Modokis. The highest number of active days during summer monsoon occurred in 2006 when no discernible ENSO event was observed. These are likely associated with the co-occurring strong positive IOD event (Cai et al., 2009; Kucharski et al., 2020). The above-normal active cycles during the strong canonical El Niño in 1997 and those during the strong El Niño Modoki during 1994 can be attributed to the opposing effect of the co-occurring strong positive IOD events in years such as 1997 (Ashok et al., 2001). This of course needs to be verified through modelling experiments. In short, we observe that both El Niños and El Niño Modokis apparently facilitate higher than normal break days in Indian summer monsoon, the former particularly so. However, an analogous unique impact of the La Nina's on active cycles is not that evident, which supports the argument of Pai et al. (2016).

Figure A2.1depicts a composite analysis of daily rainfall anomalies during break conditions associated with the two types of El Niños, El Niño Modoki, and corresponding La Niñas. A similar analysis for the active cases is shown in Figure A2.2. We see negative rainfall anomalies over most of India, except the anomalously positive rainfall anomalies along the Himalayan foothills. I do not see a big difference between the signatures of two types of El Niños, except that the canonical events seem to introduce higher deficit in daily rainfall during the breaks. Notably, the impact of El Niño Modokis on the seasonal summer monsoon rainfall along the monsoon trough (e.g., Fig. 5 of Ashok et al., 2019) is apparently opposite to that during the break monsoon days. In addition, while the El Niño Modokis and El Niños are associated with a positive rainfall anomalies in the break monsoon distribution and negative rainfall anomalies during active conditions over the Northeast India, these indications are subject to the data quality in the r region (Soraisam et al., 2018).The surplus rainfall footprints during active cases associated with all types ENSOs seem to be only confined to the monsoon trough region (Fig. A2.2), unlike those during the corresponding break conditions. The La Niña Modokis do not seem to be as proficient as the La Niñas in causing surplus rainfall in the central Indian region during the active phase of ISM (Figures A2.1 and A2.2, lower panels).

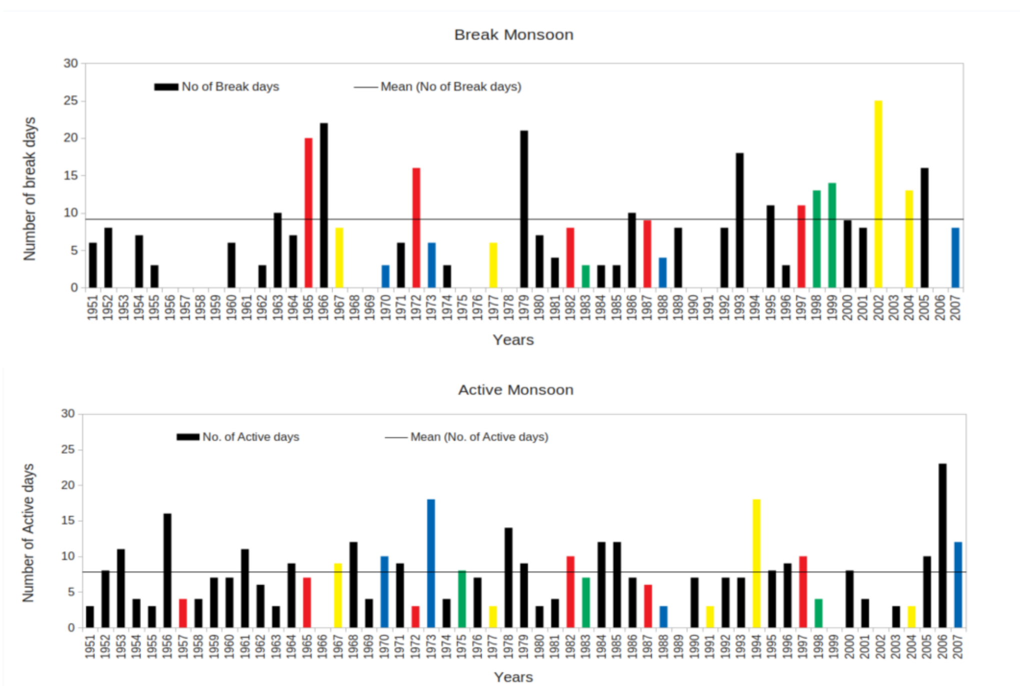

Figure A2.3: (a - Top) Histogram of break days during 1951-2007 based on Rajeevan et al., (2008) criterion. The El Niño, El Niño Modoki, La Niña, La Niña Modoki are designated by the Bars in Red, Yellow, Blue and Green, respectively. (b - Bottom) Same as Figure 3.7 (a) but for active days.

Figures A2.4 a and A2.4 b shows the composite of daily anomalous 850 hPa velocity potential and the divergent wind vectors over all the break and active cases during the 1951-2007 period. Notably, during the breaks, I see a relatively small zone anomalous convergence confined over the central tropical pacific (Fig. A2.4 a). On the other hand, during the active monsoon conditions, the zone of convergence extends well over the western pacific region (Fig. A2.4 b); this looks like an enhanced seasonal mean Walker circulation, with a strong signal over the tropical western pacific. In conformation with the active conditions, we find a convergence over the Indian sub-continent too, along with convergence from the equatorial Indian Ocean (Fig. A2.4 b). This is more prominent over the eastern portion, importantly, over the equatorial Pacific region at the level of 850 hPa, the magnitude of the divergent vectors is strong during the active phase of the Indian summer monsoon, with an opposite signature during the breaks. (Fig. A2.4 b).

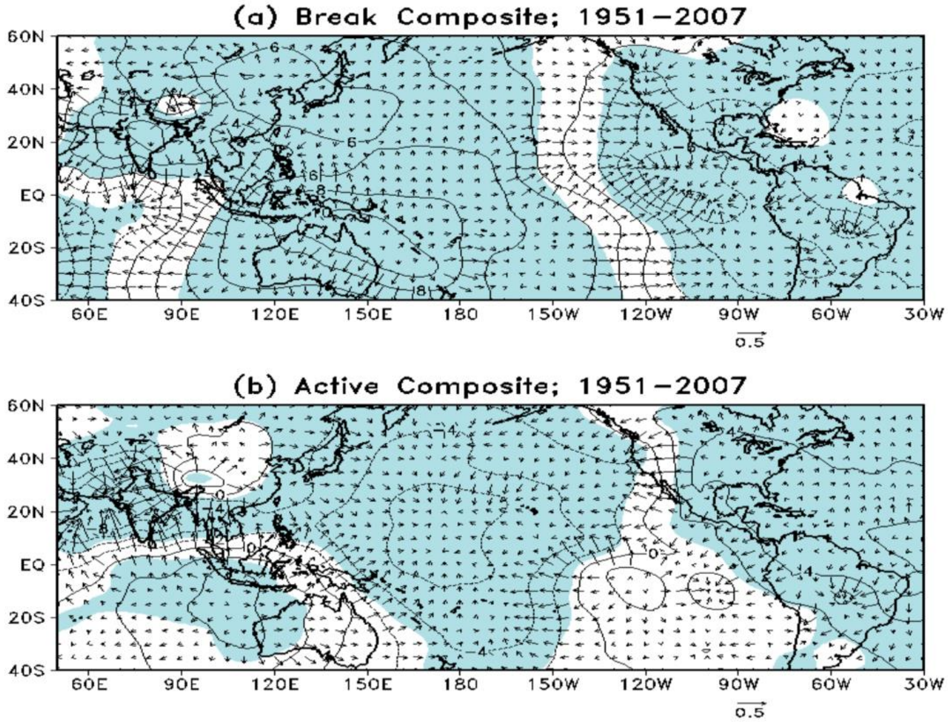

Figure A2.4: 850hPa Velocity potential anomalies (in contours, at 2 m^2/s intervals) and divergent (convergent) wind vectors for all the (a) break and (b) active cases during the 1951-2007 period. The shaded region indicates 95% confidence using two tailed Student's t test.

Figure A2.5 illustrates the composites of the daily anomalous 850 hPa velocity potential and the divergent wind vectors for summer monsoon breaks during all phases of co-occurring ENSOs and ENSO Modokis. Figure A2.5a shows that during canonical El Niños, I find a strong zone of anomalous divergence over the western Indian sub-continent. An anomalous zone of convergence over the northeast Indian region is also shown. These anomalous signatures explain the dynamics behind the rainfall anomalies during breaks associated with the canonical El Niños (Fig. A2.1). During the El Niño Modokis as well, we still see anomalous divergence signature, statistically significant at 95% confidence level. The composites of the active cases during all phases of ENSO and ENSO Modoki indicate anomalous convergence mainly over the northern Head Bay of Bengal (Fig. A2.6), except in case of La Niña Modoki where the anomalous convergence is more prominent over the Arabian Sea. We also observe a strong convergence zone (Fig. A2.6 a) in the in the tropical eastern pacific case of El Niño, and in northern tropical central Pacific region in the case of El Niño Modokis with a slight weakened convergence over the western equatorial Pacific region (Fig. A2.6 b) and vice versa in the cases of La Niña (Fig. A2.6 c) and La Niña Modoki (Fig. A2.6 d) respectively in these locations. . The anomalous convergence signal over the Indian regions fall slightly short of statistical significance during active cases associated with canonical La Niñas.

The above composite analysis, essentially a preliminary effort, when combined with Table A2.1 suggest that changes in seasonal circulation may play potential role in the active-break cycles. There seems to be a relatively stronger association between the El Niños – be it canonical or Modokis -and breaks. However, a similar relatively stronger relation between active conditions with La Niñas, which I expect because of the propensity of La Niñas to provide a favourable background condition for the active conditions, is not that conspicuous. These subtle conjectures need to be supported by further observations using multiple observations -particularly station level observations, and a more exhaustive dynamical analysis. We would also note from Figures A2.5 and A2.6 that the large scale circulation changes associated with monsoon break and active conditions due to ENSOs have their signatures as far as Australia, indicating the complex dynamics that may be involved, and need further attention. The analysis is also subject to the fact that we have not factored the impacts from other climate drivers such as the IOD, Atlantic Zonal Mode, and Madden-Julian Oscillation into our analysis.

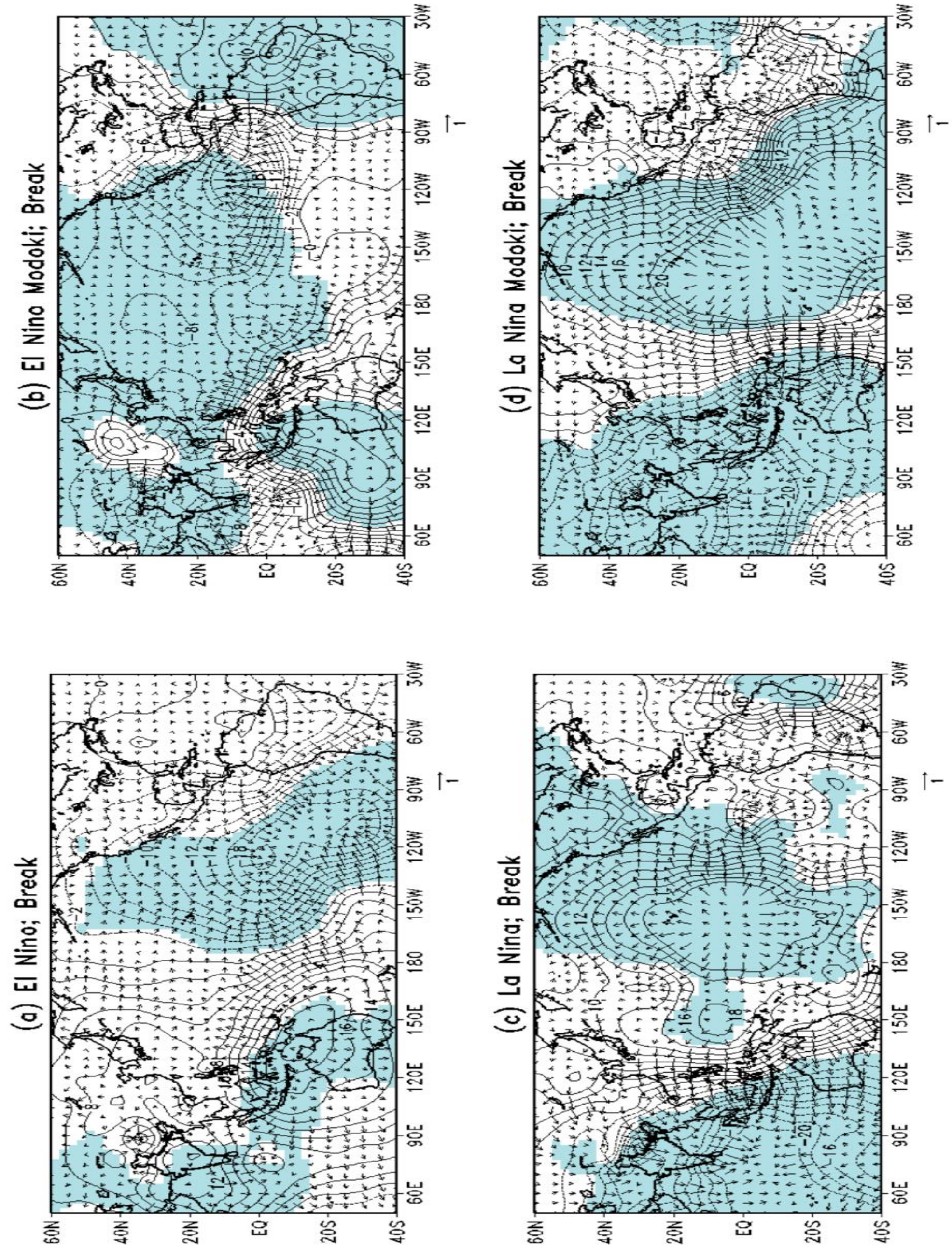

Figure A2.5: 850 hPa Velocity potential anomalies (in contours, at 2 m^2/s intervals) and divergent (convergent) wind vectors for the break cases in (a) El Niño, (b) El Niño Modoki, (c) La Niña and

(d) La Niña Modoki years. The shaded region indicates 95% confidence using two tailed Student's t test.

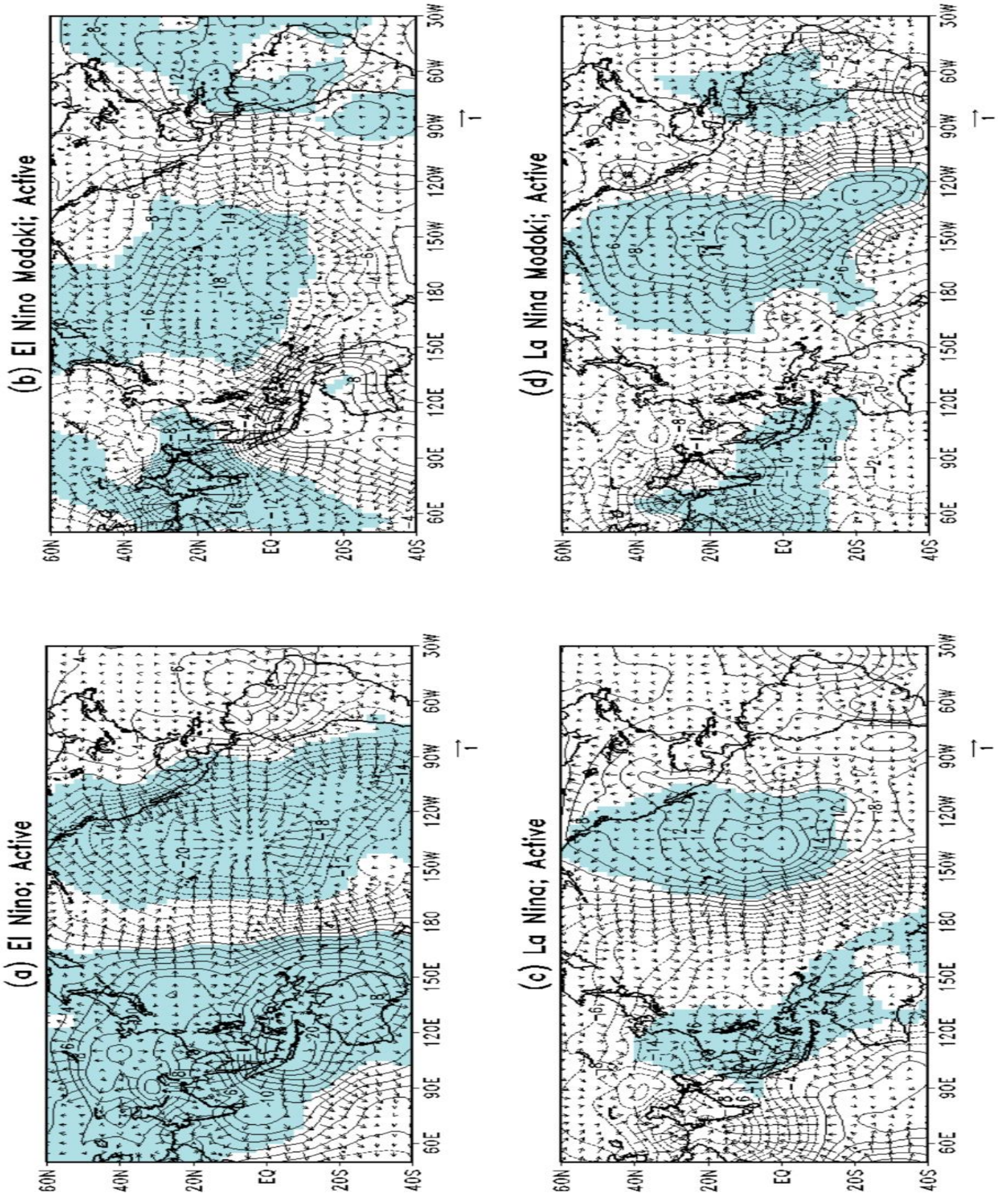

Figure A2.6: 850 hPa Velocity potential anomalies (in contours, at 2 m2/s intervals) and divergent (convergent) wind vectors for the active cases in (a) El Niño, (b) El Niño Modoki, (c) La Niña and

(d) La Niña Modoki years. The shaded region indicates 95% confidence using two tailed Student's t test.

ENSO & ENSO Modoki Index

We use the standard Niño3 and Niño4 indices (area-averaged SST anomaly over the regions 5^0N-5^0S, 150^0W-90^0W and 5^0N-5^0S, 160^0E-150^0W respectively) to define the canonical ENSO events. For ENSO Modoki, we use the ENSO Modoki Index (EMI) as defined by Ashok et al. (2007) and Marathe et al. (2015).

$$\text{EMI}= [\text{SSTA}]_A - 0.5*[\text{SSTA}]_B - 0.5*[\text{SSTA}]_C$$

with SSTA area-averaged over the regions,

A (165^0E-140^0W, 10^0S-10^0N), B (110^0W-70^0W, 15^0S-5^0N), and C (125^0E-145^0E, 10^0S-20^0N), respectively.

Criterion for Break/Active spells

In evaluating the potential impact of the ENSO Modoki on the active and break monsoon events, the rainfall anomalies are obtained by subtracting the daily rainfall climatology for the period 1951-2019 from the daily mean value. We follow the well-accepted Rajeevan et al. (2006) criterion to identify the active and break spells/phase of the ISM, which is based on daily rainfall data. According to the criterion, the active (break) episodes are identified during the peak monsoon months (July to August) as the period through which the standardized daily rainfall anomaly in the interested area exceeds (is less than) one standard deviation. If this continues for at least 3 consecutive days, then these are called as Active (Break) spells. Here, we applied the criterion to identify the active and break episodes in the monsoon core zone limited to the region 18°N-28°N, 65°E-88°E.

REFERENCES

Aihara, M., 1959: Stability properties of large-scale baroclinic disturbances in a vertically and horizontally variable zonal current. Journal ofMeteorological Society of Japan 37, 45-58.

Aikawa, T., M. Inatsu, N. Nakano, and T. Iwano, 2019: Modedecomposed equation diagnosis for atmospheric blocking development. J. Atmos. Sci., 76, 3151–3167, https://doi.org/10.1175/JAS-D-18-0362.1.

Amat H B, Pradhan M, Tejavath C T et al. (2021) Value Addition to Forecasting: Towards Kharif Rice Crop Predictability Through Local Climate Variations Associated With Indo-Pacific Climate Drivers, PREPRINT (Version 1) available at Research Square [https://doi.org/10.21203/rs.3.rs-169288/v1]

Amat HB & Ashok K (2018) Relevance of Indian Summer Monsoon and its Tropical Indo-Pacific Climate Drivers for the Kharif Crop Production Pure ApplGeophys 175(3), p1221

Andrews DG &Mcintyre ME (1976a) Planetary waves in horizontal and vertical shear: the generalized Eliassen-Palm relation and the mean zonal acceleration J Atmos Science 33, 2031-2048

Andrews DG &Mcintyre ME (1978a) Generalized Eliassen-Palm and Charney-Drazin theorems for waves on axisymmetric flows in compressible atmospheres J Atmos Science 35, 175- 185

Andrews DG, Mahlman JD and Sinclair RW (1983) Eliassen-Palm diagnostics of wave-mean flow interaction in the GFDL "SKYHI" general circulation model J Atmos Sci 40, 2768-2784

Arakawa A (1961) The variations of the general circulation in the barotropic atmosphere J Jap Meteor Soc 39, 49-58

Ashfaq, M., Cavazos, T., Reboita, M.S. et al. (2020) Robust late twenty-first century shift in the regional monsoons in RegCM-CORDEX simulations. ClimDyn. DOI: https://doi.org/10.1007/s00382-020-05306-2.

Bedi H S, Billa H S and Mukarjee N 1981 Interaction between northern middle latitude and summer monsoon circulation; Int. Conf. on early results of FGGE and large-scale aspects of monsoon experiment GARP, Tallahassee, Florida, pp. 5-25–5-29.

Berggren, R., B. Bolin, , and C. G. Rossby, 1949: An aerological study of zonal motion, its perturbations and break-down. Tellus, 1 , 14–37.

Blandford, H.F. (1886) Rainfall of India. Monsoon Monograph—India Meteorological Department, No. 3, 658.

Bonner, W. D., 1968: Climatology of the low-level jet. Mon. Wea. Rev., 96, 833–850, doi:10.1175/1520-0493(1968)096,0833:COTLLJ.2.0.CO;2.

Branstator, G., 2002: Circumglobal teleconnections, the jet stream waveguide, and the North Atlantic Oscillation. J. Climate, 15, 1893–1910, https://doi.org/10.1175/15200442(2002)015<1893:CTTJSW>2.0.CO;2.

Brunner, L., Hegerl, G. C., & Steiner, A. K. (2017). Connecting Atmospheric Blocking to European Temperature Extremes in Spring, Journal of Climate, 30(2), 585-594. Retrieved Oct 25, 2021, from https://journals.ametsoc.org/view/journals/clim/30/2/jcli-d-160518.1.xml

Bryson, R. A., and W. P. Lowry, 1955: The synoptic climatology of the Arizona summer precipitation singularity. Bull. Amer. Meteor. Soc, 36, 329-339

Buehler, T., , C. C. Raible, , and T. F. Stocker, 2011: The relationship of winter season North Atlantic blocking frequencies to extreme cold or dry spells in the ERA-40. Tellus, 63A, 212–222, doi:10.1111/j.1600-0870.2010.00492.x.

Carleton, A. M., 1986: Synoptic-dynamic character of "bursts" and "breaks" in the southwest U.S. summer precipitation singularity. J. Climatol, 6, 605-623.

Carleton, A. M., D. A. Carpenter, and P. J. Weser, 1990: Mechanisms of interannual variability of southwest United States summer precipitation maximum. J. Climate, 3, 999-1015.

Carvalho L et al., (2010) The South American Monsoon System and the 1970s climate transition International Journal of Climatology DOI:101002/joc2147

Carvalho LMV, Jones C and Liebmann B (2002) Extreme precipitation events in Southeastern South America and large-scale convective patterns in the South Atlantic convergence zone J Climate 15, 2377-2394

Carvalho LMV, Jones C, Liebmann B. 2002. Extreme precipitation events in southeastern South America and large-scale convective patterns in the South Atlantic Convergence Zone. J. Clim. 15: 2377–2394.

Carvalho LMV, Jones C, Liebmann B. 2004. The South Atlantic Convergence Zone: intensity, form, persistence, and relationships with intraseasonal to interannual activity and extreme rainfall. J. Clim. 17: 88–107.

Carvalho, L M V., A. E. Silva, C. Jones, B. Liebmann, P. L. Silva Dias, and H. R. Rocha, 2010a; Moisture transport and Intraseasonal Variability in the South America Monsoon system. Climate Dynamics, DOI 10.1007/ s00383-010-0806-2

Carvalho, LMV, Jones AE, Silva B, Liebmann, and PL Silva Dias, 2010b, The South American Monsoon System and the 1970s climate transistion, Int. J. Clim., DOI:10.1002/joc.2147

Castro, C. L., T. B. McKee, and R. A. Pilke, 2001: The relationship of the North American Monsoon to tropical and North Pacific surface temperatures as revealed by observational analysis. J. Climate, 14, 4449-4473.

Cavazos, T., Comrie, A. C. and Liverman, D. M. (2002) Intraseasonal anomalies associated with wet monsoons in SE Arizona, J. Climate, 15, 2477-2490.

Charles Jones and Leila MV Carvalho (2002): Active and Break Phases in the South American Monsoon System, Journal of Climate; Vol 15, No 8 (15 April 2002), pp 905-914

Charney JG (1969) A further note on large scale motions in the tropics J Atmos Science 26, 182–185

Charney JG and DeVore JG (1979) Multiple flow equilibria in the atmosphere and blocking J Atmos Science 36, 1205–1216

Charney JG, Shukla J and Mo KC (1981) Comparison of a barotropic blocking theory with observation J Atmos Science 38, 762–779

Charney, J. G., and P. G. Drazin, 1961: Propagation of planetary-scale disturbances from the lower into the upper atmosphere. J. Geophys. Res., 66, 83–109, https://doi.org/10.1029/JZ066i001p00083.

Charney, J. G., J. Shukla, and K. C. Mo, 1981: Comparison of a barotropic blocking theory with observation. J. Atmos. Sci., 38, 762–779.

Chatterjee, P. and Goswami, B. N., 2004, "Structure, genesis and scale selection of the tropical quasi-biweekly mode", Quart. J. Roy. Meteor. Soc., 130, 1171–1194.

Chattopadhyay J, Bhatla R & Prakash O (1994) Zonal circulation indices, 500 hPa April ridge position along 75°E and Indian summer monsoon rainfall: Statistical relationship Theoretical and Applied Climatology, 50, 35–43 https://doiorg/101007/BF00864901

Chen, T. C and Van Loon, H, 1987, Interannual variation of the tropical easterly jet, Mon. Wea. Rev. 115, 1739-1759

Cifelli, R., W. A. Petersen, L. D. Carey, S. A. Rutledge, and M. A. F. Silva Dias, Radar observations of kinematic, microphysical, and precipitation characteristics of two MCSs in TRMM-LBA, J. Geophys. Res., 107, 10.1029/2000JD000264, in press, 2002.

Cifelli, R., W. A. Petersen, L. D. Carey, S. A. Rutledge, and MAF da Silva Dias, Radar observations of the kinematic, microphysical, and precipitation chracteristics of two MCSs in TRMM LBA. J. Geophys. Res., 107(D20), 8077

Ciffelli R, Petersen WA, Carey LD, and Rutledge SA (2002) Radar observations of kinematics, microphysical, and precipitation characteristics of two MCSs in TRMM-LBA, Journal of Geophysical Research 107:101029/JD000264

Colucci, S. J., 1985: Explosive cyclogenesis and large-scale circulation changes: Implications for atmospheric blocking. J. Atmos. Sci., 42, 2701–2717, https://doi.org/10.1175/1520-0469(1985)042,2701:ECALSC.2.0.CO;2.

Colucci, S. J., A. Z. Loesch and L. F. Bosart (1981), Spectral evolution of a blocking episode and comparison with wave interaction theory,J. Atmos. Sci.,38: 2092–2111.

Cunningham, C. C. A, and I. F.A. Cavalcanti, 2006: Intraseasonal modes of variability affecting the South Atlantic Convergence Zone, Int. J. Clim, 26, 1165-1180

De, U. S., Lele, R. R. and Natu, J. C., 1998, “Breaks in South West Monsoon”, Pre-Published Scientific Report No. 1998/3, India Meteorological Department.

Della-Marta P.M., Haylock M.R., Luterbacher J., Wanner , (2007) Doubled length of western European summer heat waves since 1880 J. Geophys. Res., 112 (D15), pp. D15103-D15111

Dickinson RE (1970) Development of a Rossby wave critical level. J Atmos Sci 27: 627–633.

Dickinson, R. E., 1969: Theory of planetary wave-zonal flow interaction. J. Atmos. Sci., 26, 73–81, https://doi.org/10.1175/1520-0469(1969)026<0073:TOPWZF>2.0.CO;2.

Ding Q & Wang B (2007) Intraseasonal teleconnection between summer Eurasian wave train and the Indian monsoon Journal of Climate, 20, 3751–3767 https://doiorg/101175/JCLI42211

Douglas, A. V., , and P. J. Englehart, 1996: An analysis of the starting date for the summer monsoon in western Mexico and southeast Arizona. Proc. 20th Annual Climate Diagnostics and Prediction Workshop, Seattle, WA, U.S. Department of Commerce, NOAA, 207–211.

Douglas, M. W., , R. A. Maddox, , K. Howard, , and S. Reyes, 1993: The Mexican monsoon. J. Climate, 6 , 1665–1677.

Douglas, M. W., R. A. Maddox, K. Howard, and S. Reyes, 1993: The Mexican monsoon. J. Climate, 6, 1665-1677.

Edmon JR Hoskins BJ and McIntyre ME (1980) Eliassen-Palm cross sections for the troposphere, J Atmos Science 37, 2600– 2616

Egger J. 1978 Dynamics of Blocking Highs, J. Atmos. Sci. Volume 35

Eliasen E, Machenhauer B (1965) A study of the fluctuations of the atmospheric planetary flow patterns represented by spherical harmonics. Tellus 17:220–238.

Eliassen A, and Palm E (1961) On the transfer of energy in stationary mountain waves GeofysPubl 22(3), 23 pp, I KommisjonhosAschehoug, Oslo

Eliot, J., 1884, “Accounts of southwest monsoon storms generated in the Bay of Bengal during 1877-1881” Mem. Ind Met. Dept.2, 217-448.

Fisch G, Tota J, Machado LAT, Silva Dias MAF, Lyra RF, Nobre CA, Dolman AJ, Gash JHC (2004) The convective boundary layer over pasture and forest in Amazonia. Theoretical and Applied Climatology, 78: 47-59 doi 10.1007/s00704-004-0043-x.

Fraedrich K, Böttger H (1978) A wavenumber-frequency analysis of the 500 mb geopotential at 50°N. J Atmos Sci 35:745–750.

Fu R, Li, W (2004) The influence of the land surface on the transition from dry to wet season in Amazonia. Theor. Appl. Climatol., 78, doi:10.1007/s00704-004-0046-7. http://link.springer.com/10.1007/s00704-004-0046-7.

Fu R, Zhu B, Dickinson RE (1999) How do atmosphere and land surface influence seasonal changes of convection in the tropical Amazon? J. Climate, 12: 1306–1321.

Fultz D (1956) A survey of certain thermally and mechanically driven fluid systems of meteorological interest, in Fluid models in geophysics. Proc. 1st Sympos. on the Use of Models in *Geophys. Fluid Dynamics*, Baltimore, Sept., 1953, 27–63.

Gadgil and Gadgil, (2006) The Indian monsoon, GDP and agriculture *Economic and Political Weekly* (2006), pp. 4887-4895

Gadgil, S., 2003, "The Indian Monsoon and its variability. Ann. Rev. Earth and Planetary Sci., 31, 429-467.

Gadgil, S., and P. V. Joseph (2003), On breaks of the Indian monsoon, Proc. Indian Acad. Sci. Earth Planet Sci., 112, 529–558.

Gadgil. S. 2008, The Indian monsoon; Links to Cloud Systems over the Tropical Oceans, RESONANCE │ March 2008.

Gan MA, Kousky VE and Ropelewski CF (2004) The South America monsoon circulation and its relationship to rainfall over west-central Brazil, *Journal of Climate*, 17: 47– 66

Garreaud, R D, 2000, Cold air incursions over subtropical South America: Mean structure and dynamics. Mon. Wea. Rev., 128, 2544-2559

Goswami, B. N., 1998, "Inter-annual variation of Indian summer monsoon in a GCM. External conditions versus internal feedbacks", J. Climate, 11, 501-522.

Goswami, B. N., Ajaymohan, R. S., Xavier P. K. and Sengupta, D., 2003, "Clustering of low-pressure systems during the Indian summer monsoon by intraseasonal oscillations", Geophys. Res. Lett. 80(8), doi. l0, 1 029/2002/GLO16734.

Goswami, B. N., and R. S. Ajayamohan, 2001: Intra-seasonal oscillations and inter-annual variability of the Indian summer monsoon, J. Clim., 14, 1180 – 1198.

Goswami, B. N., R. N. Keshavamurthy, and V. Satyan, 1980: Role of barotropic-baroclinic instability for the growth of monsoon depressions and mid-tropospheric cyclones, Proc. Indian Acad. Sci. Earth Planet. Sci., 89, 79 – 97.

Goswami, B. N., R. S. Ajayamohan, P. K. Xavier, and D. Sengupta, 2003: Clustering of low pressure systems during the Indian summer monsoon by intraseasonal oscillations, Geophys. Res. Lett.,30(8), 1431, doi:10.1029/2002GL016734.

Goswami, B. N., Sengupta, D., and Suresh Kumar, G.,(1998) Intraseasonal oscillations and interannual variability of surface winds over the Indian monsoon region. Proc. Indian Acad. Sci. (Earth Planet. Sci.),107, 1–20.

Goswami, B. N., 1997, Chaos and Predictability of the Indian summer monsoon. Pramana,48, 719–736.

Govardhan D, Rao VB, Ashok K (2017) Understanding the Revival of the Indian Summer Monsoon after Breaks, J. Atmos. Science 74(5), 1417-1429, DOI: https://doi.org/10.1175/JAS-D-16-0325.1

Grimm A M., Francina Dominguez, Iracema F. A. Cavalcanti, Tereza Cavazos, Manoel A. Gan, Pedro L. Silva Dias, Rong Fu, Christopher Castro, Huancui Hu and Marcelo Barreiro, 2021, World Scientific Series on Asia-Pacific Weather and ClimateThe Multiscale Global Monsoon System, pp. 49-66.

Grimm AM, Vera C and Mechoso R (2005) The South American Monsoon System, Chang C-P, Wang B, Lau NC-G, (eds) The Global Monsoon System: Research and Forecast, WMO/TD 1266—TMRP: pp 542 http://wwwwmoint/pages/prog/arep/tmrp/documents/global_monsoon_system_IWM3pdf

Haines, K., and J. C. Marshall, 1987: Eddy-forced coherent structures as a prototype of atmospheric blocking. Quart. J. Roy. Meteor. Soc., 113, 681–704, https://doi.org/10.1002/qj.49711347613.

Hales, E. J., Jr., 1972: Surges of maritime tropical air northward over the Gulf of California, Mon. Wea. Rev., 100, 293-306.

Halley E (1686) An historical account of the trade winds and monsoons observable in the seas between and near the tropics, with an attempt to assign the physical cause of the winds Philos Trans Roy Soc London 26,153–168

Hall-McKim, E. A., A. Nowlin, F. Lo, M. Serreze, and M. Clark, 2002: Frequency analysis of intraseasonal variations in the North American monsoon system. Preprints, 13th Symp. On Global Change and Climate Variations, Orlando, FL, Amer. Meteor. Soc., CD-ROM, 14.2.

Hartmann, D. L., and M. L. Michelson, 1989: Intra-seasonal periodicities in Indian rainfall, J. Atmos. Sci., 46, 2838 – 2862.

Hartmann, D. L., and M. L. Michelson, Intraseasonal periodicities in Indian rainfall, J. Atmos. Sci., 46, 2838 – 2862, 1989.

Hartmann, D. L., and S. J. Ghan, 1980: A statistical study of the dynamics of blocking. Mon. Wea. Rev.,108, 1144–1159.

Hasanean, H. M. and Y. Y. Hafez, 2003: On the Formation of Blocking. MAUSAM, 54; PART3, 739-742. Kalnay, E., et al., 1996: The NCEP/NCAR 40-year reanalysis project. Bull. Amer. Meteor. Soc., 77, 437-470.

He, J. H., M. Wen, L. Wang, and H. Xu, 2006: Characteristics of theonset of the Asian summer monsoon and the importance ofAsian–Australian ‘‘land bridge.’’ Adv. Atmos. Sci., 23, 951–963

Held I (1975) Momentum transport by quasi-geostrophic eddies J Atmos Science 32,1494-1497

Held I (2000) The General circulation of the atmosphere Woods Hole Program in Geophysical Fluid Dynamics, 66

Herdies, D. L., A. da Silva, M. A. Silva Dias, and R. Nieto-Ferreira, 2002: Moisture budget of the bimodal pattern of the summer circulation over South America. J. Geophys. Res., 107, 8075, doi:10.1029/2001JD000997.

Hide R (1953) Some experiments on thermal convection in a rotating liquid. Quarterly Journal of the Royal Meteorological Society, 79, 161.

Higgins, R. W., , Y. Yao, , and A. V. Douglas, 1999: Interannual variability of the North American warm season precipitation regime. J. Climate, 12 , 653–680.

Higgins, R. W., , Yao Y. , , Yarosh E. S. , , Janowiak J. E. , , and Mo K. C. , 1997: Influence of the Great Plains low-level jet on summer precipitation and moisture transport over the central United States. J. Climate, 10 , 481–507.

Higgins, R. W., and W. Shi, 2000: Dominant factors responsible for interannual variability of the summer monsoon in the south-western United States. J. Climate, 13, 759–776.

Higgins, R. W., and W. Shi, 2001: Intercomparison of the principal modes of interannual and intraseasonal variability of the North American monsoon system. J. Climate, 14, 403–417.

Higgins, R. W., K. C. Mo, and Y. Yao, 1998: Interannual variability of the U.S. summer precipitation regime with emphasis on the southwestern monsoon. J. Climate, 11, 2582-2606.

Higgins, R. W., Y. Chen, and A. V. Douglas, 1999: Interannual variability of the North American warm season precipitation regime. J. Climate, 12, 653-680.

Higgins, R.W., J. E. Janowiak, and Y. Yao, 1996: A gridded hourly precipitation data base for the United States (1963-1993). NCEP/Climate Prediction Center ATLAS No.1, 47pp.

Holopainen, E., and C. Fortelius, 1987: High-frequency transient eddies and blocking. J. Atmos. Sci., 44, 1632–1645, https://doi.org/10.1175/15200469(1987)044,1632:HFTEAB.2.0.CO;2.

Horel, J. D., A. N. Hahmann, and J. E. Geisler, 1989: An investigation of the annual cycle of convective activity over the tropical Americas. J. Climate,2, 1388–1403.

Hoskins, B. J., and D. J. Karoly, 1981: The steady linear response of a spherical atmosphere to thermal and orographic forcing. J. Atmos. Sci., 38, 1179–1196, https://doi.org/10.1175/1520-0469(1981)038<1179:TSLROA>2.0.CO;2.

Jones C and Carvalho LMV (2002) Active and break phases in the South American Monsoon system J Climate 15, 905–914

Jones, C., 1990: An investigation of low-frequency variability of the large-scale circulation over South America. M.S. thesis, Department of Meteorology, University of Utah, 108 pp.

Joseph, P. V., and S. Sijikumar (2004), Intraseasonal variability of the low level jetstream of Asian summer monsoon, J. Clim., 17, 1449–1458.

Joseph, S., A. K. Sahai, and B. N. Goswami (2009), Eastward propagatingMJO during boreal summer and Indian monsoon droughts, Clim. Dyn.,32, 1139–1153, doi:10.1007/s00382-008-0412-8

Joseph, S., Sahai, A.K. & Goswami, B.N. Eastward propagating MJO during boreal summer and Indian monsoon droughts. ClimDyn 32, 1139–1153 (2009). https://doi.org/10.1007/s00382-008-0412-8

Kalnay-Rivas, E. and L. O. Merkine (1981), A simple mechanism for blocking, J. Atmos. Sci.,38: 2077–2091.

Kanamitsu M et al., (2002) NCEP-DOE AMIP-II reanalysis (R-2) Bull Am Math Soc 83, 1631–1644

Keshavamurthy, R.N&Rao, M.S.(1992) Physics of the monsoons, Aliedpublisheers, https://books.google.co.in/books?id=SDFmmk6i69cC

Keshvamurty, R. N., Satyam, V., Dash, S. K. and Sinha, H. S. S., 1980, “Shift of quasi-stationary features during active and break monsoon”, Proc. Ind.Acad.Sci., (EPA), 89, 209-214.

Kobayashi, N. 1974, Interannual variations of tropical easterly jet stream and rainfall in South Asia, Geophys. Mag. 37, 123-134

Kodama YM. 1992. Large-scale common features of subtropical precipitation zones (the Baiu frontal zone, the SPCZ, and the SACZ). Part I: characteristics of subtropical frontal zones. J. Meteorol. Soc. Jpn. 70:813–836.

Kornhuber K et al., (2017) Summertime planetary wave-resonance in the Northern and Southern Hemisphere J Clim 30, 6133–50

Koteswaram, P (1958) The easterly jet stream in the tropics Tellus, 10, p 56

KOTESWARAM, P., 1950, Upper level “lows” in low latitudes in the Indian area during southwest monsoon season and “breaks” in the monsoon. Ind. J. Met. Geophys., 1, pp. 162-64.

Koteswaram, P., 1958: The easterly jet stream in the tropics. Tellus 10(1) : 43–57, DOI DOI:10.1111/ j.2153-3490.1958.tb01984.x

Kripalani RH, Kulkarani A & Singh SV (1997) Association of the Indian summer monsoon with the northern hemisphere and mid-latitude circulation International Journal of Climatology, 17, 1055–1067

Krishnamurthy, V. and J. Shukla, 2000: Intra-seasonal and inter-annual variability of rainfall over India, J. Clim., 13, 4366-4377.

Krishnamurthy, V., and J. Shukla (2007), Intraseasonal and seasonally persisting patterns of Indian monsoon rainfall, J. Clim., 20, 3–20, doi:10.1175/JCLI3981.1

Krishnamurti, T. N., and P. Ardunay, 1980: The 10 to 20 day westward propagating mode and “breaks in the monsoons”, Tellus, 32, 15–26.

Krishnamurti, T. N. and Bhalme, H. N., 1976, “Oscillations of a monsoon system”, Part I, Observational aspects, J. Atmos, Sci., 33, 1937 – 1954.

Krishnamurti, T. N., and P. Ardunay, 1980: The 10 to 20 day westward propagating mode and ‘breaks’ in the monsoons, Tellus, 32, 15–26.

Krishnan, R., V. Kumar, Sugi, M and Yoshimura, J (2009) Internal Feedbacks from Monsoon Midlatitude Interactions during Droughts in the Indian Summer Monsoon. J. Atmos. Sci., 66, 553–578,

Krishnan, R., Zhang, C, and Sugi, M, (2000) Dynamics of Breaks in the Indian Summer Monsoon. J. Atmos. Sci., 57, 1354–1372, https://doi.org/10.1175/1520-0469(2000)057<1354:DOBITI>2.0.CO;2.

Kuo HL (1949) Dynamic instability of two-dimensional nondivergent flow in barotropic atmosphere J Meteor 6, 105–122

Kuo HL (1951) Dynamical aspects of the general circulation and the stability of zonal flow Tellus 3, 268–284

Kuo HL (1953) On the production of mean zonal currents in the atmosphere by large scale disturbances Tellus 5, 475–493

Kuo, H. L., 1953: On the production of mean zonal currents in the atmosphere by large.scale disturbances. Tellus 5, 475-493.

Lawrence, D. M., and P. J. Webster, 2001: Interannual variability of intraseasonal convection and the Asian monsoon. J. Climate, 14, 2910–2922.

Lejenas, H. and R.A. Madden, 1989: Traveling planetary-scale waves and blocking. Mon. Wea. Rev., 129, 2821-2830.

Liebmann, B., C. S. Vera, L. M. V. Carvalho, I. A. Camilloni, M. P. Hoerling, D. Allured, V. R. Barros, J. Báez, and M. Bidegain, 2004b: An observed trend in central South American precipitation. J. Climate, 17, 4357-4367.

Liebmann, B., G. N. Kiladis, C. S. Vera, A. C. Saulo, and L. M .V. Carvalho, 2004a: Subseasonal variations of rainfall in South America in the vicinity of the low-level jet east of the Andes and comparison to those in the South Atlantic convergence zone. J. Climate, 17, 3829-3842.

Liu, B. Q., J. He, and L. Wang, 2009: Characteristics of the SouthAsia high establishment processes above the Indochina pen-insula from April to May and their possible mechanism (inChinese). Chin. J. Atmos. Sci., 33, 1319–1332.

Liu, B. Q., J. He, and L. Wang, 2012: On a possible mechanism for southernAsian convection influencing the South Asian high establish-ment during winter to summer transition. J. Trop. Meteor., 18,473–484

Lorenz EN (1986) The index cycle is alive and well. In Namias Symposium, Roads, J. O., ed. California. Univ., Scripps Institution of Oceanography, La Jolla, SIO Reference 86-17, Aug., 1986. pp. 188-196

Lorenz, E. N. (1955), Available potential energy and the maintenance of the general circulation, Tellus, 7, 157– 167.

Lorenz, E.N., (1969), The predictability of a flow which possesses many scales of motion, 21. PP 19.

Lorenz, E.N., (1986), The index cycle is alive and well. In Namias Symposium, Roads, J. O., ed. California. Univ., Scripps Institution of Oceanography, La Jolla, SIO Reference 86-17, Aug., 1986. pp. 188-196.

Luo, D, 2005: A barotropic envelope Rossby soliton model for block–eddy interaction. Part I: Effect of topography. J. Atmos. Sci., 62, 5–21, https://doi.org/10.1175/1186.1.

Luo, D, J. Cha, L. Zhong, and A. Dai, 2014: A nonlinear multiscale interaction model for atmospheric blocking: The eddy-blocking matching mechanism. Quart. J. Roy. Meteor. Soc., 140, 1785–1808, https://doi.org/10.1002/qj.2337.

Luo, D, W. Zhang, L. Zhong, and A. Dai, 2019: A nonlinear theory of atmospheric blocking: A potential vorticity gradient view. J. Atmos. Sci., 76, 2399–2427, https://doi.org/10.1175/JAS-D18-0324.1.

Luo, D., 2000: Planetary-scale baroclinic envelope Rossby solitons in a two-layer model and their interaction with synoptic-scale eddies. Dyn. Atmos. Oceans, 32, 27–74, https://doi.org/10.1016/S0377-0265(99)00018-4.

Madden, R. A., and Julian, P. R., (1971) Description of a 40-50 day oscillation in the zonal wind in the tropical Pacific. J. Atmos. Sci. 28, 702-708.

Madden, R. A., and Julian, P. R., (1972) Description of global-scale circulation cells in the tropics with a 40-50 day period. J. Atmos. Sci., 29, 1109-1123.

Madhu Singh and R. Bhatla; 2020: “Intense Rainfall conditions over Indo-Gangetic Plains under the influence of Madden-Julian Oscillation”, Meteorology and Atmospheric Physics, 132(3), 441-449. https://doi.org/10.1007/s00703-019-007037.

Malurkar, S. L. 1950; Notes on analysis of weather of India and neighbourhood, memoir of the Indian meteorological department, vol. XXVIII, part IV, pp. 154-165.

Mandke S, Sahai A K, Shinde M A, Susmitha Josephand Chattopadhyay R 2007 Simulated changes inactive/break spells during the Indian summer monsoondue to enhanced CO2 concentrations: Assessment fromselected coupled atmosphere–ocean global climate mod-els; Int. J. Climatol. 27 837–859.

Mann ME et al., (2018) Projected changes in persistent extreme summer weather events: The role of quasi-resonant amplification Sci Adv 4, eaat3272

Manola I, Selten F, De Vries H and Hazeleger W (2013) Wave guidability of idealized jets J Geophys Res 118, 10432–1044

Marengo, JA., B. Libemann, AM. Grimm, V. Mishra, P. L. Silva Dias, I. F. A. Cavalcanti, L. M. V. Carvalho, E. H. Berbery, T. Ambrizzi, C. S. Vera, A. C. Saulo, J. Nogues-Paegle, E. Zipser, A. Seth, and L. M. Alves, 2010: Review recent developments on the South American Monsoon Systems, Int. J. Clim. DOI:1002/joc.2254

Mishra SK (2018) On the evolution of planetary-scale fields and genesis of monsoon depressions over the Indian region Q J Roy Meteor Soc 144, qj3189

Mo KC (2000) Intraseasonal modulation of summer precipitation over North America Mon Wea Rev, 128, 1490–1505

Mo, K. C., and Berbery E. H. , 2004: The low level jets and the summer precipitation regimes over North America. J. Geophys. Res., 109. D06117, doi:10.1029/2003JD004106.

Moore, T. J., R. L. Gall, and T. C. Adang, 1989: Disturbances along the Arizona monsoon boundary. Mon. Wea. Rev., 117, 932–941

Mullen, S. L., J. T. Schmitz, and N. O. Renno´ , 1998: Intraseasonal variability of the summer monsoon over southeast Arizona. Mon. Wea. Rev., 126, 3016–3034.

Murakami, T., 1979, “Scientific objectives of the monsoon experiment (MONEX)”, Geo. Journal 3.2 117-136/1979.

Murakami, T., L. X. Chen, and A. Xie, 1986: Relationship among seasonal cycles, low-frequency oscillations, and transient disturbances as revealed from outgoing long wave radiation data, Mon. Weather Rev., 114, 11,456 – 11,465.

Murakami, T., T. Nakazawa, and J. He, 1984: On the 40 – 50 day oscillation during 1979 Northern Hemisphere summer. part I: Phase propagation, J. Meteorol. Soc. Jpn., 62, 440 – 468.

N Schaller et al 2018, Influence of blocking on Northern European and Western Russian heatwaves in large climate model ensembles, Environ. Res. Lett. 13 054015

Nakamura, N., and C. Huang, 2017: Local wave activity and the onset of blocking along a potential vorticity front. J. Atmos. Sci., 74, 2341–2362, https://doi.org/10.1175/JASD-17-0029.1.

Nakamura, N., and C. Huang, 2018: Atmospheric blocking as a traffic jam in the jet stream. Science, 361, 42–47, https://doi.org/10.1126/science.aat0721.

Namias J (1950) The index cycle and its role in the general circulation. Journal of Meteorology, 7, 130– 139.

Pai DS, Sridhar L, Rajeevan M, Sreejith OP, Satbhai NS and Mukhopadyay B (2014) Development of a new high spatial resolution (025° × 025°) long period (1901–2010) daily gridded rainfall data set over India and its comparison with existing data sets over the region Mausam 65(1), 1–18

Pai, D., Bhate, J., Sreejith, O. and Hatwar, H. (2011) Impact of MJO on the intraseasonal variation of summer monsoon rainfallover India. Climate Dynamics, 36, 41–55

Pant, G.B. and Rupa Kumar, K., 1997, "Climate of South Asia", John Wiley & Sons, Chichester, New York, USA.

Pant, P. S., 1983, "A physical basis for changes in the phases of the summer monsoon over India", Mon.Wea.Rev., 106, 771-781.

Paradise, A., C. B. Rocha, P. Barpanda, and N. Nakamura, 2019: Blocking statistics in a varying climate: Lessons from a ''traffic jam'' model with pseudostochastic forcing. J. Atmos. Sci., 76, 3013–3027, https://doi.org/10.1175/JAS-D-19-0095.1.

Parker, S. S., J. T. Hawes, S. J. Colucci and B. P. Hayden, 1989: Climatology of 500 mb cyclones and anticyclones, 1950-1985. Mon. Wea. Rev., 117, 558-570.

Parthasarathy B, Rupa Kumar K and Munot AA (1993) Homogeneous Indian monsoon rainfall: variability and prediction, Proc Indian Acad Sci (Earth Planet Sci), 102(1), 121-155

Pattanaik, DR and Satyan, V (2000) Fluctuations of Tropical Easterly Jet during contrasting monsoons over India: A GCM study. Meteorology and Atmospheric Physics, 75 (1-2). pp. 51-60.

Petersen, W. A., and S. A. Rutledge, Regional variability in tropical convection: Observations from TRMM, J. Clim., 14, 3566– 3586, 2001.

Petersen, Walter A., Stephen W. Nesbitt, Richard J. Blakeslee, Robert Cifellim Paul Hein, and Stephen A. Rutledge, 2002; TRMM Observations of Intraseasonal Variability in Convective Regimes over the Amazon. J. Climate. 15, 1278-1294

Petoukhov V, Rahmstorf S, Petri S and Schellnhuber HJ (2013) Quasi-resonant amplification of atmospheric planetary waves as a mechanism for recent Northern Hemisphere weather extremes Proc Natl Acad Sci USA 110, 5336–5341

Raghavan K (1973) Break monsoon over India; *Mon. Weather Rev* 101 33–43

Rajeevan M, Gadgil S and Bhate J (2010) Active and break spells of the Indian summer monsoon J Earth Syst Sci 119, 229–247

Rajeevan M., J. Bhate, J. D. Kale, B. Lal, 2006: High resolution daily gridded rainfall data for the Indian region: analysis of break and active monsoon spells. Curr Sci 91:296–306.

Rajeevan, M., S. Gadgil, J. Bhate, 2008: Active and break spells of Indian summer monsoon. National Climate Centre Research Report No. 7/2008, India Meteorological Department, Pune, 44 pp. http://www.imdpune.gov.in

Ramage, C. S., 1971, "Monsoon Meteorology", Int. Geophys. Ser. 15, Academic Press, San Diego, USA.

Ramamurthy, R., 1969: Monsoons of India: some aspects of the 'break' in the southwest monsoon during July-August, Forecasting Manual, Part IV, No. 18.3. India Meteorological Department, Poona, 13.

Raman CRV and Rao YP (1981) Blocking highs over Asia and droughts over India, Nature 289, 271–273

Ramanadham, R., Visweswara Rao, P. & Patnaik, J.K. Break in the Indian summer monsoon. PAGEOPH 104, 635–647 (1973). https://doi.org/10.1007/BF00875908

Ramaswamy C (1956) The Indian southwest monsoon Paper read at the Seminar in the International Meteorological Institute, Stockholm, Sweden

Ramaswamy C (1962) Breaks in the Indian summer monsoon as a phenomenon of interaction between the easterly and the subtropical westerly jet streams Tellus 14, 337–349

Ramaswamy, C., 1971, Satellite determined cloudiness in tropics in relation to large–scale flow patterns, Part I, studies of different phases of the Indian southwest monsoon, Indian J. Met. Geophys. 22, pp. 289–298.

Ramaswamy, C., and R. S. Pareek, 1978: The south-west monsoon over India and its teleconnections with the middle and upper tropospheric flow patterns over the southern hemisphere. Tellus,30, 126–135.

Ramesh K. and Dessai U R P, 2004, A new criterion for identifying breaks in monsoon conditions over the Indian subcontinent, Geophysical Research Letters, Vol (31), Issue-18, https://doi.org/10.1029/2004GL020562

Rao V.B, 1971: Dynamic instability of the zonal current during a break monsoon,Tellus XXIII.

Rao, G. V. and S. Erdogan, 1989: The atmospheric heat source over the Bolivian Plateau for a mean January. Bound. Layer Meteorol., 46, 13-33

Rao, K. G., Desbois, M., Roca, R., and Nakamura K., (2004) Upper tropospheric drying and the ‘‘transition to break’’ in the Indian summer monsoon during 1999, Geophys. Res. Lett., 31, L03206, DOI: 10.1029/2003GL018269.

Rao, K. V., and S. Rajamani, 1970: Diagnostic study of a monsoondepression by geostrophic baroclinic model. Indian J. Meteor.Geophys., 21, 187–194

Rao,Kusuma G., M. Desbois, R. Roca, and K. Nakamura (2004) Uppertropospheric drying and the ‘‘transition to break’’ in the Indiansummer monsoon during 1999, Geophys. Res. Lett., 31, L03206, doi:10.1029/2003GL018269

Rex D F 1950 Blocking action in the middle troposphere and its effect upon regional climate. II. The climatology of blocking action Tellus, 2, 275-301.

Rex, D. F., 1950: Blocking action in the middle troposphere and its effect upon regional climate. Part I: An aerological study of blocking action. Tellus,2, 196–211. https://doi.org/10.1111/j.2153-3490.1950.tb00331.x

Rickenbach, TM., R, Nieto Ferreria, J. Halverson, DL Herdies, and MAF silva Dias, 2002; Modulation of convection in the southwestern Amazon basin by extratropical stationary fronts, J. Geophys. Res. 107, DOI: 10.1029/2000JD000263

Rodwell, M. J., 1997, “Breaks in the Indian Monsoon: The influence of southern hemisphere weather systems”, J. Atmos. Sci., 54, 2597-2611.

Rossby CG (1939) Relation between variations in the intensity of the zonal circulation of the atmosphere and the displacements of the semi-permanent centers of action J Mar Res 2, 38-55

Samanta D, Dash MK, Goswami BN, & Pandey PC (2016) Extratropical anticyclonic Rossby wave breaking and Indian summer monsoon failure Climate Dynamics, 46, 1547–1562 https://doiorg/101007/s00382-015-2661-7

Sathiyamoorthy V, Pal PK, Joshi PC. (2007). Intraseasonal variability of the Tropical Easterly Jet. Meteorology and Atmospheric Physics 96(3-4): 305–316, DOI 10.1007/s00703-006-0214-7

Sathiyamoorthy, V., P. K. Pal, P. C. Joshi, 2007: Intraseasonal variability of the Tropical Easterly Jet. Meteorology and Atmospheric Physics 96(3-4): 305–316, DOI 10.1007/s00703-006-0214-7

Schamm K, Ziese M, Raykova K, Becker A, Finger P, Meyer-Christoffer A, and Schneider U (2016) GPCC Full Data Daily Version 10: Daily Land-Surface Precipitation from Rain Gauges built on GTS based and Historic Data Research Data Archive at the National Center for Atmospheric Research, Computational and Information Systems Laboratory

Schneider T (2006) The general circulation of the atmosphere Annual Reviews of Earth and Planetary Sciences 34, 655-688

Shukla , J., 1987: Interannual variability of monsoon, Monsoons, edited by J. S.Fein and P. L. Stephens, pp. 399 – 464, John Wiley, New York.

Shukla and Mo 1983, Seasonal and geographical variation of blocking, Mon. Wea. Rev. 111, 388-402

Shutts, G. J. (1983). The propagation of eddies in diffluent jetstreams: Eddy vorticity forcing of ‘blocking’ flow fields. Quarterly Journal of the Royal Meteorological Society, 109(462), 737–761. https://doi.org/10.1002/qj.49710946204

Shutts, G. J., 1983: The propagation of eddies in diffluent jetstreams: Eddy vorticity forcing of ‘blocking’ flow fields. Quart. J. Roy. Meteor. Soc., 109, 737–761, https://doi.org/10.1002/QJ.49710946204.

Sikka and Grossman, 1981, Summer MONEX chronological Weather Summary, International MONEX Management Centre, New Delhi, India

Sikka, D. R., and S. Gadgil, 1980: On the maximum cloud zone and the ITCZ over Indian longitude during southwest monsoon, Mon. Wea. Rev., 108, 1840–1853.

Silva Dias, P. L., M. A. F. Silva Dias, and D. S. Moreira, Mesoscale reanalysis, Proceedings 15th Conference on Hydrology, paper presented at 80th AMS Annual Meeting, Long Beach, Calif., 9–14 January, Am. Meteorol. Soc., Boston, Mass., 2000.

Singh, S.V., R. H. Kripalani and D. R. Sikka, 1992: Interannual variability of the Maddan-Julian Oscillatios in Indian summer monsoon rainfall, J. Climate, 5, 973-979.

Siu, L. W., & Bowman, K. P. (2020). Unsteady Vortex Behavior in the Asian Monsoon Anticyclone, Journal of the Atmospheric Sciences, 77(12), 4067-4088. https://journals.ametsoc.org/view/journals/atsc/77/12/JAS-D-19-0349.1.xml

Souza EB, Kayano MT, and Ambrizzi T (2005) Intraseasonal and submonthly variability over the eastern Amazon and Northeast Brazil during the autumn rainy season Theoretical and Applied Climatology 81, 177–191

Sperber, K. R., J. M. Slingo, and H. Annamalai, 2000: Predictability and the relationship between subseasonal and interannual variability during the Asian summer monsoons, Q. J. R. Meteorol. Soc., 126, 2545 – 2574.

Srivastava AK, Rajeeva M &Kshirsagar SR (2014) Examining pathways for modulation of Indian summer monsoon rainfall by extratropical tropospheric temperature pattern International Journal of Climatology, 34(14) https://doiorg/101002/joc3940

Srivatsangam S Hsiao CN (1978) Parametric study of large-scale eddy properties. II - The zonal scale, Journal of the Atmospheric Sciences, DOI: 10.1175/1520-0469(1978)035<1220:PSOLSE>2.0.CO;2.

Starr V (1948) An essay on the general circulation of the earth’s atmosphere J Meteor 5, 39–43

Starr, V. P., and R. M. White, 1954: Balance requirement of the general circulation. Geophys.Res. Papers No. 35, Geophys. Res. Directorate,AFORO.

Syono, S., and M. Aihara, 1957: Some characteristic features of barotropic disturbances. Journal of meteorological society of Japan 35, 56-64.

Taljaard, J. J., 1972: Synoptic meteorology of the Southern Hemisphere. Meteorology of the Southern Hemisphere, Meteor. Monogr., No. 35, Amer. Meteor. Soc., 139–213.

Tanaka, 1998, Numerical simulation of a life-cycle of a atmospheric blocking and the analysis of potential vorticity using a simple bartropic model. J. Meteor. Soc. Japan, 76, 963-1008

Trenberth KE (1986) An assessment of the impact of transient eddies on the zonal flow during a blocking episode using localized Eliassen-Palm flux diagnostics J Atmos Science 43, 2070-2087

Tung KK (1986) Nongeostrophic theory of zonally averaged circulation Part I: Formulation J Atmos Science 43, 2600

Umakanth U, Kesarkar AP, Rao TN, Rao S (2014) An objective criterion for the identification of breaks in Indian summer monsoon precipitation. Atmos Sci Lett 16:193–198

Umakanth U, Vellore RK, Krishnan R et al,(2019) Meridionally Extending Anomalous Wave Train over Asia During Breaks in the Indian Summer Monsoon, Earth Syst Environ 3, 353–366 (2019) https://doiorg/101007/s41748-019-00119-8

Umakanth, U., Vellore, R.K., Krishnan, R. et al. Meridionally Extending Anomalous Wave Train over Asia During Breaks in the Indian Summer Monsoon. Earth Syst Environ 3, 353–366 (2019). https://doi.org/10.1007/s41748-019-00119-8

Unninayar, M. S., and T. Murakami, 1978: Temporal variations in the northern hemispheric summer circulations. Indian J. Meteor. Hydrol. Geophys.,29, 170–186.

Van Loon, H., 1956: Blocking action in the Southern Hemisphere. Part 1. Notos, 5, 171–175

Vera C et al., (2006) Toward a unified view of the American monsoon systems J Climate 19 (20), 4977–5000

Vernekar AD, Thapliyal V, Kripalani RH, Singh SV, Kirtman B. 1993. Global structure of the Madden–Julian oscillations during two recent contrasting summer monsoon seasons over India. Meteorological and Atmospheric Physics 52: 37–47.

Wallace, J.M., 1975: Diurnal variations in precipitation and thunderstorm frequency over the conterminous United States. Mon. Wea. Rev., 103, 406-419.

Wang B, Webster P. J., and Teng H., 2005, Antecedents and self-induction of active-break south Asian monsoon unraveled by satellites, Geophysical Research Letters, Vol (32), Issue-4, https://doi.org/10.1029/2004GL020996

Webster PJ, and Curtin DG (1975) Interpretations of the EOLE experiment: II Spatial variation of transient and stationary modes J Atmos Science 32, 1848-1863

Webster, P. J., V. O. Magan˜a, T. N. Palmer, J. Shukla, R. A. Tomas, M. Yanai, and T. Yasunari, Monsoons, 1998: Processes, predictability, and the prospects for prediction, J. Geophys. Res., 103(C7), 14,451 – 14,510.

Webster, P., Magana, V., Palmer, T., Shukla, J., Tomas, R., Yanai, M. and Yasunari, T., 1998, "Monsoon processes, predictability and the prospects for prediction", J.Geophys, Res, 103, 14451-14510.

Wei, W., Zhang, R., Wen, M., Kim, B., & Nam, J. (2015). Interannual Variation of the South Asian High and Its Relation with Indian and East Asian Summer Monsoon Rainfall, Journal of Climate, 28(7), 2623-2634. Retrieved Oct 25, 2021, from https://journals.ametsoc.org/view/journals/clim/28/7/jcli-d-14-00454.1.xml

Whitham GB (1960) A note on group velocity. J Fluid Mech 9:341–352.

Whittaker, L. M. and L. H. Horn, 1981: Geographical and seasonal distribution of North American cyclogenesis, 1953-1977. Mon. Wea. Rev., 109, 2312-2322.

Wolfe, K., Wu, X. and Liu, R.H. (2003) Antioxidant Activity of Apple Peels. Journal of Agricultural and Food Chemistry, 51, 609-614. http://dx.doi.org/10.1021/jf020782a

Wright, A. D. F., 1974: Blocking action in the Australian region. Tech. Rep. 10, Bureau of Meteorology, Australia, 29 pp

Wu, G. X., and Coauthors, 2007: The influence of the mechanical and thermal forcing of the Tibetan Plateau on the Asian climate. J. Hydrometeor., 8, 770–789

Yasunari T (1986) Low-frequency interactions between the summer monsoon and the northern hemisphere westerlies Journal of the Meteorological Society of Japan, 64, 693–708

Yasunari T., 1986, Low-Frequency Interactions between the Summer Monsoon and the Northern Hemisphere Westerlies, J. of the Met. Society of Japan, Vol-64 (693-708)

Yasunari, T., 1980: A quasi-stationary appearance of the 30–40 day period in the cloudiness fluctuations during the summer monsoon over India, J. Meteor. Soc. Japan, 58, 336–354.

Yasunari, T., 1981: Structure of an Indian summer monsoon system with around 40-day period, J. Meteorol. Soc. Jpn., 59, 336 – 354.

Yeh, T. C., 1949: On energy dispersion in the atmosphere. J. Meteor., 6, 1–16, https://doi.org/10.1175/1520-0469(1949)006,0001:OEDITA.2.0.CO;2

Zhang, W., and D. Luo, 2020: A nonlinear theory of atmospheric blocking: An application to Greenland blocking changes linked to winter Arctic sea ice loss. J. Atmos. Sci., 77, 723–751, https://doi.org/10.1175/JAS-D-19-0198.1.

Zhou J and Lau KM (1998) Does a monsoon climate exist over South America? J Climate 11, 1020-1040

Zhou J, Lau K-M. 1998. Does a monsoon climate exist over South America? Journal of Climate 11: 1020–1040